

**Understanding Material Flow at the Interface of Friction Stir Lap Welding
(FSLW) of Al-to-Cu plates**

Doddy Parningotan

A thesis submitted to Auckland University of Technology

In fulfilment of the requirements for the degree of Doctor of Philosophy (PhD)

2019

School of Engineering, Computer and Mathematical Sciences

Auckland University of Technology

Abstract

Aluminium to copper bimetal parts have seen wide use in electrical componentry. A continuous interface between the two alloys is necessary in order to have unhampered electron path. Friction stir welding, especially in a lap configuration (FSLW), is a proven method in the production of continuous welds with dissimilar metals, producing a metallurgical joint in the form of interfacial intermetallic layer formed in between the plates. However, from existing literature there is no evidence of a discontinuity-free interface in aluminium-to-copper FSLW. More specifically, no parameter optimisation of penetration depth (d_p) and tool rotation speed (ω) were conducted to establish a continuous weld interface. In addition, material flow, especially in the vicinity of the pin bottom region is still unknown. Therefore, a series of experiments using three different pins, left-hand threaded pin, scriber pin, and pin that have its last thread at the bottom manually filed were conducted with the intention of modifying the flow in the bottom region of the pin. Variation of d_p , ω and tool tilt angle also utilized to investigate their effect toward the material flow, as well as to possibly find the optimum parameter window.

Optimum parameters to produce a continuous Al-to-Cu welds using a conventional left-hand threaded pin a range of d_p between 0.15 - 0.29 mm that combined with ω and travel speed (v) of either 1400 and 40 mm/min or 1000 rpm and 56 mm/min. However, the d_p range is too narrow for manufacturing convenience. In addition, it was revealed, despite the optimum ω and v were known, achieving a consistent continuous interface in a weld as well as the reproducibility were difficult. Flow analysis was then conducted by means of keyhole observation and stop action method. It was revealed that welding using d_p exceeding the workable range that resulted in the formation extensive copper flashes in retreating (RS) and advancing (AS) side. During the process, in the rear half of the pin, the flash in AS side folded inward to the stir zone. It was driven by the vortex flow induced by pin threads. These extensive copper can be broken into big elongated fragments and together with the folded RS flash can potentially blocked the aluminium downflow. Thus, creating voids in the vicinity of the weld's interface. Furthermore, the inconsistency was hypothesized to be caused by non-uniform intermetallic shearing in last thread at the bottom of the pin.

To solve the first problem, a series of welds were conducted with a pin with a 1 mm in diameter scribe pin, fixed 2 mm off from the centre of the bottom surface of the pin. With a scribe pin, 0.5 mm in length, using parameters of ω of 1400 rpm and v of 40 mm/min the scribe penetration depth ($d_{p-scribe}$) range was extended to 0.2 - 0.5 mm. Copper flash bent outward from the stir zone, creating unhampered material flow in the scribed area. However, a $d_{p-scribe}$ less than 0.2 mm led to a decrease in down flow fluidity in the scribe area, and as a result, an extensive gap formed in the weld zone. Tilting the tool closed the majority of the gap. However, a critical $d_{p-scribe}$ of 0.2 mm was applied forming a completely discontinuity free interface. Additionally, material down flow was of importance in driving the copper fragments away from the weld interface. The diminished downward flow was insufficient in driving the copper fragments away from the scribed area, with the fragments and aluminium in the scribed area transforming into a region of thick and brittle intermetallic. Weld keyhole analysis was used in visualising the flash formation and material flow for these scribe pin trials.

To justify the previously drawn hypothesis, FSLW was then conducted using a pin that manually filed to remove the last thread in the pin bottom for the purpose to produce constant intermetallic shearing behind the pin. A consistent, discontinuity-free weld interface, with similar features throughout the weld, was produced using a ω of 1400 rpm, v of 40 mm/min, and d_p of 0.1 mm, verifying the hypothesis. The interface was characterized by thick interfacial intermetallic layer from the RS to the middle of the interface, with a 50 μ m thick of Al_2Cu cluster particles just above the interface, with the cluster appearing to be driven away from the interface in the middle to AS. Extensive copper flashes in both the retreating and AS were formed however, the absence of thread in the bottom region of the pin, diminished or removed the vortex flow, preventing flash folding into the stir zone. This also demonstrated in the weld using d_p of 0.2 and 0.5 mm. The absence of Al_2Cu clusters in welds at a deeper d_p 's, produced enlarged copper fragments, too large to be completely transformed into Al_2Cu particles. These fragments along with the driven away Al_2Cu were used in visualising the aluminium down flow. The extended copper flash in welds with d_p 's of 0.2 and 0.5 mm served as an anchor that made the shear tensile test breaking load value larger than weld with a d_p of 0.1 mm. Fracture analysis confirmed fracturing to occur at the interfacial

intermetallic layer in the weld with a d_p of 0.1 mm, as opposed to fracturing occurring in the mixed stir zone (MSZ) for at the other d_p 's.

Particles usually found dispersed in the stir zone in weld produced with a ω equal or more than 1000 rpm were confirmed with EBSD to be Al_2Cu , similar to the interfacial intermetallic layer that is adjacent to aluminium stir zone. The composite-like structure, which is the dispersion of Al_2Cu particles in the stir zone, was formed by the reaction between copper fragments and surrounding aluminium. With, denseness of the structure depending on the amount of copper fragments. Copper was introduced into aluminium matrix during the process. As temperature increased, the solubility limit increase, then further reduced. The previously dissolved copper got out of the aluminium matrix into the grain boundary and formed Al_2Cu fragments. These fragments the grew and further liquefied as they react with their surrounding aluminium. The amount of liquefaction and denseness depends on the amount of copper fragments. Interfacial intermetallic growth was also investigated by analysing multipass FSLW using optimum parameter for left-hand threaded pin. It was seen that the growth of the interfacial intermetallic layer was not fully governed by volume diffusion, and was formed by dispersion of dense Al_2Cu particles directly atop of the interface.

Acknowledgment

I would like to express my utmost gratitude to my two supervisors, Assoc. Prof. Timotius Pasang and Prof. Zhan Chen. I thank my primary supervisor, Assoc. Prof. Timotius Pasang, for his trust in me, giving me the chance to study here, in AUT and I thank him for his guidance towards the completion of this thesis. His insight plus his direct, humorous and easy-going style making all meeting sessions always productive. I thank my secondary supervisor, Prof. Zhan Chen, for his guidance with his expertise in friction stir welding. I thank him for shaping my way of thinking with on point suggestions and all those rigorous meeting sessions. Without this, I would still be oblivious about what is PhD all about. Most importantly, I thank him for giving me the chance to be involved in the industrial research fellowship.

I also like to express my sincere gratitude to Mr. Mark Tarrant, Altus (previously known as NALCO) and Callaghan innovation. I thank them for their trust and generosity for choosing me as their research fellow and for granting me the funding needed for this PhD journey. I would also like to thank Dr. Baguley for his help during the research fellowship. His expertise in electrical engineering help me in investigating the electrical performance of my samples.

I would express my appreciation to Mr. Jim Crossen, Mr. Ross Jamieson, Mr Mark Masterston, Mr. Tom Jones, Mr. Tim Luton, Mr. Makirai Henry, Mr. Stephen Hartley and Mr. Patrick Connor for their help in machine operation trainings and miscellaneous workshop expertise. Without them, this study would not have been possible.

Special thanks have to be expressed to my fellow PhD student friends. Dr. Nurul Razak, Dr. Kuroush Darvish, and Dr. Mahros Darsin for their companionship during this long journey. Special Thanks for Dr. Karl Davidson for his help in proof reading and his insight in academic writing and the precious, smoking buddies, Dr. Yuan Tao and Dr. Mana Azizi. I owe the completion of my study to their massive help and support.

Most importantly, I would like to express my deepest gratitude to my wife, Novita, for her patience, support, love and sacrifices. I also thank my big family in Indonesia. I thank them for their support, encouragement and constant prayer. I would have quit a long time ago without their supports.

Table of content

Abstract	II
Acknowledgment	V
Table of content.....	VI
List of figures	IX
List of tables.....	XVII
Nomenclature	XVIII
Attestation of Authorship.....	XIX
Chapter 1: Introduction	1
1.1 Aluminium 6060-T5, commercially pure copper and Al-Cu bimetal	1
1.1.1 Aluminium background.....	1
1.1.2 Aluminium 6060-T5.....	2
1.1.3 Copper background	3
1.1.4 C11000 commercially pure copper	4
1.1.5 Al - Cu Bimetal	5
1.2 Fusion welding	5
1.2.1 Fusion welding of similar metal.....	5
1.2.2 Fusion welding of dissimilar metal	6
1.3 Friction stir welding	8
1.3.1 Tools and Pins material selection and design.....	10
1.3.2 Material flow and flow related defects.....	12
1.4 Zinc Electrowinning and Al-Cu bimetal application	15
Chapter 2: Literature review	18
2.1 Effect of ω and v on Al - to - Cu FSLW interface quality	18
2.2 Effect of dp on Al - to - Cu FSLW interface quality and material flow in the pin bottom region	21

2.3	Review on friction stir scribe technology	26
2.4	Review on Al - Cu interfacial intermetallic growth in Al-to-Cu FSLW	30
2.5	Objectives.....	32
Chapter 3: Experimental procedures		33
3.1	Materials and dimensions of weld pieces.....	33
3.2	Machine, work pieces clamping and position adjustment.....	33
3.3	Tool design and material	39
3.4	Welding conditions	44
3.5	Temperature monitoring.....	45
3.6	Stop action procedure	47
3.7	Keyhole examination.....	47
3.8	Metallurgical examination and measurement	48
3.9	Mechanical testing.....	49
Chapter 4: Effect of welding parameters on interfacial continuity on welds produced using left-hand threaded pin		51
4.1	Effect of dp on interfacial continuity.....	51
4.2	Effect of rotational speed (ω) on interfacial continuity	57
4.3	Flow analysis on the vicinity of pin bottom zone during FSLW	64
4.4	Further analysis on the effect of bottom-most thread on the interfacial continuity.....	71
4.5	Microstructure Evolution in the stir zone.....	78
4.5.1	Formation of composite like structure in stir zone.....	78
4.5.2	Interfacial intermetallic growth behaviour	83
4.6	Summary	86
Chapter 5: FSLW with scriber pin		88
5.1	Effect of depth of scriber penetration ($dp - scriber$) on interfacial continuity	88

5.2	The importance of down flow on the formation of intermetallic	96
5.3	The effect of 2.5° tilt angle to interfacial continuity	97
5.4	Analysis on material flow in the pin bottom during FSLW	101
5.4.1	Flow in the bottom region in weld with 0° tilt	101
5.2.2	Flow in the bottom region in weld with 2.5° tilt	105
5.5	Summary	108
Chapter 6:FSLW using pin with unthreaded portion at its bottom		110
6.1	Weld interface consistency and the effect of penetration (dp) on interfacial continuity.....	110
6.1.1	Consistency of the weld	110
6.1.2	The effect of dp on interfacial continuity	112
6.2	Flow analysis on the filed thread region	115
6.3	Mechanical properties and fracture surface analysis.....	116
6.4	Summary	121
Chapter 7: Conclusion and future works.....		123
7.1	Conclusion.....	123
7.2	Future works.....	125
Reference.....		126
Appendix		140

List of figures

Figure 1 – 1	Microstructural zones of fusion welding [14].	6
Figure 1 – 2	(a) Al - Cu laser welding in lapping configuration (b) higher magnification of the weld root showing extensive cracks in intermetallic that formed in the weld root [24].	7
Figure 1 – 3	Schematic drawing of FSW [38], [39].	8
Figure 1 – 4	Typical FSW [38], [39]	9
Figure 1 – 5	Common tool shoulder and pin features [39], [47].	10
Figure 1 – 6	Bands of periodically deposited material behind the pin [50].	12
Figure 1 – 7	Nunes kinematic model for FSW material (a) rigid-body rotation (b) uniform flow, (c) maelstrom or vortex flow, (d) combined flow model resulting in two material currents, straight through and maelstrom current. [51], [56]	13
Figure 1 – 8	Material flow behind the pin [60], [61]	13
Figure 1 – 9	Process schematic of zinc refinery [62], [63].	14
Figure 1 – 10	(a) Plan view schematics of electrodes arrangement [64](b) anode/cathode arrangement [65] (c) one of cathode configuration (d) Bimetal part as a connection from copper busbar to aluminium cathode [66].	16
Figure 2 - 1	σ vs T model of aluminium alloys with two strain rates of 1 and 10 s^{-1} [68].	18
Figure 2 - 2	Type of defects in FSW [60], [61].	19
Figure 2 - 3	FSW interface in Saeid et al. work with a constant ω of 1180 rpm and v of (a) 30,(b) 60, (c) 95, (d) 118 and (e) 190 mm/min [72].	23
Figure 2 - 4	Weld interfaces from Firouzdor and Kou, with a ω of 1400 rpm. (a) weld interface using v of 38 mm/min, (b) void formed in the interface in RS region, (c) voids in copper flash hooks (as polished condition), (d) weld interface using v of 203 mm/min (e) typical voids formed in the interface, (f) voids formed in the copper flash hook [93].	24
Figure 2 - 5	Weld using a ω of 600 rpm and v of 32 mm/min, (b) channel formed in weld shown in a, (c) weld using ω of 600 rpm and v of 15mm/min, (d) weld using ω of 825 rpm and v of 32 mm/min [73].	25

Figure 2 - 6	Weld interface produced using a ω of 1550 rpm and v of 15 mm/min [73].	25
Figure 2 - 7	Interface produced by scriber pin [99]–[101].	27
Figure 2 - 8	Energy density VS dp – scriber on weld quality [102].	27
Figure 2 - 9	Microcrack in the well bonded weld [102].	28
Figure 2 - 10	Al-to-Fe FSLW using $\omega = 710$ rpm and $v = 80$ mm/min with (a) $d_p = -0.3$ mm and (b) $d_p \approx 0$ mm [35].	28
Figure 2 - 11	Al-to-Ti FSLW using $\omega = 1400$ rpm and $v = 20$ mm/min with (a) $d_p \approx 0$ mm, and (b) $d_p > 0$ mm [37].	29
Figure 3 - 1	(a) Plan view of the plate & dimensions; (b) side view of the lapping plates; (c) magnification of circled area E in Fig. 3 - 1b showing thickness of the lapping plates.	34
Figure 3 - 2	Schematic of Al-to-Cu FSLW in this study	34
Figure 3 - 3	(a) Retrofitted Lagun milling machine used throughout the study; (b) Tool rotation speed control in the side of the machine; (c) speed gauge.	35
Figure 3 - 4	(a) Z axis control lever to control dp circled red and labelled as 2 in Fig. 3 - 2; (b) Scale in Z axis control lever.	36
Figure 3 - 5	(a) Travel speed control lever circled red and labelled as 1 in Fig. 3 - 2; (b) travel speed selection.	36
Figure 3 - 6	Bolting system used in this study.	37
Figure 3 - 7	(a) Pin down until pressing the paper tight; (b) Gauge fastener circled red and gauge marker circled in green; (c) Zero position.	37
Figure 3 - 8	Tool penetration with total displacement of 6.2 mm for $dp = 6.1$ mm; (b) Rotating pin penetrates into the lapping plates ready to traverse.	38
Figure 3 - 9	Schematic of dp in normal pin.	38
Figure 3 - 10	Schematic of dp in scriber pin.	39
Figure 3 - 11	(a) Concave shoulder tool; (b) Tool dimension.	40
Figure 3 - 12	(a) Scroll shoulder tool with shoulder head; (b) scroll feature; (c) Tool dimension.	41
Figure 3 - 13	(a) Scroll shoulder tool with shoulder head and scriber in the pin bottom surface; (b) scriber position in the pin bottom surface; (c) pin and scriber dimension.	42

Figure 3 - 14	(a) Concave shoulder tool with scribe pin in the pin bottom surface; (b) Tool dimension.....	43
Figure 3 - 15	Pin with bottom most root and crest manually filed.....	43
Figure 3 - 16	Right picture is the faulty thread. For comparison, good threads can be seen in the left.....	44
Figure 3 - 17	(a) Lateral cross section schematic of welds on first series; (b) Plan view schematic of RS overlap configuration for normal pin multipass FSLW.....	45
Figure 3 - 18	Plan view and dimension of thermocouple groove in Al plate; (b) Cross section of the plate; (c) Higher magnification details circled and labelled as D in Fig. 3 - 11b showing the groove depths.	46
Figure 3 - 19	Data logger USB-2416 from Measurement Computing.....	46
Figure 3 - 20	(a) Plan view of sample cutting schematic; (b) longitudinal cross section of sample cutting schematic.	47
Figure 3 - 21	Keyhole sectioning schematics of welds produced with (a) left-hand threaded pin; (b) scribe pin; (c) tilted scribe pin; (d) pin without the last thread at the bottom.	48
Figure 3 - 22	Method of measuring actual d_p	49
Figure 3 - 23	Shear tensile test sample dimension	50
Figure 4 - 1	$dp - aim = 0.5\text{mm}$ interface (a) P1 $d_p = 0.51\text{ mm}$; (b) P2 $d_p = 0.54\text{ mm}$; (c) P3 $d_p = 0.62\text{ mm}$; and (d) P4 $d_p = 0.55\text{ mm}$	52
Figure 4 - 2	$dp - aim = 0.3\text{ mm}$ interface (a) P1 $dp = 0.29\text{ mm}$; (b) P2 $dp = 0.19\text{ mm}$; (c) P3 $dp = 0.33\text{ mm}$; and (d) P4 $dp = 0.36\text{ mm}$	53
Figure 4 - 3	$dp - aim = 0.2\text{ mm}$ interface (a) P1 $dp = 0.15\text{ mm}$ (area 3 will be discussed in chapter 4.4); (b) P2 $dp = 0.23\text{ mm}$ (area 1 and 2 will be examined and discussed in chapter 4.2 and 4.4); (c) P3 $dp = 0.27\text{ mm}$; and (d) P4 $dp = 0.34\text{ mm}$	53
Figure 4 - 4	SEM image of typical interface of the weld in Fig. 4 - 3b (a) Area 1 in figure 4 - 3b; (b) Magnification of the boxed area in Fig. 4 - 4a; (c) Area 2 in figure 4 - 3b; (d) Magnification of the boxed area in Fig. 4 - 4b.	55
Figure 4 - 5	EDS examination on intermetallic layer and dispersed intermetallic pieces.	56
Figure 4 - 6	Al - Cu binary phase diagram.[124]	57

Figure 4 - 7	(a) SEM image of area taken for EBSD examination; (b) and (e) patterns obtained for point 1 and 22 respectively; (c) and (f) pattern analysis; (d) and (g) analysis results.	58
Figure 4 - 8	SEM micrograph weld made by second tool with $\omega = 500$ rpm, $v = 56$ mm/min (a) Transversal cross section of the weld interface; BE image of typical weld interface showed in area (b) 1; (c) 2; and (d) 3 in a.	59
Figure 4 - 9	SEM micrograph weld made by second tool with $\omega = 710$ rpm and $v = 56$ mm/min, (a) Transversal cross section of the weld interface; (b) typical weld interface; (c) magnified area 1 in b; (d) another typical interface with another layer of crumbled intermetallic below the Al - Cu interface; and (e) enlarged interface of area 2 in d.	61
Figure 4 - 10	SEM micrograph weld made by second tool with $\omega = 1000$ rpm and $v = 56$ mm/min (a) Transversal cross section of the weld interface; Typical weld interface shown in area (b) 1; (c) 2; and (d) 3 in a; and (e) intermetallics dispersed in stir zone are shown in area 4 in a.	62
Figure 4 - 11	SEM micrograph weld made by second tool with $\omega = 1400$ rpm and $v = 56$ mm/min (a) Transversal cross section of the weld interface; (b) Typical weld interface showed in area 1 in a; (c) magnified area 3 in b; and (d) area 2 in a.	63
Figure 4 - 12	Temperature History.....	64
Figure 4 - 13	(a) Edge of the keyhole transversal cross section (sample 1); (b) Position 1 in a; (c) Position 2 in b; (d) Position 3 in b; (e) Position 4 in a; (f) Position 5 in a.	65
Figure 4 - 13	Continued	66
Figure 4 - 14	(a) Keyhole transversal cross section 2mm before the middle (sample 2); (b) Position 1 in a; (c) Position 2 in a; (d) Position 3 in b; (e) Position 4 in c; (f) Position 5 in a; (g) Position 6 in a.	68
Figure 4 - 15	(a) Transversal cross section of the middle of the keyhole (sample 3); (b) Position 1 in a; (c) Position 2 in a; (d) Position 3 in b; (e) Position 4 in c; (f) Position 5 in a; (g) Position 6 in a.	69
Figure 4 - 15	Continued	70

Figure 4 - 16	(a) Keyhole transversal cross section 2mm after the middle (sample 4); (b) Position 1 in a; (c) Position 2 in a.	71
Figure 4 - 17	SEM examination on interface weld in Fig. 4 - 3a (a) SE mode examination; (b) BE mode examination.	72
Figure 4 - 18	(a) Stereo microscope image of longitudinal cross section of the lower region of the pin; (b) Stereo microscope image of region below the pin marked as 1 in a; (c) SEM in BE mode of 4 in b; (d) Transversal cross section pin from RS to mid area; (e) Enlarged area 1 in d.	73
Figure 4 - 19	(a) Stereo microscope image of longitudinal cross section is showing slope region of the raising interface in the trailing part of the pin inside the last root region of the pin (region 2 in Fig. 4 - 17a); SEM BE image of region of (b) 1 and (c) 2 in a.	75
Figure 4 - 20	(a) Stereo microscope image of region 3 in Fig. 4 - 17a showing trailing part of the pin outside the pin periphery; (b) SEM BE mode image of trailing interface further away from the pin.	76
Figure 4 - 21	(a) FSLW used to investigate the pin location on the peak temperature; (b) Temperature history of weld in a.	77
Figure 4 - 22	(a) Temperature history of weld in Fig. 4 - 3; (b) Enlarged area boxed in a showing temperature under the pin.	79
Figure 4 - 23	(a) Recirculation flow with small copper fragments and intermetallic in the Aluminium grain boundaries in area 7 in Fig. 4 - 14a; (b) SEM image of area 1 in a; (c) SEM image of area 2 in a. Area circled red is still in the form of copper.	80
Figure 4 - 24	(a) Al ₂ Cu dispersed particle dense region in Fig. 4 - 15a; (b) SEM image of Fig. 4 - 15c; (c) Another area in less dense region near area in Fig. 4 - 15c; (d) SEM image of circled region in c.	81
Figure 4 - 25	SEM image from 3 different regions in x500 magnification (a) Microstructure in recirculation flow, area 7 in Fig. 4 - 14a; (b) Microstructure in less dense stir zone in area 2 of Fig. 4 - 15c; (c) Microstructure of dense area 1 of Fig. 4 - 15c.	82
Figure 4 - 26	(a) Multipass FSLW using welding parameter of weld in Fig. 4 - 9; (b) Typical interface of second lap; (c) Typical interface of third lap.	84

Figure 4 - 27	Temperature history of multipass FSLW starting from thermocouple placed in first weld. Insert shows the peak of first and second pass in temperature more than 400 °C.....	85
Figure 5 - 1	FSLW scriber with $\omega = 1400$ rpm, $v = 40$ mm/min and $d_p - scriber \approx 0$ mm.	88
Figure 5 - 2	FSLW scriber with $\omega = 1400$ rpm, $v = 40$ mm/min and $d_{p-scriber} = 0.1$ mm (a) OEM image of the interface; (b) Hook region pointed by red arrow in a; (c) SEM image of region 1 in a; (d) SEM image of region 2 in a.	89
Figure 5 - 3	Plan view of scribing action schematic. (a) Initial scribing action in the front periphery of the scribing region; (b) second scribing action in the rear periphery of the scribing region; (c) longitudinal cross section of the incomplete second scribing action.....	91
Figure 5 - 4	FSLW scriber with $\omega = 1400$ rpm, $v = 40$ mm/min and $d_{p-scriber} = 0.2$ mm (a) OEM image of the interface; (b) SEM image of the region pointed by black arrow in a; (c) SEM image of the region pointed by red arrow in a; (d) SEM image of typical interface of this weld; (e) SEM image of stir zone in boxed region in a.....	93
Figure 5 - 5	FSLW scriber with $\omega = 1400$ rpm, $v = 40$ mm/min and $d_{p-scriber} = 0.5$ mm (a) OEM image of the weld's interface; (b) Area 1 in a; (c) turbulence zone in a; (d) SEM image of mixed stir zone (MSZ) in the weld's interface.	95
Figure 5 - 6	(a) Normal left-hand thread pin and (b) "Faulty" thread used to diminish the down flow.....	96
Figure 5 - 7	Weld interface using faulty thread pin (a) OEM image of the stir zone showing thick intermetallic formed by the Cu fragments and Al; (b) Hardness of matrix in intermetallic region; (c) Copper fragment hardness in intermetallic region; (d) Hardness of the region near big cracks in circled red area in a.....	97
Figure 5 - 8	$\omega = 1400$ rpm, $v = 40$ mm/min, $d_{p-scriber} = 0.1$ mm, tilt angle = 2.5° (a) OM image of the interface; (b) Continuous interface of this weld; (c) Typical interface showing discontinuity formation; (d) Closer look at the gap; (e) Al ₂ Cu fragments in the stir zone; (f) MSZ fracturing in the interface; (g) Higher magnification of circled red area in f.....	99

Figure 5 - 9	$\omega = 1400$ rpm, $v = 40$ mm/min, $d_{p-scriber} = 0.2$ mm, tilt angle = 2.5° (a) OM image of the interface; (b) One of typical interface above thick MSZ; (c) OM image of b; (d) Another typical interface with continuous interfacial intermetallic layer.....	100
Figure 5 - 10	(a) OM image of the edge of scribed area; (b) Bottom corner of pin in RS, area 1 in a; (c) Bottom corner of pin in AS, area 2 in a.....	102
Figure 5 - 11	OM image of the middle of the keyhole.....	103
Figure 5 - 12	OM image of rear edge of the scribed area.	104
Figure 5 - 13	OM image of rear edge of the pin periphery.	104
Figure 5 - 14	(a) interface of area outside the pin periphery; (b) Interface further away from a; (c) Stagnant zone from b.....	105
Figure 5 - 15	Scriber pin positions comparison, (a) back (initial position) and front (dashed) side; (b) back (initial position) and flank (dashed) side; (c) analysis of $d_{p-scriber}$ difference; (d) diagram of pin position.....	106
Figure 5 - 16	Figure 5 -16 Keyhole analysis taken from FSLW weld with scriber using $\omega = 1400$ rpm, $v = 40$ mm/min, $d_{p-scriber} = 0.2$ mm, tilt angle = 2.5° . (a) Section taken from the region in front of the scribing area; (b) Section taken from behind of the scribing area.	108
Figure 6 - 1	Back of the pin (a) filed bottom pin; (b) left hand threaded pin.....	110
Figure 6 - 2	Interface 1 produced using parameters of $\omega = 1400$ rpm and $v = 40$ mm/min with $dp = 0.1$ mm.(a) Interface 1 cross section;(b) SEM of typical interface from RS to mid, boxed red in a; (c) typical interface of mid to AS, marked 1 on a; (d) another typical interface of mid to AS, marked 2 on a.	111
Figure 6 - 3	Interface 2 from the same weld as Fig. 6 - 2. (a) Interface 2 cross section; (b) SEM of typical interface from RS to mid, marked 1 in a; (c) SEM of typical interface from mid to AS, marked 2 in a.	112
Figure 6 - 4	Weld produced with $\omega = 1400$ rpm, $v = 40$ mm/min and $dp = 0.25$ mm (a) OM image of the interface; (b) large fragments laid on top of the interface, marked 1 in a; (c) typical interface taken from area marked 1 in a; (d) another typical interface taken from area marked 2 in a;.....	113

Figure 6 - 5	Weld produced with $\omega = 1400$ rpm, $v = 40$ mm/min and $dp = 0.5$ mm (a) OM image of the interface; (b) typical interface of the weld; (c) another typical interface of the weld showing minor discontinuity.	114
Figure 6 - 6	Transversal cross section of one fourth of the keyhole. The threadless region is ~ 1.4 mm in height.....	115
Figure 6 - 7	Transversal cross section of three fourth of the keyhole.....	116
Figure 6 - 8	Fractured tensile shear sample of welds with (a) dp of 0.1 mm; (b) dp of 0.2 mm; (c) dp of 0.5 mm.	117
Figure 6 - 9	(a) Fracture surface of broken tensile shear test sample of weld with dp of 0.1 mm; (b) fracture surface on the aluminium side; (c) fracture surface of copper side.....	118
Figure 6 - 10	(a) Fracture surface of broken tensile shear test sample of a weld with a dp of 0.2 mm; (b)-(c) aluminium side fracture surface; (d)-(e) fracture surface of copper side.....	119
Figure 6 - 11	(a) Fracture surface of broken tensile shear test sample of a weld with a dp of 0.5 mm; (b)-(c) aluminium side fracture surface; (d)-(e) fracture surface of copper side.....	120
Figure 6 - 12	EDS examination spots of Fig. 6 - 11d.....	121

List of tables

Table 1 - 1	Group of aluminium wrought alloy [2].....	1
Table 1 - 2	Copper and copper alloys	4
Table 1 – 3	Advantages of FSW [38], [44].....	8
Table 1 – 4	Tool material and attributes [39], [47].....	9
Table 1 - 5	Tool features design variations and advantages [39], [47].	11
Table 2 - 1	Past studies on interfacial features in conjunction with dp in Al - to - Cu FSLW.....	22
Table 4 - 1	Chemical composition in atomic % of EDS displayed in Fig. 4 - 5.	56
Table 6 - 1	Chemical composition in atomic % of Fig 6 - 12.	121

Nomenclature

d_p - Depth of Penetration.

$d_{p-scriber}$ - Depth of Scriber Penetration.

$l_{scriber}$ – length of scriber.

ω - Tool Rotation Speed.

v - tool travel speed.

T_{enter} – Temperature 4 mm before the peak of temperature.

T_{pass} – Temperature 4 mm after the peak of temperature.

T_{peak} – Peak temperature of the weld.

$T_{eutectic}$ – Eutectic Temperature.

LoC – Lack of Consolidation.

RS - Retreating side.

AS - Advancing side.

MSZ – mixed stir zone.

IMC – Intermetallic compound

SEM = Scanning Electron Microscope

EDS – Energy dispersive spectroscopy

EBSD – Electron backscattered diffraction

BE – Backscattered Electron

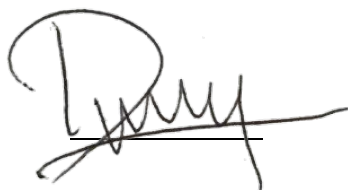
SE – Secondary Electron

HV – Hardness Vickers

Attestation of Authorship

I hereby declare that this submission is my own work and that, to the best of my knowledge and belief, it contains no material previously published or written by another person (except where explicitly defined in the acknowledgements), nor material which to a substantial extent has been submitted for the award of any other degree or diploma of a university or other institution of higher learning.

Signed

A handwritten signature in dark ink, featuring a large, stylized initial 'D' followed by several loops and a long horizontal stroke extending to the right.

Date 04/06/2019

Chapter 1: Introduction

1.1 Aluminium 6060-T5, commercially pure copper and Al-Cu bimetal

1.1.1 Aluminium background

Sir Humphry Davy, a British chemist, discovered aluminium (Al) in 1808. He named this metal after alumina whose name was derived from Latin word alum, which means bitter salt. However, he never succeeded to isolate the metal. In 1825, Danish chemist named Hans Christian Ørsted, succeeded to produce a very small amount of aluminium by reducing aluminium chloride with potassium amalgam. Two years after Ørsted, Friedrich Wöhler in Germany with the same method succeeded to obtain a very small amount of aluminium lumps and demonstrate aluminium's lightweight and malleability. In France, around 1854, Henri Sainte-Claire Deville demonstrated that relatively low-cost sodium than potassium can also be used. This led to the establishment of first commercial plant that produced small amount of aluminium in 1855. However, the process was expensive because sodium and potassium were produced with electrolytic process [1].

Table 1 - 1 Group of aluminium wrought alloy [2].

Designation	Major alloying element
1xxx	None
2xxx	Cu
3xxx	Mn
4xxx	Si
5xxx	Mg
6xxx	Mg and Si
7xxx	Zn
8xxx	Other than above (iron, lithium or tin)
9xxx	Reserved for the future

The development of large-scale electrical generating industrial instruments happened in 1886, at the same time, Paul Héroult in France and Charles hall in United States, independently developed direct electrolytic decomposition of Al_2O_3 . They discovered that when electric current is driven through molten cryolite containing dissolved Al_2O_3 at 980 °C, molten aluminium is deposited in cathode. This process together with the process to produce alumina developed by Karl Josef Bayer in 1888, lead to the modern production of aluminium that we know of today [1].

Aluminium is one of the most versatile metal with a very board application from a simple, soft and ductile wrapping foil to a complicated and demanding engineering application. Aluminium density is 2.7 g/cm^3 , which is about one-third of lesser compared to steel (7.8 g/cm^3). With light weight and the strength of some alloys [3], aluminium also have excellent corrosion resistance to environment that would cause steel to rust owing to the formation of aluminium oxide on its surface when exposed to oxygen. Furthermore, the oxide of aluminium is not in the form of flakes like in steel, and it doesn't peel off and expose fresh surface to further oxidation [3]. In addition, aluminium is second most used in structural application and rivals copper (Cu) in electrical application, although its thermal conductivity is about 50 to 60% than copper aluminium is twice on equivalent basis and is the most abundance amount of structural metal, about 8% of the earth's crust [1] [3].

Aluminium alloy is categorized into two major categories wrought and cast alloy. Wrought alloy is alloy that is produced in the form of billet or ingot which then formed into various shapes by various metal forming processes such as forging, rolling drawing, extruding etc., and cast alloy is alloy that is used in parts cast to produce semi-finished products which further made into end products. Since aluminium used in this study is not from cast alloy category, further discussion will be emphasized on wrought alloy category. Wrought alloys, depending on their major alloying element, are divided into various groups that can be seen in Table 1 below. The group designation is following the system developed by aluminium association (AA) [2], [3].

2xxx, 6xxx, 7xxx, and some of 8xxx aluminium groups are heat-treatable. The major alloying elements are forming second phase precipitates and improve the mechanical properties with precipitation hardening strengthening mechanism [2], [4].

1.1.1.1 Aluminium 6060-T5

6060-T5, aluminium used in this study, is belong to the 6xxx series. Its main alloying elements are magnesium and silicone, which combination will form into magnesium silicide (Mg_2Si) phase as the basis of its precipitation hardening. This series is the most common alloy due to its good machinability and weldability, making them highly versatile applications in various industries. In addition, because this series is easy to be extruded, it is available in wide range of shape and size from sheets and plates to complex structural shapes. 6060-possesses similar properties as one of the most common alloys used in this series that is 6063, which is commonly used in structures,

appliance parts, automotive parts, electrical and electronic parts, etc. Note that T5 is the temper condition where aluminium is cooled down from elevated working temperature condition with artificial aging performed subsequently [2], [4].

In term of electrical application performance, the electrical resistivity of 6060 is about the same with 6063, which is around 54% international annealed copper standard (IACS) in the same volume as copper and 180% IACS in the same weight as copper. Furthermore, 6060 is still comparable to 1350 from 1xxx series that is commonly used for electrical conductors which have around 61-62% IACS in the same volume as copper and 200-210% IACS in the same weight as copper [5], [6]. This shows that 6060 is a good substitute for 1350 with far better formability.

1.1.2 Copper background

Together with gold (Au) and tin (Sn), copper is one of the first metals that humankind utilized. Copper have been utilized since 10,000 years ago. Even the earliest artefact made from smelted metal was dated as early as 7000 B. C. The discovery of alloying copper with Sn led to the beginning of Bronze Age in the Middle East around 3000 B. C. It allows the manufacture of various things starting from weapons, house appliances, and decorative items, and even used in construction. The alloying with Zinc (Zn), and brass, were also widely used. The discoveries of brass artefact from Greeks and Romans era demonstrate the metal's excellent corrosion resistance.

Industrial revolution making it possible to produce copper in higher amount and higher purity, as well as various kinds of copper alloys. In this era, copper demonstrated its excellence in conducting electricity, heat and corrosion resistance that made copper widely used now in the modern era, with the majority of usage being in the electrical application. In 1997, the majority of copper consumption in US is used for electrical conductivity. Most of the applications is in the form of wires and cables. The electrical conductivity is expressed in a percentage of IACS, which is equal to 100 times the ratio of volume resistivity of the annealed copper standard ($17.2 \times 10^{-4} \mu\Omega.m$) at 20 °C to the value of the material measured. The highest purity of copper able to produced today, 99.999%, have the conductivity of 103% IACS.

Based on its alloying, copper alloys are divided into 9 categories, which can be seen in Table 1 - 2. Because copper that is used in this study is belong to these coppers' category. The unified numbering system (UNS) was used to distinguish copper and copper alloys from one and another. UNS numbering system is a five-digit number and

preceded by the letter C. Designation number from C10000 to C79999 is classified as wrought alloys and designation number from C80000 to C99999 is classified as cast alloys. Out of these two groups, the alloying composition are grouped into categories listed in Table 1-2 above.

Table 1 - 2 Copper and copper alloys

Alloy categories	Description
Coppers	Containing 99.3% of Cu
High-Copper alloys	Containing up to 5% alloying elements
Copper-Zinc alloys (brasses)	Containing up to 40% of Zn
Copper-tin alloys (phosphor (P) bronzes)	Containing up to 10% of Sn and 0.2% P
Copper-aluminium alloys (aluminium bronzes)	Containing up to 10% of Al
Copper-silicon alloys (silicon (Si) bronzes)	Containing up to 3% of Si
Copper-nickel (Ni) alloys	Containing up to 30% of Ni
Copper-zinc-nickel alloys (nickel silvers)	Containing up to 27% of Zn and 18% Ni
Special alloys	Containing elements to enhance specific characteristic

1.1.3 C11000 commercially pure copper

Commercially pure copper is a wrought copper that belongs to the first Coppers alloy group with the content of copper being at least 99.3%. This type of alloy group is known to be superior in electrical conductivity and mainly used in electrical and electronic applications [7]. To be specific, commercially pure coppers are designated by UNS number of C10100 to C13000 [8]. Comprise of oxygen-free coppers (C10xxx) that is made by induction melting, electrolytic tough pitch copper (C11xxx) that is refined electrolytically, and phosphorus-deoxidized copper (C12xxx) that is made by deoxidizing the copper until the oxygen content drop to 0.02 - 0.04%. However, the most used type of copper for electrical purposes such as busbar, cable, windings etc., is the C11000 grade, that is the most commonly utilized grade [9]. In addition to their excellent conductivity of 100 - 101.5% IACS, C11000 is also very ductile, making it easy for them to be fabricated into various forms [7], [8].

1.1.4 Al - Cu Bimetal

Al - Cu bimetal is commonly used in various electrical applications. To be specific, Al - Cu bimetal parts are used as a bridge to pass electricity current from a specific part of an electrical device or cathode and anode to an aluminium or copper busbar in a direct-current bus system. Al - Cu bolted joint resistance can increase more than 30 times after 5 years. As an attempt to extend the life service of the joint, the Al - Cu interface that was previously bolted was then welded to seal the joint from contaminant so that the resistance would not drop after some times of usage. However, due to the formation of thick and brittle intermetallic, the parts went through mechanical failure [10]–[12]. The introduction of solid state joining technique such as roll and explosive bonding was proven to be successful to expand the life service of the Al - Cu bimetal to more than 10 years [11].

1.2 Fusion welding

Welding, according to Messler, in general “is a process in which materials of the same type or class are joined together through the formation of primary (and, occasionally, secondary) bonds under combined action of heat and pressure” [13]. Similarly welding according to ISO standard R 857 (1958) is “an operation in which continuity is obtained between parts for assembly, by various means”. Continuity can be interpreted as the absence of physical discontinuities or gaps in atomic level. Different with mechanical fastening, no matter how tight the joint is, physical gaps will always present. Continuity also does not always mean homogeneous in chemical composition across the welding interface. For example, stainless steel can be joined with the same alloy (homogeneous) or different alloy (heterogeneous), as well as cast iron can be welded with bronze filler [13].

1.2.1 Fusion welding of similar metal

In fusion welding, the joint is established by heating the abutting interfaces above the melting or liquidus point of pure and alloys, respectively, and then the interface is put together in their liquid state, either with or without filler, so that atomic continuity will be formed after the interface solidified. Typical fusion welding of similar metal interface with distinct zones such as Fusion zone (FZ), heat-affected zone (HAZ), and base metal can be seen in right hand side of Figure 1 - 1. In addition, in some alloy such as Al 2024, Al 6061, etc., partially melted zone (PMZ) could be formed in between base metal and FZ, as shown in the left hand side of Fig. 1 - 1 [14].

The fundamental process of fusion welding, depending on the heat generation source can be divided into four: (1) Chemical energy from combustible fuel or exothermic reaction (oxyfuel gas welding & aluminothermic welding); (2) Electric arc either from a non-consumable or consumable electrode, whereas the latter acts as filling material as well (gas-tungsten arc welding, plasma arc welding, gas-metal arc welding, shielded-metal arc welding, submerged arc welding, etc.); (3) Joule heating that is produced by direct current flow through the plates which are positioned in a circuit (spot welding); (4) High intensity flux of beam that is fast-moving particles (laser welding, electron beam welding, microwave welding, etc.) [14].

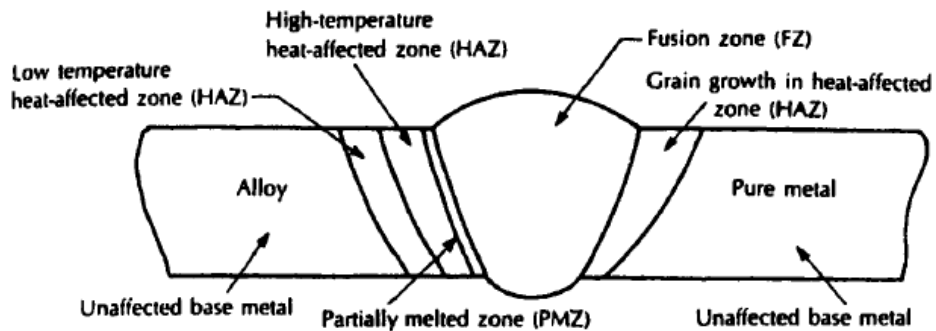


Figure 1 - 1 Microstructural zones of fusion welding [14].

1.2.2 Fusion welding of dissimilar metal

Dissimilar metal welding is proven hard to achieve due to difference in material properties such as thermal expansion, melting point etc. However, it is still doable except if thick intermetallic compound after the weld solidified formed. Two of which are fusion welding of Cu - Fe [15]–[17] and Fe - Ni based alloys [18], [19]. As for Al - Mg [20]–[23][23], Al - Ti [23]–[25], Mg - Ti [23] and Al - Cu [24], [26], [27] metal couples, except for Mg - Ti for being immiscible [20]–[23], there is a common agreement that the intermetallic that formed is brittle and have adverse effect on the joint's mechanical properties.

For Al - Cu fusion welding, Al - Cu intermetallic is readily formed in temperature greater than 120 °C, owing to its high affinity in said temperature [10], [28]–[31]. This intermetallic tends to form and grow excessively. Example can be taken from laser welded Al - Cu in lapping configuration in Fig. 1 - 2a. Higher magnification of the weld root shows that cracks are formed extensively (Fig. 1 - 2b). The cracks stopped at the border of the weld root/copper vase metal are indicating that there is a significant

difference in toughness. Moreover, no cracks can be seen in upper region of the weld where copper dilution in aluminium matrix was low to none [24].

Studies have shown that the thicker the intermetallic [11], [28], [32], [33], the lower its mechanical properties. The critical thickness for the interfacial Al - Cu intermetallic in order for the joint to retain its integrity, meaning that it would break in the HAZ, is not more than 2.5 μm [28], [33]. The crack mode changes from ductile, in the HAZ, to intergranular fracture in $\text{Al}_2\text{Cu}/\text{AlCu}$ border when the intermetallic exceeds the critical thickness and further growth changes the mode to transgranular fracture in all intermetallic [28], [33], as shown in Fig 1- 2b. In addition, the increase in intermetallic thickness in Al - Cu system is also directly proportional to the increase in electrical resistivity [28], [31], [34] because these Al - Cu intermetallic compounds have covalent bond, making them non-conductive in nature [28], [31].

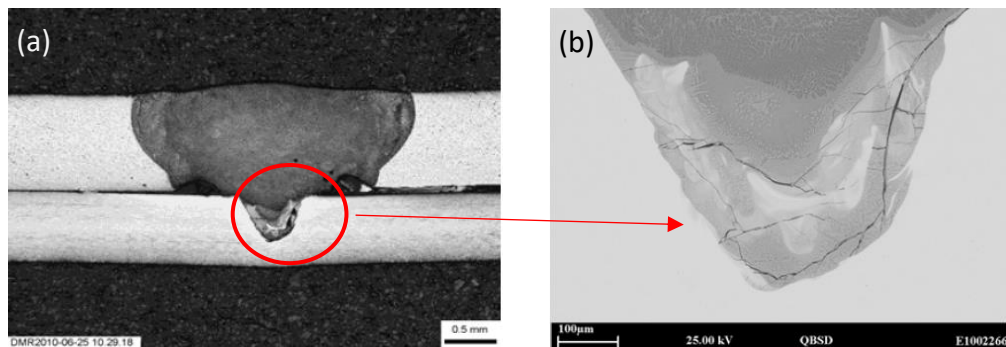


Figure 1 - 2 (a) Al - Cu laser welding in lapping configuration (b) higher magnification of the weld root showing extensive cracks in intermetallic that formed in the weld root [24].

Although attempts have been made to reduce the interfacial intermetallic in dissimilar metal fusion welding in general [23], [27], the presence of molten state during welding makes it difficult to avoid the formation of intermetallic. Furthermore, fusion welding in lap configuration, where the melting starts from the top plate all the way to the bottom plate, ensures material mixing in molten state that lead to the formation of intermetallic as shown in Fig 1 - 2 a and b [24].

Because of these reasons, solid state welding, where no melting involved in the process, is the best method to join dissimilar metals especially in lapping configuration. Friction stir welding (FSW), one of solid state welding technique, is proven to be able to produce a relatively good joints with an interfacial layer of intermetallic, such as the metallurgical joint in Al-to-Fe [35], [36] and Al-to-Ti [37] that are produced under one process, without the need of additional heat treatment to establish metallurgical joint.

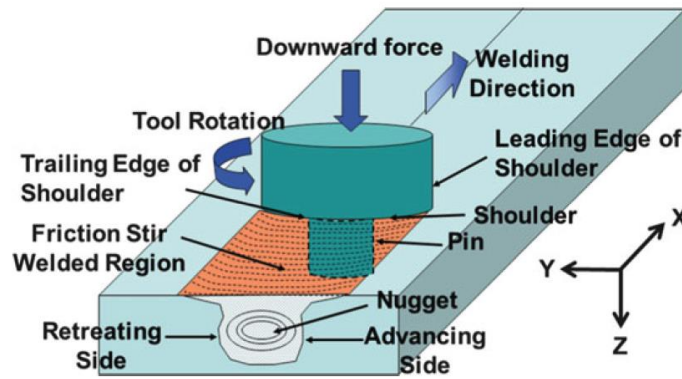


Figure 1 - 3 Schematic drawing of FSW [38], [39].

1.3 Friction stir welding

FSW is a solid state joining technique invented by Wayne Thomas and colleagues at TWI in the United Kingdom in 1999, which was initially utilized to weld aluminium alloys that could not be welded with conventional fusion welding methods [39]–[43]. The process itself is exceptionally simple; weld is established by using a non-consumable rotating tool with specially designed shoulder and pin that is inserted into abutting edges of plates, or in this study lapping plates, to be joined and subsequently traversed along the joint line [38], [39], [44]. Fig. 1 - 3 clearly explains how the FSW process in general, however additional elaboration is needed to further understand about retreating side (RS) and advancing side (AS). It can be seen in Fig. 1 - 3 that the tool rotates counter clockwise and traverses into the paper. Based on the tool position and rotation direction, the RS is in the left side where the tool rotates in an opposite direction with the tool's travel direction. Whereas, the AS is in the right side of the pin that rotates in the same direction with tool's travel direction.

Table 1 - 3 Advantages of FSW [38], [44].

Metallurgical benefits	Environmental benefits	Energy benefits
<ul style="list-style-type: none"> • Solid-phase process • Low distortion • Good dimensional stability and repeatability • No loss of alloying elements • Excellent mechanical properties in the joint area • Fine recrystallized microstructure • Absence of solidification cracking • Replace multiple parts joined by fasteners • Weld all aluminum alloys • Post-FSW formability 	<ul style="list-style-type: none"> • No shielding gas required • Minimal surface cleaning required • Eliminate grinding wastes • Eliminate solvents required for degreasing • Consumable materials saving, such as rags, wire, or any other gases • No harmful emissions 	<ul style="list-style-type: none"> • Improved materials use (e.g., joining different thickness) allows reduction in weight • Only 2.5% of the energy needed for a laser weld • Decreased fuel consumption in lightweight aircraft, automotive, and ship applications

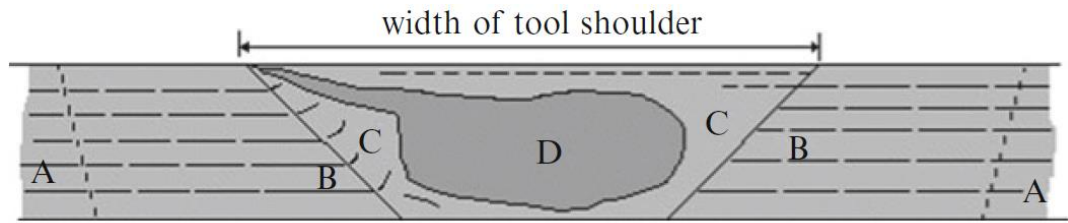


Figure 1 - 4 Typical FSW [38], [39]

The main advantage of FSW in dissimilar metal welding is its solid-state nature, because the process normally occurs below the melting point or solidus line of an alloy [39], [44]–[46]. This means that the welded material will not transform into molten state during the process, thus avoiding the formation of thick intermetallic, which is brittle in nature, effectively reducing the joint's mechanical properties and if cracked, when used in electrical applications, reducing the electron path, reducing the joints conductivity. Beside this important advantage for dissimilar metal welding, advantages of FSW over fusion welding in general are summarized in Table 1 - 3 [38], [44].

Table 1 - 4 Tool material and attributes [39], [47].

Material attributes	Tool material class				
	Tool steels	Superalloys	Refractory metals	Carbides, cermets, and ceramics	Superabrasives
Strength (room temperature)	Good	Excellent	Excellent	Excellent	Excellent
Strength (at processing temperature)	Good	Very good	Excellent	Good	Excellent
Fatigue strength	Very good	Excellent	Very good	Excellent	Very good
Fracture toughness	Very good	Very good	Very good	Good	Poor to good
Wear resistance	Good	Good	Very good	Good	Excellent
Chemical inertness	Good	Very good	Good	Good	Excellent
Availability	Excellent	Very good	Very good	Very good	Very good
Cost	Excellent	Very good	Poor to acceptable	Good	Poor to acceptable

Pioneered by Threadgill, there are extensive studies on FSW microstructures to date [38], [39], [48]. Despite of this, many of them still use the early definitions of the zones. Different microstructural zones in FSW weld nugget can be seen in Fig. 1 - 4. Explanation of the zones as follows [38], [39]:

- A. Unaffected base material: this zone was secluded from the weld and deformed, moreover it was not experienced microstructure and mechanical properties changes, despite the probability that it may undergo a thermal cycle from the weld.

- B. Heat affected zone (HAZ): this zone has undergone a thermal cycle from the weld and has been experiencing microstructural and mechanical properties changes. However, plastic deformation does not take place in this region.
- C. Thermomechanically affected zone (TMAZ): this region experiences deformation, which is caused by the influence exerted by the tool rotation and plastic deformation of the material as well as the friction heat of the process. Moreover, this zone does not undergo recrystallization, making it distinguishable from recrystallization zone or weld nugget.
- D. Weld nugget: Where significant amount of material was processed, and fully recrystallized, and commonly known as stir zone. This was previously occupied by the rotating pin during process.

1.3.1 Tools and Pins material selection and design

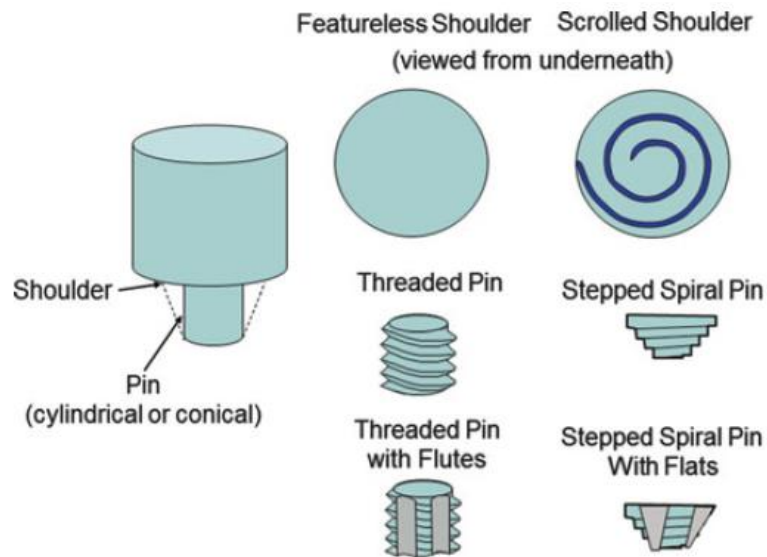


Figure 1 - 5 Common tool shoulder and pin features [39], [47].

In FSW, the tool has three main functions, which are, heating up the material, moving the material to establish joint, and containing the heated material beneath the tool shoulder. Heating is established by friction between the rotating tool, shoulder and pin, with the severely deformed material of the plates. The localized heating softens the material around the pin, and as the rotating tool traverse, the material in front of the pin moves to the back of the pin, filling the space behind the pin. In addition, the shoulder keeps the majority of the material beneath it to flow strictly under it without flowing out excessively [38]. Due to these functions, the tool material needs to have certain attributes to be able to perform these tasks without experiencing deformation. Table 1 - 4 is the summary of various tool materials that are usually used in FSW [38], [39].

Table 1 - 5 Tool features design variations and advantages [39], [47].

Tool feature	Design variation		Advantage
Shoulder	Convex with scroll	Curved geometry	Allows joining of different thickness work-pieces. Scroll contains material within shoulder
		Tapered geometry	-do-
	Concave (standard design)	Smooth surface	Concavity preserves material within shoulder region. Requires tool tilt.
		Scrolled surface	Allows welding without tool tilt. Minimizes normal tool force and thickness reduction in weld zone.
Pin	Cylindrical	Flat bottom	Easier too machine. Commonly used design
		Round bottom	Reduces tool wear during plunge and improves joining at weld root.
		With flats	Increased plastic strain and temperature in nugget region
	Conical	Threaded cone	Low transverse force compared to cylindrical pins.
		Stepped spiral	Robust design and used for high temperature materials welding
		With flats	Increased plastic strain and temperature in nugget region
	Whorl MX Triflute Threadless Retractable		Reduces transverse force on tool
			Refined version of whorl pin
			Useful in aggressive tool wear situation
			Allows closure of exit hole

It is important for shoulder and pin to have certain features to control the material flow. Originally, the diameter ratio of shoulder and pin was 4:1. However, it was revealed that shoulder has the highest contribution towards heat generation [49]. To control the heat input, lower ratio of 3:1 to 2:1 can be used [39]. Generally, the shoulder can be made flat, concave (most common shoulder shape), or convex, additional scroll is needed for this. Flat, featureless and concave shoulder has to be run with a tilt angle, making the trailing part of the shoulder forged the material behind the pin. Scroll shoulder feature is usually machined in a flat shoulder, protruding out or sinking in of the shoulder surface. Then main function of this feature is driving the material inward to the base of the pin. This type of shoulder can be run with no tilt angle, meaning that the weld can run in any direction and can run in curved surfaces, while the convex shoulder can be used to weld plates with uneven thickness.

The shape and features of the pin have a big influence in material flow. The most common shape is cylindrical and truncated conical. The addition of features mainly functioned to induce vertical flow from shoulder area to bottom of the pin. Changing the pin from cylindrical to truncated-conical promotes more down force and better downward flow as the consequence. For the pin features, both threaded and stepped

spiral promote vertical flow with stepped spiral pin having twice as much displaced down material volume than threaded pin, in the contrary to featureless pin, where the material flows only from the front to the back of the pin. Moreover, the addition of flats and flutes on the pin promotes changes in material flow by acting as paddles and promotes local turbulent resulting in wider weld nugget and reduction in traversing force. That means it is easier for the tool to travel forward than pin without flats or flutes, in other words, faster travel speed can be carried out [38], [39], [47]. The summary of advantages of various shoulder and pin can be seen in Table 1 - 5.

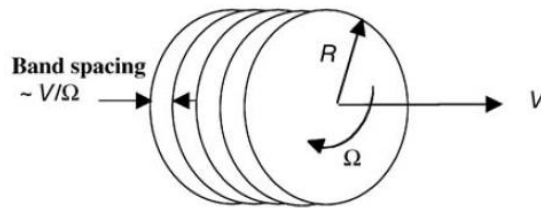


Figure 1 - 6 Bands of periodically deposited material behind the pin [50].

1.3.2 Material flow and flow related defects

Large temperature difference on the interface of the tool and workpiece confine the thermally soften plasticized region within a region restricted by thermally and mechanically unaffected base material, tool shoulder and backing plate. The volume of this thermally soften material depends on FSW parameter such as rotation speed, travel speed, as well as pin tool design and the properties of the material itself. The soften region is displaced around the tool and deposited behind the pin in the shape of bands. The length of these bands of deposited material is equal to the distance of the tool travel to complete one tool rotation (Fig. 1 - 6) [50], [51].

Over the years, attempts on studying the material flow have been conducted extensively. Various methods such as marker [52]–[54], tracer [55]–[57], stop action [53], [55], [57], [58] and pin breaking technique [59] have been implemented. However, flow models from Nunes et al. [51], [56] study can represent FSW flow in general.

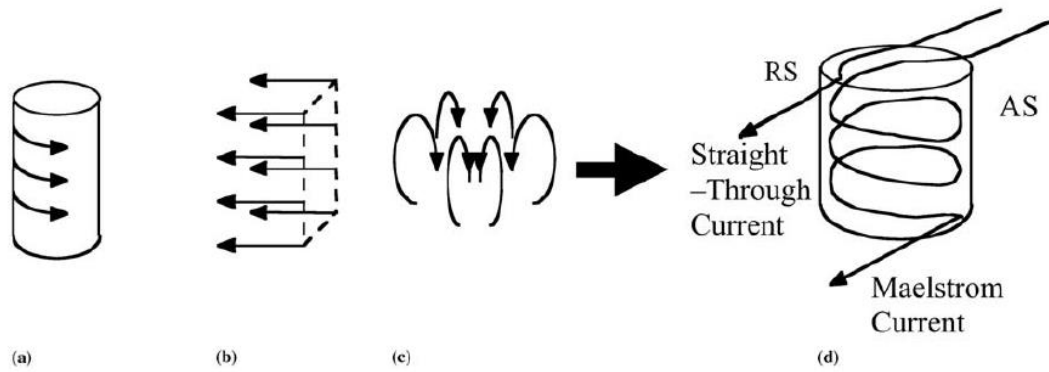


Figure 1 - 7 Nunes kinematic model for FSW material (a) rigid-body rotation (b) uniform flow, (c) maelstrom or vortex flow, (d) combined flow model resulting in two material currents, straight through and maelstrom current. [51], [56]

In Nunes et al. [51], [56] model or the Nunes kinematic model, flow around the pin is formed from three different incompressible flows. First flow is the rigid-body rotation, where the material attached to the pin body and rotated with the same rotation speed with it. The pin wall acts as the boundaries, from top, the shoulder, to the bottom of the pin and expands to the edge of the shoulder or to where the plastic flow change is slipping (rotates slower than the tool's rotation speed) to the outer side of the shoulder, with slight increase of thickness in the RS to allow material displacement to the back of the pin as the pin moves forward (Fig. 1 - 7a). The second flow is uniform flow, where the flow speed is equal but in the opposite direction to the travel direction of the tool (Fig. 1 - 7b). In a flow field combination of first and second flow, tool approaches the metal with a certain travel speed, joins the rotating pin at the first flow surface, and rapidly carries around the pin at the same speed as the tool's rotation speed in an arching trajectory and deposits behind the tool as the tool move further away forward [51], [56].

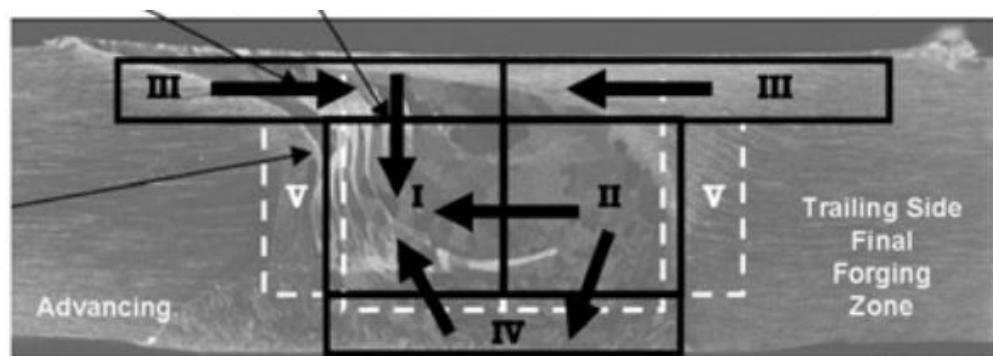


Figure 1 - 8 Material flow behind the pin [60], [61]

The third flow is the maelstrom or vortex flow where the material flow is encircling the pin and bringing material up towards the shoulder and in to the centre of the shoulder or base of the pin, then displaced down. After reaching the bottom, material goes out of the maelstrom flow (Fig. 1 - 7c). This flow is caused by the threads feature on the pin [51], [56].

The three flows combined are producing two material flow currents, which are straight through and maelstrom currents. The straight through current happened in the RS with mechanism explained in the first flow. While, maelstrom current comes from the AS in the front of the pin with mechanism explained in second flow. As the material radially displaced inward at the shoulder, the shoulder is keeping the material from exiting the material around the pin and under the shoulder. This trapped material then flows around the pin and as the pin rotates, the straight through current fills the RS side in front of the pin. Because of this, the remaining maelstrom current is only able to get out in the AS of the weld behind the pin after the material that was picked up from the RS on the front of the pin displaced to the RS behind the pin (Fig. 1 - 7d) [51], [56].

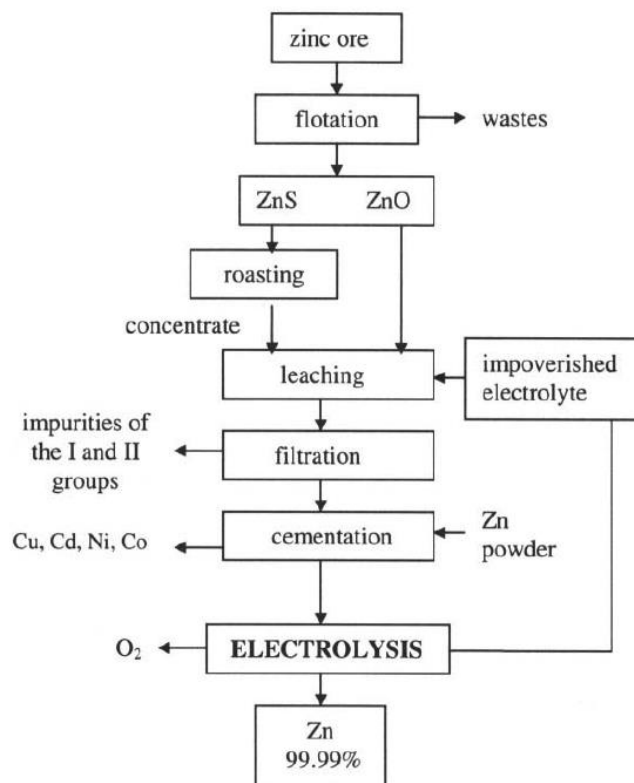


Figure 1 - 9 Process schematic of zinc refinery [62], [63].

Flow behind the pin can be best represented by Arbegast's model [60], [61]. In this model, there are five zones as can be seen in Figure 1 - 8. Material flow from the front

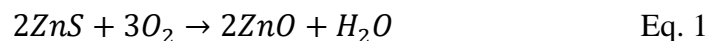
side of the pin passes through to zone II, some material around the pin displaced into zone I and some displaced downward, some can travel further into zone IV under the pin and move upward again to combine with the material in zone I. Material in zone III is material that is dragged across from RS to AS. The material from RS in zone III is then forced to move to zone I due to new material stream entering zone III in AS. Zone IV usually appears under very hot condition, high tool rotation speed and/or low travel speed, where the downward flow is turned upwards into recirculating pattern. In lap joints, this will result in hooking formation or sheet thinning.

Several defects that commonly occur in FSW can be explain with this model. Excessive material flows from zone III to zone I result in nugget collapse. Insufficient material from zone II, III, or IV due to flash, raised crown, sheet lifting or sheet separation can lead to insufficient material entering zone II, III or IV and will cause less material to enter zone I, that manifested as volumetric defects such as lack of filling at surface, wormhole or lack of consolidation, microvoids or scalloping. Insufficient material flowing into zone IV will lead to lack of penetration defect, while on the contrary, excessive material flow into zone IV can cause root flow defect [60], [61].

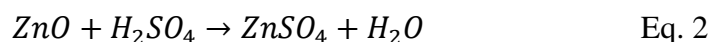
1.4 Zinc Electrowinning and Al-Cu bimetal application

Electrowinning is a method of metal refining by electrolysis of aqueous solutions or melts that contain the metal's salts by utilizing insoluble anode [63]. Electrowinning is the last step of metal refinement. Since metals found in nature in the form of sulphides and oxides ores, the refinement steps usually consist of (Figure 1 - 9) [62], [63]:

1. Ore enrichment, removing the wastes usually by floatation, which produces a concentrate of metal sulphides and/or oxides.
2. Roasting, transforming the metal sulphide into oxide (equation 1) so that it becomes metal oxide that is soluble in sulphuric acid (equation 2).



3. Leaching, separation of some unwanted impurities by dissolving the metal oxide into dilute sulphuric acid creating a solution of metal sulphate (equation 2).



Two main groups of impurities that are separated in this stage are as follows:

1. Fe, Si, Al, Sb, Bi, Ge, Sn
2. Pb, Ag, SiO₂

4. Refining of leach, further leaching process to eliminate most of remaining impurities. This can be conducted by increasing the pH of the solution by precipitation by adding Zn powder for cementation or hydrogen sulphide to remove impurities such as Cu, Cd, Ni, Co.
5. Electrolysis (in this case Electrowinning), extraction of metal from the previous solution by cathodic deposition in an electrochemical plant.

The reactions on the process' respective electrode are as follows:

In the cathode, cathodic deposition of zinc occurred:



In the insoluble anode, oxygen evolution occurred:

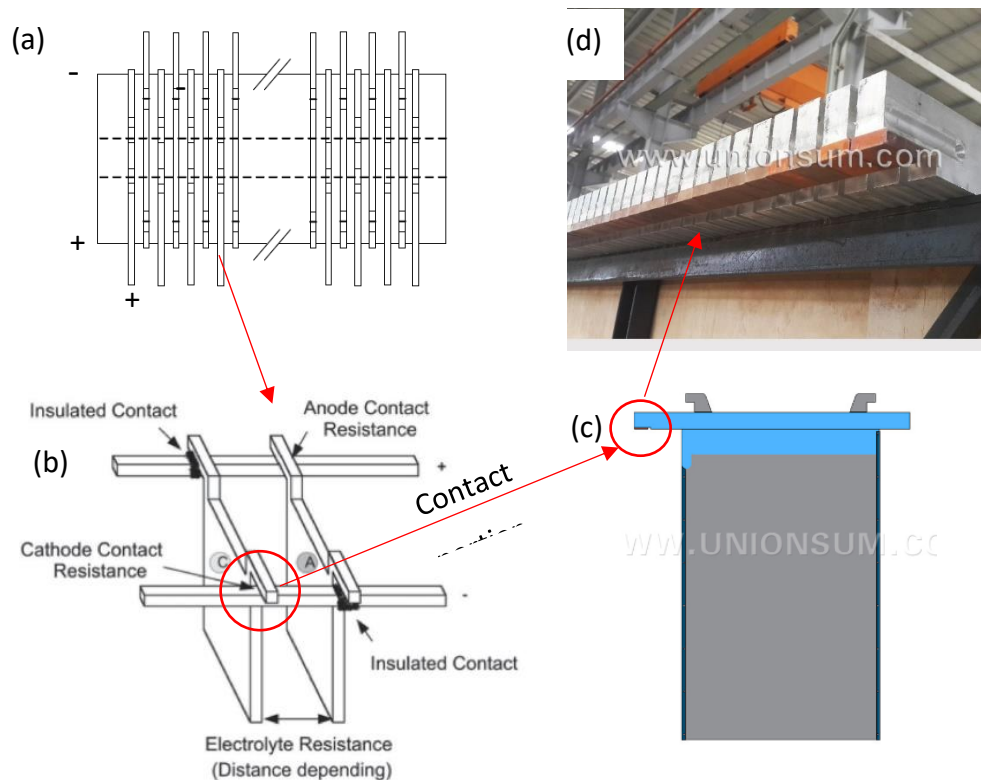


Figure 1 - 10 (a) Plan view schematics of electrodes arrangement [64] (b) anode/cathode arrangement [65] (c) one of cathode configuration (d) Bimetal part as a connection from copper busbar to aluminium cathode [66].

In electrowinning plants, the electrodes are arranged in a chemical tank in such way, so that the anodes placed intermittently with cathodes with distance of 4.5 cm, which is the usual distance between the electrodes. Schematic of the arrangement can be seen in Fig. 1 - 10a. The cathode head bar is seated in the negatively charged pole busbar, with the other end of the head bar seated in an insulated contact of positively charged busbar and

the active part of the electrode suspended in the electrolyte. Meanwhile, the anode head bar is seated in positively charged busbar and the other end is seated in an insulated contact of negatively charged busbar. The electrodes contact arrangement can be seen in Fig. 1 - 10b. [64], [67].

In order to connect aluminium cathode to copper busbar without having any concern of oxide formation between cathode and busbar that could increase the resistance and reduce the process efficiency, an Al - Cu bimetal part can be fixed on the part that is in contact with the busbar to establish copper-to-copper contact. One example of cathode configuration can be seen in Fig. 1 - 10c. In addition, one example of configuration of bimetal placement in cathode can be seen in Fig 1 - 10d.

Chapter 2: Literature review

In this chapter, the interface quality in Al - to - Cu FSLW is reviewed based on a few factors such as the effect of rotation speed (ω), travel speed (v), and depth of penetration (d_p) as well as interfacial intermetallic growth behaviour and the application of scribe pin on dissimilar metal FSLW. From review of the appropriate literature the knowledge gap can be established forming the basis of the research.

2.1 Effect of ω and v on Al - to - Cu FSLW interface quality

In FSW, material fluidity is important in order to continuously flow and fill the space in left by the advancing tool. Welding parameters effect on material flow can be understood in Equation's 5 and 6 taken from the work by Cui et al. [68]. The relation of ω with the welding temperature (T) is represented in Equation 5, and shows that an increase in ω proportionately influences the welding temperature.

$$T = T_0 + T_f(1 - e^{-q\omega}) \quad \text{Eq. 5}$$

This increase further impacts the material flow as visualised in Equation 6 whereby, the flow stress of the material (σ) drops as T increases.

$$\sigma = \alpha^{-1} \sinh^{-1} \left\{ (A^{-1} \dot{\epsilon} \exp(Q/RT))^{1/n} \right\} \quad \text{Eq. 6}$$

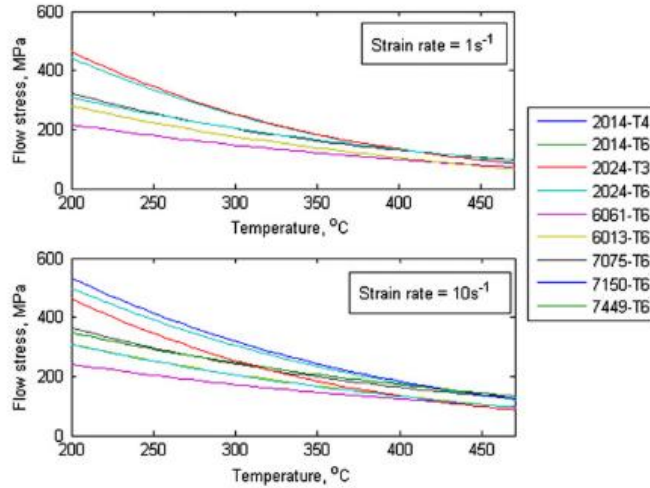


Figure 2 - 1 σ vs T model of aluminium alloys with two strain rates of 1 and 10 s^{-1} [68].

Based on results of Equation 6, σ from a wide range of aluminium alloys have been plotted with respect to temperature as presented in Fig. 2 - 1, for two strain rates ($\dot{\epsilon}$) of 1 and 10 s^{-1} . It can be observed that increases in the welding temperature lead to a decrease in σ of the material, improving material flow during the welding process.

However, as temperature rises σ values converge, suggesting a theoretical minima in σ with further increases in temperatures. While, Abdollah - Zadeh et al. [69] concluded that an increase in v for a constant ω results in a similar influence on weld temperature as a reduction in ω at a constant v .

Welding temperature related defects in FSW are presented in Fig. 2 - 2 below. The occurrence of flow related defects proved the hypothesis of a parameter window of optimum FSW conditions, forming a close to defect free weld. Parameters outside this window are considered either too hot or too cold, with high and low respective welding temperatures. Cold conditions commonly lead to a lack of fill in the surface, wormhole, or defects along the advancing side (AS), and excessive surface flash, galling on the surface and nugget collapse defects in hot conditions [60], [61].

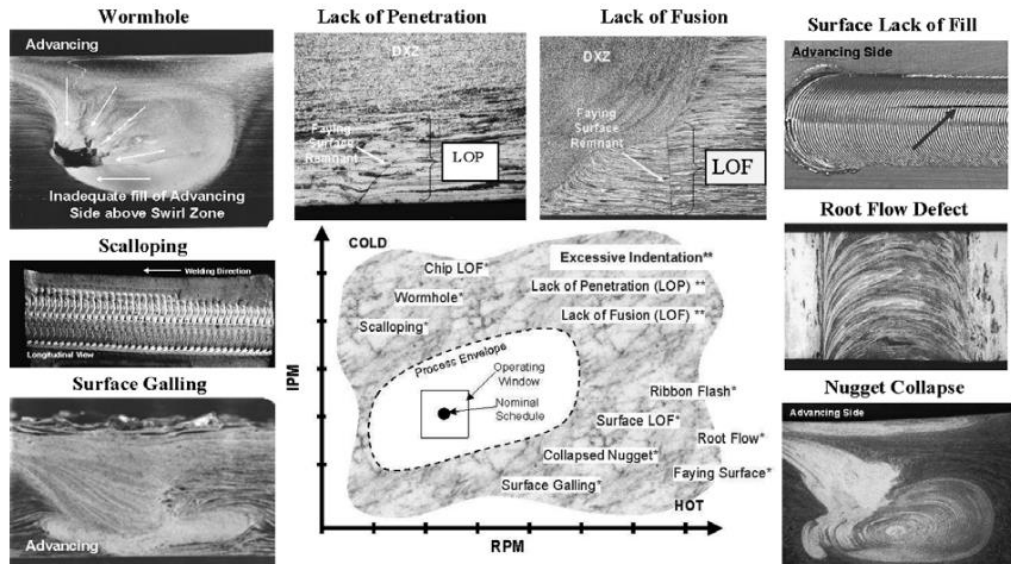


Figure 2 - 2 Type of defects in FSW [60], [61].

As in Al - to - Cu FSLW, studies on the effect of ω and v were conducted by Elrefaey et al. [70], Abdollah-Zadeh et al.[70], [71], Saeid et al. [72] and Bisadi et al. [73]. The earliest work on Al - to - Cu FSLW was conducted by Elrefaey et al. [70], [71], with welds produced over a range of rotation speeds ($\omega = 1000, 1500$ and 2000), each coupled with v from $200 - 300$ mm/min and a d_p of 0.1 mm into copper. A black structure formed in aluminium side of stir zone in the welds with ω 's larger than 1000 rpm, extending further to the AS with increases in v . On the copper side, mixed stir zone (MSZ) formed in close to the Al - Cu interface, with similar observations made in low ω welds, similar structure in aluminium side was similar to weld with high ω . However, no black and grey structures can be seen in this weld. Weld quality was

determined by application of the peel test, highlighting the slight decrease in failure load when v increased from 200 to 300 mm/min and improvement when ω increased from 1000 to 2500 rpm. Welds produced at ω 's of 1500 and 2500 rpm led to high breaking loads with, fracture occurring in the layer structures or mixture zone, identified by XRD to contain hard and brittle AlCu and Al₄Cu₉ intermetallics.

In Abdollah - Zadeh et al.'s work [69], a series of welds using ω 's ranging from 750 to 1500 rpm were conducted, each coupled with v 's ranging from 30 to 375 mm/min. No microstructural comparison on weld interfaces was conducted however, a black area consisting of mechanically mixed copper and aluminium layer composed of Al - Cu intermetallics; AlCu, Al₂Cu and Al₄Cu₉ was found, similar to that observed by Elrefaey et al. [70], [71]. A shear tensile test was used to determine weld quality, with the finding of an increasing trend in failure load to a maxima, declining afterward with increasing ω for a constant v . The same trend was observed when decreasing v with ω set as a constant. Although no microstructural evidence on the Al - Cu interface was reported, it was stated that low failure load was caused by cold weld condition resulting in the imperfect joint and brittle intermetallic compound existing in the interface. With the compound forming at higher temperatures as a result of the increase in ω or decrease in v .

Similar findings were reported in Saeid et al.'s work [72], where a series of experiments on FSW AA1060-pure copper were conducted with a constant ω of 1180 rpm and range of v from 30 to 190 mm/min. The weld interface was analysed, although lacking detailed insight. The black area in the stir zone near the interface was reduced with the increase in v , which was interpreted as a reduction in copper particles into the aluminium due to reduced degree of mixing. The copper fragments triggered micro cracks, that were believed to be the reason for the lower failure load prior to reaching a maximum at a v of 95 mm/min. With, the lower failure load at v 's more than 95 mm/min was caused by the formation of cavities. The authors further observed the high failure load to result from the balance between formation of cavities and micro cracks however, a detailed microstructural analysis on the interface was not conducted.

Bisadi et al. conducted another similar study in which welds were produced in a range of ω from 600 to 1550 rpm, each coupled with a v of 15 and 32 mm/min [73]. Weld analysis was conducted using the ω^2/v ratio relating to the T of the process, as taken from Equation 7 by Arbogast [60].

$$\frac{T}{T_m} = K \left(\frac{\omega^2}{v \times 10^4} \right)^\alpha \quad \text{Eq. 7}$$

Also observed was the low T process yielding interfaces with cavities. In addition, as the T of the weld increases, intermetallic formation and microcracks in the interface region increase as well, in turn leading to the decrease in the maximum failure load. Moreover, contrary to Bisadi et al. and Arbegast, high temperature (T) welds also led to cavity formation, especially in the hottest weld occurring at a ω of 1550 and v of 15 mm/min. The author cited this to be caused by the diffusion of aluminium into the copper. However, experiment by Xue et al. [33] and Peng et al. [74] suggest otherwise. Both found Kirkendall tunnels evident in the region between copper base metal and the Al - Cu intermetallics zone, forming between the Al_4Cu_9 intermetallic and adjacent copper base metal. Thus implying copper in aluminium diffusion is faster than aluminium in copper. In addition, a lamellar structure is common in Al - to - Cu FSW [71], [75], [84]–[92], [76]–[83], consisting of a aluminium intercalation with copper or vice versa, instead of copper full of voids.

Evident from literature is a process parameter window suited in producing an optimum weld, with weld quality assessed by peel and tensile shear test. However, there is no consensus on the ideal combination of ω and v to obtain a discontinuity free interface. Additionally, a thorough investigation on the microstructural evolution in stir zone still required, in order to avoid micro cracking initiation along the interface between aluminium and copper particles in dark area in aluminium stir zone.

2.2 Effect of d_p on Al - to - Cu FSLW interface quality and material flow in the pin bottom region

A limited number of studies on Al - to - Cu FSLW have been conducted over the years, thus the effect of d_p on weld interface quality is poorly known. Elrefaey et al. vaguely revealed its influence on the interface quality, with a weak weld interface leading to sample breakage during preparation when the pin was positioned at $d_p = 0$ [70], [71]. Despite these findings, a microstructural study on the failed interface was not conducted and the cause of the breakage be it; no bonding or brittle intermetallic formation was not established. Contrastingly, in FSLW of Al - steel [35] and Al - Ti [37] metal couples the highest strength was achieved by using a d_p of 0 with a thin continuous interfacial intermetallic layer formed in the metal interface. Optimum ω and v to obtain of close to discontinuity free interface. In A1100H24 to tough pitch copper welds with a d_p of 0.1

mm the formation of MSZ in the copper side close to the interface and no extensive copper flash hooks formed in RS and/or AS is apparent. This MSZ of mechanically mixed aluminium and copper, further develops into Al_4Cu_9 and AlCu intermetallics. However, no interfacial comparison between welds with same ω and v with different d_p were conducted. Moreover, no information regarding interfacial continuity was ever established.

Table 2 - 1 Past studies on interfacial features in conjunction with d_p in Al - to - Cu FSLW.

	d_p	Al/Cu Thickness	Remarks on Interfacial features and continuity
Elrefaey et al. [70], [71]	0 mm	2/1 mm	Low strength, broke in sample preparation, no interfacial examination.
	0.1 mm		MSZ intermetallic that consist of Al_4Cu_9 and AlCu that in Cu, no remarks on interfacial continuity.
Abdollah-Zadeh et al. [69]	0.2 mm	4/3 mm	Mechanically mixed Cu - Al rich layer with Al_2Cu , Al_4Cu_9 and AlCu formation near the interface, no remarks on interfacial continuity
Saeid et al. [72]	0.2 mm	4/3 mm	Interface move further into bottom plate, lost symmetry in higher v .
Firouzdor et al. [93]	0.2 mm	1.6/1.6 mm	Extended Cu flash hook in retreating side (RS), bent into stir zone. Voids in the interface.
Bisadi et al. [73]	1.2 mm	2.5/3 mm	RS hook might form and fold, forming voids.
Beygi et al. [94]	Excessive into Cu	1.5/3 mm (roll bonded to 3 mm)	RS hook may from and fold into stir zone creating void.
Andrade et al. [81]	0.2 mm	1/3 mm	MSZ was formed in the interface, no remarks on interfacial continuity.

Interfacial features of d_p of different depths from literature are listed in Table 2 - 1 with their respective parameters differing for each study. Interfacial features of welds using a d_p of 0.2 mm can be seen in works by Abdollah - Zadeh et al [69], Saeid et al. [72], Firouzdor and Kou [93] and Andrade et al. [81]. The first two works show that the interface moved further into the bottom copper, with the formation of MSZ in the copper side near the interface. This MSZ consists of intermetallics similar to the work mentioned above by Elrefaey et al [70], [71]. However, with the addition of Al_2Cu . In the work by Saeid et al. [72], the interface was seen to lose its symmetry at higher v (Fig. 2 - 3). In their analysis they cited Cederqvist and Reynolds [95], who noted loss in

symmetry to be caused by the lack of vertical transport, itself initiated by the pin threads. Suggesting that the mechanism pushing the Al - Cu interface down into the copper is the aluminium vertical transport. However, it is important to notice that during the FSW process, the pin penetrated 0.2 mm deep into the copper. In addition, based on the material flow study using shot tracer by Colligan [55] , tracers beneath the pin only slightly move upward highlighting the lack of vertical transport. Contrary to Colligan's finding, Saeid et al. observed the weld interface on the RS at v 's of 118 and 190 mm/min (Fig. 2 - 3d and c) to rise more than the interface on the AS, rising close to original Al - Cu interface.

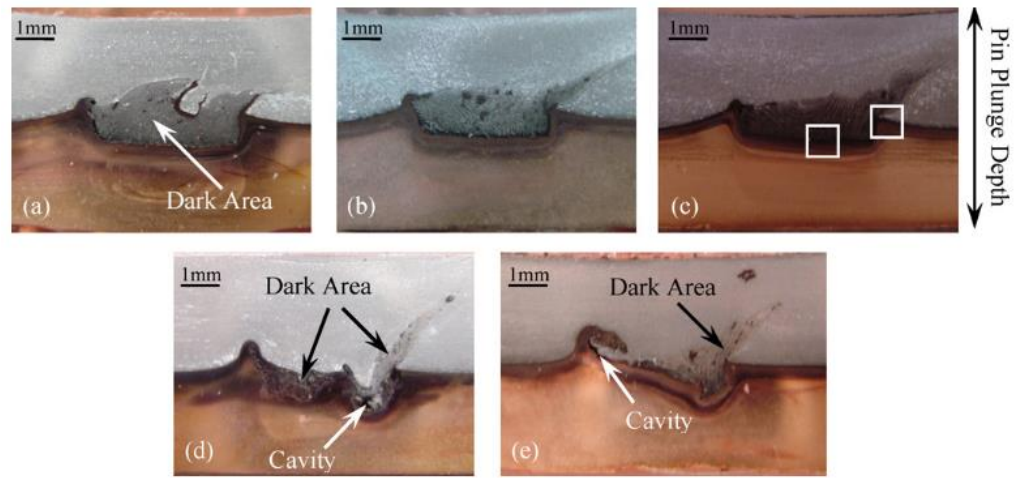


Figure 2 - 3 FSW interface in Saeid et al. work with a constant ω of 1180 rpm and v of (a) 30, (b) 60, (c) 95, (d) 118 and (e) 190 mm/min [72].

Interfacial features in the work by Firouzdor and Kou were seen to differ to that observed by Abdollah - Zadeh et al. and Saeid et al. [93]. An extended Cu flash hook that bent towards the stir zone (Fig. 2 - 4a) was evident in welds made at an ω of 1400 rpm, v of 38 mm/min and d_p of 0.2 mm. However, contrary to Saeid et al.'s result [72], another weld using an elevated v of 203 mm/min produced similar hooking features with similar d_p and a lower v (Fig. 2 - 4d). Voids were present in both, primarily in the RS area, with similar observations made by Shen et al. [96] in Al - to - steel FSLW. A denser MSZ formed in the Cu In the weld interface produced at a v of 38 mm/min. While in Andrade et al's work [81], no extensive RS hook formed in their weld.

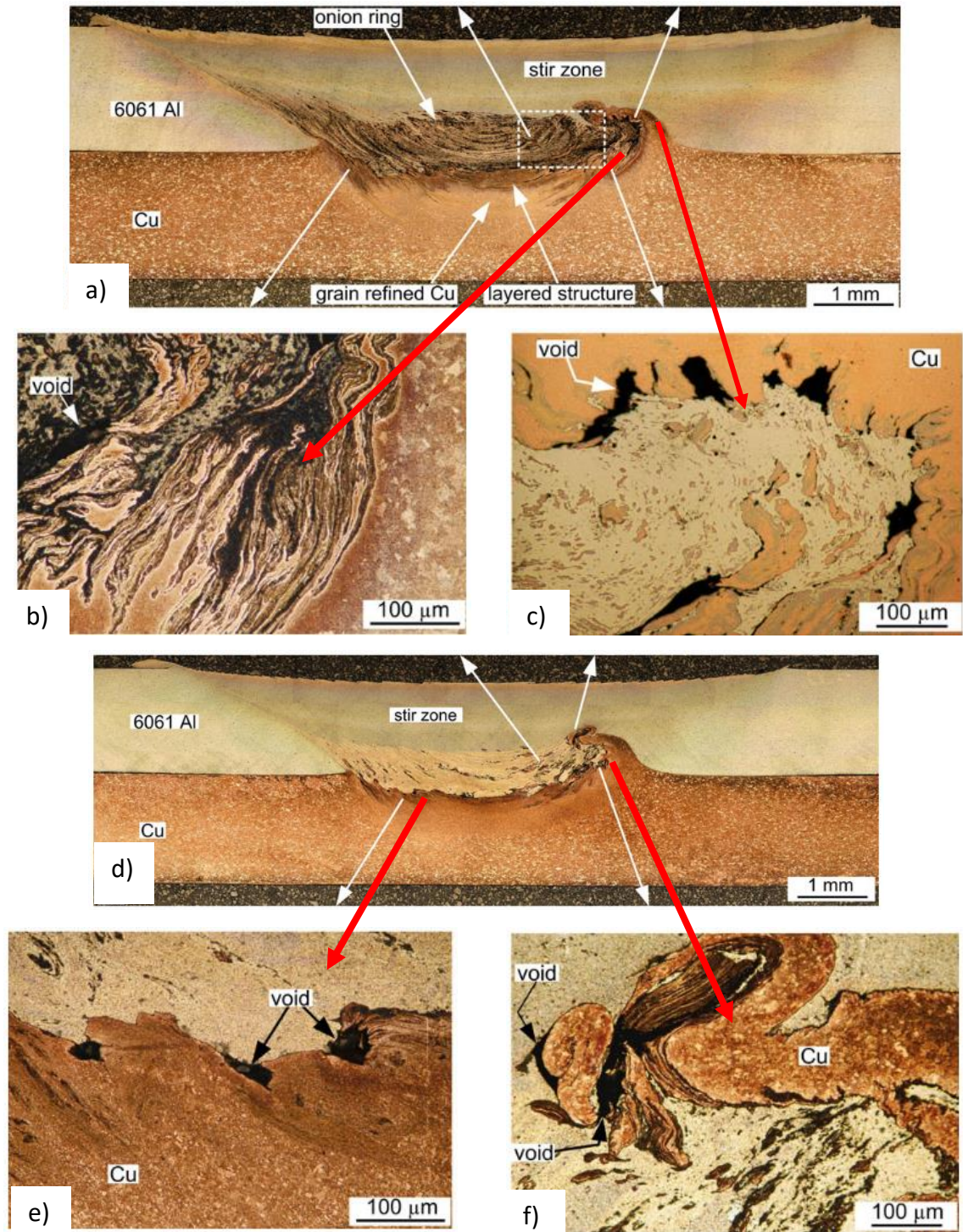


Figure 2 - 4 Weld interfaces from Firouzdor and Kou, with a ω of 1400 rpm. (a) weld interface using v of 38 mm/min, (b) void formed in the interface in RS region, (c) voids in copper flash hooks (as polished condition), (d) weld interface using v of 203 mm/min (e) typical voids formed in the interface, (f) voids formed in the copper flash hook [93].

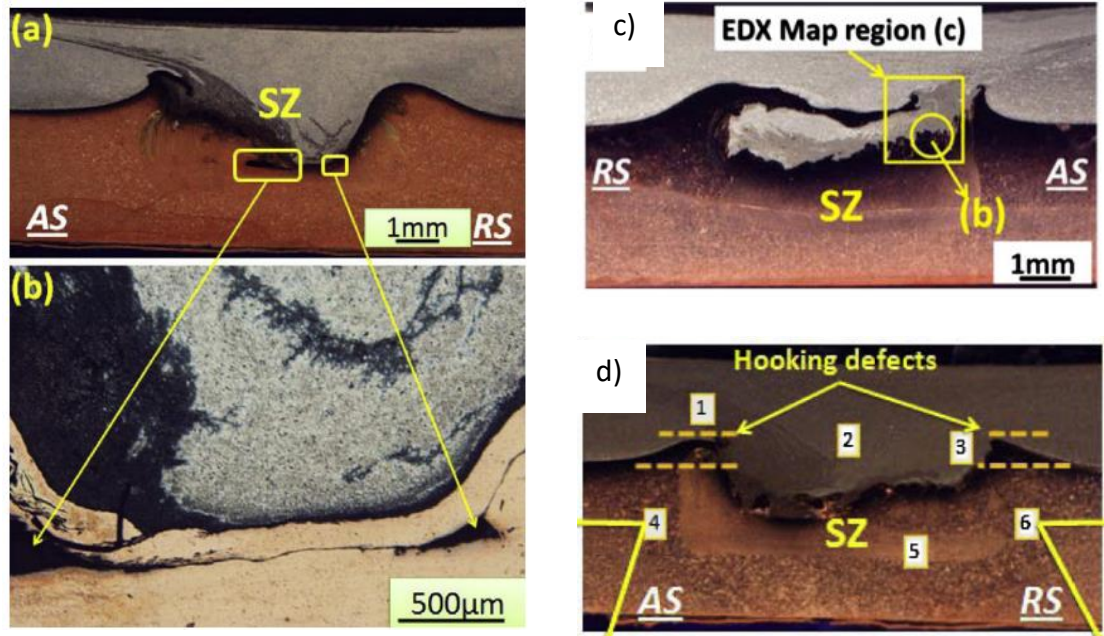


Figure 2 - 5 Weld using a ω of 600 rpm and v of 32 mm/min, (b) channel formed in weld shown in a, (c) weld using ω of 600 rpm and v of 15mm/min, (d) weld using ω of 825 rpm and v of 32 mm/min [73].

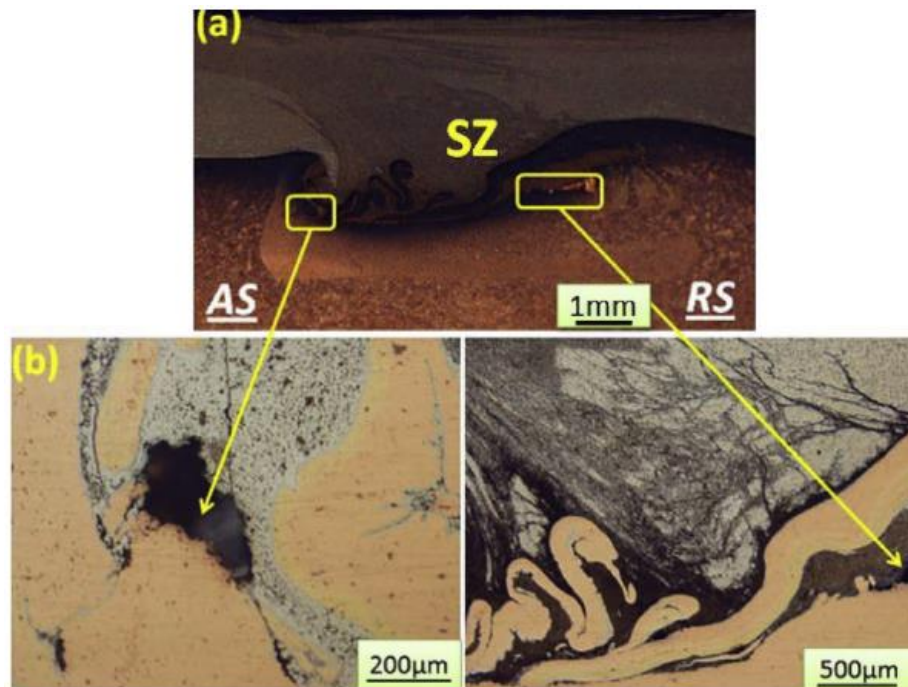


Figure 2 - 6 Weld interface produced using a ω of 1550 rpm and v of 15 mm/min [73].

Excessive d_p is reported in the work by Bisadi et al. [73] and Beygi et al. [94]. Bisadi et al. found channel and void defects on the interface mainly along the retreating and AS of welds at a ω of 600 rpm and v of 32 mm/min (Fig. 2 - 5), and a ω of 1550 rpm and v of 5 mm/min (Fig. 2 - 6) respectively. A greater examination of these channels (Fig. 2 - 5b) and voids (Fig. 2 - 6b and c) showed that these defects formed due to the folding of

the retreating and AS copper flash. A reduction of v from 32 to 15 mm/min for a constant ω of 600 rpm leads to the folding of the RS flash, eliminating channels (Fig. 2 - 5c). Further, AS flash was seen in this weld to be not as extensive as other works. Copper flash was removed completely after increasing ω from 600 to 825 rpm as presented in Fig. 2 - 5d however, with no evidence of interfacial continuity in a defect free interface. Another extreme use of d_p is evident in the work by Beygi et al. [87], whereby the total penetration from aluminium to copper was 2.6 mm. However, determining the penetration toward bottom copper was challenging as both lapping plates were roll bonded to a thickness of 3 mm while, void defects formed on the RS under the folded copper flash.

Based on this literature it can be postulated that excessive penetration into copper bottom plate may cause channel and void defects due to copper flash folding into the stir zone, in turn restricting aluminium flow in the fill region under the folded copper flash. However, there is no consensus on the formation of the copper flash hook in the stir zone and how FSW parameters affect it. No evidence of interfacial continuity was evident from literature. However, less voids in the interface are seen with shallower d_p 's of 0.1 - 0.2 mm in a narrow d_p range. Because of this, the intention is to widen the d_p range adding flexibility to the process thus, it is important to further study the effect of d_p 's with a range greater than what is currently known. Also it is important to determine and understand the flow in the bottom region of the pin as well as the copper flash formation mechanism in order to determined ways to overcome it.

2.3 Review on friction stir scribe technology

Joining dissimilar metals with different thermal and physical properties including; melting point, hardness, etc. is challenging for most joining methods. This can in turn lead to materials with lower melting points liquefying and being squeezed out from the intended joint interface, as shown in Al - to - Mg FSLW by Firuouzdor and Kou [97]. This can be overcome in FSLW of dissimilar metals, where the harder and/or higher melting point material is placed on the bottom and the incorporation of scribe in the bottom of the pin originally designed to avoid overheating of top plate [97] as well as pin wear [35], [37], [98], as is commonly observed in conventional FSW.

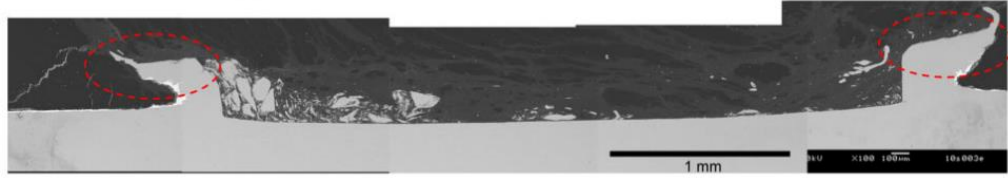


Figure 2 - 7 Interface produced by scribe pin [99]–[101].

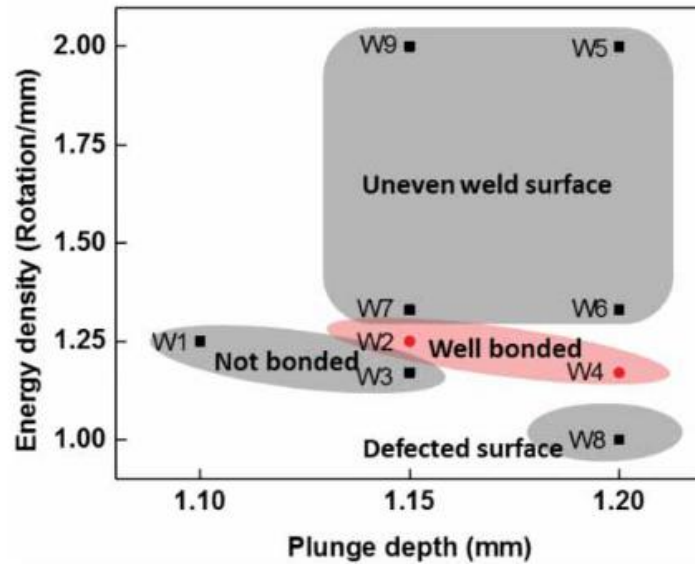


Figure 2 - 8 Energy density VS $d_{p-scriber}$ on weld quality [102].

The incorporation of the scribe into the pin was first realised by Hovanski et al. [101] naming his invention as friction stir scribe technology, consisting of a scribe cutter integrated into the tool's pin that is placed radially off from the centre of the pin bottom surface (in this study 2 mm off from the centre). Scribe pins are commonly made from alloys including; nickel, titanium, tungsten, steel, carbide steel, polycrystalline cubic boron nitride, silicon nitride, rhenium, boron, or combinations of these alloys. The scribe protrudes to a predetermined length from the bottom pin surface and is plunged into the harder bottom plate to a defined depth, creating two RS and AS hooks bending in the opposite direction to the stir zone (Fig. 2 - 7)[101].

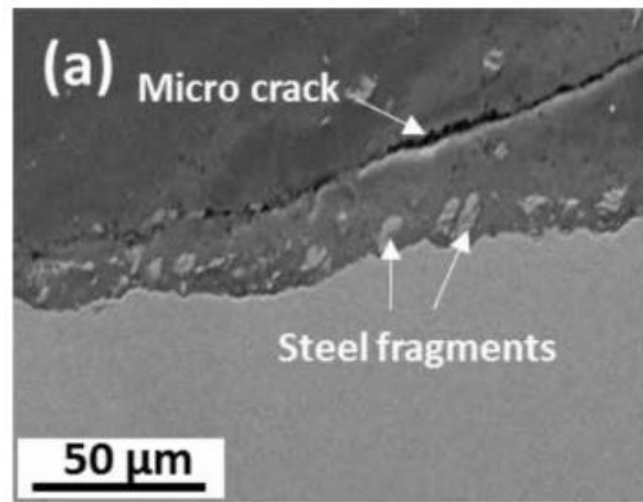


Figure 2 - 9 Microcrack in the well bonded weld [102].

Until now, little is known about the material flow, the interface formation mechanism and the interfacial continuity of FSW made with scriber pins. The most common features that exist in the interface, besides the RS and AS hooks, is the existence of fragments scribed from the bottom plate and trapped in the weld nugget close to the scribed interface [99], [102]–[108]. Owing to the interlocking nature of the RS and AS hooks formed, joints produced with the scriber pin have higher strengths than those without the pin as observed by Mahoney et al. in tensile shear tests [99].

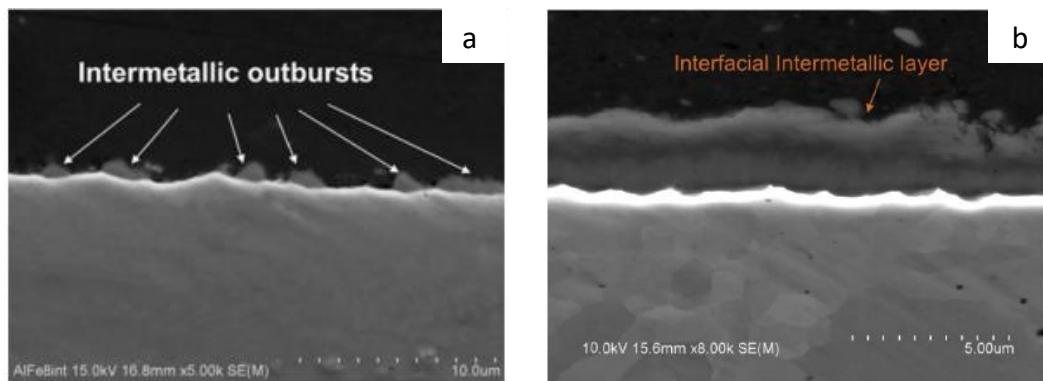


Figure 2 - 10 Al-to-Fe FSLW using $\omega = 710$ rpm and $v = 80$ mm/min with (a) $d_p = -0.3$ mm and (b) $d_p \approx 0$ mm [35].

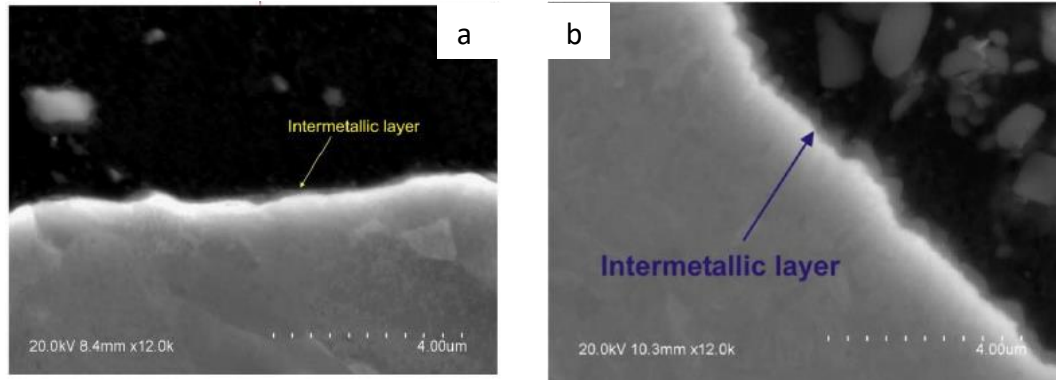


Figure 2 - 11 Al-to-Ti FSLW using $\omega = 1400$ rpm and $v = 20$ mm/min with (a) $d_p \approx 0$ mm, and (b) $d_p > 0$ mm [37].

A more in depth investigation into weld quality using various combinations of ω , v , and scribe penetration depth towards the bottom plate ($d_{p-scriber}$) was conducted by Wang et al. on aluminium to galvanized steel welds [102]. The optimum process window was attained by plotting energy density, relating the heat input per welding distance (ratio of ω/v) against $d_{p-scriber}$. From this analysis it was found that for the same $d_{p-scriber}$, welds with high energy density produce uneven weld surfaces (High to low energy density welds of W9, W7, W2 and W3 in Fig. 2 - 8), while conversely cold welds lead to no bonding and a defect dominated interface. However, at a nominal input, increasing $d_{p-scriber}$ by 0.05 mm results in a interface quality change from no bonding to well bonded as evident from W1 to W2 and W3 to W4 in Fig. 2 - 8. Despite the categorisation “well bonded”, the author observed evidence of a microcrack just above the weld interface, in which the upper and lower side of the crack do not match with one another upon higher magnification imagery in Fig. 2 - 9. Furthermore, there is a region of dispersed steel fragments below the crack suggesting difference in flow between the upper and lower region of the crack. By virtue of this lack in knowledge, better understanding about flow in the scribed region is required.

The greater majority of literature on FSLW with scribe consist of metal couples with large hardness and melting point differences including; Mg - steel [99], [100], Al - steel [102], [103], [106], [107], [109], [110], and polymer - Al [104]. At this time there is no knowledge on the application of a scribe tool on alloy couples containing similar mechanical properties e.g. Al - Cu, highlighting the literature gap that will be investigated in this study.

2.4 Review on Al - Cu interfacial intermetallic growth in Al-to-Cu FSLW

Intermetallic formation and growth mechanics in FSLW is clearly defined in the work by Chen *et al.* [35] on Al-to-Fe FSLW and Yazdanian [36] on Al-to-Ti FSLW. Differing intermetallic continuities and thicknesses are observed by the authors, through the variation of penetration depth for similar ω and v 's. Further noted is the evidence of greater frictional heat at full or slight penetration of the tool, as opposed to the bottom of the pin located above the interface. In Al-to-Fe FSLW by Chen *et al.*, welding was performed using a $\omega = 710$ rpm and $v = 80$ mm/min. At a $d_p = -0.3$ mm, with the bottom of the pin positioned 0.3 mm above the Al-Fe interface in the Al side, a Al-Fe intermetallic formed as an outburst with a thickness of ~ 1 μm (Fig. 2 - 10a). However, at $d_p \approx 0$ mm, with the pin slightly penetrating into the Fe plate or just grazing the Fe surface, a continuous Al-Fe intermetallic layer with an average thickness of 1.5 μm was formed in the interface (Fig. 2 - 10b) [35]. As for Al-to-Ti FSLW conducted by Yazdanian *et al.*, welding was performed at a $\omega = 1400$ rpm and $v = 20$ mm/min. At a $d_p \approx 0$ mm, same condition as Al - Fe, very thin continuous Al - Ti intermetallics with the average thickness of ~ 200 nm layer formed in the interface (Fig. 2 - 11a). However, at $d_p > 0$ mm with the pin penetrating the Ti plate, the greater friction heat only produced a continuous Al-Ti intermetallic with an average thickness of ~ 250 nm (Fig. 2 - 11b) [36]. This shows that the Al-Fe intermetallic nucleation rate (\dot{R}_n) is slow, restricting the formation of a stable nucleus, resulting in intermetallics forming as outbursts. However, once a stable nucleus is formed, intermetallics grow at a rapid rate. Considering the Al-Ti intermetallic behaviour, when the pin was positioned just touching the Al-Ti interface, continuous intermetallics formed with a $d_p \approx 0$ mm showing that the Al-Ti intermetallic \dot{R}_n is rather fast. However, with greater friction heat produced at a $d_p > 0$ mm (no exact d_p value as penetration monitored by increase in monitored down force), the Al-Ti intermetallic was only ~ 50 nm thicker than when the $d_p \approx 0$ mm. Thus, suggesting that Al-Ti intermetallic growth is rather slow. With respect to Al-Cu FSW, Al-Cu intermetallic formation and growth behaviour is still unknown, thus its behaviour forms one of the aims of this study.

Attempts to study the growth behaviour of the interfacial intermetallic layer in dissimilar metal FSW are evident in literature for various metal couples including; Al - Fe [35], [36], [111]–[113][35], [36], [112]–[115], Al - Mg [116], Al - Ti [36], [37], and Al - Cu [33]. A post weld heat treatment was implemented in most of these studies, as an attempt to grow the interfacial intermetallic further. Heat treatment processes were

conducted across range of temperatures and holding times depending on the material combination, with the thickness of the interfacial intermetallic measured at each of the holding times tested. The squared value of the material thickness is plotted against the holding time, with data proving that the square value of intermetallic thickness increases linearly with holding time at a specific temperature. Thus suggesting that intermetallic growth follows the parabolic growth kinetics expressed by Equation 8 below.

$$th^2 = dt \quad \text{Eq. 8}$$

Whereby; th is the interfacial intermetallic layer, d is the growth rate constant and t the holding time. Interfacial intermetallic growth governed by volume diffusion or otherwise can be determined by plotting the measured th^2 vs t and performing regression linear analysis on the plot. Data fitting closely with the regression line denotes interfacial intermetallic growth to be governed by volume diffusion, allowing for the growth rate of the intermetallic to be determined. However, the exact growth behaviour of interfacial intermetallics in dissimilar FSW's still unknown. Some studies suggest the growth behaviour to be volume controlled [33], [113], [116] however, Movahedi et al. observed different results. They found that interfacial intermetallic growth in Al - to - Fe FSLW is not governed by volume diffusion and that a high level of stored energy in the Al side could affect the growth behaviour. The stored energy was investigated through determining the average misorientation angle between crystallographic orientations and applying kernel average misorientation (KAM) analysis [112].

A different approach to understand interfacial intermetallic growth was conducted by Wei et al. [114] in the FSLW of Al - to - Fe. A $\omega = 950$ rpm together with various v 's from $60 - 375 \text{ mm min}^{-1}$ were used with, interfacial intermetallic from corresponding parameter couple measured and the d value was determined by using equation 9. Subsequently, t growth, or holding time, was determined by using Equation 9 as follows.

$$t = \frac{D_{\text{shoulder}}}{v} \quad \text{Eq. 9}$$

Where, t is the "holding time", D_{shoulder} is the shoulder diameter, and v is the travel speed. Wei et al. found that the calculated d in FSW is in the order of 10^{-13} which is 10^4 higher than d in equilibrium state, 10^{-17} [117]. They stated that the enhancement on d was probably activated not only by temperature but also severe plastic deformation induced by the stirring action during FSW however, this was not demonstrated in their work.

Specifically, in Al - Cu system FSW, Xu et al., applied a post weld heat treatment, demonstrating that the growth behaviour of interfacial intermetallic layer is governed by volume diffusion. However, the temperature used to further grow the interfacial intermetallic was done externally, not from the FSW process itself [117].

2.5 Objectives

The literature review highlighted that the optimum parameter combinations of; ω , v and d_p , required to produce discontinuity-free interfaces in Al-to-Cu FSLW are still unknown. Furthermore, there is a lack of understanding on material flow under the pin during the FSLW process. This knowledge is important in understanding the defect formation mechanism, as to prevent their existence. Equally important is furthering the knowledge on the growth kinetics of the interfacial intermetallic as well as microstructural evolution in the stir zone during the process.

Based on this knowledge gap, the objectives of this study are as follows:

1. To find the optimum parameters (ω and/or d_p) to achieve a discontinuity-free weld interface in left-hand threaded, scriber and manually filed bottom thread pin.
2. To understand material flow in the bottom region of the pin, first in left-hand threaded pin followed by scriber and manually filed bottom thread pin as a response to findings in welds with the first pin.
3. To investigate the application of scriber pin in Al-to-Cu FSLW.
4. Further investigation on microstructural evolution and interfacial intermetallic growth during the FSLW process.

Chapter 3: Experimental procedures

The two main objectives of this research are to:

- Establish the optimum processing condition (ω , v and tooling condition) for Al - to - Cu FSLW via a series of experiments using a left-hand threaded pin, scriber pin and a pin that has the bottom thread manually filed. Defect types that could impair the electron path in the Al - Cu interface are identified and the cause of the defects, as well as their formation are revealed.
- Investigate the interfacial intermetallic formation and growth behaviour during the FSLW process.

Details on experimental, measuring technique and analytical designs and procedures used to fulfil the objectives are explained in this chapter.

3.1 Materials and dimensions of weld pieces

Aluminium 6060-T5 and commercially pure copper plates with thickness of 6 and 3 mm respectively were used in this study, with chemical compositions each material presented in Table 3 - 1. The plates were cut into 300 x 100mm sections and assembled by lapping aluminium atop of copper following the plate dimension and lapping configuration schematic can be seen in Fig. 3 - 1a to c. Lapping plates were divided into two 150 mm sections, with ~120 mm long welds conducted in each section.

Table 3 - 1 Chemical composition of aluminium 6060-T5 and commercially pure copper

Materi als	Mn	Fe	Mg	Si	Cu	Zn	Ti	Cr	Ni	Pb	Oth ers	Al
6060- T5	0.10	0.10 - 0.30	0.35 - 0.60	0.30 - 0.60	0.10	0.15	0.10	0.05	-	-	0.15	Bal.
Cu	-	0.05	-	0.01	Bal.	0.3	-	-	0.03	0.03	-	0.02

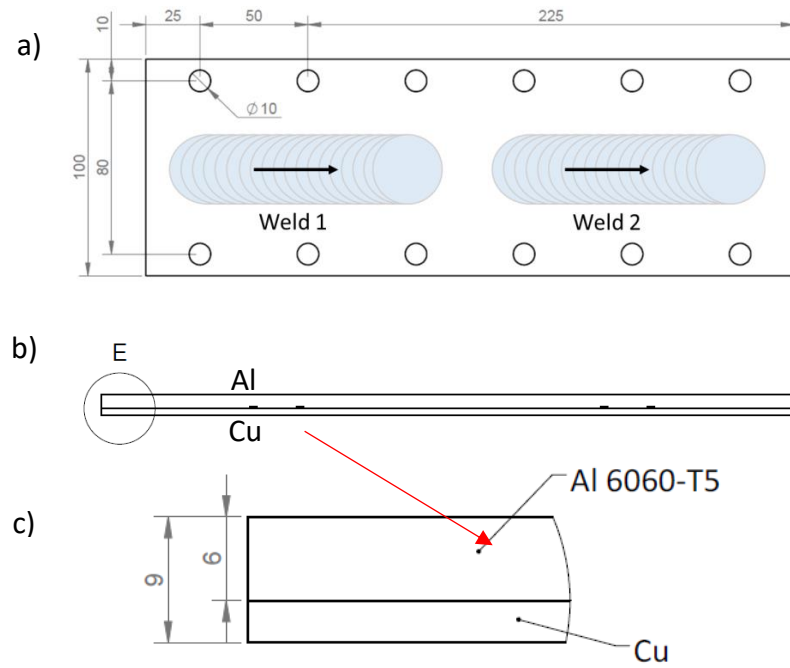


Figure 3 - 1 (a) Plan view of the plate & dimensions; (b) side view of the lapping plates; (c) magnification of circled area E in Fig. 3 - 1b showing thickness of the lapping plates.

3.2 Machine, work pieces clamping and position adjustment

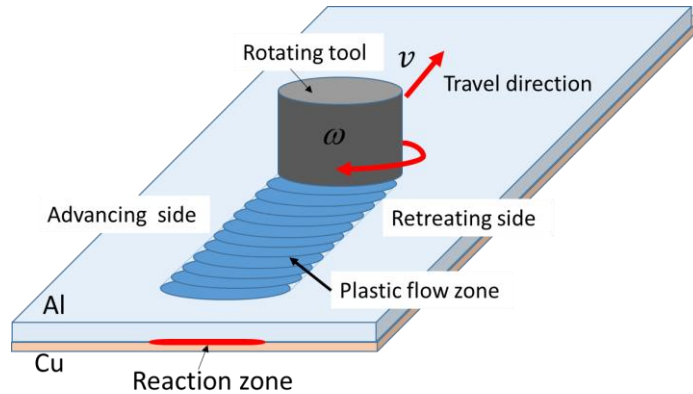


Figure 3 - 2 Schematic of Al-to-Cu FSLW in this study

The principle of FSLW is described as a solid-state fabrication process whereby a rotating tool with the rotation speed of ω is plunged into lapping plates of aluminium and copper to a pre-set penetration depth (d_p). The rotating tool traverses to a certain length of weld moving with a travel speed of v , leaving behind a plastic flow zone and reaction zone in the interface between aluminium and copper. After the specified weld length was established, the tool traverse was terminated and the rotating pin pulled from the lapping plate as per the process schematic in Fig. 3 - 2. A detailed systematic

explanation of the process from controlling the machine, setting zero position for accurate penetration, plate and pin positioning is described herein.

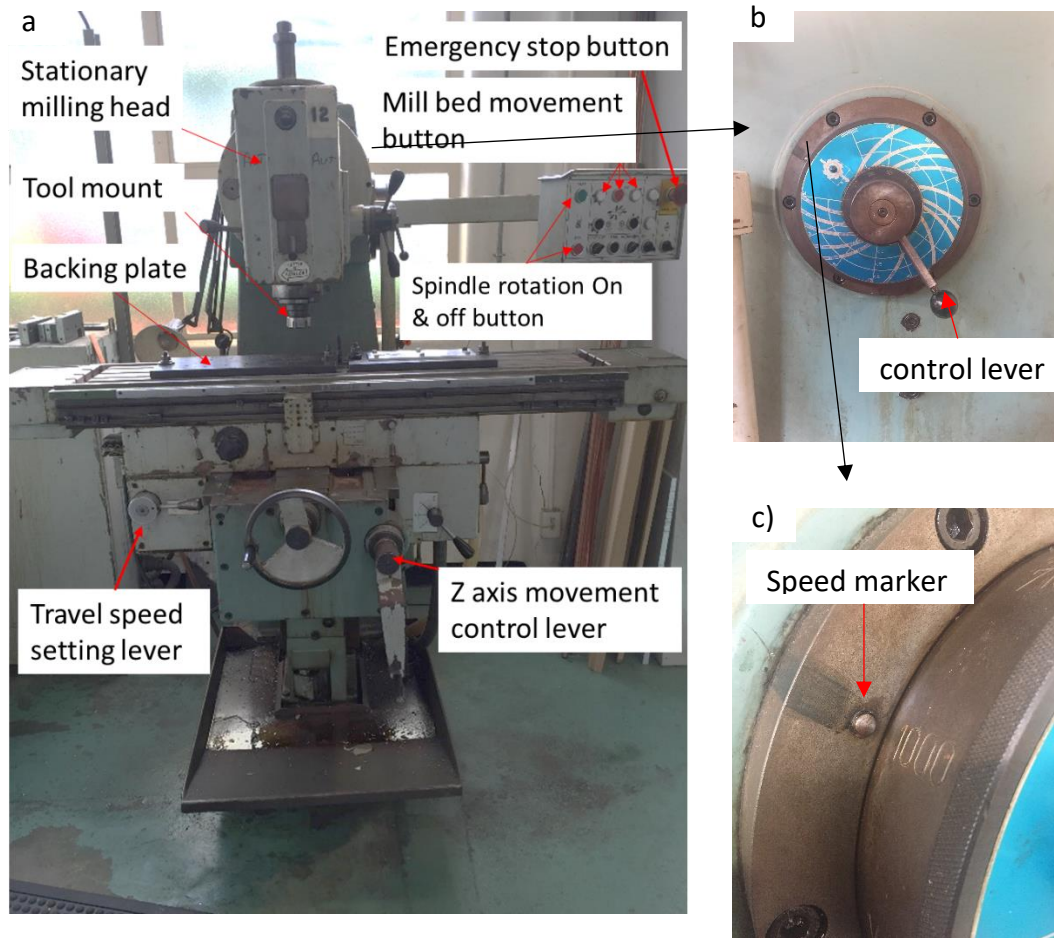


Figure 3 - 3 (a) Retrofitted Lagun milling machine used throughout the study; (b) Tool rotation speed control in the side of the machine; (c) speed gauge.

A retrofitted Lagun milling machine was used for FSLW experiments (Fig. 3 - 3a). The FSW tool was mounted in the tool mount of the milling head. The lapping plates were fixed on a backing plate of the milling bed and set to travel along the X-axis. Tool rotation and mill bed movement are controlled via the control panel in the upper right of Fig. 3-3a. The control panel is equipped with emergency stop button used in terminating movement of the machine for the experiment, with the tool suddenly stopped, embedding it in the lapping plates. To the right of the stationary milling head is the rotation-speed control lever (Fig. 3 - 3b), used in changing the tool rotation speed by rotating the lever clockwise. The selected speed is set to align with the selection gauge marker (Fig. 3 - 3c) to engaging the gears.

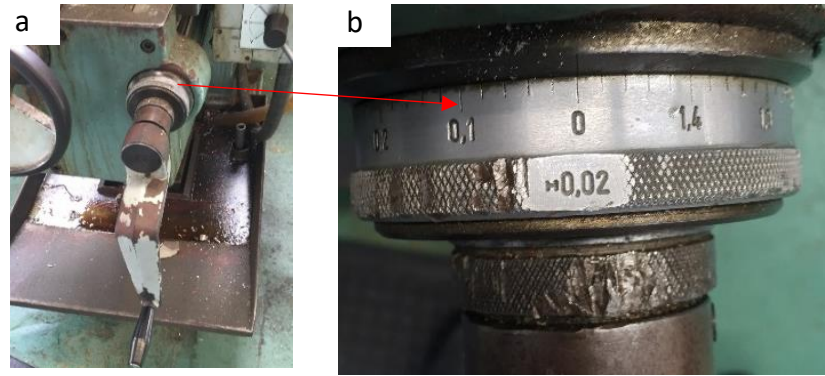


Figure 3 - 4 (a) Z axis control lever to control d_p circled red and labelled as 2 in Fig. 3 - 2; (b) Scale in Z axis control lever.

Fig 3 - 4a shows the Z-axis control lever used in manually controlling the penetration, as shown in lower right of Fig. 3 - 3a. Clockwise rotation of the lever moves the milling bed up, simulating pin advancement towards the lapping plates and subsequently penetrating to a pre-set depth, with vice versa simulating pin retraction from the plates. One rotation of the lever displaces the milling bed 1.5mm, with increments taken at 0.02 mm intervals (Fig 3 - 4b).

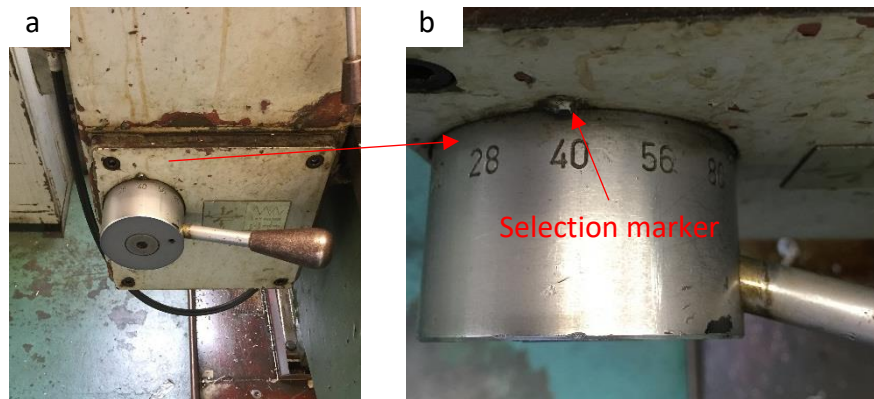


Figure 3 - 5 (a) Travel speed control lever circled red and labelled as 1 in Fig. 3 - 2; (b) travel speed selection.

Mill bed movement or travel speed was selected by using the control lever seen in the lower left side of Fig 3 - 3a as shown in more detail in Fig. 3 - 5a. Travel speed was enabled by rotating the lever so that the selected speed aligns with the selection marker facing upward (Fig. 3 - 5b)



Figure 3 - 6 Bolting system used in this study.

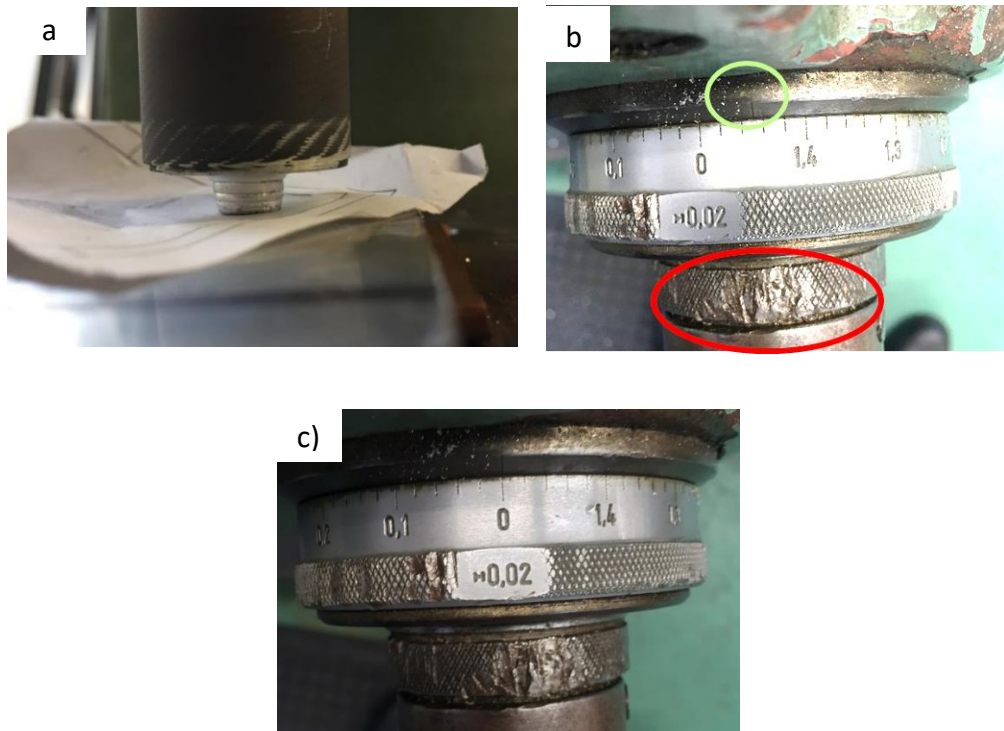


Figure 3 - 7 (a) Pin down until pressing the paper tight; (b) Gauge fastener circled red and gauge marker circled in green; (c) Zero position.

Lapping plates were affixed to a backing plate by six bolts along each side of the plates, preventing material displacement due to thermal expansion, common in high temperature processing (Fig. 3 - 5). A detailed drawing including dimensions of the bolt holes and their locations is shown in Fig. 3 - 1a.

In order to accurately reach the pre-set d_p , the zero pin position must be established first. In this study, the zero pin position was established by pinning down a 0.1 mm thick piece of paper, pressing it tight enough to establish contact but not to tear the paper upon removal as seen in Fig. 3 - 7a. The Z-axis lever gauge was then adjusted by first loosening the gauge fastener (circled red in Fig. 3 - 7b), and turning the gauge so

that the 0 indication aligned with the marker as circled green in Fig. 3 - 7b. The final gauge position at the 0 position is depicted in Fig. 3 - 7c.

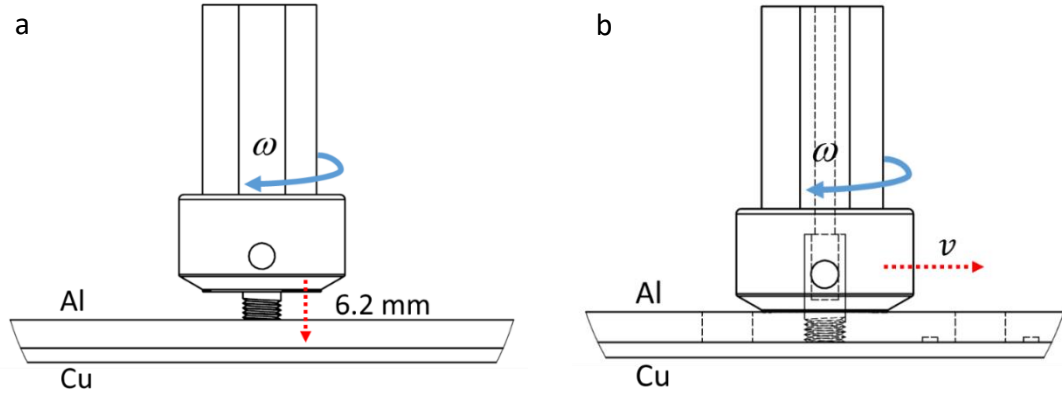


Figure 3 - 8 Tool penetration with total displacement of 6.2 mm for $d_p = 6.1$ mm; (b) Rotating pin penetrates into the lapping plates ready to traverse.

After setting the zero pin position, tool rotation is turned on and the Z-axis control lever is rotated 4 times (1 revolution = 1.5 mm) plunging into the aluminium plate (6 mm). This is followed with a further rotation to the pre-set depth, with 0.1 mm added to compensate the paper thickness. As an example, evident in Fig. 3 - 8a, if a d_p of 6.1 mm is desired, the lever completes a full rotation four times, with an additional 0.1 mm for the copper penetration and 0.1 mm compensating paper thickness, totalling a displacement of 6.2 mm. After reaching the pre-set depth, the mill bed movement control was turned on to a pre-set direction, used in controlling the tool forward speed, up to a certain length of weld (Fig 3 - 8b). After weld termination the mill bed movement is turned off and the tool is subsequently retracted from the welded plates and finally, the tool rotation is then turned off.

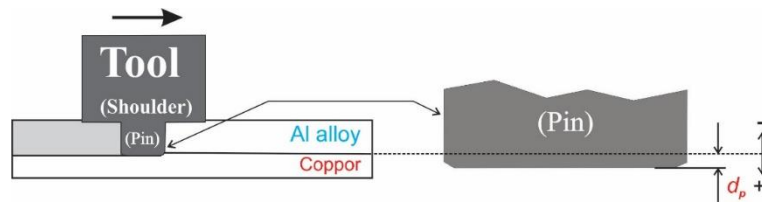


Figure 3 - 9 Schematic of d_p in normal pin.

In this study d_p is defined as the relative position of the bottom of the pin to the copper plate surface. Considering the left-hand threaded pin without scriber (hereafter referred as normal pin), a positive penetration value was determined when the pin bottom surface penetrated into the copper bottom plate. Whilst, pin position right in the Al - Cu plate interface is considered as $d_p = 0$ and pin position away from the copper surface

(still in Al) was considered as negative d_p , as seen in the schematic of pin penetration in Fig. 3 - 9.

Whereas for the normal pin with scribe fixed on its bottom surface (hereafter referred as scribe pin), Scriber penetration ($d_{p-scriber}$) is the penetration of scribe into copper, while the penetration of pin bottom still considered as d_p . Therefore:

$$l_{scriber} - d_{p-scriber} = d_p \quad \text{Eq. 10}$$

Where:

$l_{scriber}$ = length of scribe

$d_{p-scriber}$ = penetration of scribe into copper

d_p = position of pin bottom

A detailed schematic of scribe penetration is shown in Fig. 3-10.

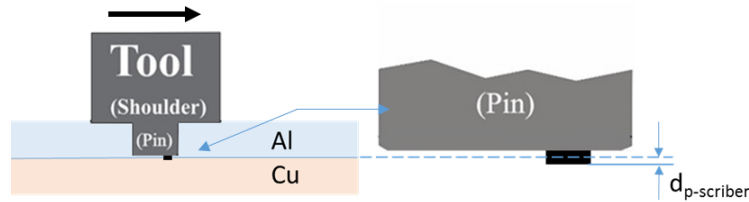


Figure 3 - 10 Schematic of d_p in scribe pin.

3.3 Tool design and material

Five tool designs are used in this study, the first consisting of a concave shoulder 25mm in diameter and a cylindrical left-hand threaded pin 8 mm in diameter. Pin length was adjusted depending on penetration depth into the Cu bottom plate. The d_p for preliminary trials was 0.5, 0.3 and 0.2 mm, thus corresponding to a pin length measured from the base of the shoulder of 6.5, 6.3 and 6.2 mm respectively. Detailed tool drawings and dimensions for this tool are detailed in Fig. 3 - 11a and b. This tool was predominantly used in the preliminary investigation, and was incorporated with a tilt angle of 2.5°. The tilt angle led to the concave section of the tool shoulder acting as a reservoir, providing material to be driven down by the left threaded pin.

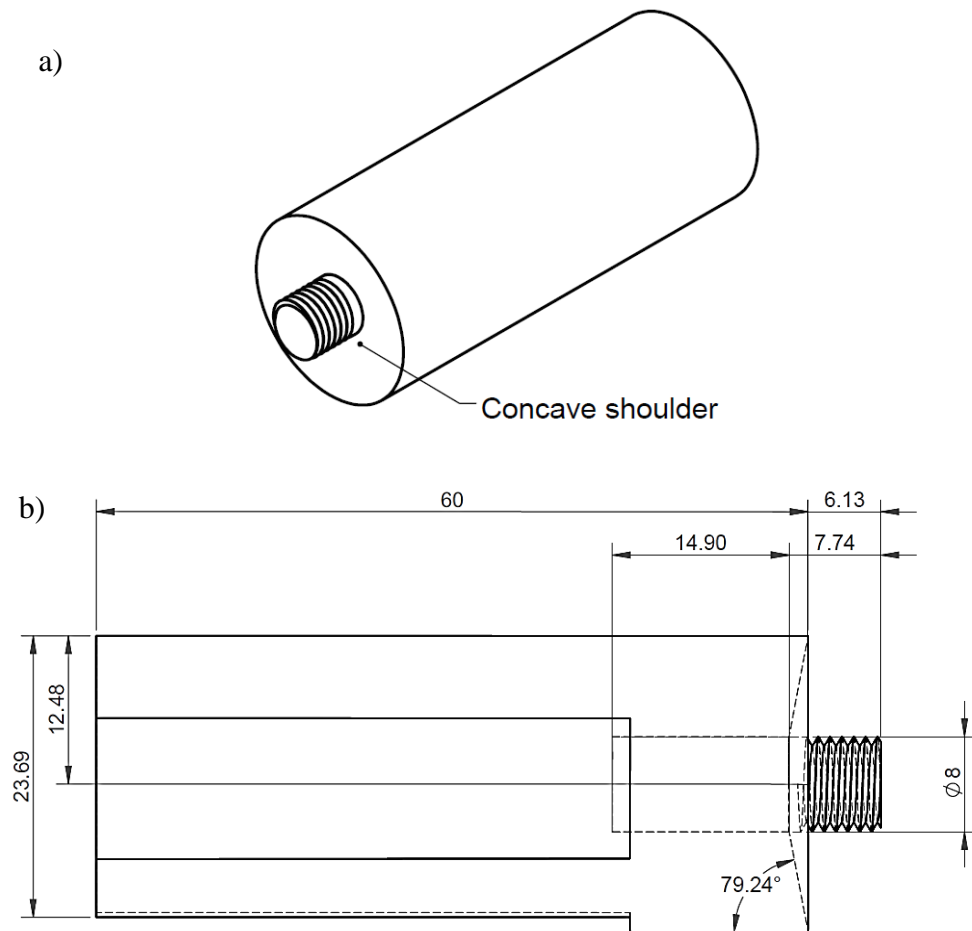


Figure 3 - 11 (a) Concave shoulder tool; (b) Tool dimension.

The second tool used in this study was a scroll shoulder tool incorporating a cylindrical left-hand thread pin with the same shoulder and pin diameter as the first tool (Fig. 3 - 12a). A scroll shoulder was chosen to eliminate the need to tilt the tool, allowing tool traversal in any direction without the requirement to change the tilt direction of the milling head each time the welding direction is changed. The shoulder head feature was added to reduce the excessive surface flash from forming (Fig. 3 - 12b). As evident in Fig. 3 - 12c the two counter clockwise concentric scrolls protrude 0.5 mm from the shoulder base each with a width of 1.5mm, forming two counter clockwise concentric channels. These channels act as a material passage that is scooped from the outer periphery of the scroll feature during the process and funnelled into the base of the pin, driven downward by the left hand threaded cylindrical pin.

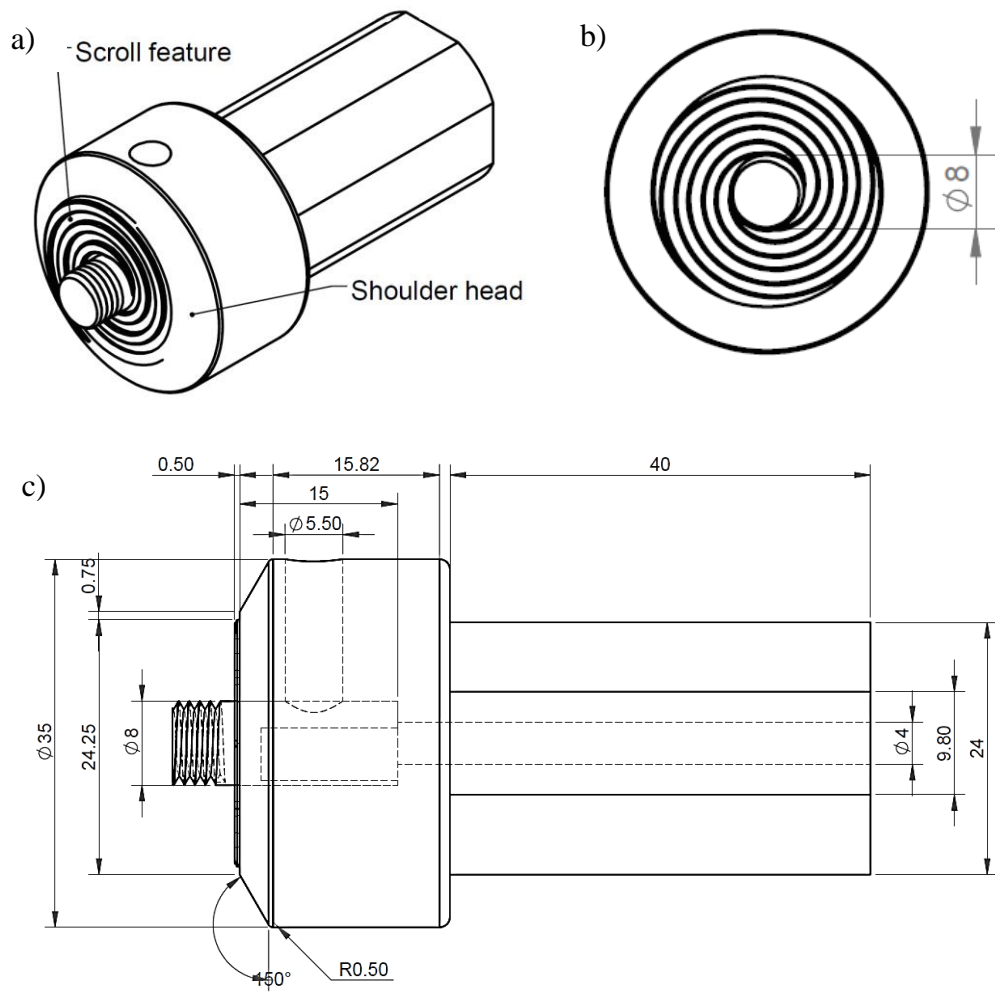


Figure 3 - 12 (a) Scroll shoulder tool with shoulder head; (b) scroll feature; (c) Tool dimension.

The third tool is similar in design to the second tool with the addition of a high speed steel scriber pin 1mm in diameter (Fig. 3 - 13a). The scriber was fixed in the bottom pin surface and placed 2 mm off from the center of the pin surface, protruding as long as 0.7 mm as shown in Fig. 3 - 13b and c [101]. The scriber penetrated 0.2 mm into the Cu bottom plate, leaving a 0.5 mm gap between the aluminum and copper interface with the bottom of the pin. In this setup, pin length was set to 5.5 mm from the base of the shoulder. This scriber was used to reduce or eliminate the inward hooking, decreasing the possibility of void formation by creating a mechanical interlocking feature in the form of bent outward hooks [101], [102], [118]–[121].

The fourth tool utilised in this study has a concave shoulder, left-hand thread pin with scriber pin in the same configuration as previous tool (Fig 3-14). A detailed drawing of the tool is presented in Fig 3-14b, with welds made applying a 2.5° tilt along the tool's length.

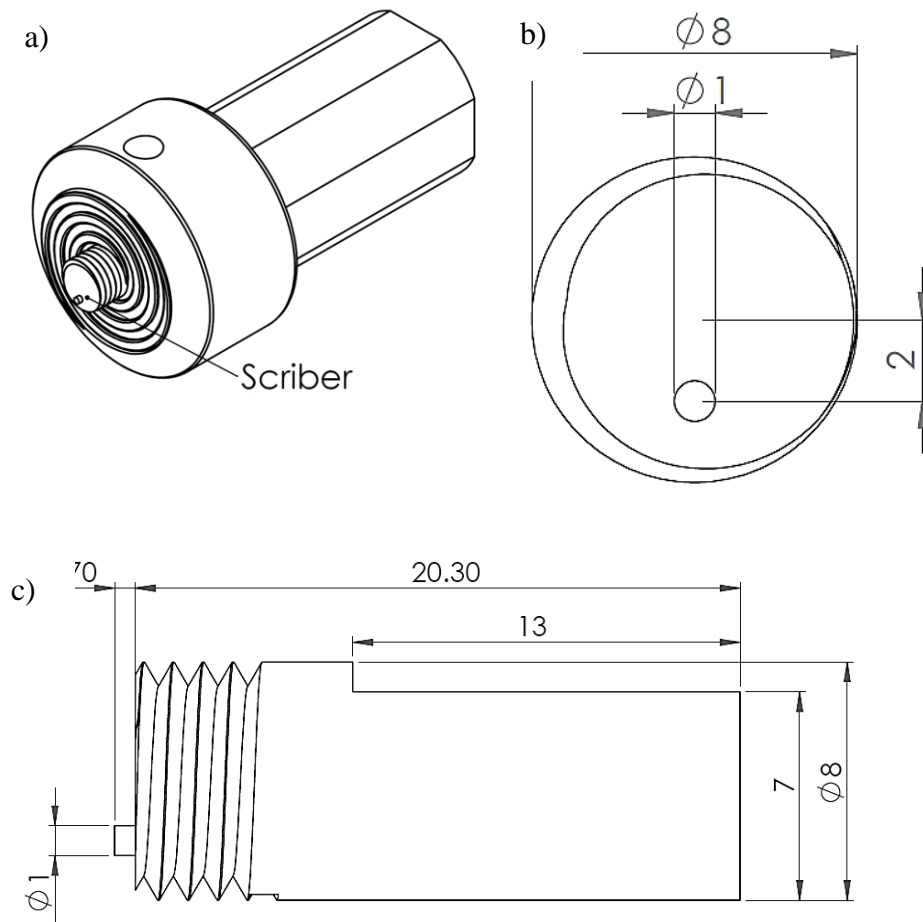
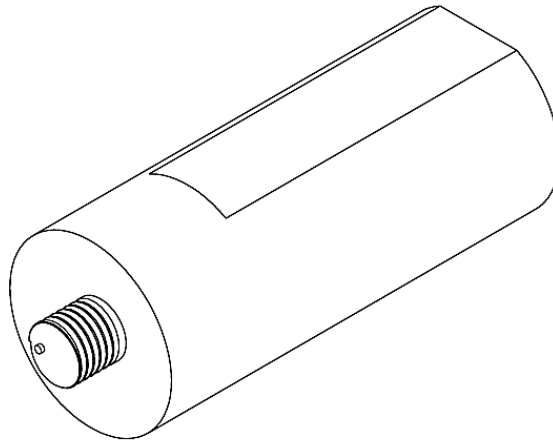


Figure 3 - 13 (a) Scroll shoulder tool with shoulder head and scriber in the pin bottom surface; (b) scriber position in the pin bottom surface; (c) pin and scriber dimension.

A scroll shoulder tool with left-hand thread pin, in which the last thread on the bottom of the pin was manually filed was the fifth tool type used in this study. As filing was done manually, exact dimensions of the filed region is unknown, however the final shape of the pin is similar to the drawing in Fig 3-15.

Similar in design to the third tool, the sixth and final tool seen in Fig 3-16 utilised threads with machining defects made to diminish material down flow and to study down flows importance on interfacial continuity in FSLW with scriber pin.

a)



b)

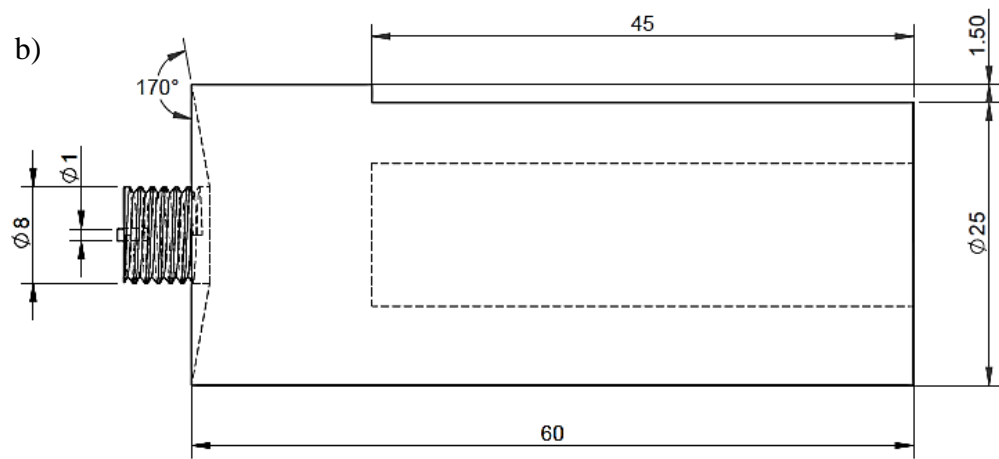


Figure 3 - 14 (a) Concave shoulder tool with scribe pin in the pin bottom surface; (b) Tool dimension.

Manually filled

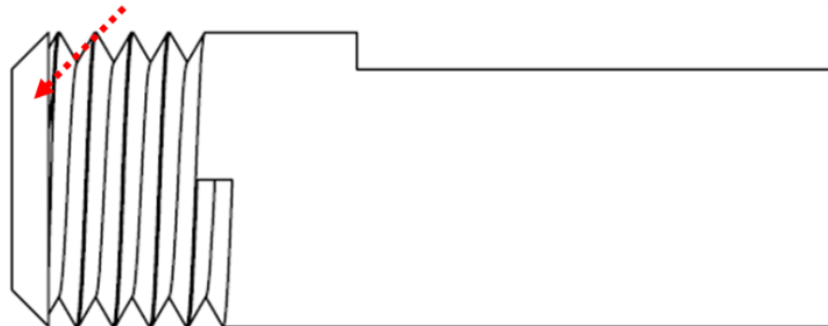


Figure 3 - 15 Pin with bottom most root and crest manually filed

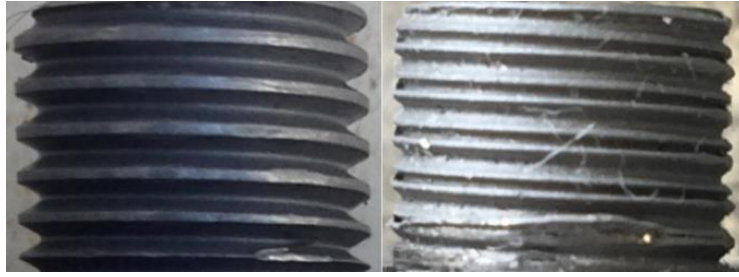


Figure 3 - 16 Right picture is the faulty thread. For comparison, good threads can be seen in the left.

3.4 Welding conditions

Multiple single pass welds were conducted to establish the ideal parameters where a (close to) discontinuity free welds could be achieved. A series of experiments were conducted using the first and second tool, with variation in welding parameters such as ω , v and d_p . Welds conducted with the first tool used d_p 's of 0.2, 0.3 and 0.5 mm, with the purpose of investigating the effect of pin penetration on the quality of the weld interface. In specifically, the formation of copper flash hooks in the retreating side (RS) and advancing side (AS) area and their influence on the interfacial continuity of the welds, as well determining the optimum d_p . These trials were conducted using a ω of 1400 rpm and v of 40 mm/min. Using the second tool, FSLW's were produced at ω 's between 500 - 1400 rpm with a single v of 56 mm/min and used to investigate the effect of ω on the interfacial continuity of the weld interface. The flow in the lower part of the pin was studied by conducting a stop action method. Welds produced with a ω of 1400 rpm, v of 40 mm/min and d_p of 0.1 mm were produced and abruptly stopped mid process by pressing the milling machine's emergency stop button, embedding the tool in the weld.

A second series of trials followed the same principle as the first however, FSLW was conducted with the addition of scriber using the third tool type with d_p 's of 0, 0.1 and 0.2 mm and a ω of 1400 rpm and v of 40 mm/min. Following, the fourth tool type was used to investigate the influence of tilt angle towards the quality of the welds in FSLW with scriber pin. For these trials a tilt angle of 2.5° was incorporated with d_p 's of 0.1 and 0.2 mm. In order to study the flow, stop action was also performed in this part of the study.

The third series of trials used the fifth tool with the filed bottom thread pin, with d_p 's of 0.1, 0.2, 0.5 and 0.7 mm, ω of 1400 rpm and v of 40 mm/min. a stop action trial was conducted at a ω of 1400 rpm and v of 40 mm/min with a d_p of 0.3 mm.

Multipass FSLW's were subsequently conducted in order to understand intermetallic growth kinetics with welds produced at a $\omega = 1000$ rpm, $v = 56$ mm/min and $d_p = 0.15$ mm taken from the second series of first part of the study. An overlap of about 1mm in the AS side was evident between passes, resulting in the second and third lap starting 7 mm to AS of the previous lap, with each pass starting after the plate temperature cooled down to room temperature. Overlapping was chosen to preserve the maximum interface area, avoiding rewelding of the interface by the subsequent pass. Transversal and plan view schematics are presented in Fig. 3 - 17a and b respectively, showing the overlapping and thermocouple placement in the middle of first and second lap of the weld.

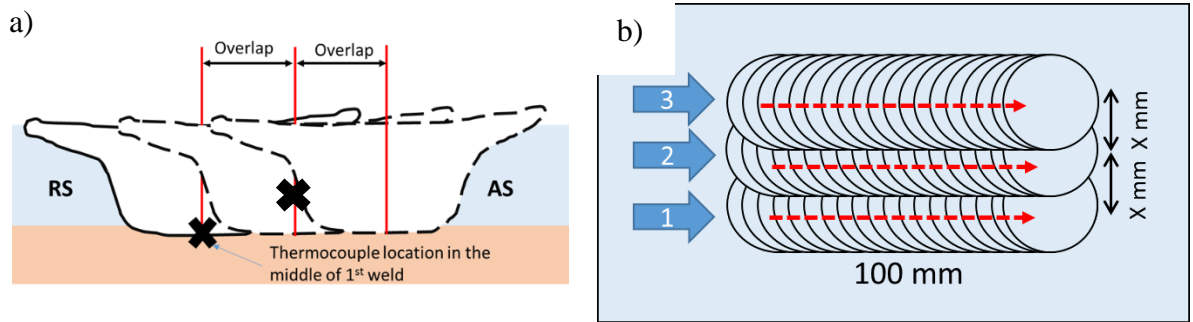


Figure 3 - 17 (a) Lateral cross section schematic of welds on first series; (b) Plan view schematic of RS overlap configuration for normal pin multipass FSLW.

3.5 Temperature monitoring

Temperature measurements were taken during the weld process using 1.5 mm K-type thermocouples. Two thermocouples were placed in separate grooves machined in the Al plate on the surface adjacent to Cu surface. As seen in Fig. 3 - 18a to c. grooves are located ± 10 mm from the second bolthole along one side of each section (each section is 150 mm long), with each groove 1 mm deep and 50 mm long from one edge to the middle of the plate. The hot junction of the thermocouple was placed centrally in the end of the groove in the middle of the plates between Al and Cu, intersecting with the welding path right in the middle of the pin bottom surface.

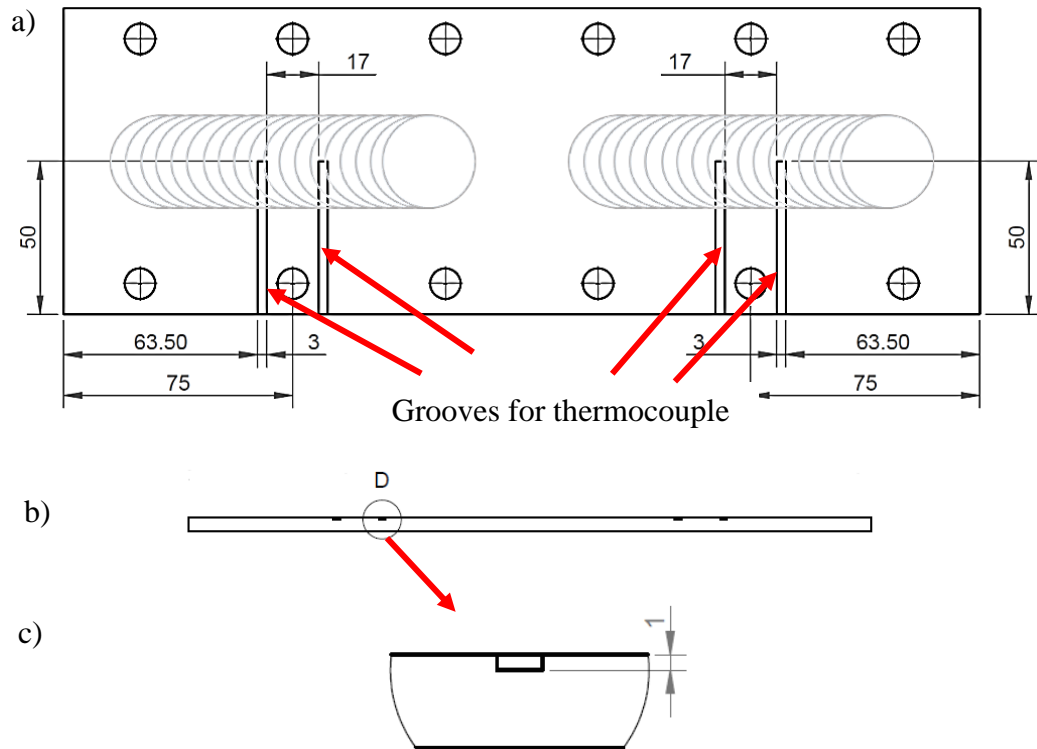


Figure 3 - 18 Plan view and dimension of thermocouple groove in Al plate; (b) Cross section of the plate; (c) Higher magnification details circled and labelled as D in Fig. 3 - 11b showing the groove depths.

Temperature measurements were recorded using a multi-channel USB-2416 data logger (Fig. 3 - 19) with Daqami software from Measurement Computing. A measurement frequency of 50 Hz was used corresponding to a recording rate of 25 measurements in 1 second for each of 2 channels.



Figure 3 - 19 Data logger USB-2416 from Measurement Computing.

3.6 Stop action procedure

In order to study the flow in the lower region of the pin, a quick stop action was employed by manually stopping tool rotation mid process via pressing of the emergency stop button. For metallographic examination purposes, the frozen pin was first cut along the outer periphery of the tool following the black dashed line presented in Figure 3 - 20a, and then along the longitudinal cross section following the red dashed line with the side observed pointed by the red arrow. The cut longitudinal sample was further sectioned in the pin area following black dashed line in figure 3 - 20b.

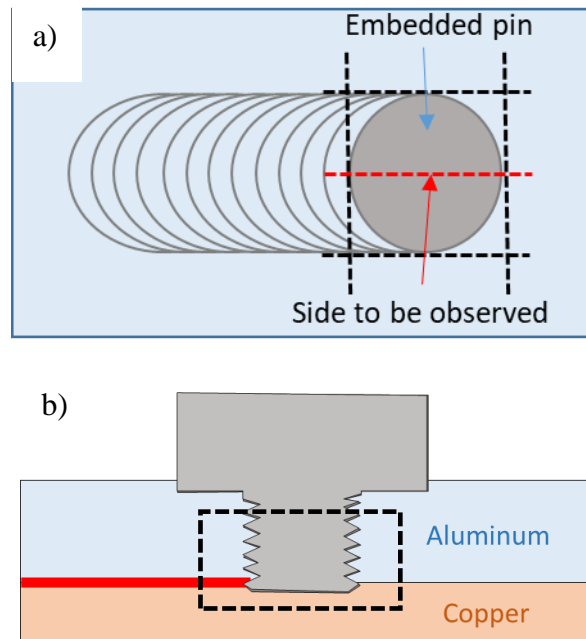


Figure 3 - 20 (a) Plan view of sample cutting schematic; (b) longitudinal cross section of sample cutting schematic.

3.7 Keyhole examination

To further study the flow in the lower area of the pin, the weld's Keyhole, opening remaining in the weld after pin removal, was sectioned as per the schematics in Fig 3 - 21a to d for the; normal left hand threaded, scriber pin, tilted scriber pin and pin without the last thread at the bottom respectively. Four samples were sectioned from the Keyhole produced in the weld with normal left-hand threaded pin. The first sample was taken from the very edge of the key hole and the third sample taken from the cross section of the middle of the keyhole, to study the material flow in the edge and middle of the pin respectively. Samples two and four were taken 2mm before and after sample three as evident from Fig. 3 - 21a. These samples were taken to study the flow in a quarter and three quarter of the pin respectively.

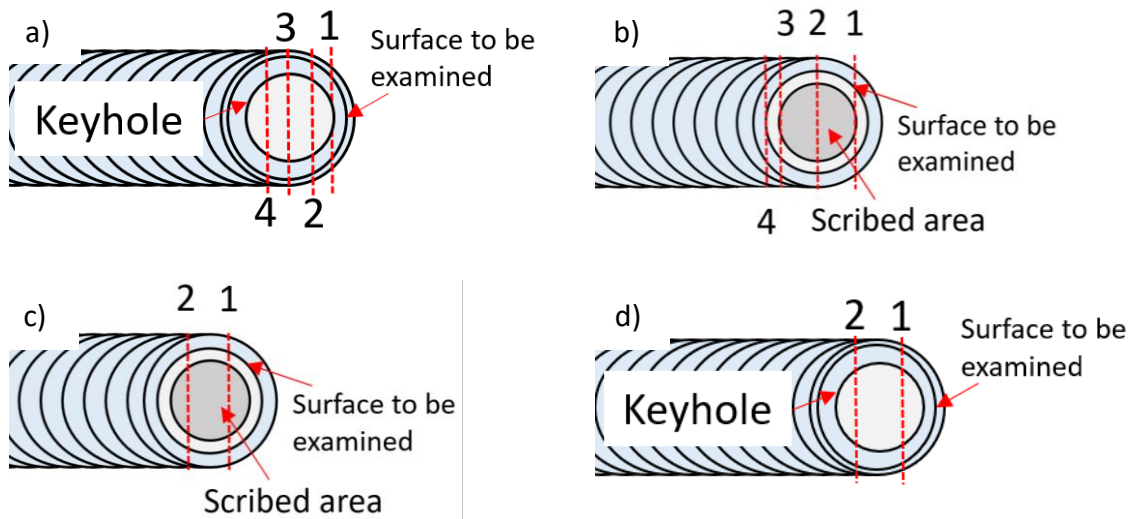


Figure 3 - 21 Keyhole sectioning schematics of welds produced with (a) left-hand threaded pin; (b) scriber pin; (c) tilted scriber pin; (d) pin without the last thread at the bottom.

With respect to the keyhole formed in the weld made using a scriber pin tool (Fig. 3 – 21b), four main samples were sectioned. Sample one and three were taken from the front and rear edge of the scribed area, 2.5 mm from the centre of the keyhole. Whilst, sample two was taken from the middle of the keyhole/scribed area, and sample four taken from the rear edge of the keyhole, 1.5 mm from the scriber area. An additional two samples were taken from the area just outside the keyhole. These two samples were obtained by grinding layer by layer from sample four. These samples represent the flow in the front edge of the scribing zone, middle of the pin, rear edge of the scribing zone and in the rear edge of the pin periphery.

Finally, two sections were sampled from keyholes produced from welds using a tilted scriber pin (Fig. 3 - 21c) and pins without the last thread at its bottom (Fig. 3 - 21d). These two locations were taken from a quarter and three quarter of the keyhole, representing material flow in the front and rear of the pin. The surface facing the direction of tool travel was examined, so that the RS is in the left-hand side and AS in the right-hand side of the image respectively.

3.8 Metallurgical examination and measurement

FSLW samples were sectioned using Electric discharge machining (EDM) for metallurgical examination as to minimise vibration during sectioning, reducing the possibility of intermetallic cracking. The cross section normal to welding direction was selected for metallurgical observation and so samples were hot mounted in a phenolic polymer, ground with silicon carbide abrasive paper rotating disks from 180 to 2400

grit, and finally polished with both a 3 and 1 μm cloth using a TegraPol-25 automatic polishing machine until a mirror like finish. The polished samples were then rinsed and ultrasonically cleaned in ethanol.

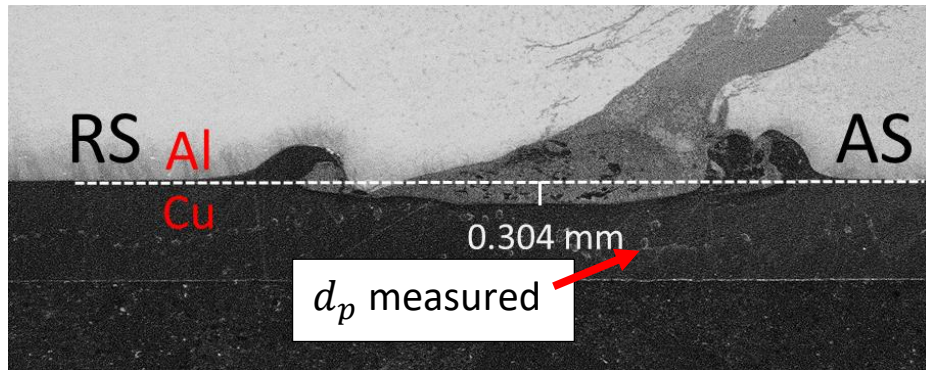


Figure 3 - 22 Method of measuring actual d_p

An Olympus BX51M stereo microscope was used for low magnification macro and microstructure examination imagery. Higher magnification imagery was taken on a FE Hitachi SU-70 scanning electron microscope equipped with electron back scattered diffraction (EBSD) detector. Secondary electron (SE) and Backscattered electron signals (BSE) were used for topography examination as well as for phase differentiation on the weld interface to distinguish the intermetallic layer in the interface without the requirement for chemical etching. EBSD examination was also used for intermetallic determination.

Low magnification images of the lateral cross section of the welded interface were used to measure the actual d_p . As represented in Fig. 3 - 22, images were taken up to the flat region (original unpenetrated Al - Cu interface) outside the stir zone (SZ) in AS and RS on the left and right hand side of the image respectively. A straight line was drawn across the penetrated zone with the original unpenetrated Al - Cu interface used as a basis of the line. In the weld zone a straight perpendicular line was drawn from the deepest weld zone interface to the pre-penetration interface line and measured. This was measured as a d_p of 0.304 mm in the example seen in Fig. 3 - 22 with, all measurements were conducted using ImageJ software.

3.9 Mechanical testing

Mechanical properties were investigated by tensile shear and micro hardness tests for welds used with the sixth tool. Tensile testing was conducted using a Tinius Olsen machine with a constant pulling speed of 3 mm/min. samples used in tensile shear

testing were made in accordance to the schematic in Fig. 3 - 23 with, a support plate used to maintain parallelism of the joint to the loading direction.

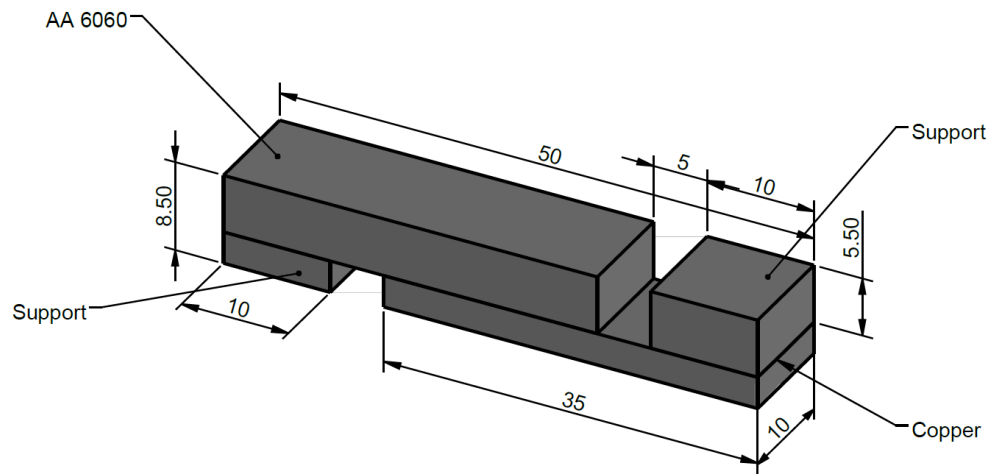


Figure 3 - 23 Shear tensile test sample dimension

Vickers micro hardness tests were conducted to investigate the mixed stir zone (MSZ), interfacial intermetallic layer and composite like structures that were commonly formed in this study. The testing area was narrow, hence tests were performed using an indentation load of 50 gf with a dwell for 10 seconds.

Chapter 4: Effect of welding parameters on interfacial continuity on welds produced using left-hand threaded pin

This chapter discusses the effect of depth of penetration (d_p) and rotational speed (ω) on the weld interface quality, specifically on interfacial continuity on welds that is using conventional left-hand threaded pin. Further analysis to understand the material flow, especially in the bottom area of the pin was then carried out by means of keyhole analysis and stop action method. Analysis on microstructural evolution on the weld stir zone (SZ) was also performed. The purpose of this study is to find the optimum parameter for a close to discontinuity free interface as well as to understand the material flow in the bottom of the pin to be able to further devise conditions in order to achieve discontinuity free weld interface.

4.1 Effect of d_p on interfacial continuity.

Three FSLW experiments were conducted by using tool number one that is concave featureless shoulder with left-hand threaded pin, with welding parameters of $\omega = 1400$ rpm and $v = 40$ mm/min, and three different aims of d_p 's, which are 0.5, 0.3 and 0.2 mm respectively, in order to investigate the effect of d_p on the quality of the weld interface. Welds used in this study were part of preliminary study with travel length of 180 mm. Samples were taken from four different positions to represent starting, middle, and end position. Starting position was taken 2 cm from the starting position, two middle positions were taken 3.5 cm and 7 cm from starting position sample, and end position was taken 3.5 cm from the second middle position. The positions hereafter were designated as P1, P2, P3 and P4 respectively. Due to the preliminary nature of these welds, inaccuracy in the effort of reaching the aimed d_p was experienced. However, these welds were able to reveal important points that will be discussed in following paragraphs. $d_p \approx 0$ mm was not pursued because no joints can be established using this d_p range.

For the first weld, where d_{p-aim} of 0.5 mm were applied, actual measurement of d_p were not equal to initial d_{p-aim} . The measured d_p for P1 - P4 were 0.51, 0.54, 0.62, and 0.55 mm respectively. In all four positions, copper flash hooks were extensively formed and bent towards the middle of the stir zone in retreating side (RS) and advancing side (AS) (Fig. 4 - 1a-b). Except for P1 (Fig 4 - 1a), the formed hooks extend approximately up to two-thirds the length from RS to middle of the weld. In addition, despite of having deeper d_p , more than 0.05 mm if compared to P2 and P4, P2 - P4 have similar copper

RS hooks. It can also be seen in P1 - P4, that there are extensive elongated copper fragments dispersed in the stir zone. The existence of elongated copper fragments close to the tip of copper RS hook in P3 (Fig. 4 - 1c) is suggesting that these elongated copper fragments might be broken off from the elongated RS hooks during the process in the back of the pin. However, the elongated fragments seems to be peeled layer-per-layer under the AS hooks. It is important to point out that cavities were formed in the P1 - P4 stir zones (Fig. 4 - 1a and b), in the Al - Cu interface vicinity, with P2 - P4 (Fig. 4 - 1b to d) having larger cavities than P1 (Fig. 4 - 1a).

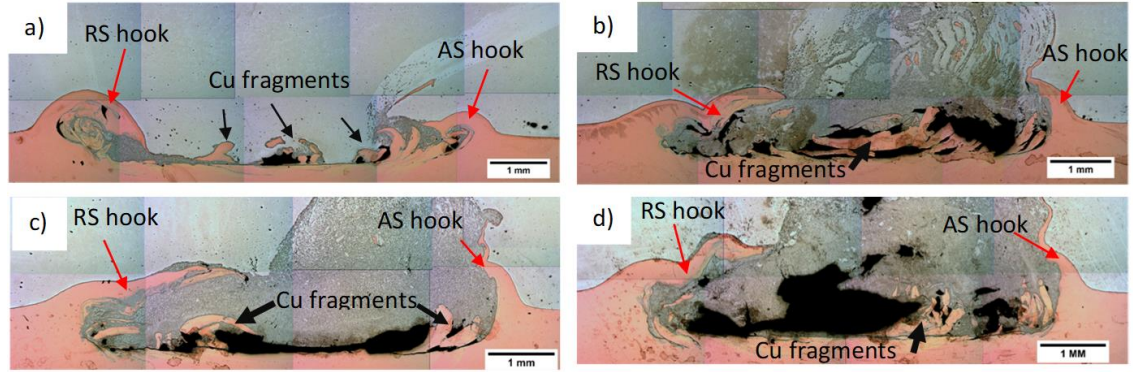


Figure 4 - 1 $d_{p-aim} = 0.5 \text{ mm}$ interface (a) P1 $d_p = 0.51 \text{ mm}$; (b) P2 $d_p = 0.54 \text{ mm}$; (c) P3 $d_p = 0.62 \text{ mm}$; and (d) P4 $d_p = 0.55 \text{ mm}$.

In the second weld with $d_{p-aim} = 0.3 \text{ mm}$, copper RS and AS hooks did not form extensively in P1 (Fig. 4 - 2a) and P2 (Fig. 4 - 2b), with hooks in P1 somewhat curved outwards from the stir zone. Fine fragments can be seen dispersed in the stir zone of P1 and P2. As for P2, having shallower d_p of 0.19, caused the copper fragments dispersing in its stir zone to be coarser than P1 with d_p of 0.3 mm. Unlike previous weld, the extensive fragments seen in Fig. 4 - 2b were dispersed slightly farther from Al - Cu interface. Moreover, no cavities can be seen in these two positions. Copper RS hook in P3 (Fig. 4 - 2c), in a weld with d_p of 0.33 mm, was formed extensively similar to P3 - P4 of the previous weld (Fig. 4 - 1b and c). Despite of the similarity, much lesser amount and size of copper fragments in the stir zone can be seen. Moreover, no cavities are formed in the stir zone. However, more defined Al - Cu interface is suggesting that interfacial crack occurred in this position. In P4, the d_p was slightly deepened to 0.36 mm. But despite of that, it did not produce same or even more extensive copper RS hook, yet, rather short copper RS hook was formed in this position, as well as extensive copper fragments along with cavities in the Al - Cu interface vicinity that can be seen in the stir zone (Fig. 4 - 2d).

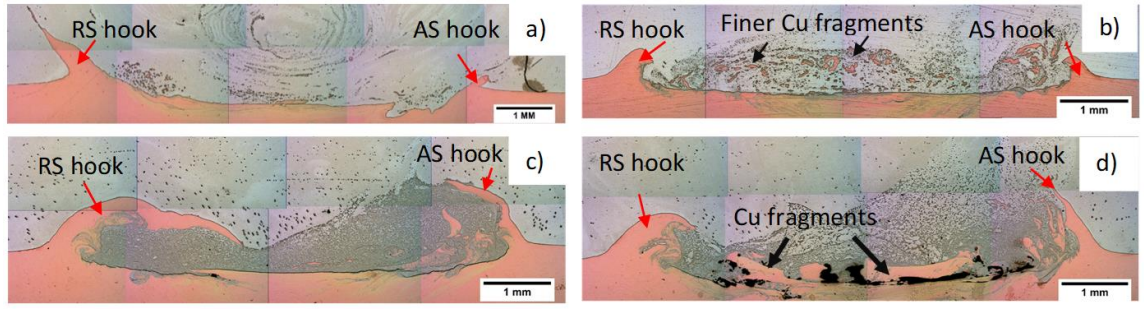


Figure 4 - 2 $d_{p-aim} = 0.3$ mm interface (a) P1 $d_p = 0.29$ mm; (b) P2 $d_p = 0.19$ mm; (c) P3 $d_p = 0.33$ mm; and (d) P4 $d_p = 0.36$ mm

In welding with d_{p-aim} of 0.3 mm, the actual d_p of P1 - P4 are 0.20, 0.23, 0.27, and 0.34 mm respectively. Copper RS and AS hooks in P1 - P3, as can be seen in Fig. 4 - 3a to c, are not extensive and bent away from the stir zone. Little amount of fine copper fragments can be seen dispersing in the stir zone and no cavities can be seen forming in the stir zone, specifically in the Al - Cu interface vicinity. In P4, where the d_p went deeper to 0.34 mm, the copper RS hooks were extensively formed, similar to P3 from previous weld (Fig 4 - 2c). Again, similar to P3 from previous weld, no large cavities and defined Al - Cu interface can also be found in this weld (Fig. 4 - 3d).

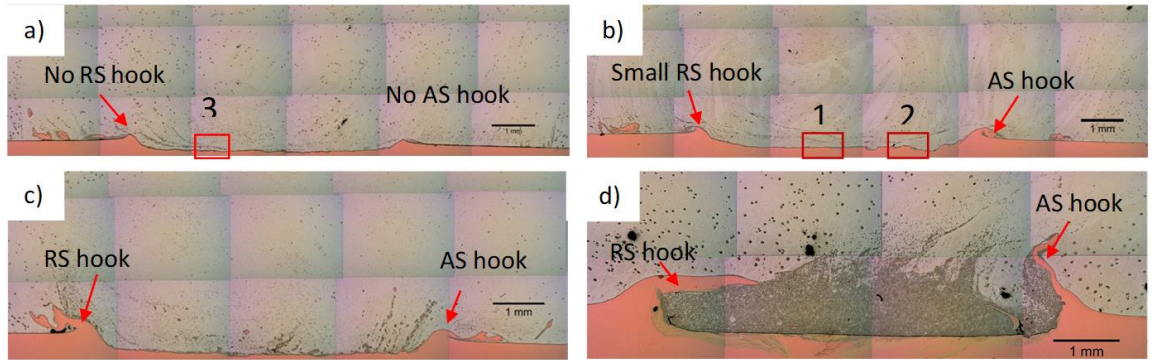


Figure 4 - 3 $d_{p-aim} = 0.2$ mm interface (a) P1 $d_p = 0.15$ mm (area 3 will be discussed in chapter 4.4); (b) P2 $d_p = 0.23$ mm (area 1 and 2 will be examined and discussed in chapter 4.2 and 4.4); (c) P3 $d_p = 0.27$ mm; and (d) P4 $d_p = 0.34$ mm.

Observation on the weld interface using tool number one, emphasizing on left-hand threaded pin, and on the relation of d_p to the quality of Al - Cu interface can be summarized as follows:

- In d_p with range < 0.3 mm, hook is small, with very low to none cavities (particularly good if $d_p \leq 0.2$ mm). In this range of d_p , copper RS and AS hooks fold in the opposite side from the stir zone. Cu hooks are not formed extensive enough to be able to be folded by the aluminium flow coming from RS to AS behind the pin.

- In d_p with range 0.3 - 0.36 mm, as a response of deeper pin penetration into the bottom copper plate, copper RS and hook can be formed extensively and be driven to hook into the stir zone by the aluminium flow coming from RS to AS behind the pin. However, when d_p reached 0.36 mm, the copper RS hook started to break into extensive elongated copper fragments and flowed into the stir zone. When this happens, cavities formation is possible.
- In $d_p \geq 0.5$ mm, it can be seen that weld with $d_p = 0.5$ mm (Fig. 4 - 1a) has rather similar feature as weld with $d_p = 0.36$ mm (Fig. 4 - 2d), which implying that weld with d_p range of 0.36 - 0.50 might have similar interfacial morphology. As the d_p increase to 0.54 mm, again, the extensive forming of copper RS hook was happened as well as the breaking of the extensive RS hook into elongated copper fragments which then deposited in the stir zone, more specifically in the vicinity of Al - Cu interface. In this range of d_p , cavities can be formed extensively.
- Extensive copper hooks along with big extensive copper fragments are responsible for the cavities formation that is by blocking the aluminium to flow to Al - Cu interface. However, it was shown that elongated copper fragments have more impact on aluminium blockage as shown in P3 in weld with $d_{p-aim} = 0.3$ mm (Fig. 4 - 2c), and in P4 in weld with $d_{p-aim} = 0.2$ mm (Fig. 4 - 3d), where these interfaces have extensive RS hook without the formation of big elongated copper fragments, despite of the cracked Al - Cu interface.
- Al - Cu interfacial continuity is more likely to be achieved by using d_p range of 0.15 - 0.29 mm.

Several range of d_p in all preliminary results tend to have distinct features; the value of d_p will be considered as a representation of a weld with d_p as designated constant.

Optimum d_p can be represented by Fig. 4 - 1b and Fig. 4 - 3b for high and low (adequate) d_p namely 0.54 and 0.23 mm respectively. For high d_p , as shown in Fig. 4 - 1b, large Cu pieces along with flash curved towards the stir zone, blocking the material flow. As a result, cavities were formed in the interface region. Using lower d_p values, close to discontinuity free interface could be achieved. Small Cu particles are present in the stir zone and the flash curves outward (Fig. 4 - 3b). This clearly shows that there was no blockage toward the flow of material that flowed to the interface during welding, although there was some localized interfacial intermetallic cracking occurred (Fig. 4 - 4d). It is shown that there are around 8 μm thick of intermetallic layers formed

in the interface shown in Fig. 4 - 4b. A layer of irregular shape blocky particles can also be seen dispersing in the stir zone, which has grown between the Al grains (Fig. 4 - 4a).

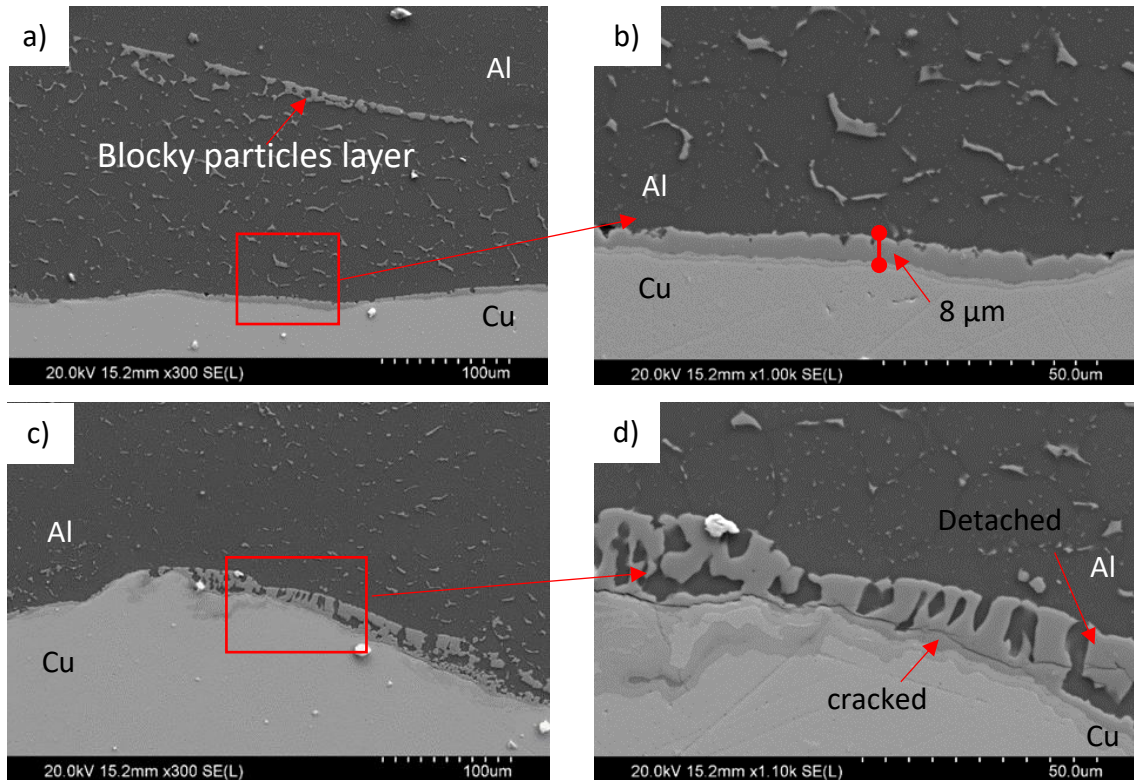


Figure 4 - 4 SEM image of typical interface of the weld in Fig. 4 - 3b (a) Area 1 in figure 4 - 3b; (b) Magnification of the boxed area in Fig. 4 - 4a; (c) Area 2 in figure 4 - 3b; (d) Magnification of the boxed area in Fig. 4 - 4b.

Higher magnification of the interface can be seen in Fig 4 - 4b. There are blocks of particles “dispersed” in the stir zone and it seems to form in a network manner in Al grain boundaries, while the layers, right at the interface, seem to have been sheared. On the other hand, Fig. 4 - 4c shows the blocky intermetallic formed in the Al - Cu interface. Higher magnification of these blocky interface can be seen in Fig. 4 - 4d. It is shown that these blocky particles are cracked and detached from the interface. From Chen et al. [59], it is known that material will still flow from RS to AS behind the pin. This continuous aluminium flow may exert a sufficiently high shear stress to the intermetallic layer, cracking the layer. A cracked layer may be further pushed away by the flow. This may be the reason for the “dispersed” particles in the stir zone. Further discussion on the formation of dispersed blocky particles will be discussed in chapter 4.5.

To identify the composition of the dispersed material and to ensure whether the dispersed particle is the same material as the outer interfacial intermetallic layer

(adjacent to aluminium), first, EDS examination on the dispersed particle and outer interfacial intermetallic layer was conducted and followed by EBSD examination. In EDS examination, first we look at BE image in Fig 4 - 5. Same shade of grey colour indicates that dispersed intermetallic particles are the same with the outer layer, which adjacent to Al. Note that the darkest shade of grey is aluminium. Then, EDS beams were shot in the outer layer intermetallic and followed by a shot done toward the dispersed particle. Result can be seen in table 4-1, where atomic percentage of Al and Cu in outer layer intermetallic are 55.74 % and 44.26 % in atomic percentage respectively, while dispersed particle intermetallic are 57.84 % and 42.16 % in atomic percentage (as indicated in Tan et al. [86] work as well) respectively. This result was situated between Al_2Cu and AlCu region as shown with shaded grey area Al - Cu binary diagram in Fig. 4 - 6. However, due to the limited test area, $< 5 \mu\text{m}$, the vicinity of the test area might be detected as well. Thus, reducing the accuracy of the result.

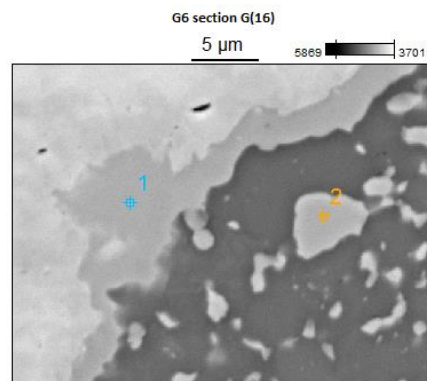


Figure 4 - 5 EDS examination on intermetallic layer and dispersed intermetallic pieces.

Table 4 - 1 Chemical composition in atomic % of EDS displayed in Fig. 4 - 5.

Atom %	Al	Cu
pt1 (outer layer)	55.74	44.26
pt2 (dispersed particle)	57.84	42.16

More accurate examination was then conducted using electron backscattered diffraction (EBSD). Multiple shots were conducted starting from the dispersed intermetallic particle to the outer layer intermetallic (Fig 4 - 7a). Point 1 and 22 were taken to represent the comparison. Point 1 (Fig. 4 - 7b to d) and 22 (Fig. 4 - 7e to g) were identified as khatyrkite, which is the mineral name for Al_2Cu [122]. It was confirmed that the outer layer, as shown in several previous FSW works [33], [78], [86], [123], and the dispersed particle intermetallic are the same, which is Al_2Cu .

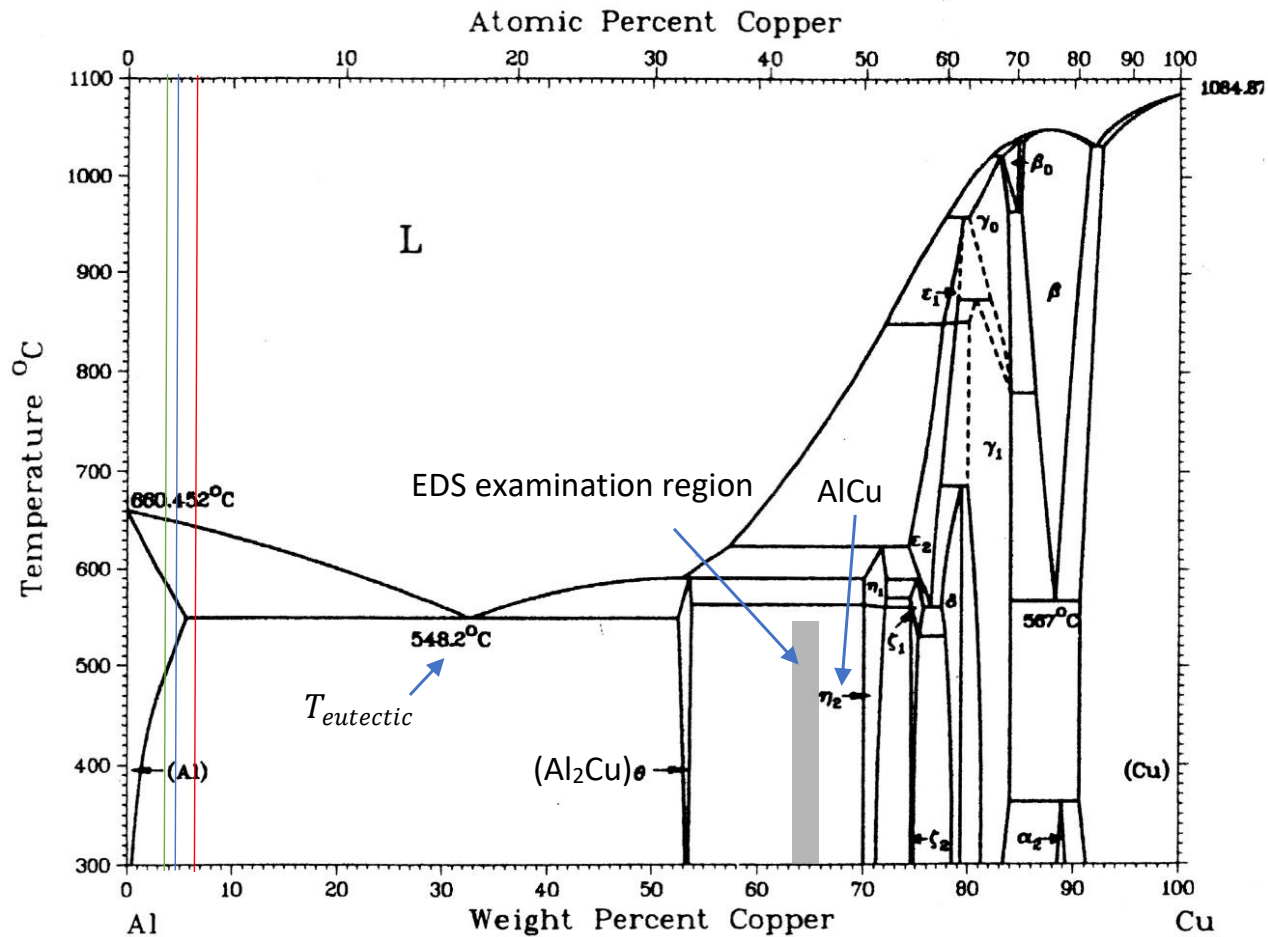


Figure 4 - 6 Al - Cu binary phase diagram.[124]

4.2 Effect of rotational speed (ω) on interfacial continuity

Despite the weld in Fig. 4 - 3b is having near discontinuity free interface; the interfacial layer is too thick. It is known that the optimum interfacial intermetallic in order to be able to withstand external force without breaking is 2.5 μm . A thicker interfacial intermetallic than that will cause it to experience brittle fracture through itself [28], [33]. Therefore, it becomes a necessity to find an optimum parameter that produces a discontinuity free interface with thinner interfacial intermetallic layer. Based on the previous observations, further experiments were then conducted to study the effect of ω on achieving discontinuity free FSLW interface using d_p that aimed at 0.2 mm. However, for operational simplification, a second tool namely scroll shoulder with left hand threaded pin, was used for this study.

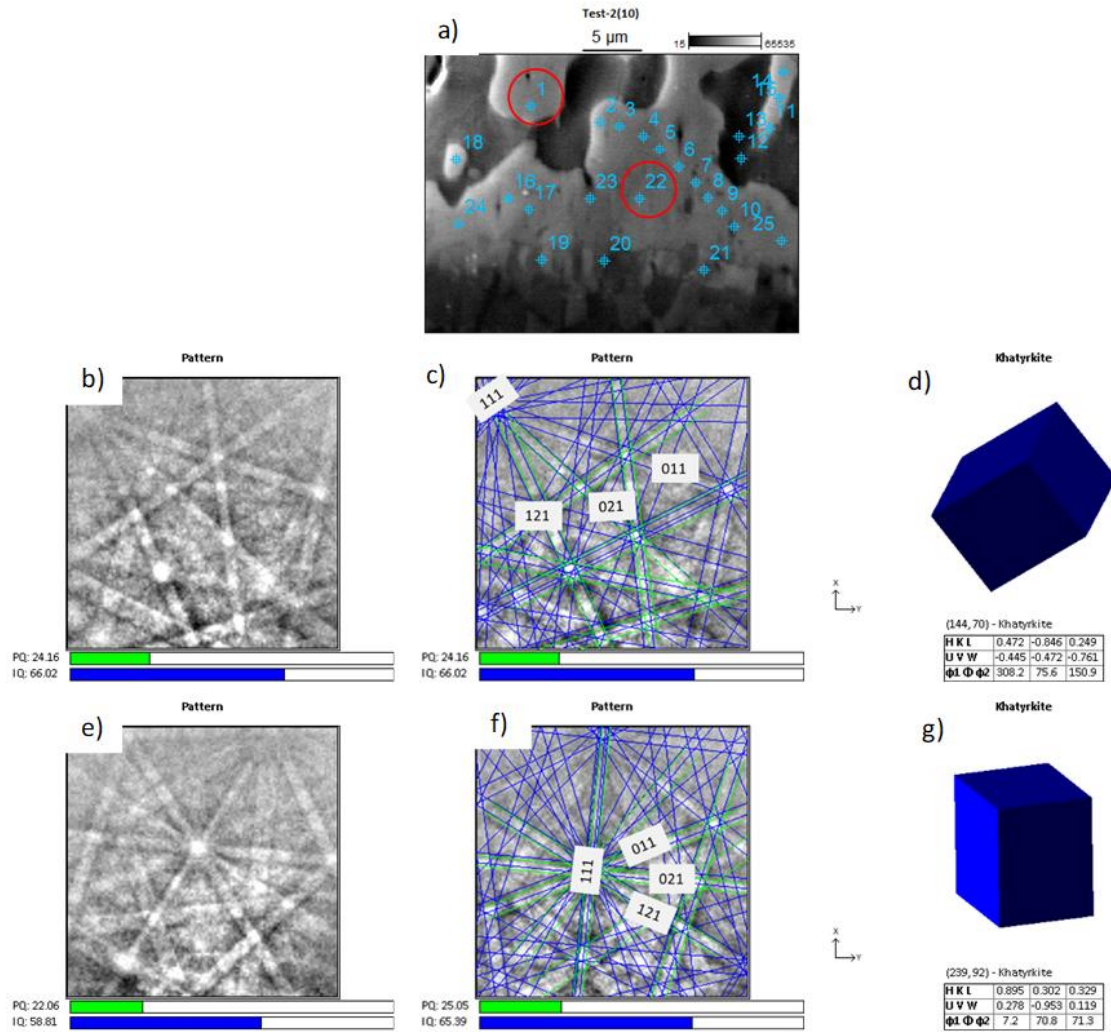


Figure 4 - 7 (a) SEM image of area taken for EBSD examination; (b) and (e) patterns obtained for point 1 and 22 respectively; (c) and (f) pattern analysis; (d) and (g) analysis results.

In welding with $\omega = 500$ rpm and $v = 56$ mm/min, no voids and no big Cu particles are present in the stir zone (Fig. 4 - 8a). However, higher magnification of various typical interfaces of this weld, as shown in Fig. 4 - 8b to d, shows that aluminium was not joined to the reaction zone in the bottom of the pin. The separated surfaces of aluminium and copper facing one and another were not matching. This dismissed the occurrence of intermetallic layer brittle fracture. There are different shades of grey showed in BE image implying that once upon a time during the process, aluminium reached copper, and mixed to form a mixed stir zone (MSZ). This mixture will then, with the help of frictional heat, be reacted and turned into intercalated layers of aluminium, copper and intermetallic MSZ near the separated aluminium and copper. In addition, in Fig. 4 - 8d, there are some aluminium left in the bottom zone just above MSZ, suggesting that intermetallic shearing by aluminium down flow occurred right

after or simultaneously with the formation of MSZ. However, it might not completely sheared the aluminium off. When the last stream of aluminium down flow reached the sheared surface, last coming aluminium was probably not able to reach the reaction zone or it just slightly grazed the reaction zone, thus failed to force the joining with the previously sheared copper surface and resulting in gapping interface as seen in Fig. 4 - 8b to d.

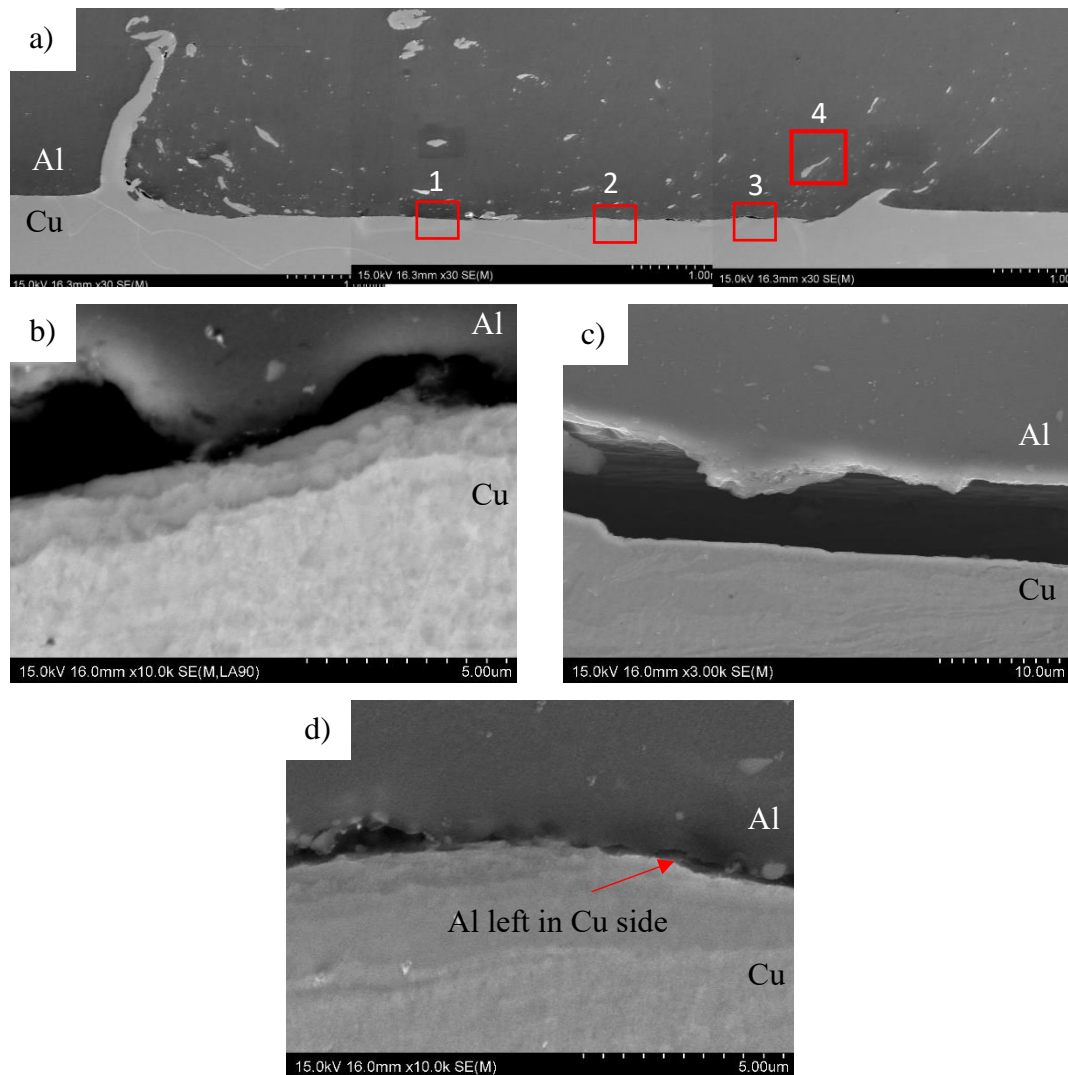


Figure 4 - 8 SEM micrograph weld made by second tool with $\omega = 500$ rpm, $v = 56$ mm/min (a) Transversal cross section of the weld interface; BE image of typical weld interface showed in area (b) 1; (c) 2; and (d) 3 in a.

Similar joining difficulties also occurred in welding with $\omega = 710$ rpm and $v = 56$ mm/min. The whole transversal cross section of the weld can be seen in Fig. 4 - 9a. Fig. 4 - 9b and d are the typical interface of this weld. Fig. 4 - 9c, enlarged area in Fig. 4 - 9b marked by 1, shows that the MSZ intermetallic in copper side is sheared. Aluminium

left in this area that was separated from the aluminium above implies that the same mechanism as in previous weld occurred in this weld as well. However, the absence of gapping interface suggests that aluminium down flow in this weld have more fluidity, which enables it to reach the bottom of the pin copper surface. The existence of aluminium layer that is not joined into aluminium stir zone above and MSZ intermetallic in copper side below is suggesting that series of aluminium flow have occurred. However, in some area the last flow cannot reach the sheared copper surface, leaving a layer of aluminium in between as can be seen in Fig. 4 - 9c. Another typical interface of this weld showed a cracked like interface (Fig. 4 - 9d). However, higher magnification of the marked area 2 in Fig. 4 - 9d showed that separated aluminium - intermetallic MSZ interface was not matched with the previous weld. Enlarged interface is given in Fig. 4 - 9e. It can be seen that the copper side surface is rather irregular. On the contrary, aluminium side is rather flat. This implies that although the aluminium down flow is more fluid than the previous weld, it still cannot fill the crevices in the irregular surface.

The next FSLW condition is $\omega = 1000$ rpm and $v = 56$ mm/min, Fig. 4 - 10a shows that continuous interface could be achieved. Typical interfaces of this weld can be seen in Fig. 4 - 10b to d. The first interface type, as shown in Fig. 4 - 10b, does not have extensive interfacial intermetallic. In copper side, MSZ intermetallic was formed and indicated by different shades of grey in BE image, which means different compounds exist in copper near Al - Cu interface. In second type, Fig. 4 - 10c, there are three layers formed in the interface. The outer most layer was able to extensively grow outward toward aluminium. This indicates that Al down flow was able to force the joining of aluminium to the copper surface, allowing the layer to continue to grow. In some area, the intermetallic formed was very thick, as shown in Fig. 4 - 10d. This is the result of coming from the thick MSZ that was completely transformed into intermetallic due to excessive frictional heat. The existence of grainy structure with same colour with the fully converted MSZ is suggesting that the thick intermetallic was formed first by the densely dispersed Al_2Cu intermetallic particle, which deposited near MSZ by the down flow, become denser and at one point turned completely into thick intermetallic layer as seen in the right-hand side of Fig. 4 - 10d. Micro hardness test on fully converted intermetallic area showed that this structure has hardness of HV 507. This is significantly harder than copper and aluminium base metal, which are HV 79 and 60 respectively, thus exhibiting the brittle nature of the welded interface, Al_2Cu in

particular. In aluminium side, a quite dense intermetallic particle can be seen dispersing in the stir zone (Fig. 4 - 10e).

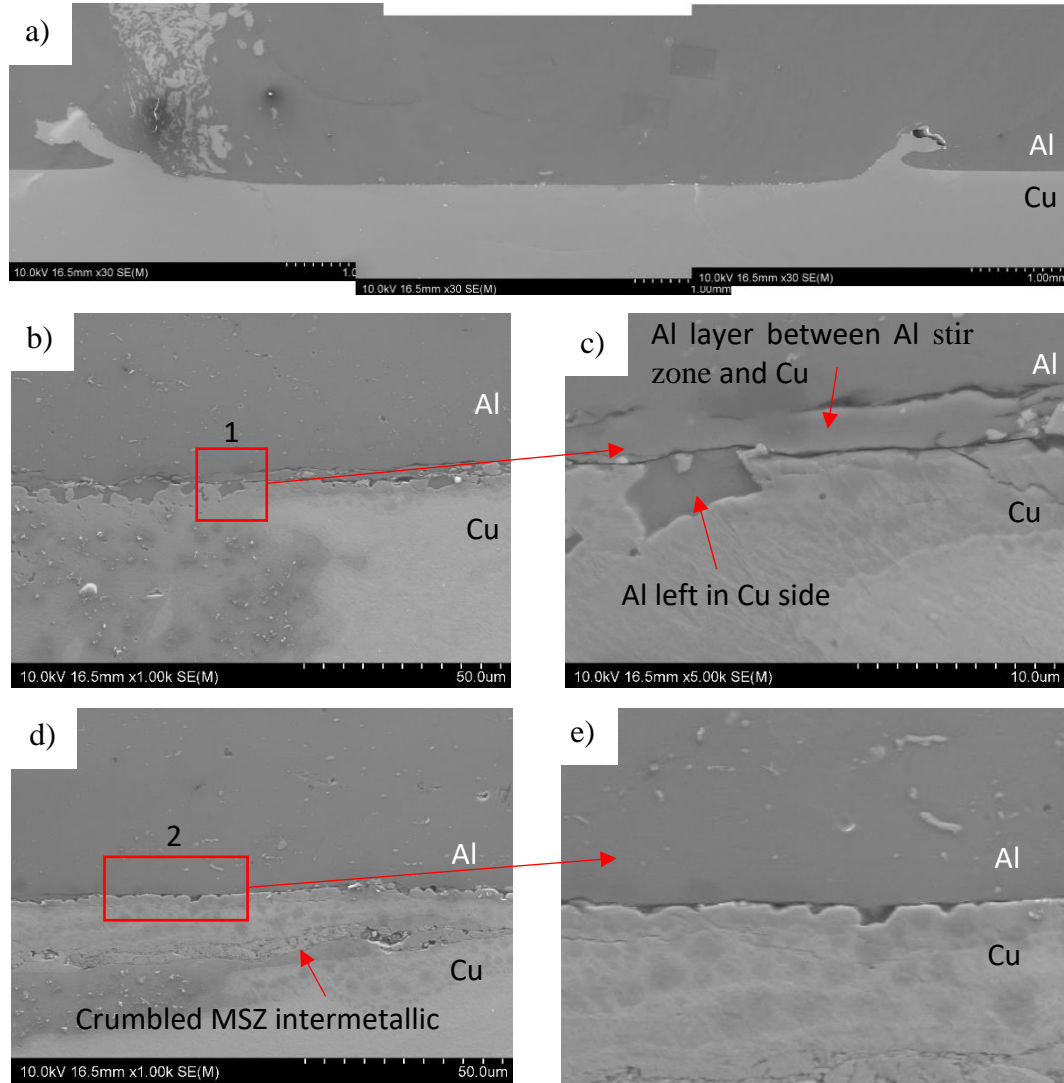


Figure 4 - 9 SEM micrograph weld made by second tool with $\omega = 710$ rpm and $v = 56$ mm/min, (a) Transversal cross section of the weld interface; (b) typical weld interface; (c) magnified area 1 in b; (d) another typical interface with another layer of crumbled intermetallic below the Al - Cu interface; and (e) enlarged interface of area 2 in d.

For the weld made using the highest ω of 1400 rpm, voids are present in stir zone (Fig. 4 - 11a). Typical interface of the weld showed cracked interface; it can be seen in Fig. 4 - 11b. Examination using higher magnification as shown in Fig. 4 - 11c reveals that the majority of the cracked interface have propagated between the Al_2Cu and two inner layers, which is AlCu in particular. This is also in accordance with previous studies [33], [125]. Moreover, Moreno et al. [126] in their study stated that Al_2Cu and AlCu have low interfacial strength as a result of their difference in lattice structure, where Al_2Cu being tetragonal and AlCu being monoclinic and orthorhombic. The mechanism

of intermetallic layer formation is the same with the previous parameter. However, judging from the crack morphology, it was not caused by the shear flow associated with the down flow. This is because the outer layer that adjacent to aluminium, seems to have grown extensively at one point. It is possible that the layer cracked during sample preparation. During welding, melting has occurred in the stir zone as suggested by the presence of eutectic structures in Fig. 4 - 11d. Melting could be a reason for voids formation, although in this work this has not been studied further.

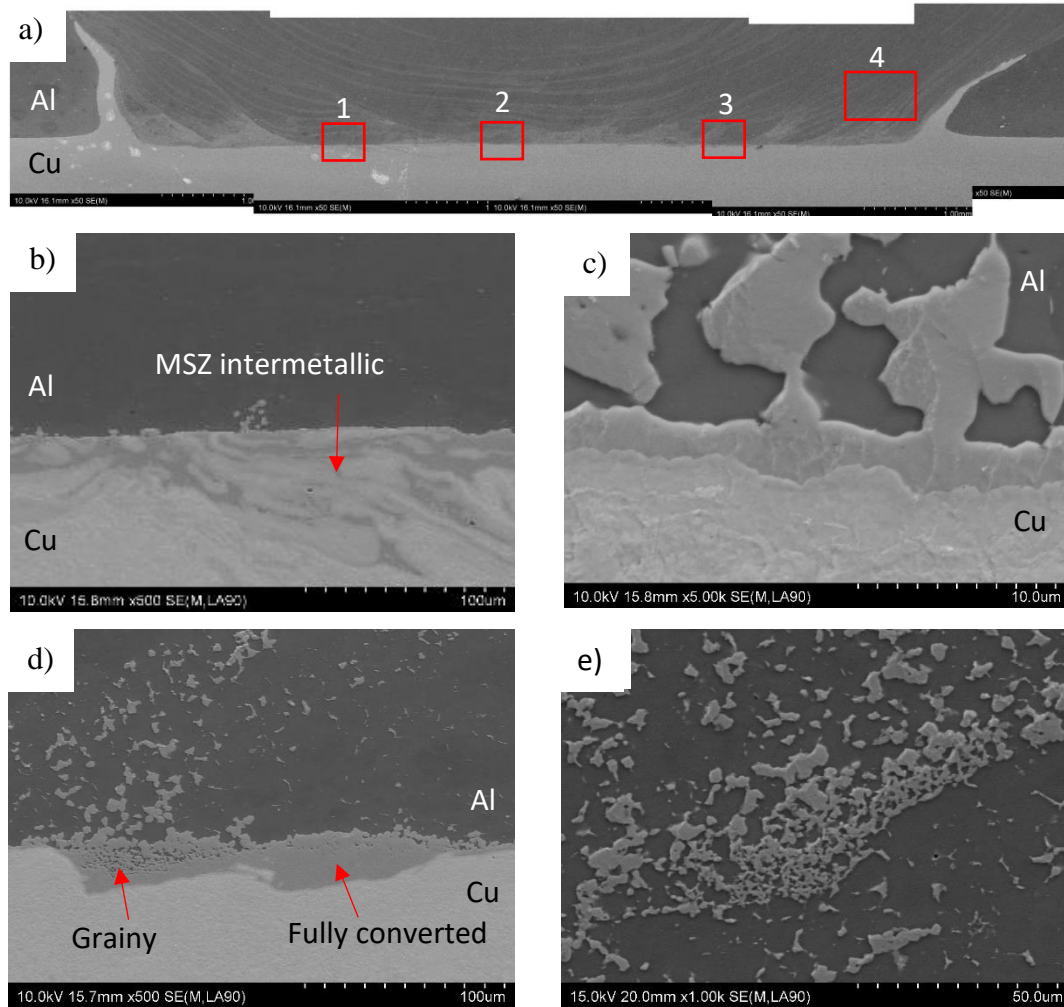


Figure 4 - 10 SEM micrograph weld made by second tool with $\omega = 1000$ rpm and $v = 56$ mm/min (a) Transversal cross section of the weld interface; Typical weld interface shown in area (b) 1; (c) 2; and (d) 3 in a; and (e) intermetallics dispersed in stir zone are shown in area 4 in a.

Now we examine welding temperature history and relate them to the microstructural features explained in previous sections. In this study, v used was 56 mm/min (just under 1 s for the pin to travel for 1 mm). This means there is one point in a FSLW weldment (in this case, thermocouple hot junction) was rubbing against the pin bottom for 8 s. As the pin travelled pass the point, the temperature increased and reached the peak right

before the pin leaves the point. Temperature peaks for 500, 710, 1000, and 1400 rpm were 440, 490, 580, and 590 °C respectively (Fig. 4 - 12). Temperature record for 500 rpm welding was not synchronized due to a difference in scan frequency. This rise in welding temperature with the increase in ω confirmed the work by Cui et al. [68] who analysed Upadhyay and Reynold's [127] study and formulated it as follows:

$$T = T_0 + T_f(1 - e^{-q\omega}) \quad \text{Eq. 11}$$

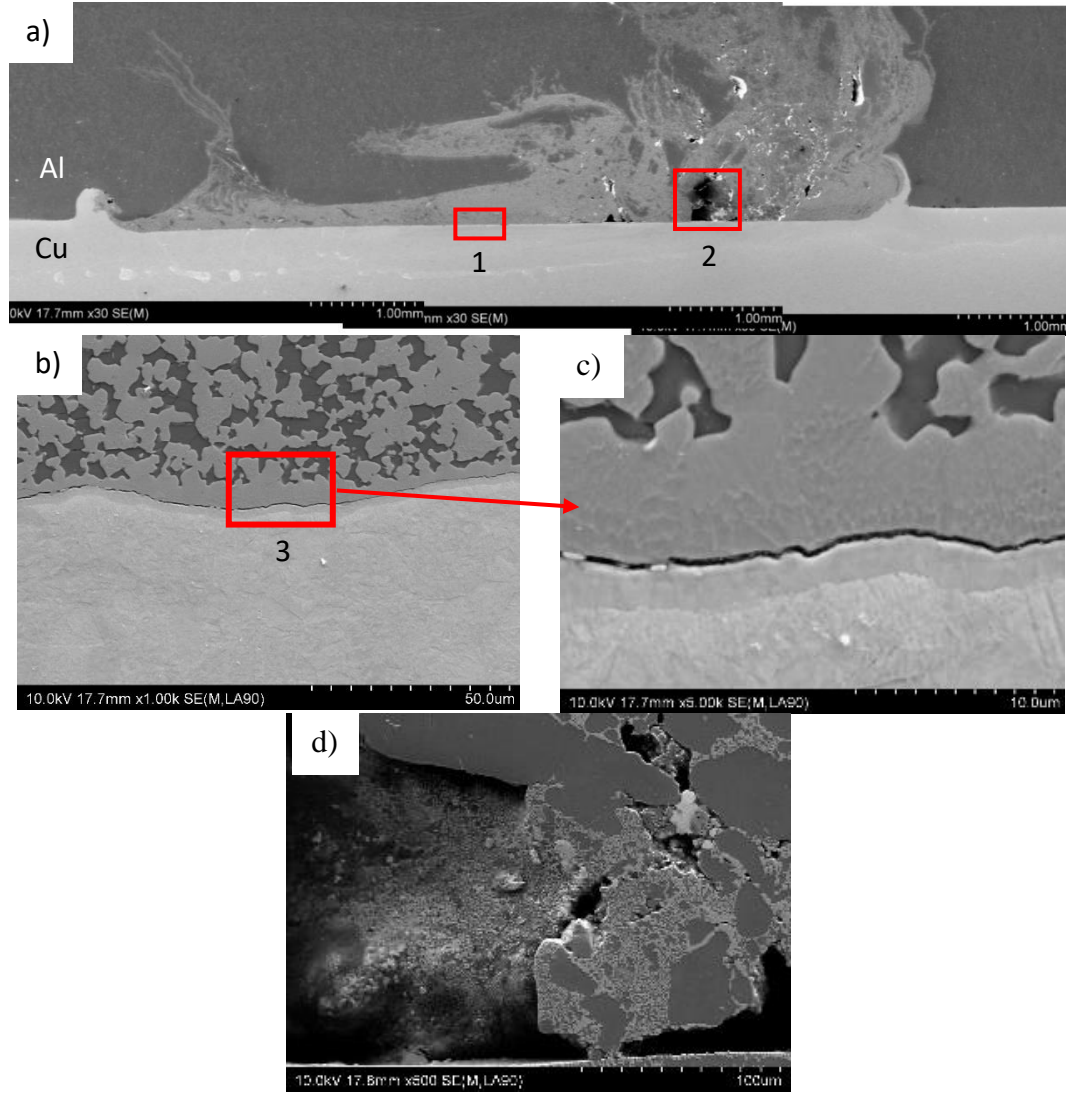


Figure 4 - 11 SEM micrograph weld made by second tool with $\omega = 1400$ rpm and $v = 56$ mm/min (a) Transversal cross section of the weld interface; (b) Typical weld interface showed in area 1 in a; (c) magnified area 3 in b; and (d) area 2 in a.

Referring to the phenomenon of stir flow and re-welding, again from Cui et al. [68], with higher temperature the flow stress (σ) of the stirred material will be lower. This relation can be seen equation 12. Furthermore, flow stress of the stirred material will decrease and converge as the temperature is increasing towards the melting. Which means as the temperature rises, it will be easier for the stir zone material to flow

downward and to fill spaces. Furthermore, both peak temperatures for 1000 and 1400 rpm welding were above Al-Cu eutectic point (548 °C). This means that there is a possibility that the down flow stream behind the pin for this welding has a little part of molten state. The presence of eutectic structure in the stir zone supports this theory.

$$\sigma = \alpha^{-1} \sinh^{-1} \left\{ \left(A^{-1} \dot{\epsilon} \exp(Q/RT) \right)^{1/n} \right\} \quad \text{Eq. 12}$$

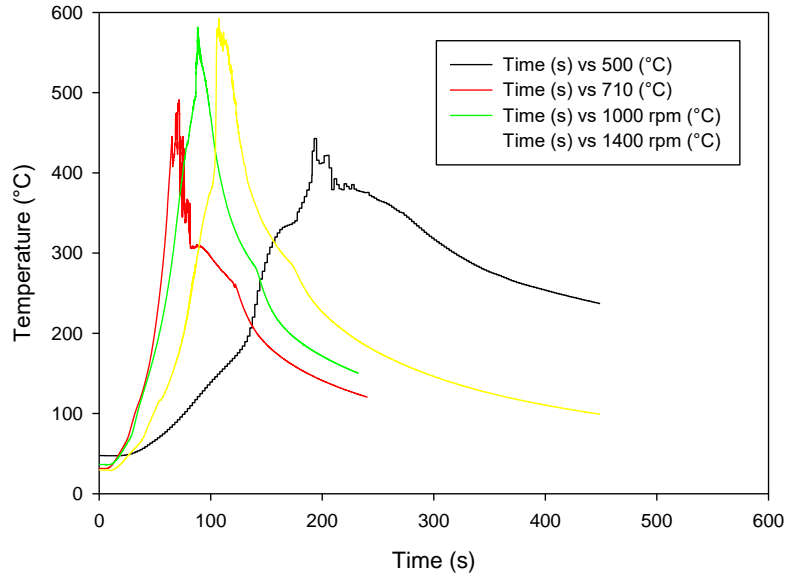


Figure 4 - 12 Temperature History.

4.3 Flow analysis on the vicinity of pin bottom zone during FSLW

It was found that in order to avoid hooking defect and more likely to achieve near continuous weld interface, 0.15 - 0.29 mm should be used as the d_p . However, such range is very narrow. Better understanding of the flow in the lower area of the pin is needed in order to find ways to expand the d_p range while avoiding the formation of RS copper hook that could lead to formation of interfacial discontinuities in the form of cavities.

For that purpose, keyhole in the end of weld in Fig. 4 - 3 was examined. As described in section 3.8, four samples were taken to portray the material flow as the pin traverses through during process. Analysis was emphasized on the lower region of the interface. The weld interface in Fig. 4 - 3d is right behind the keyhole that is examined in this section. Therefore, what is described in this analysis is the formation of the said interface.

Sample 1 represents the phenomenon happened when pin started to interact with the original Al - Cu interface. It can be seen in Fig. 4 - 13a that copper flash in RS and AS already were extended upward for about 1.8 mm. This raise of copper flash is a compensation for pin penetration that occupying a certain volume at copper surface. The empty region in between the raised copper flash is the region occupied by the pin. Higher magnification in Fig. 4 - 13b shows that copper fragments exist above the copper flashes, in the saw tooth structure. The saw tooth structure is most likely formed by material movement from AS to RS and driven by the rotating left hand threaded pin. Note that sample 1 is in the front half of the pin, whereas the material movement is from AS to RS. This implies that there are mechanisms that cause the fragmentation of copper in top of both flashes and recirculation flow that bring the fragments upward as far as the shoulder flow zone as shown in 4 - 13d. These fragments were flown further to the shoulder flow zone (Fig. 4 - 13e) indicating that there is a recirculation flow in the opposite direction to the aluminium flow inside and around the pin threads.

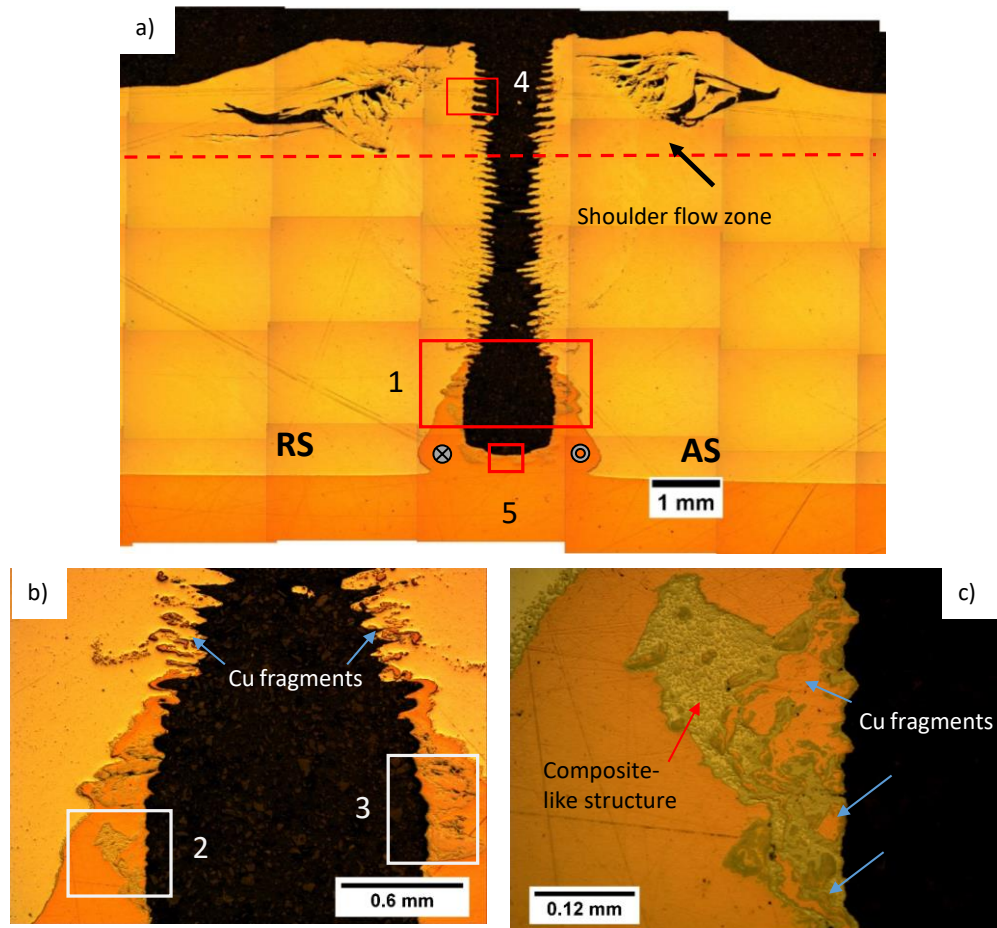


Figure 4 - 13 (a) Edge of the keyhole transversal cross section (sample 1); (b) Position 1 in a; (c) Position 2 in b; (d) Position 3 in b; (e) Position 4 in a; (f) Position 5 in a.

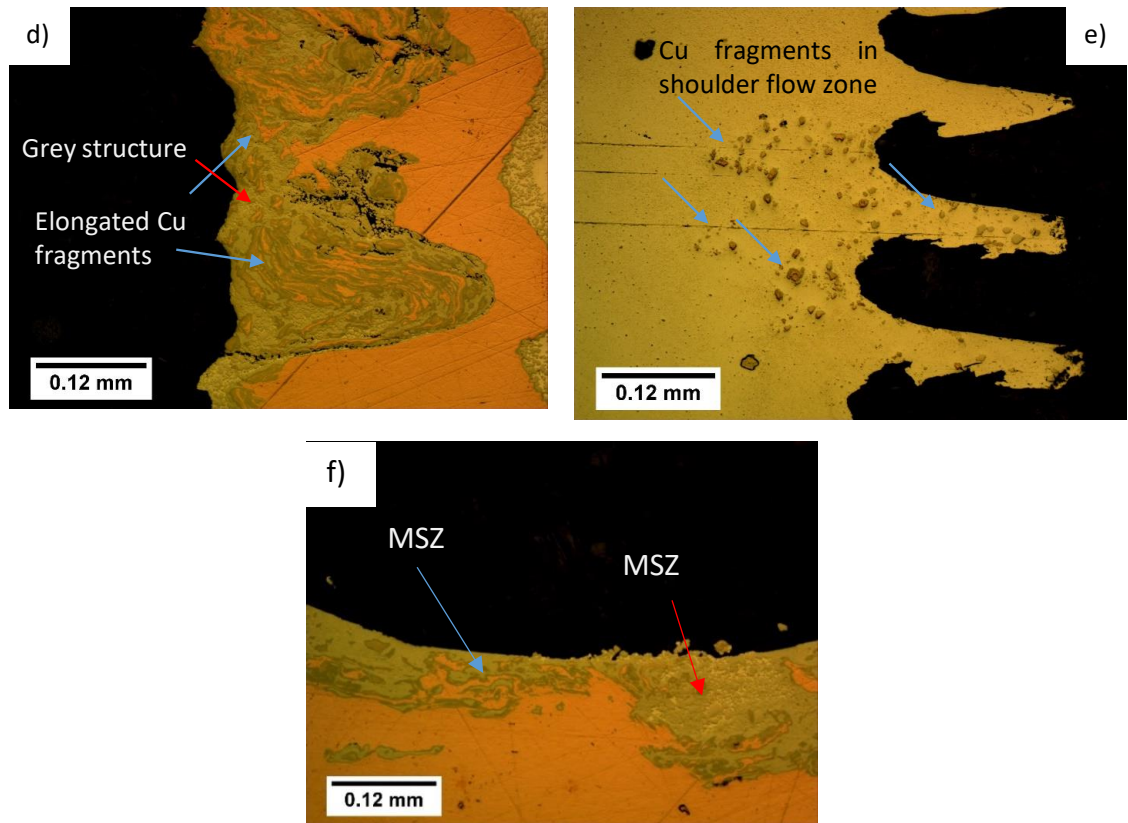


Figure 4 - 13 Continued.

Further examination on the inside of the copper flashes can be seen in Fig. 4 - 13c and d showing area 2 and 3 in Fig. 4 - 13b, which are the inside of flashes on RS and AS respectively. It can be seen in Fig 4 - 13c that there are copper fragments (indicated by blue arrow), tangerine coloured, and grey coloured grainy structures that are rich in Al - Cu intermetallic phase, which dispersed in aluminium matrix (yellowish in colour), and formed composite-like structure (indicated by red arrow). While in Fig 4 - 13d, smaller elongated copper particles were intercalated (indicated by blue arrow) in same grey coloured structure (indicated by red arrow). Similar structures can be seen in other works [75], [76], [79], [83], [86], [89]–[92], [128]. This implies that once upon a time, the inside of the hook filed with aluminium and the aluminium shred the inside wall of the flash as it travel from AS to RS and downward in a ring vortex flow driven by the pin.

In the base of the raised copper region, Fig. 4 - 13f, intercalated and composite like structures can be seen to form more than 0.1 mm deep. The presence of this rather thick mixture of aluminium, copper and Al - Cu intermetallic implies that significant amount of aluminium was driven to this region, mixed with copper and formed these structures

which also known as MSZ. This strongly confirm the existence of vertical downward flow induced by the left hand thread as suggested by Schneider et al. [51], [56].

Sample 2 (Fig. 4 - 14a) depicts the flow in a quarter of the pin during process. In figure 4 - 14a it can be seen that copper flash hooks extend way up as far as approximately 2 mm and 1.6 mm for RS and AS flashes respectively. The void area in between flashes is wider than previous sample due to more volume of pin occupied this area. Morphology of RS flash is wavy in structure (Fig. 4 - 14b). Higher magnification in Fig 4 - 13d shows that there is a lining of composite-like structure containing grey particle (pointed by blue arrow) with some elongated copper fragments (pointed by red arrow) in aluminium matrix as seen in RS flash in previous sample in Fig. 4 - 13c, which is especially thick in the curved part. As for AS flash (Fig. 4 - 14c), the morphology is not as wavy as RS flash and thicker than RS flash. Also, there is a quiet similar lining to RS flash. However, the matrix where copper fragments situated is grey in colour, similar with grey particle dispersed in composite like structure in RS flash (Fig. 4 - 14e). This indicates that the aluminium matrix have been fully converted into similar compound as the dispersed grey particles in RS composite like structure lining. Note that from section 4.2 it is known that the dispersed particles in the stir zone is Al_2Cu . Furthermore, it is implied that the grey matrix is most likely formed by dense Al_2Cu particles dispersed in aluminium matrix that grew over time converting aluminium matrix into Al_2Cu . The conversion was driven by high temperature from frictional heat between aluminium and copper supplied from the matrix itself and copper fragments. Further analysis on the formation of dispersed Al_2Cu particles will be discussed in section 4.5. In the copper surface between RS and AS flashes inside the area that was occupied by the pin (Fig. 4 - 14f and g), MSZ that consists of copper intercalation on Al_2Cu matrix was formed, similar to figure 4 - 13f. This also confirms the existence of aluminium down flow that drove aluminium downward even further to the bottom of the pin and mixed it with copper to form MSZ. However, this contradicts to the observation in the work of Liu et al. [129]. In their work, they found that no stirring below the pin could be seen. However, since same material is used (Al 6005 - T6), it is impossible to determine the occurrence of material mixing, moreover the origin of material, whether form top or bottom plate.

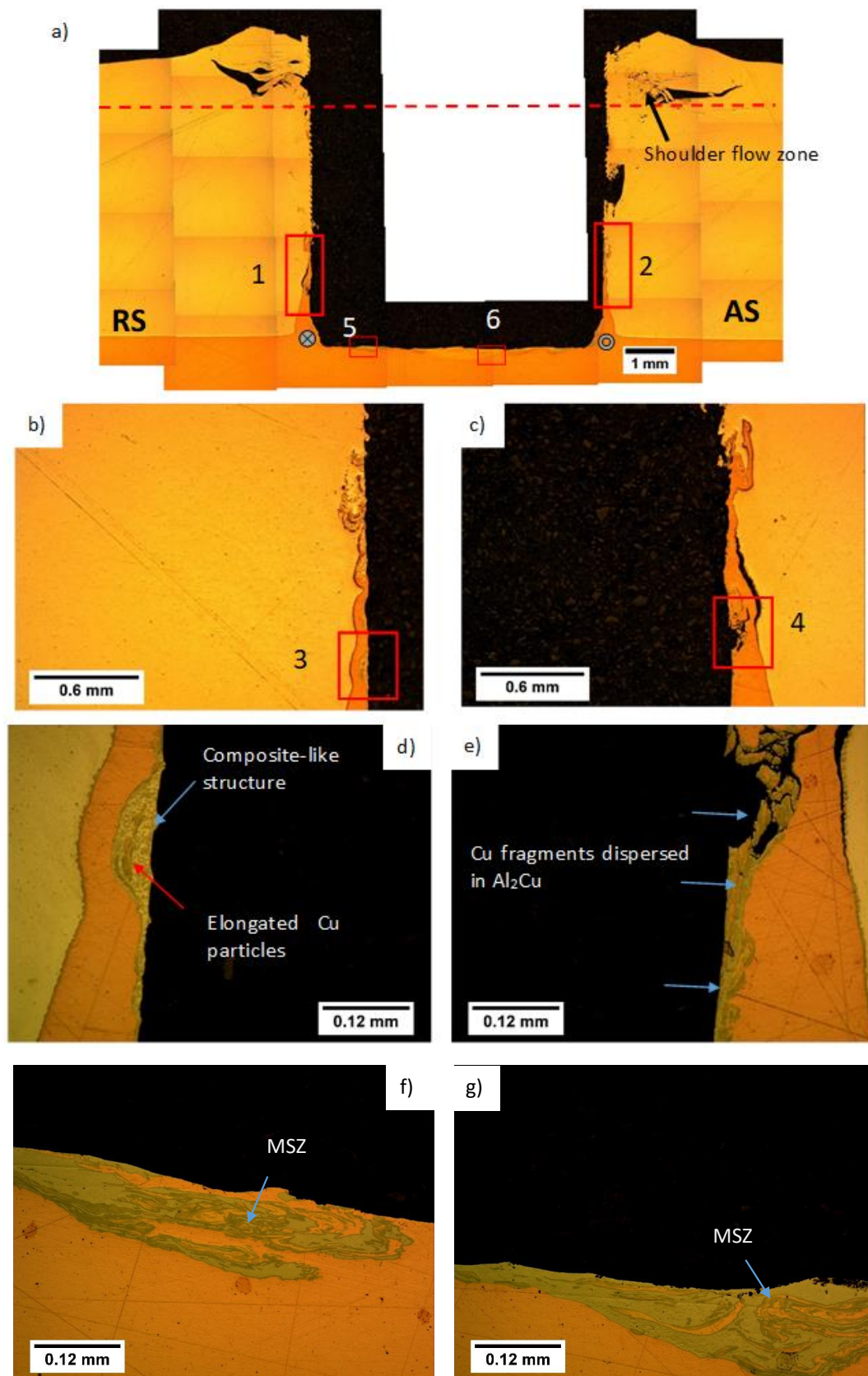


Figure 4 - 14 (a) Keyhole transversal cross section 2mm before the middle (sample 2); (b) Position 1 in a; (c) Position 2 in a; (d) Position 3 in b; (e) Position 4 in c; (f) Position 5 in a; (g) Position 6 in a.

Sample 3 represents the material flow in the half of the pin during process (Fig. 4 - 15a to g). Most of the features in this weld are similar to features in sample 2 (Fig. 4 - 15b to e). RS and AS flash extend to about the same length as flashes from previous sample. Similar MSZ was also formed in this sample (Fig. 4 - 15g). However, in some surfaces, aluminium was able to reach the copper surface with minimum amount of mixing, forming Al_2Cu layer in the copper surface (Fig. 4 - 15f).

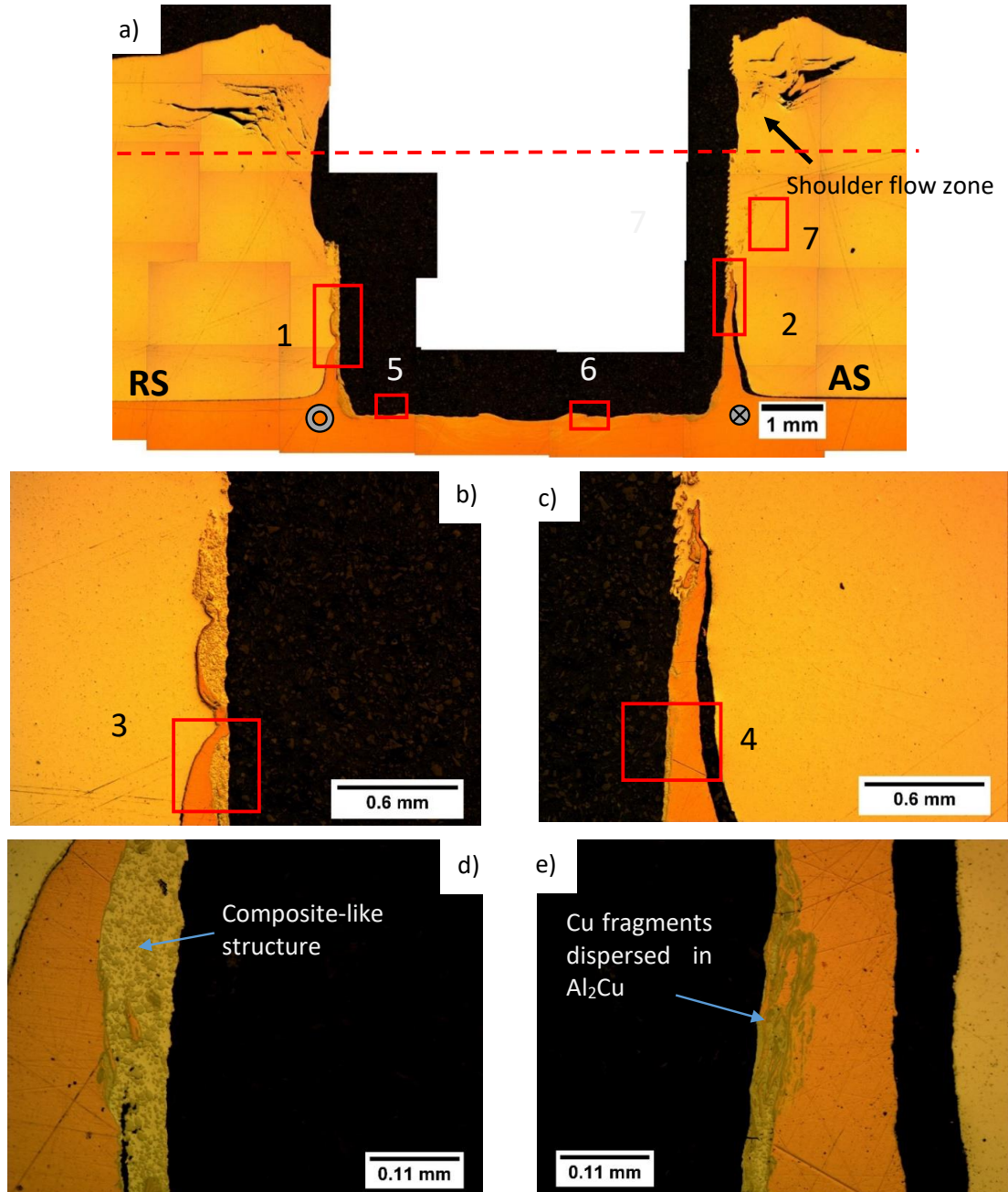


Figure 4 - 15 (a) Transversal cross section of the middle of the keyhole (sample 3); (b) Position 1 in a; (c) Position 2 in a; (d) Position 3 in b; (e) Position 4 in c; (f) Position 5 in a; (g) Position 6 in a.

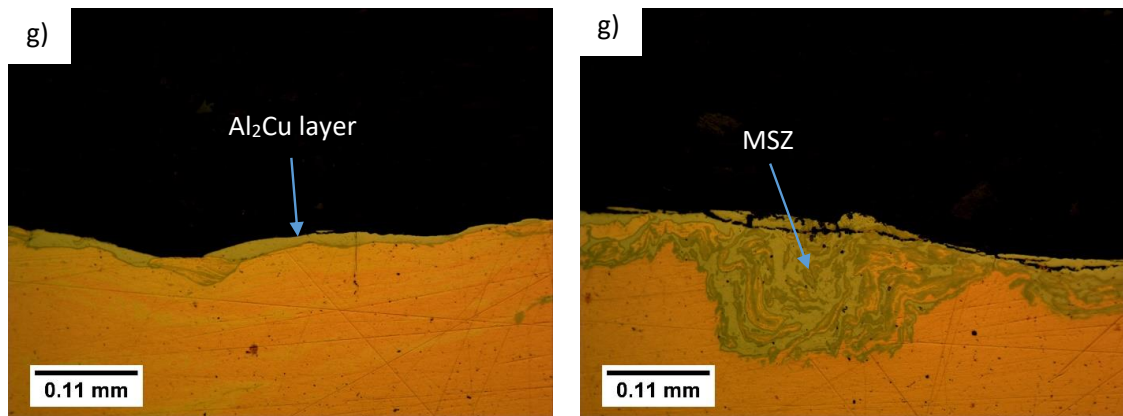


Figure 4 - 15 Continued.

Sample 4, showing the material flow in the three fourth of the pin during process. RS flash was already bent toward the stir zone (Fig. 4 - 16a). In stir zone, dense Al_2Cu intermetallic particles were dispersed in aluminium matrix (Fig. 4 - 16b) forming composite like structure. This dense intermetallic particle seems to grow in network manner in the aluminium grain boundaries. Eutectic structures can also be observed in this area. The existence of eutectic structure signifies the occurrence of melting. In Fig. 4 - 16c, the stir zone is not too dense of Al_2Cu particles, thus eutectic structures are also formed in the aluminium grain boundaries. Copper particle (tangerine coloured on lamellae structured eutectic pointed by red arrow in Fig. 4 - 16c) still exists along with the grey coloured Al_2Cu particle that is formed in eutectic formation. This suggests that copper particles have a role in Al_2Cu particles dispersion and eutectic structures formation in stir zone.

These composite-like structures were present in welds in Fig. 4 - 1a to d, 4 - 2b to d, and 4 - 3d. Except for Fig 4 - 2b, most of these welds have d_p more than 0.33 mm. Although Fig. 4 - 2b has d_p of 0.19 mm, there are a lot of copper particles in its stir zone. This suggest the role of the copper fragments exist in stir zone on dispersed Al_2Cu particles. On welds with d_p more than 0.33 mm, this copper fractures are most likely shredded from the inner sides of both RS and AS flashes as the pin traverse, and from the tip of the flash where the down flow collide with the tip of the flash, creating fragments of copper. These fragments then immediately follow the maelstrom current induced by the pin thread in between the flashes down to copper surface. As for the less dense area in upper region of stir zone, the supply of copper fragments is most likely restricted from the upper region of the rising flash, carried up by the recirculation flow.

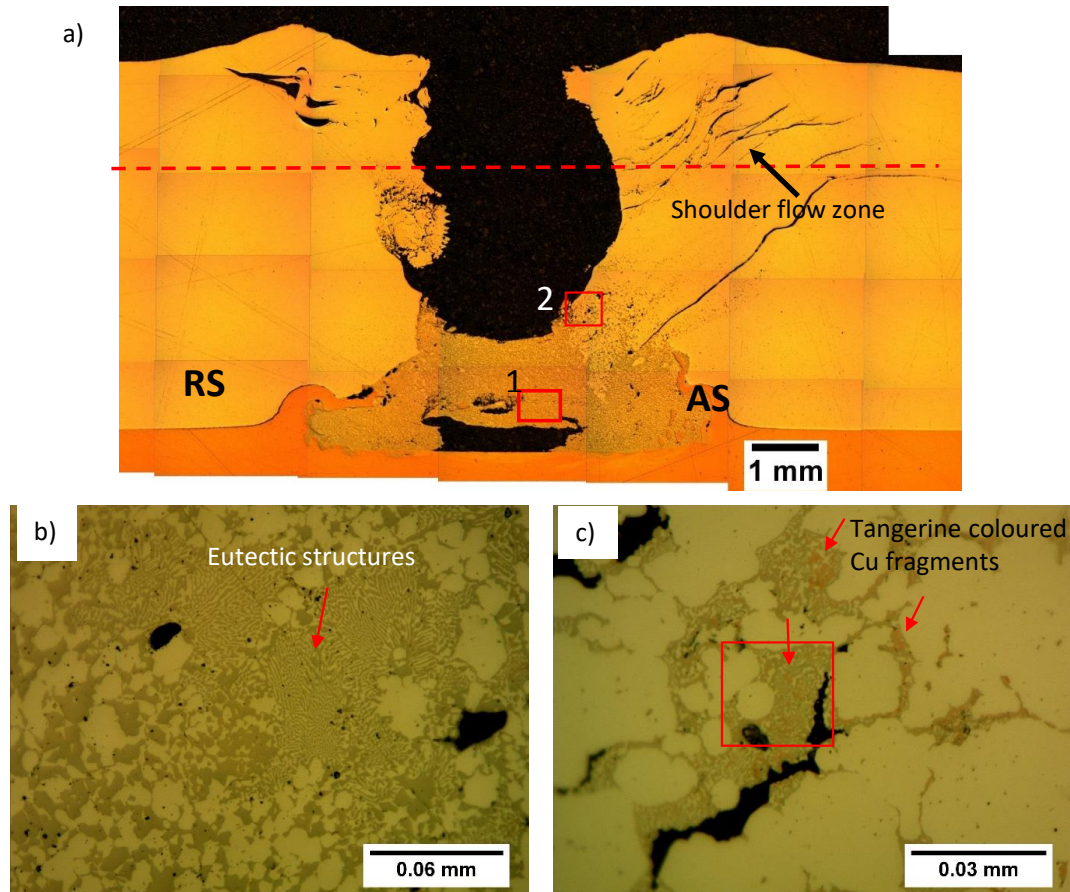


Figure 4 - 16 (a) Keyhole transversal cross section 2mm after the middle (sample 4); (b) Position 1 in a; (c) Position 2 in a.

4.4 Further analysis on the effect of bottom-most thread on the interfacial continuity

Further analysis on the interface continuity was conducted on P1 and P2 interface of weld with $d_{p-aim} = 0.2$ mm in Fig 4 - 3a and b. First, we look at P1 (Fig 4 - 3a). SEM examination (Fig. 4 - 17a) on the interface reveals that no joint was established in this weld. There is a gap between copper and aluminium with white structure lining (presumably intermetallic) in the aluminium side, suggesting that the interface was joined once, but it was cracked at some point. However, BE mode reveals that there is another layer between the previously thought to be a gap. The layer consists of light and white dark grey fragments. Note that same colour in BE means same composition, where light grey is similar to dispersed Al_2Cu in stir zone and dark grey is the colour of aluminium matrix. This means that the interlayer between aluminium and copper is a mixture of aluminium and copper fragments.

The interface, from different positions of the same weld as above, as shown in P2 of Fig. 4 - 3b, was then examined for comparison. The interface has near discontinuity free condition, which typical interfacial feature can be seen in Fig. 4 - 4b and d. Thick

interfacial intermetallic layer can be seen to form between aluminium and copper. There are three visible layers between them, with the one adjacent to aluminium being Al_2Cu . The Al_2Cu layer seems to be sheared, judging from the rather flat sheared surface (Fig. 4 - 4b). The other layer in this interface can be seen in Fig. 4 - 4d. The Al_2Cu layer is not sheared as in previous interface. The layer is blocky and cracked suggesting that this is the original shape of this layer before being sheared as in the previous.

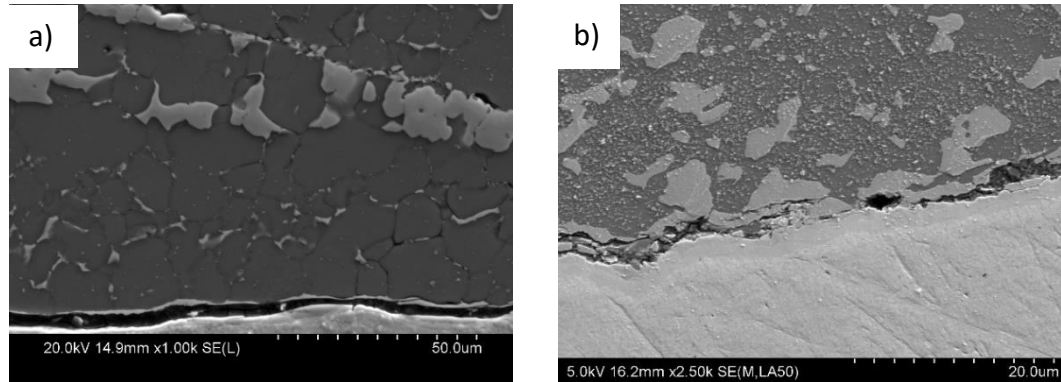


Figure 4 - 17 SEM examination on interface weld in Fig. 4 - 3a (a) SE mode examination; (b) BE mode examination.

Based on this findings, further examination towards the material flow in the lower region of the pin especially in the trailing part of the pin was needed. Therefore, tool stop action was conducted afterwards. Longitudinal cross section of the interface of the embedded pin was observed. The parameter of this weld was ω of 1400 rpm and v of 40 mm/min. Detail on the method and sample sectioning can be seen in chapter 3.7.

The longitudinal cross section of the embedded tool in the pin bottom region is shown in Fig. 4 - 18a. The original Al - Cu interface is slightly forged up in front of the pin and there are fragments of copper filling the bottom-most root of the thread despite of the bottom pin surface positioned somewhat on the same level. Interestingly, the interface in the trailing region of the pin is lifted 0.1 mm from the original unwelded Al - Cu interface. In the bottom of the pin there is a dark layer that is increasing in thickness, and reaching the thickest in about three fourth of the pin length from the front. Higher magnification of the layer shows a white structure intercalated in fine grained copper (stripes structure) (Fig 4 - 18b). In addition, the BE image in Fig 4 - 18c shows that these white structures containing Al_2Cu fragments (grey structures) are dispersed in aluminium. Furthermore, stripes structured copper in BE image shows no difference in compound.

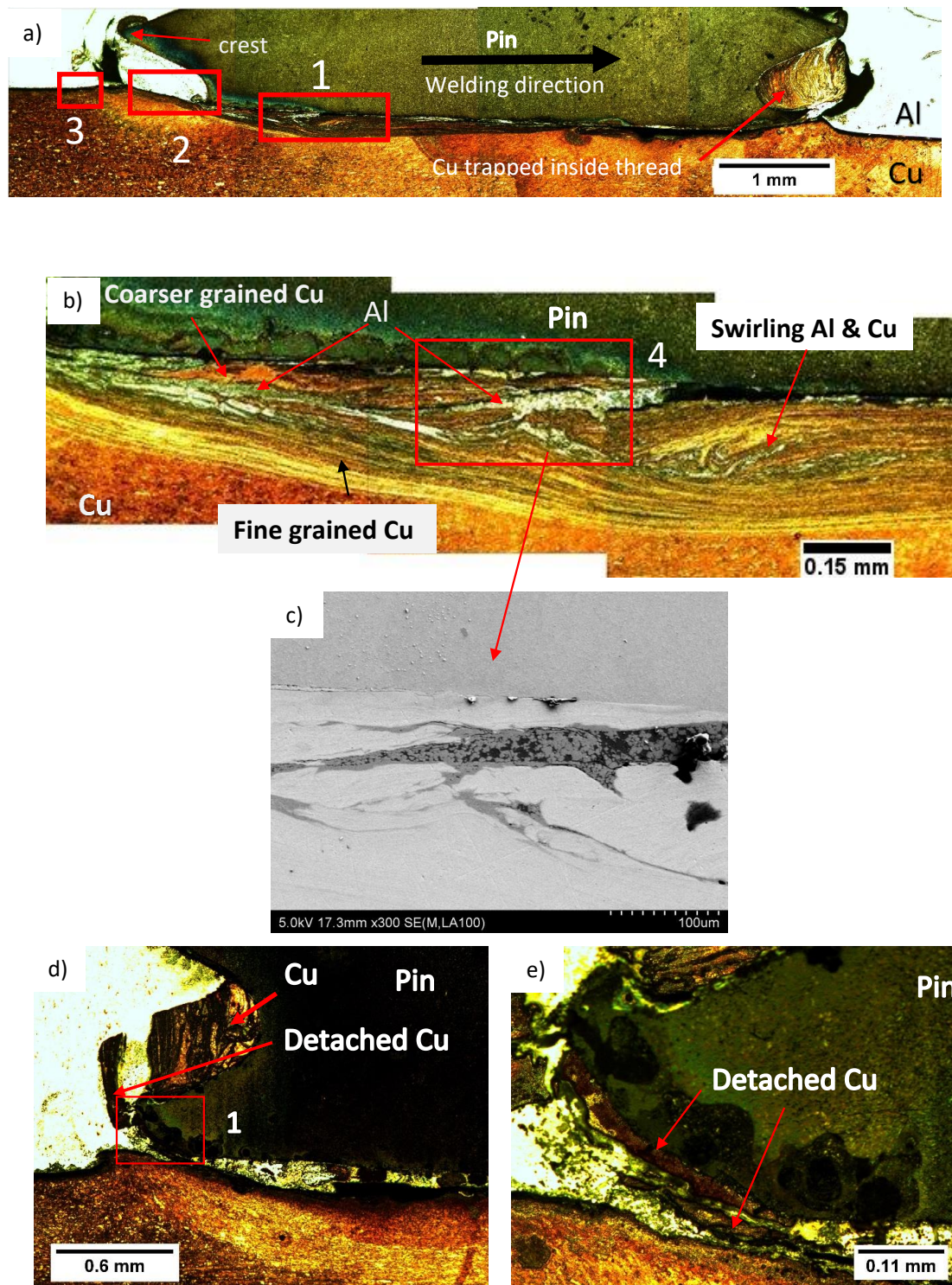


Figure 4 - 18 (a) Stereo microscope image of longitudinal cross section of the lower region of the pin; (b) Stereo microscope image of region below the pin marked as 1 in a; (c) SEM in BE mode of 4 in b; (d) Transversal cross section pin from RS to mid area; (e) Enlarged are 1 in d.

Along with these two distinctive structures, there are copper with coarser grain. The existence of these two different grained coppers implies that these structures undergo different degrees of plastic deformation. Where more severe plastic deformation was happened to the striped structure with finer grain than the coarser one. The fine-grained

copper presumably is the copper directly below the pin surface that is affected or swirled along with the rotating pin. This swirling region is restrained by the copper base metal and rotating pin in beneath and above it respectively, creating a localized region with small elongated grain as in the stripes structured region. While the coarse copper most likely came from copper that was picked up by the bottom root of the thread along with aluminium, it flew down into pin bottom and mixed with the bottom copper that forming MSZ. To support this notion, transversal cross section of the embedded pin in RS to mid region was examined (Fig. 4 - 18d). It is shown that there is a chunk of copper detached from bigger chunk of copper situated in the root of the thread. This implies that copper that is picked up in the roots of the thread will periodically detached from the bigger chunk. Higher magnification in Fig. 4 - 18e clearly shows that elongated fragments have flown towards the bottom of the pin.

The formation mechanism of the MSZ in this study is somewhat different with the one stated in studies by Galvao et al. [76], [88], [130]; they stated that this structure is formed due to heterogeneous mixture inside the shear zone, which then deposited behind the pin as it travels. In this study, it is clear that the main formation happened in the bottom of the pin.

Fig. 4 - 19a shows higher magnification of optical microscope image of the region 2 in Fig. 4 - 18a behind the pin in lower region. Although the pin was only slightly plunged into copper, aluminium and copper were flown into the pin bottom. There, MSZ was formed. As the pin moved forward, this MSZ was behind the pin, but still inside the thread's root, and pushed upward and immediately sheared by aluminium flow inside the root thread. This immediate shearing action is shown in Fig. 4 - 19b. The MSZ was sheared to a plane that was indicated by the bottom red dashed line. Unlike the swirling and mixing nature of MSZ structure below the pin surface in the slope region of raising interface, an average of 0.7 mm thick of fine-grained copper layer evidently was formed just below the slanted interface (pointed by red arrow in 4 - 19a). This indicates that the previously formed MSZ was completely sheared off. This fracturing action plastically affects about 0.7 mm of copper layer below the sheared interface, while being restrained by the copper base metal below the layer. In addition, there is a structure similar to MSZ just above the hump. This might be a part of MSZ from the pin bottom surface that was squeezed out from the pin bottom. However, it was immediately sheared by the aluminium down flow. This implies that once the MSZ is pushed out from the pin bottom, it will turn into brittle intermetallic MSZ that is easily fractured by the aluminium flow.

Although the Al - Cu interface seems to be gapping in stereo microscope image, BE image shows that there is another layer formed in this region (Fig. 4 - 19b). Higher magnification of the region between the red dashed lines reveals that in the Al - Cu interface there is a structure that consist of aluminium (dark grey), copper (light grey) and Al_2Cu (moderate grey similar to dispersed particles) (Fig. 4 - 19c). This clearly captured the fracturing process of MSZ by the aluminium flow. The existence of Al_2Cu layer in the interface of aluminium and the fractured MSZ might be caused by the copper fragment that was picked up during the fracturing process.

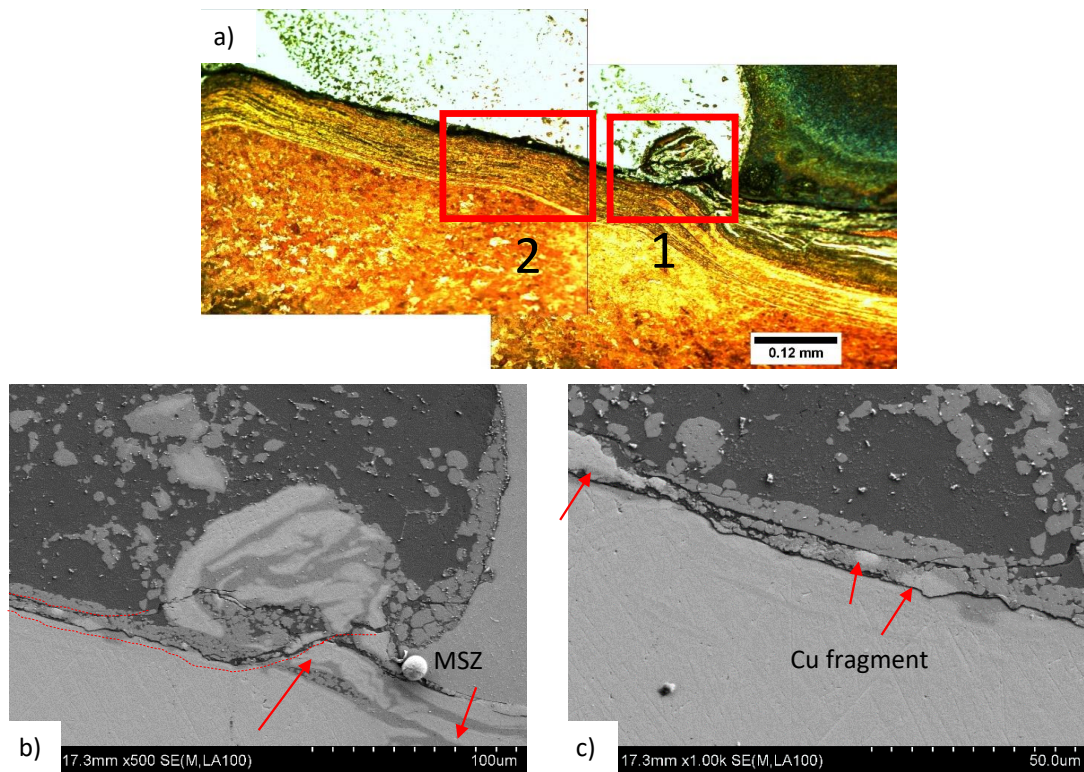


Figure 4 - 19 (a) Stereo microscope image of longitudinal cross section is showing slope region of the raising interface in the trailing part of the pin inside the last root region of the pin (region 2 in Fig. 4 - 17a); SEM BE image of region of (b) 1 and (c) 2 in a.

In Fig 4 - 20a, it is shown that the slope region of the raising interface reached its peak and the fracturing action still occurred until approximately 10 layers of detaching aluminium from the shear layer behind the pin. This is marked by the fine grained copper formed after the peak. It is important to notice that the thickness of deposited material (λ) for parameter used in this experiment in particular is approximately 0.028 mm/rev . Detail as follows:

$$\lambda = \frac{v}{\omega} \quad \text{Eq. 13}$$

$$\lambda = \frac{40\text{mm/min}}{1400\text{rev/min}}$$

$$\lambda = 0.028 \text{ mm/rev}$$

This would mean that in one revolution, the pin will advance for 0.028 mm and deposited 0.028 mm of thick material. Since the length of fine grained layer after the peak is around 0.28 mm, it can be concluded that after the peak there were 10 layers of aluminium that were still fracturing and trying to drive away the fractured MSZ intermetallic.

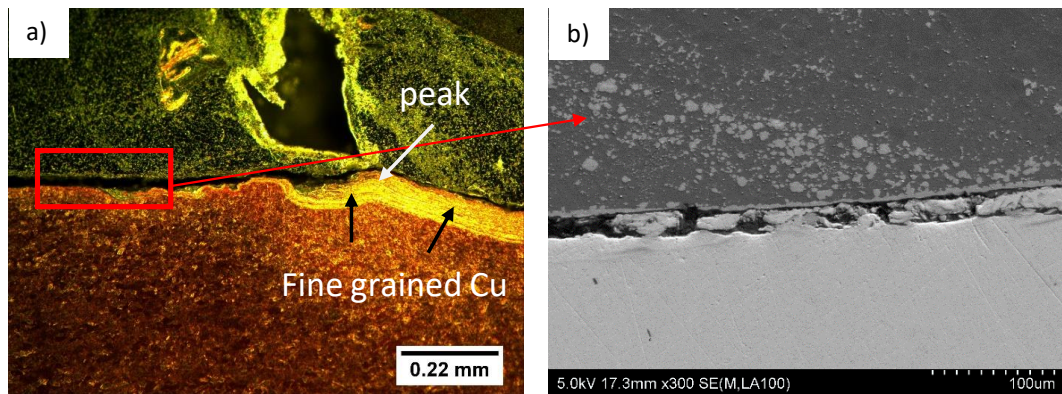


Figure 4 - 20 (a) Stereo microscope image of region 3 in Fig. 4 - 17a showing trailing part of the pin outside the pin periphery; (b) SEM BE mode image of trailing interface further away from the pin.

The detached trailing aluminium flow was stopped from filling the gap because the pin stopped suddenly; this explains the void. This backflow fracturing was still continuing after 10 revolutions creating the flat final interface. Fig 4 - 20b shows the longitudinal cross section of the final flat interface of the weld. There is a region full of aluminium, copper and Al_2Cu fragments flanked by Cu and Al similar to Fig 4 - 19c but with larger fragments and in some area insufficiently filled with or even completely devoid of aluminium and/or fragments. In addition, some fragments are still intact on the bottom plate, suggesting the MSZ intermetallic fracture fragments were not driven away completely. These fragments presumably prevented aluminium flow from filling in between the fragments. This incomplete fracturing most likely is a defect of formation mechanism for the interface from Fig. 4 - 3a. However, if the fractured fragments can be driven away completely, aluminium will be able to reach the previously fractured surface without any hindrance from the remaining fragments of MSZ intermetallic.

With the analysis of MSZ fracturing and knowing that there is a possibility of obtaining close to continuous as well as discontinuous interface, it could imply that the bottom-

most thread could be the reason for the inconsistency in obtaining discontinuity free interface. The suggested mechanism is as follows. It was analysed that in one revolution, the tool would advance as far as 0.028 mm and deposit a layer of aluminium in the previously fractured MSZ surface. Furthermore, as the pin rotates and advances, the bottom crest will look like as if it was moving further down to approach then completely shear or fracture away the slopping region (Fig. 4 - 19a).

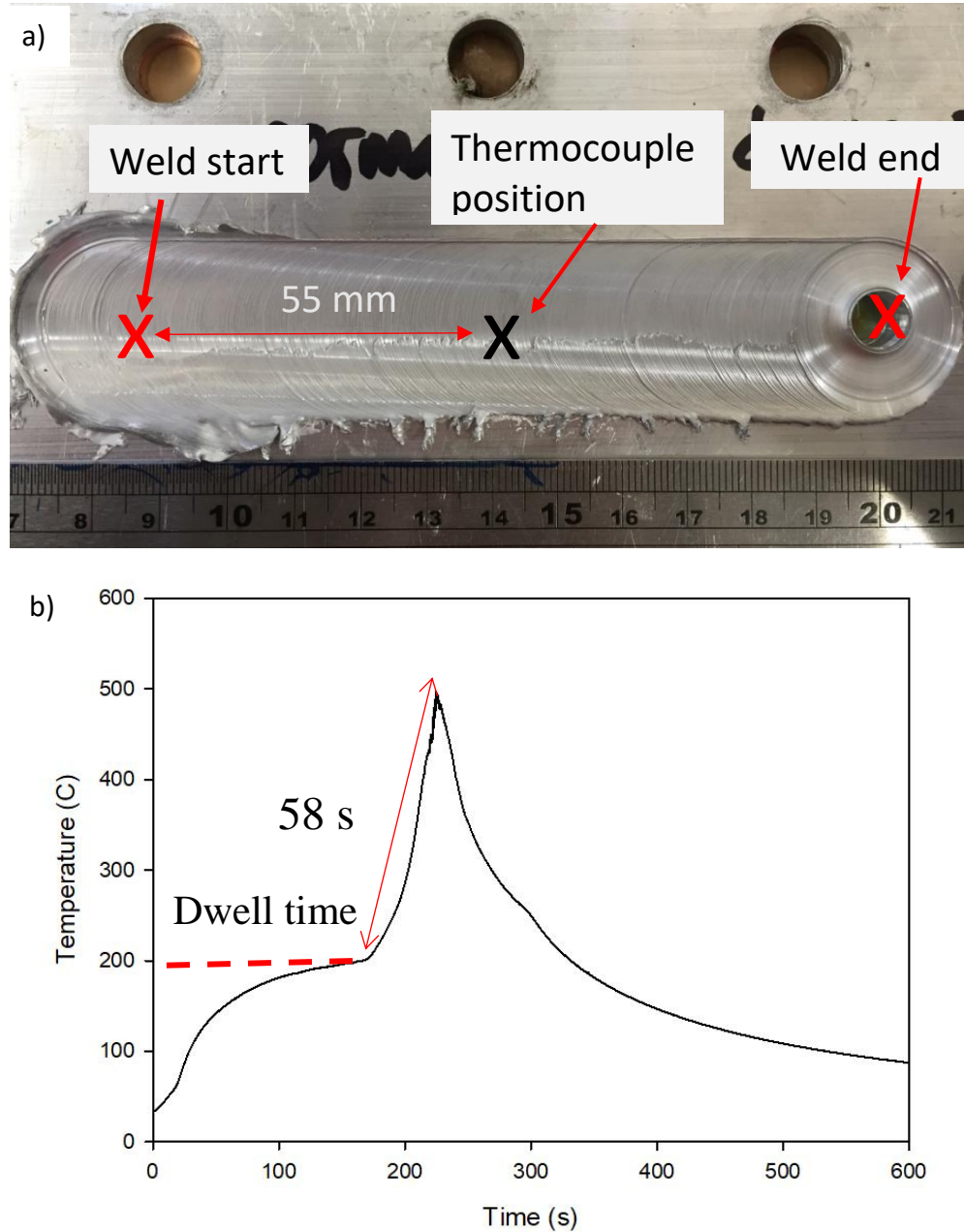


Figure 4 - 21 (a) FSLW used to investigate the pin location on the peak temperature; (b) Temperature history of weld in a.

Still referring to the crest position on Fig 4 - 18a, it is important to notice that, in one pin revolution, the crest will be in the same position as before. Therefore, after the crest moves and reaches bottom pin surface level, it will further disappear to be replaced by

another root and this root will immediately be filled with another sloping raised interface. Note that the pin only advanced for 0.028 mm in one rotation. This means that until the sloping region of the raised interface is out of the pin periphery, this region will undergo repeating process as described above.

Despite of these findings and analysis, how to obtain discontinuity free interface is still uncertain. However, in the lower thread, bottom-most crest and root, interaction with the Al - Cu interface behind the pin is repeatedly creating and shearing a sloping region of raised interface. This might be the cause of the uncertainty. This hypothesis will be further tested with two types of pins, scriber and manually filed bottom pin. These two pins were conditioned so that the interface shall be constantly sheared in one mechanism that is by aluminium stream behind the pin.

4.5 Microstructure Evolution in the stir zone

4.5.1 Formation of composite like structure in stir zone

To further understand the microstructural evolution in FSW, first, it is important to know the temperature history starting from the pin enters the original Al - Cu interface until it passes completely. To do so, a special weld was conducted. Approximately 115 mm long weld was conducted with parameters of $d_p = 0.2$ mm, $\omega = 710$ rpm, and $v = 56$ mm/min. Thermocouple was sandwiched between aluminium and copper plate, 55 mm from the weld starting point (middle point of the pin) (Fig. 4 - 21a). The rotating pin was then plunged into the lapping aluminium and copper. Before it traversed, the rotating pin was left to dwell until the temperature reached 200 °C. In this way, travel time from starting position to the thermocouple spot can be distinguished. From temperature history in Fig. 4 - 21b, it is known that time to reach peak temperature (T_{peak}) is 58 s, which is close to calculation as follows:

$$56 \text{ mm/min} = 0.933 \text{ mm/s} \quad \text{Eq. 14}$$

Time to travel for 55 mm:

$$\frac{0.933 \text{ mm}}{1 \text{ s}} = \frac{55 \text{ mm}}{x \text{ s}} \quad \text{Eq.15}$$

$$x = \frac{55}{0.933}$$

$$x = 59 \text{ s}$$

Based on this, it can be concluded that peak temperature happens in the middle of the pin bottom.

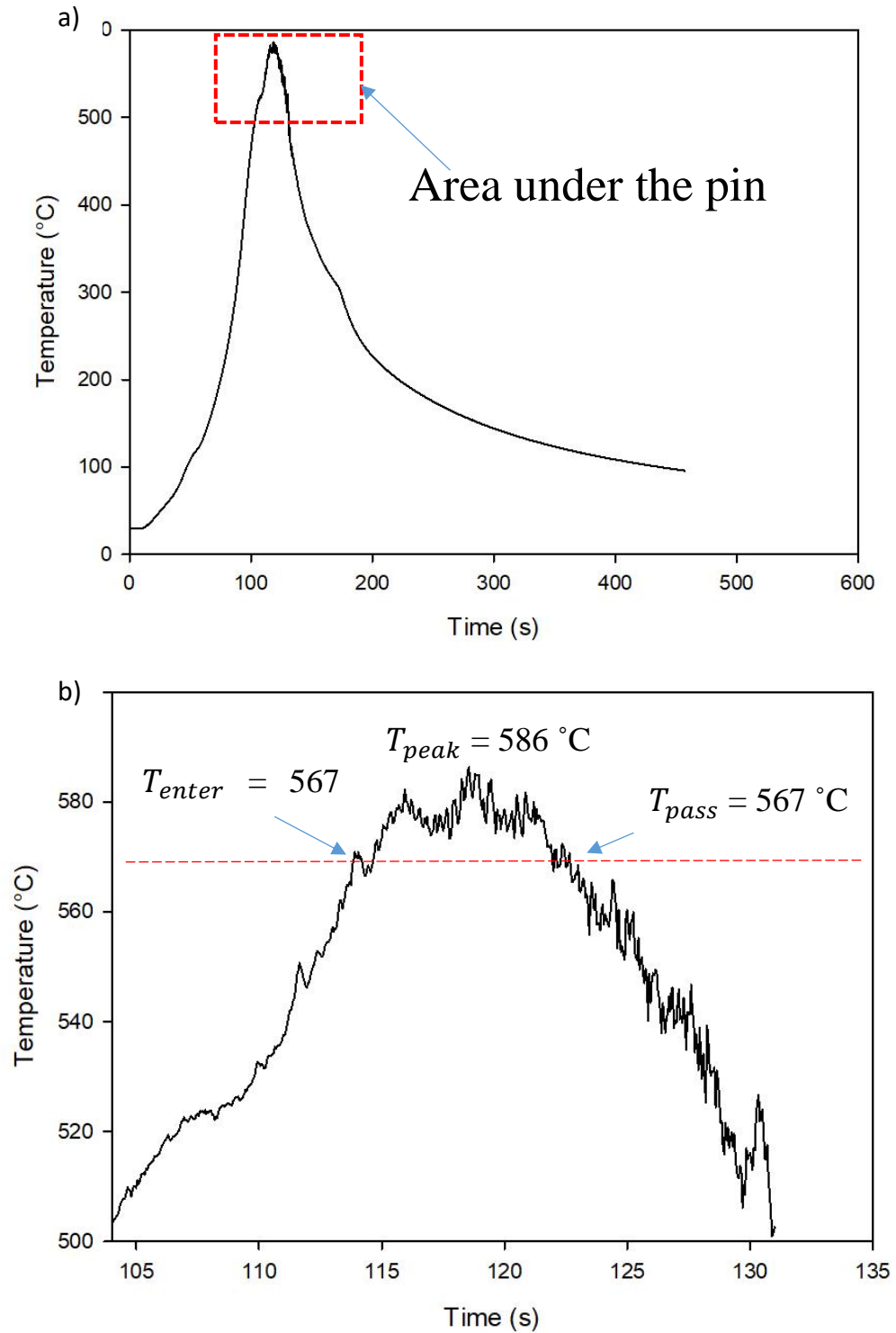


Figure 4 - 22 (a) Temperature history of weld in Fig. 4 - 3; (b) Enlarged area boxed in (a) showing temperature under the pin.

For microstructural study, weld in Fig 4 - 3 was used. The temperature history of the weld is shown in Fig. 4 - 22a. The pin used in this study was 8 mm in diameter, meaning that the area passed by the pin was ± 4 mm from T_{peak} . Knowing this, the

temperature, when the pin was starting to enter until it was completely passing through the original Al - Cu interface, can be determined. From Fig. 4 - 22b temperatures when the pin enters (T_{enter}), peaks and pin passes through (T_{pass}) were known to be 567, 586 and 567 °C respectively. This means that region just before and after the pin was already above the eutectic temperature ($T_{eutectic}$) of Al - Cu binary system (T_{enter} and T_{pas} shown with blue line and T_{peak} shown with green line in Fig. 4 - 6).

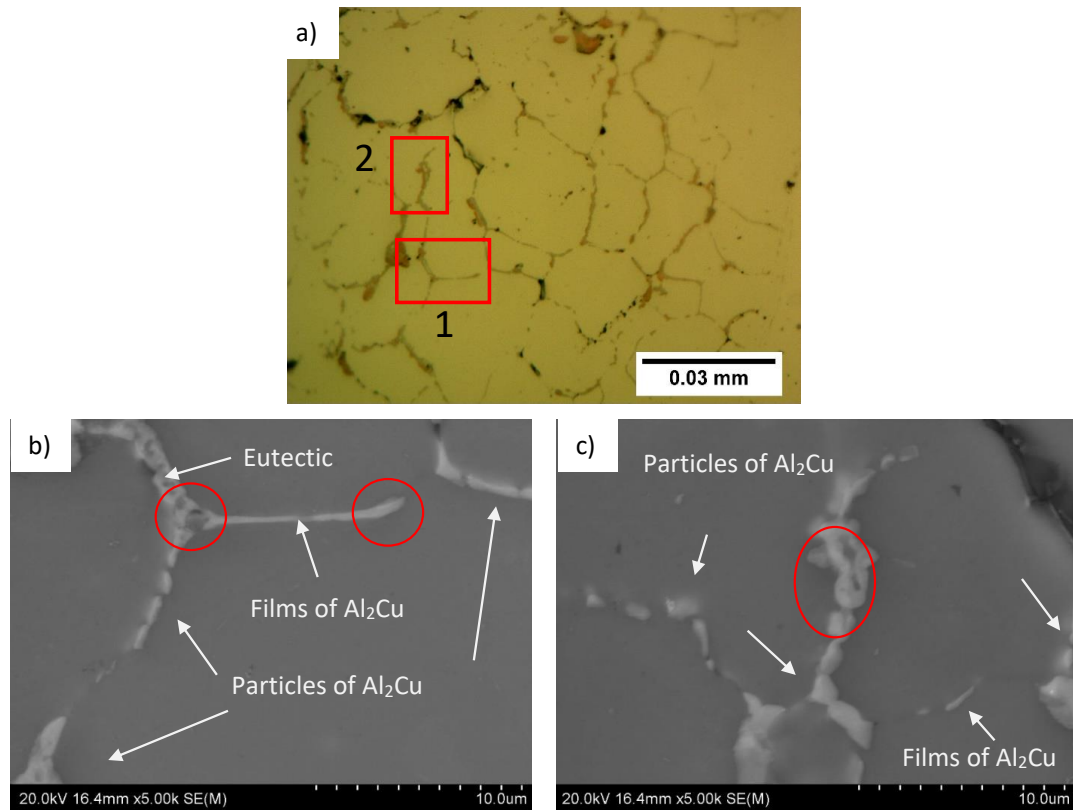


Figure 4 - 23 (a) Recirculation flow with small copper fragments and intermetallic in the Aluminium grain boundaries in area 7 in Fig. 4 - 14a; (b) SEM image of area 1 in a; (c) SEM image of area 2 in a. Area circled red is still in the form of copper.

Based on this, now the microstructural evolution can be discussed. It is implied that some copper fragments flow upward above the tip of the raised RS and AS of copper flash. Investigation on a representative of area 7 in Fig 4 - 15a (Fig. 4 - 23a) using a stereo microscope, shows structure with a mixture of grey (assumed as Al_2Cu intermetallic (θ)) and structure with tangerine colour (copper fragments). However, these two structures cannot be distinguished by BE image. Fig. 4 - 23b and c are SEM of examination on area 1 in Fig. 4 - 23a in BE mode. In these images, areas circled in red are still in the form of copper, while structures with same colour are α -aluminium + Al_2Cu lamellar eutectic structure and film of Al_2Cu formed in aluminium grain boundaries. This film of Al_2Cu according to Fallet et al. [131] is a result from divorced

eutectic growth where two components of the structure grow independently. This mechanism usually occurred in hypoeutectic composition, where the primary elements (in this study aluminium) fraction is significantly higher than the second (in this study copper). In a condition where a small liquid phase has its width comparable to the eutectic spacing, the second phase, in this case Al_2Cu , maybe solidified into a single particle, dispersed blocky particles in stir zone, or film between the dendrites [132], [133] as seen in Fig. 4 - 23b and c.

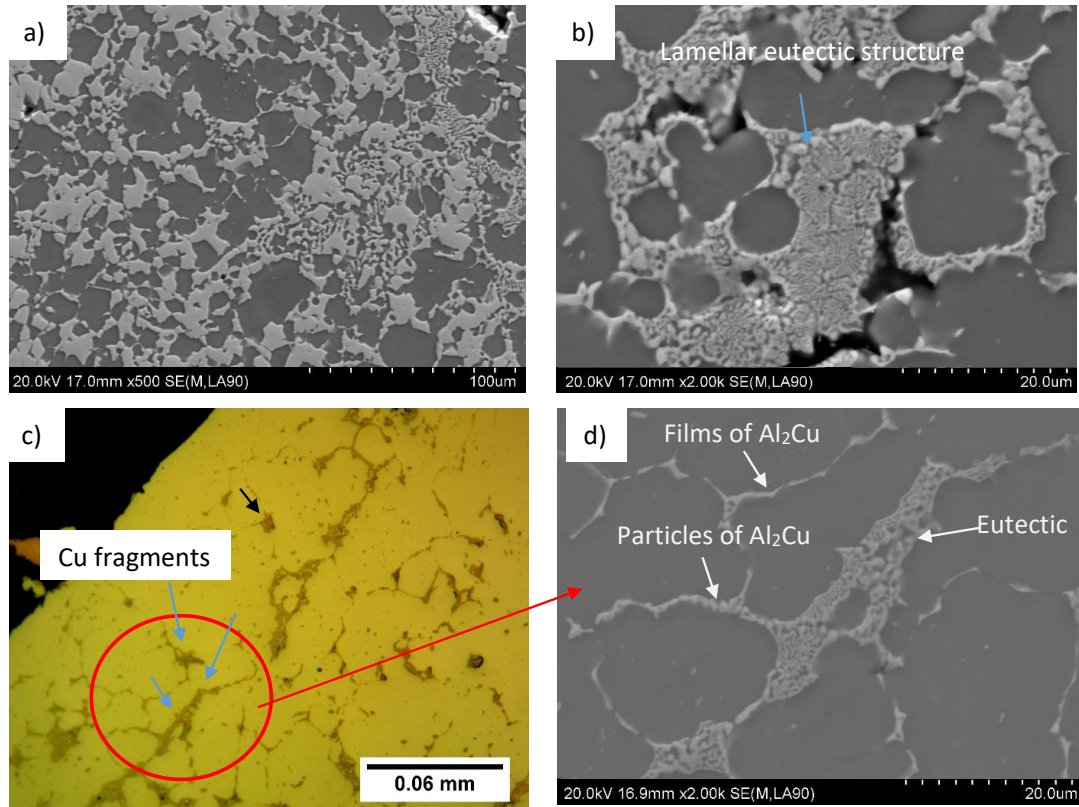


Figure 4 - 24 (a) Al_2Cu dispersed particle dense region in Fig. 4 - 15a; (b) SEM image of Fig. 4 - 15c; (c) Another area in less dense region near area in Fig. 4 - 15c; (d) SEM image of circled region in c.

Further examination on the stir zone of Fig. 4 - 16a and b was then conducted. A mixture of lamellar eutectic structure with network of large blocky and thin layer of Al_2Cu is evident in Fig 4 - 24a. The blocky and thin layer intermetallics were formed in aluminium grain boundaries. However, the blocky particles have grown excessively. In Fig 4 - 24b lamellar eutectic intermetallic was formed in aluminium grain boundaries. If we take a look at microscope image in Fig. 4 - 24c (pointed by blue arrow), copper fragments still exist along with the eutectic structure. In another area near Fig. 4 - 24c and d, mixture of lamellar eutectic, particles of Al_2Cu , and films of Al_2Cu were formed in the grain boundaries of aluminium (Fig. 4 - 24d). The lamellar eutectic structure is similar to Yang et al. [134] finding.

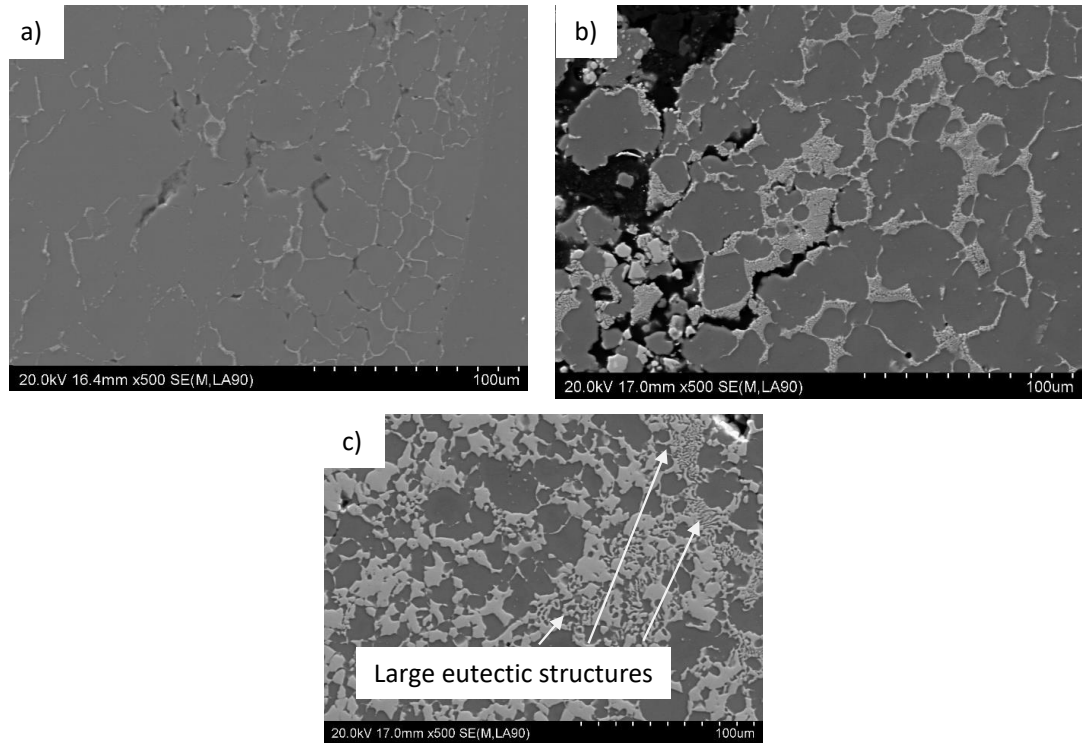
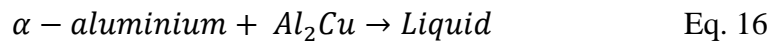


Figure 4 - 25 SEM image from 3 different regions in x500 magnification (a) Microstructure in recirculation flow, area 7 in Fig. 4 - 14a; (b) Microstructure in less dense stir zone in area 2 of Fig. 4 - 15c; (c) Microstructure of dense area 1 of Fig. 4 - 15c.

In Yang et al.[134] work, they used 2219 aluminium alloy which have 6.5 wt-% copper processed by friction stir spot welding (FSSW). It can be seen in Al - Cu binary phase diagram (red line in Fig. 4 - 22) that the solubility limit of this alloy exceeds the solubility limit of copper in α - aluminium. As a consequence, Al_2Cu particles are present in α - aluminium matrix. When the temperature is increased to $T_{eutectic}$, melting occurs with eutectic reaction as follows:



As the temperature drops, the liquid phase solidifies into lamellar eutectic or divorced eutectic which is Al_2Cu surrounded by α - aluminium.

However, in this study, no pre-existing Al_2Cu particles existed in aluminium matrix since the maximum amount of copper exist in alloy used in this study was only up to 0.1 at.%. Supply of copper obtained from copper fragment fractured during FSW. Since the pin T_{enter} reached 567 °C, the copper fragments were readily dissolved into aluminium matrix as much as 4 - 5 wt.% as well as forming Al_2Cu in Al - Cu fragments interface. As the temperature rose to T_{peak} , the solubility of copper further decreased to about 3 wt.%. The excess copper was expelled to aluminium grain boundaries; it reacted with

aluminium to form Al_2Cu in the grain boundaries and further supported the growth of existing Al_2Cu in the grain boundaries. However, in the same time, it reacted with surrounding aluminium to form liquid phase.

The amount of liquefaction is highly depended on the amount of copper fragments and the grain size of aluminium. As a comparison, SEM images of three different locations with same magnification are presented in Fig. 4 - 25a to c. Fig. 4 - 25a is taken from area 7 in Fig. 4 - 15a. This area is above the tip of raised copper flash. The supply of copper fragments is assumed to be coming from recirculation flow that carries fragments fractured from impingement of aluminium maelstrom flow in the pin vicinity with the tip of raised copper flash. Due to barrier created by the raised copper flash, not all aluminium down flow was able to flow through to the bottom of the pin. Some of the excess aluminium recirculated back to the shoulder flow zone carrying copper fragments from the tip of the raised flash.

Figure 4 - 24b is a less dense stir zone area 2 in Fig. 4 - 16c. This area is depicting three quarter of pin passing through original Al - Cu weld; it situated approximately 1.9 mm above the original Al - Cu interface. The material in this area might undergo another revolution and receive copper fragments from the upper side of the raised copper flash in RS, as the AS flash is already situated below this region. As a reminder, the flashes of RS and AS in sample 2 and 3 were raised to about 2 and 1.6 mm respectively. For dense stir zone in Fig. 4 - 25c, the copper fragments were supplied from all sides of copper raised flash. Due to excessive amount of copper fragments, when liquid phases were formed in their interfaces, these liquid phases easily grow and joined together forming large area of lamellae eutectic structure that can be seen in Fig. 4 - 25c. Moreover, the temperature dropped below $T_{eutectic}$ after the pin passed as far as approximately 4 mm. This further allows the growth of liquid phase. In addition, as the temperature were cooling down the remaining unreacted copper turned into Al_2Cu aiding the growth of dispersed Al_2Cu , thus, explaining the denseness of the stir zone.

4.5.1 Interfacial intermetallic growth behaviour

From analysis in section 4.4, it was revealed that interfacial intermetallic was formed under the pin then continuously sheared into fractures. It is impossible to pin point when and where the nucleation and growth of interfacial intermetallic happened. Knowing this, study on intermetallic growth in a single pass weld of Al - Cu dissimilar metal would not be valid. Therefore, multipass FSLW was conducted for this purpose. 1 mm

overlap in AS was used to preserve 7 mm interface without being re-welded by the overlapping weld that was using the parameters of $\omega = 1000$ rpm, $v = 56$ mm/min, and d_p aimed at 0.2 mm.

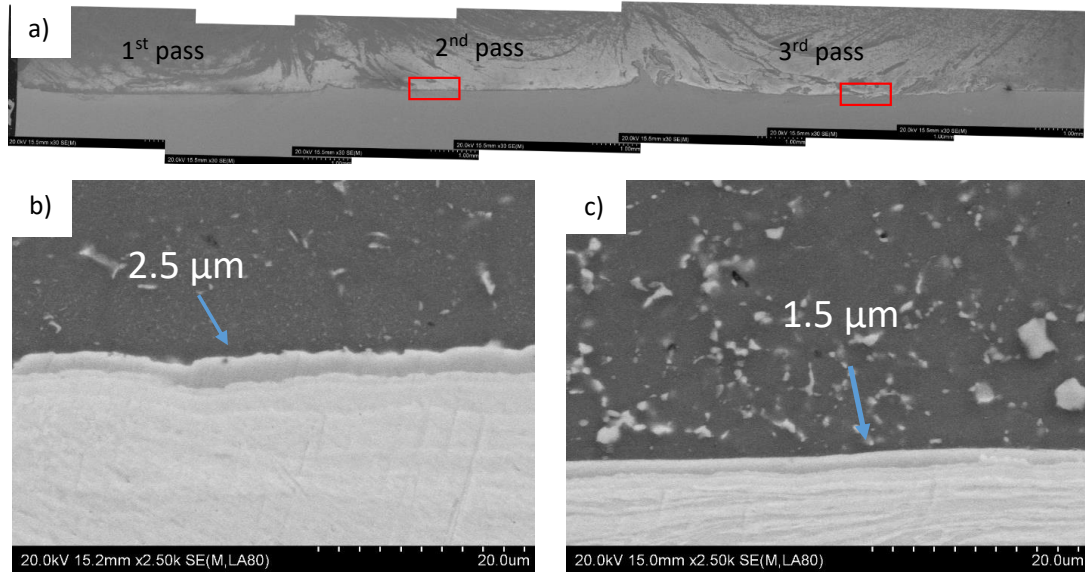


Figure 4 - 26 (a) Multipass FSLW using welding parameter of weld in Fig. 4 - 9; (b) Typical interface of second lap; (c) Typical interface of third lap.

Result of the multipass welding can be seen in Fig. 4 - 26a. Thickness of interfacial intermetallic from the second (Fig. 4 - 26b) and third (Fig. 4 - 26c) passes were measured and compared. Third pass interface represents single pass interface, while the second pass represents a single pass that experienced another heating cycle from subsequent pass. The temperature was measured using thermocouple placed in the first pass. The thermocouple placement schematic is given in Fig. 3 - 17a. It measured three temperature cycles, namely black, red and green curves that represent the first, second and third temperature histories (Fig 4 - 27). The second pass experienced two temperature cycle from first and second pass welding. While the third pass is only experienced one temperature cycle generated from itself. The outer interfacial intermetallic layer, Al_2Cu , thicknesses were 2.5 and 1.5 μm, for second and third passes respectively. The interfacial intermetallic layer in the second pass was 1 μm thicker than the third pass. From the insert of the temperature history in Fig. 4 - 27, it can be seen that the second pass experienced another temperature cycle. It went through 28s above 400 °C that peaked at approximately 480 °C. This suggests that this additional temperature cycle was responsible for the 1 μm growth. However, calculation made with equation 17 using growth rate constant for Al_2Cu taken from Xu et al. [33] works of $1.53 \times 10^{-3} \mu\text{m}^2/\text{s}$, showed that in order to grow 1 μm, it would need approximately

653 s. While, interfacial intermetallic layer only grows to about 0.21 μm in 28s on 400 $^{\circ}\text{C}$ heating condition.

$$d^2 = kt \quad \text{Eq.17}$$

Where d is the intermetallic thickness, k is the growth rate constant, and t is the heating time.

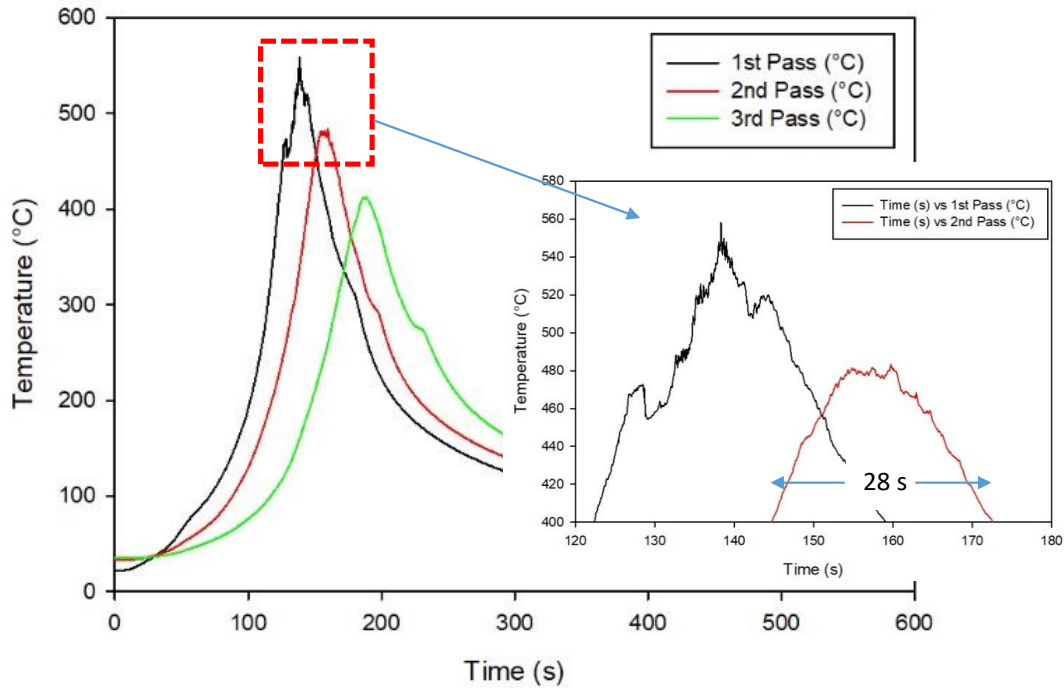


Figure 4 - 27 Temperature history of multipass FSLW starting from thermocouple placed in first weld. Insert shows the peak of first and second pass in temperature more than 400 $^{\circ}\text{C}$.

The calculation shows that the growth rate of Al_2Cu is rather slow and it is saved for multipass process without having to experience excessive growth during interfacial intermetallic growth in the preceded interface. The 1 μm in the interfacial intermetallic growth kinetics in the first lap might be caused by the difference in material mechanical mixing, that is possible due to the uncertainty induced by the pin's bottom thread. The severe plastic deformation occurred during process is known to produce dislocation [44], [135] and grain refinement [44], [52], [136], [137] in the stir zone, making it possible to increase the intermetallic layer growth kinetics by short circuit diffusion [78], [138]. Diffusions along dislocation and grain boundaries, or short-circuit diffusion, are known to be easier and faster than bulk diffusion, as it needs lesser atom to move in order to make way for the diffusing atom to pass through [139]. In addition, the activation energy for this mechanism is 0.1 - 0.3 lower than the bulk diffusion [139]. It

is shown in Fig. 4 - 23a and 24a that the copper fragments existed in the aluminium matrix boundaries. Making the diffusion of copper into its surrounding easy and fast. The deposition of copper fragments right on top of the interface, with the addition of intercalation of aluminium and copper found in MSZ, is possibly accelerating the growth of interfacial intermetallic.

4.6 Summary

From the studies conducted using traditional left-hand threaded pin, it is found that:

1. The optimum d_p to obtain voids free interface is in range of 0.15 - 0.29 mm. However, if using d_p more than the effective range, extensive copper flash hooks, especially in RS, will be formed. The extensive hooks may be fractured into elongated copper particles that block the aluminium down flow creating voids in the stir zone area close to the interface.
2. Although close to discontinuity free interface can be achieved with ω of 1400 rpm and v of 40 mm/min, 0.8 μ m thick interfacial intermetallic will potentially give rise to intermetallic cracking. Further experiments using various ω with a constant v show that continuous intermetallic with considerably thin interfacial intermetallic layer can be achieved with ω of 1000 rpm and v of 56 mm/min.
3. Due to narrow aim of d_p , it is important to study the flow on the formation of the extensive copper flash hooks in order to avoid the formation effectively and overcome the narrow aim of d_p . The study is carried by examining the key hole of the weld. It was revealed that, penetration to copper as far as 0.3 mm, will result in the formation of copper flashes in RS and AS that extend up for about 2 mm and 1.6 mm respectively. Elongated fragments most likely come from the fracturing occurred in the tip of the raised copper flashes. The Al down flow around the pin will impinge the tip and fracture the copper. The copper fragments will then be caught in the maelstrom flow inside the pin and between the flashes. If the fragments are big enough, they will block the aluminium down flow and form cavities. The impingement produces a recirculation flow that carries a small amount of copper up, even further to the shoulder flow zone. In addition, dense stir zone is the result of copper fragments that are picked up not only from the tip of the flashes but also from the inner wall of the flashes.
4. There is uncertainty in how the process of reaching discontinuity free interface occurred. Stop action method was used to investigate the phenomenon.

Examination on the transversal cross section area in the bottom of the pin reveals that aluminium and copper (picked up by the bottom root of the thread) are driven to the bottom of the pin and mixed along with the existing copper under the pin to form MSZ. These materials are being driven to the bottom of the pin, and as a compensation, materials are being lift up especially from behind the pin. MSZ that just squeezed out from the bottom of the pin was immediately fractured by the flow inside the root behind the pin. This fracturing occurred until 10 rotations after the pin passed. Complete fracturing and furthermore driving away the MSZ fragments completely are needed to achieve discontinuity free interface. The bottom-most thread is causing uneven shearing to the interface. This could be the reason for the uncertainty. Further experiments using two pins with constant amount of interfacial shearing by the aluminium stream behind the pin will be conducted in chapter 5 and 6.

5. For microstructure evolution, it was concluded that the main reason for the existence of Al_2Cu and eutectic structure in stir zone was caused by copper fragments reaction with the aluminium during FSLW. Al - Cu fragments interface will form Al - Cu intermetallic due to temperature exposure above the T_{eutectic} , thus forming Al_2Cu . Some of the copper will dissolve into aluminium matrix. As the temperature rises, solubility of copper in aluminium matrix is decreased. Copper in the aluminium matrix gets out to the grain boundaries and forms Al_2Cu and further supports the growth of interfacial Al_2Cu . These Al_2Cu in the grain boundary and Al - Cu fragments interface will further react with surrounding aluminium and liquefy. The amount of liquefaction and denseness depends on the amount of copper fragments. Small amount of copper will result in limited liquefaction and as the temperature cools down, it will form divorced eutectic due to the limited spacing between phases.
6. It was implied that the growth of interfacial intermetallic growth was accelerated by the rigorous mixing of material in single pass welding. However, in multipass welding, the effect of welding temperature of the subsequent pass, would have very small impact on the interfacial intermetallic layer growth.

Chapter 5: FSLW with scriber pin

In this chapter, FSLW was conducted using a tool with the addition of scriber pin on the bottom of the pin. This method was originally used to widen the d_p range, because of its ability to make the copper flash to fold outside of the stir zone [99]–[101], [118], [119]. The effect of d_p , ω and tilt angle on interfacial continuity were investigated. Welding was carried out with deliberately broken thread pin to study the importance of down flow on FSLW with scriber. Ultimately, flow in the bottom pin and scriber area will be studied by examining the weld's keyhole. The main purpose of this study is to find the optimum weld parameters, as well as to understand the welding flow in FSLW with scriber.

5.1 Effect of depth of scriber penetration ($d_{p-scriber}$) on interfacial continuity

With the intention of overcoming the formation of copper flash hooks that bent inside the stir zone, a scriber cutter with length of the scriber ($l_{scriber}$) of 0.5 mm made of HSS was fixed in the pin bottom surface, positioned 2 mm off the centre of pin bottom surface. This was originally applied in dissimilar metal FSLW, aiming to eliminate the necessity of pin penetrating into the harder bottom plate, and avoiding the pin to wear out and melt on the harder material due to higher temperature generated from higher tool rotation needed to plastically deform the bottom plate. In addition, there are interlocking features formed at bottom plate namely outward hooking (bent the opposite way from stir zone) of the bottom plate flash.

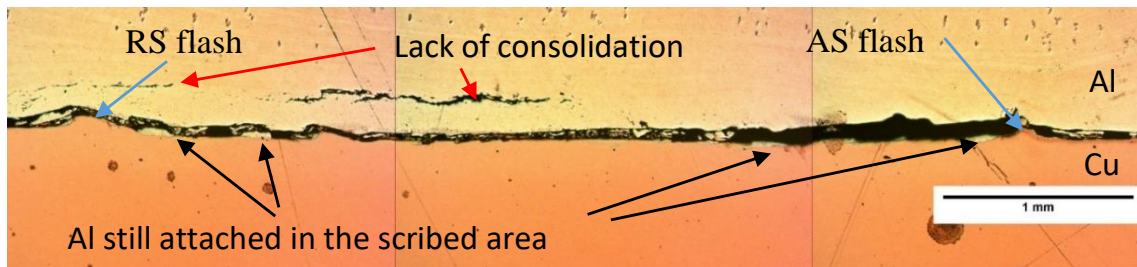


Figure 5 - 1 FSLW scriber with $\omega = 1400$ rpm, $v = 40$ mm/min and $d_{p-scriber} \approx 0$ mm.

Parameters used on this study were $\omega = 1400$ rpm and $v = 40$ mm/min, along with variation of scriber penetration into copper, $d_{p-scriber}$'s of ~ 0 , 0.1, 0.2 and 0.5 mm respectively, which purpose was to study the effect of penetration on copper flash formation, that potentially causing voids if formed excessively as shown in section 4.2. First experiment was conducted with $d_{p-scriber}$ of around 0. This means that the scriber

only slightly penetrated into the copper surface leaving a distance between pin bottom and copper surface for about 0.5 mm.

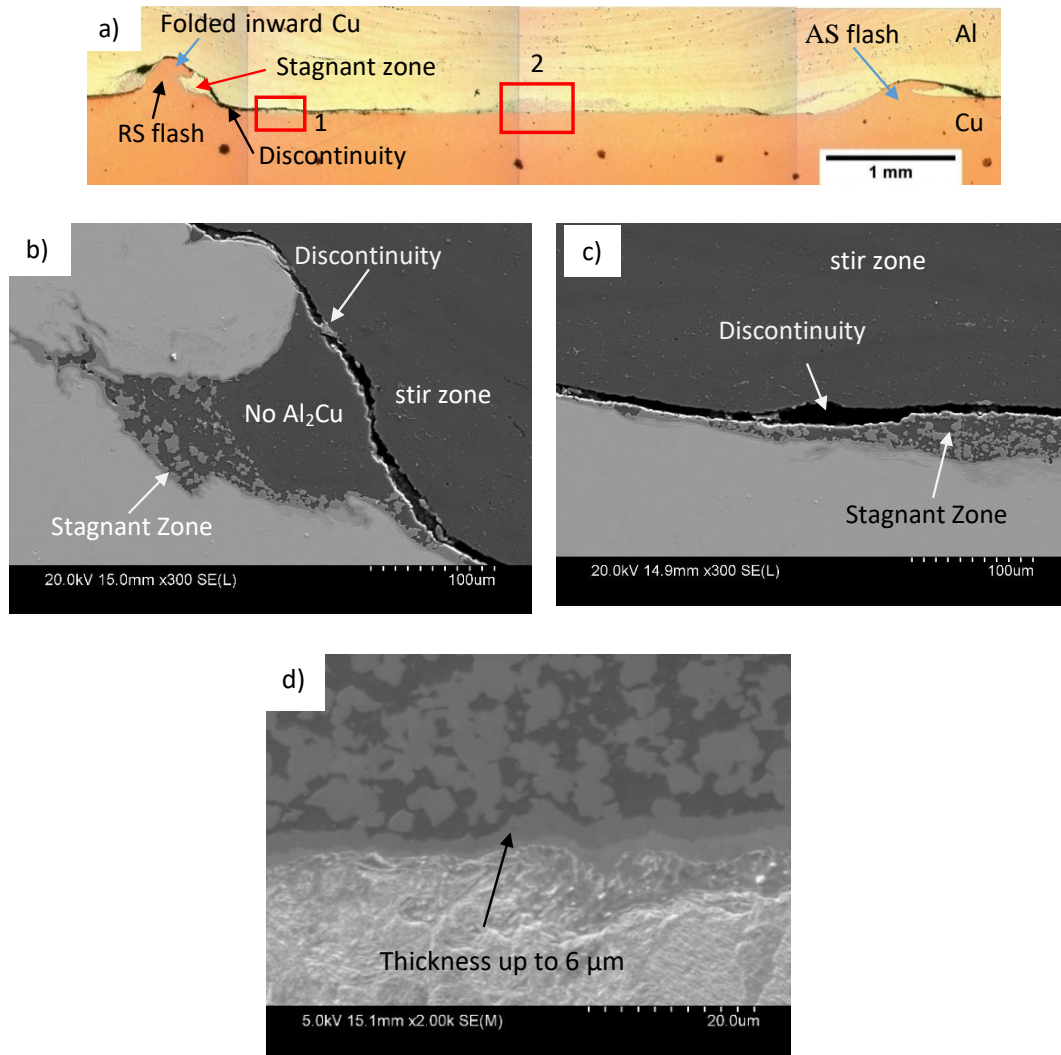


Figure 5 - 2 FSLW scriber with $\omega = 1400$ rpm, $v = 40$ mm/min and $d_{p-scriber} = 0.1$ mm
(a) OEM image of the interface; (b) Hook region pointed by red arrow in a; (c) SEM image of region 1 in a; (d) SEM image of region 2 in a.

Slight penetration was indicated by two copper humps formation in retreating side (RS) and advancing side (AS) as shown in Fig. 5 - 1. From the same figure, it clearly can be seen that no joint can be established in the weld's interface, showed by a gap between aluminium and copper. However, in some area (pointed by black arrows), there were aluminium stuck to the scribed copper surface. This implies that at some point during process, aluminium is driven further to the bottom of the pin and reached the scribed area. However, not all aluminium reacts with copper scribed despite of having the same welding parameters as used in section 4.1, which have shown the ability to form welds with thick interfacial intermetallic layer in the weld interface. Furthermore, this weld was separated upon cutting. There are crack-like features formed parallel above the

gapping interface. This is an indication of lack of consolidation (LoC) of the deposited aluminium behind the pin as explained in the following. The LoC in FSW is usually occurred in a cold weld with low ω and/or high v [60], [61]. However, in the contrary with the literatures, the LoC was formed in RS to mid area. This LoC was formed 0.2 mm above the original Al - Cu interface, while the bottom of the pin placed 0.5 mm above the original Al - Cu interface. This means that the LoC was formed below the pin. In other works this region was named region IV in Arbegast's model [60], [61] and swirl zone [59]. According to the Arbegast model (Fig. 1 - 8), material in region IV came from region II that moved further downward. While the LoC defect in the model was formed in between region IV and I and caused by loss of material from zone II and III, causing insufficient material flowing into zone I [60], [61]. However, no LoC defect can be seen 0.5 mm above AS. This means that RS to mid LoC is not a volumetric defect caused by insufficient material supply.

The 0.5 mm distance between pin bottom and Al - Cu implies that there was no friction heat, which normally generated by the friction between pin body and between pin bottom surface with Cu surface (usually occurred in pin without scriber), generated in this area especially outside the scribed area periphery. In addition, copper have high thermal diffusivity of $117 \text{ mm}^2/\text{s}$ that made temperature loss from the scribed area happened rapidly. Because of this, aluminium in this area lose its fluidity and the ability to consolidate with deposited aluminium, moreover, with copper in scribed area.

In welding with $d_{p-scriber}$ of 0.1 mm, copper flash extended as far as 0.3 mm upwards from the original Al - Cu interface. However, instead of folded outward, as shown in literatures [99]–[101], [118], [119], the RS Cu flash bent inward into the stir zone (pointed by blue arrow in Fig. 5 - 2a). Again revering to Arbegast material flow model in Fig. 1 - 8 [60], [61], this is most likely caused by the material flow in zone IV as it entered the zone from zone III, the material flow from RS to AS pushes the already raised Cu flash in RS. The position of the flash peak, being at 0.1 mm below the bottom surface of the pin, allowed this to happen. There is an apparent discontinuity starting from the left side of the RS flash down to the stir zone, propagating close to Al - Cu interface, up to a third $l_{scriber}$ interface before the middle of the weld. SEM examination on the discontinuity in the area is pointed by red arrow in Fig. 5 - 2a showed in Fig 5 - 2b. The gap morphology showed no matching surface between adjacent gap surfaces indicating that the gap is not a crack. There is a zone below the hooking copper flash in RS that have a region with Al_2Cu particles dispersion strictly

near the Al - Cu interface and another region with no Al_2Cu dispersion above up to the gap. This implies that this area was stagnant and not touched by the incoming aluminium flow behind the pin. This stagnation zone was probably formed during the inward RS folding formation. This hooking structure prevent the incoming to shear the region beneath the folded copper. Fig. 5 - 2c showed the gap in the scribed region of the weld that is marked in region 1 in Fig. 5 - 2a. There is another stagnation zone with thickness up to approximately $40\text{ }\mu\text{m}$ with dense Al_2Cu dispersed in aluminium up to the gap interface. However, in the aluminium stir zone above the gap, the Al_2Cu formed is not as big and dense as in the stagnation zone.

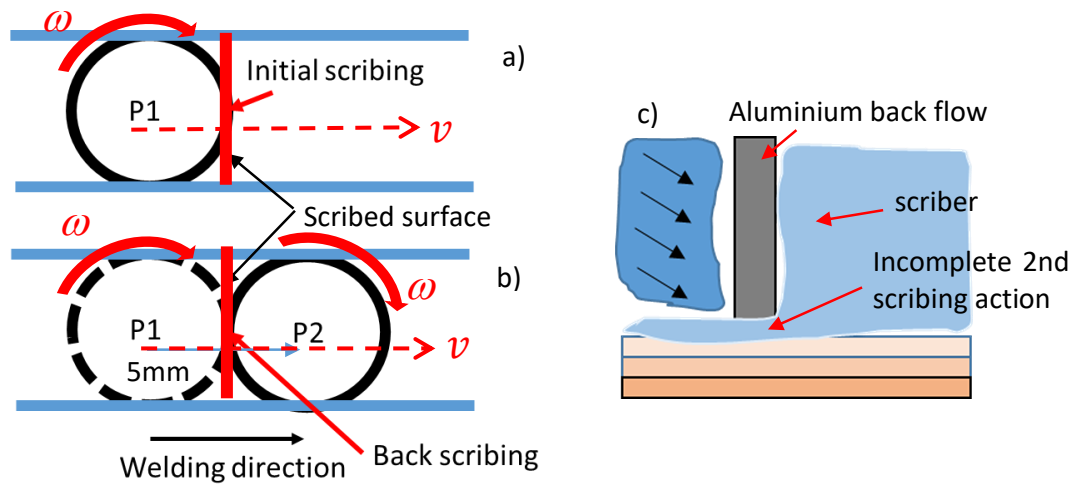


Figure 5 - 3 Plan view of scribing action schematic. (a) Initial scribing action in the front periphery of the scribing region; (b) second scribing action in the rear periphery of the scribing region; (c) longitudinal cross section of the incomplete second scribing action.

To understand how this stagnant zone is formed, it is important to understand the scribing action itself. In a scribing process, one surface as thick as the scriber diameter (thick red line in Fig. 5 - 3a and b) is scribed two times. As a reminder, scriber is a pin with 1 mm diameter, placed 2 mm off the centre of the pin. When the tool rotates, this scriber creates a scribing zone with a diameter of 5 mm that is concentric with the pin bottom surface. The scriber will scribe a surface as wide as its diameter (represented by vertical red line drawn through in Fig. 5 - 3a to b). Fig. 3 - 5a is showing the first position (P1) of the tool when the initial scribing in the front side of the scribing zone happened. As the pin traverse 5 mm forward, the pin moved to position 2 (P2 in Fig. 5 - 3b) and the scribed surface, positioned in the trailing side of the scribing zone periphery, was scribed once again on the trailing side of the scribing zone periphery (back scribing) as can be seen in the schematic in Fig. 5 - 3b.

In between initial and back scribing, most likely aluminium reached this area and reacted with the scribed copper fragments, it reacted to form a composite-like structure, a dispersion of Al_2Cu in aluminium. When the back scribing takes place, the scriber moved from RS to AS scribing the previously scribed surface in initial scribing. However, due to the machine vibration, it might not completely scribe all reaction zone, there is a zone left out, which is the composite-like structure producing stagnation zone as can be seen in Fig. 5 - 2b, c and e. Loss of aluminium backflow fluidity behind the pin and especially under the pin that happened in weld with $d_{p\text{-scriber}}$ of ~ 0 , also happened in this weld. Apparently, 0.4 mm distance between the bottom of the pin surface with the original Al - Cu interface was still causing similar problem as previous weld. The lack of fluidity with the addition of steep flow path makes it hard for aluminium back flow to shear or even to join the stagnation zone. But another flow that came to the scribed area that was not obstructed with the copper was able to join the stagnation zone. This can be seen in the interface after the discontinuity. The schematic mechanism of the discontinuity formation can be seen in Fig. 5 - 3c. Interfacial intermetallic formed in this weld can reach up to 6 μm . Although no interfacial intermetallic crack can be seen in this weld, previous studies showed that when Al - Cu interfacial intermetallic is thicker than 2.5 μm , the joint is more susceptible to have brittle crack along the interfacial intermetallic [28], [33].

In welding with $d_{p\text{-scriber}} = 0.2$ mm, both Cu flash in RS and AS bent outward (Fig. 5 - 4a) similar to the one in existing literatures [100], [101]. The copper flash extends up to 0.4 mm. Given the $d_{p\text{-scriber}} = 0.2$ mm and $l_{\text{scriber}} = 0.5$ mm, the distance between the original Al - Cu interface with the summit of the flash is only 0.3 mm. This implies that the amount of copper that was scribed, is substantial enough to produced extensive Cu flash in RS and AS. It was extended quite significant but restricted by the bottom surface of the pin. The movement of scriber from AS to RS and RS to AS in front and back of the scribing zone respectively created a stream of material that pushed the copper flash in the opposite direction of stir zone. In this stage, still under the pin bottom surface, the height of the flashes was 0.3 mm from the original Al - Cu interface. However, as the tool moved forward and the flashes got out from the bottom of the pin surface restriction, it rose further to 0.4 mm.

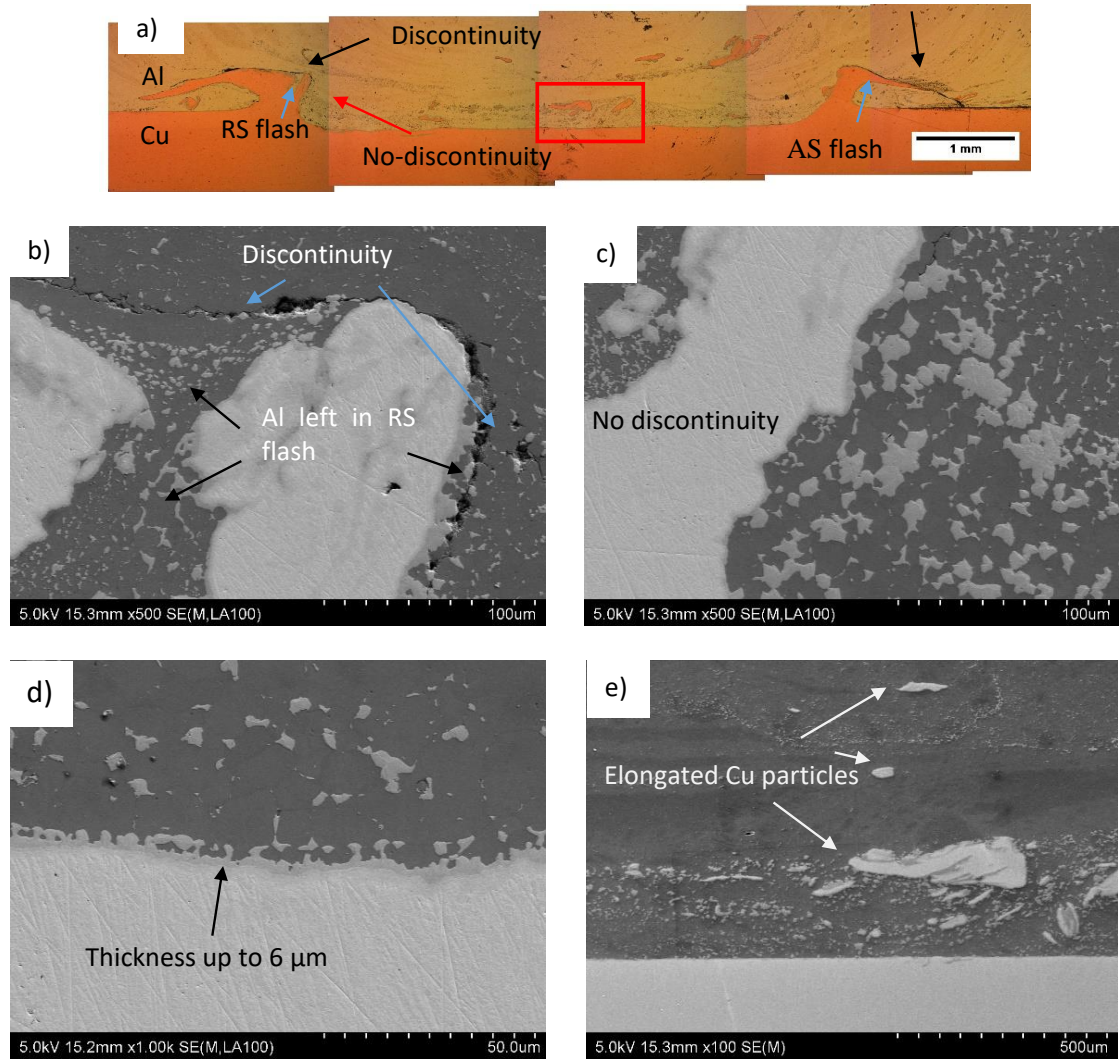


Figure 5 - 4 FSLW scribe with $\omega = 1400$ rpm, $v = 40$ mm/min and $d_{p-scriber} = 0.2$ mm
(a) OEM image of the interface; (b) SEM image of the region pointed by black arrow in a; (c) SEM image of the region pointed by red arrow in a; (d) SEM image of typical interface of this weld; (e) SEM image of stir zone in boxed region in a.

No major gap and/or voids visibly was found in the scribed interface. However, apparent discontinuity can be seen in Al - Cu interface on regions on RS and AS flash that are pointed by black arrow in Fig. 5 - 4a. SEM examination shown in Fig. 5 - 4b of RS flash pointed by black arrow shows that this discontinuity is not in the form of crack in the Al - Cu interface in the RS flash. The discontinuity propagated is not only between Al - Cu interface, but also between some aluminium that exist in the RS flash. The discontinuity continues to propagate down along the copper flash as pointed by the blue arrow. However, the discontinuity stops to propagate in this region. This is shown by examination of the region pointed by red arrow in Fig. 5 - 4a that can be seen in detail in Fig. 5 - 4c, which is the area further below from Fig. 5 - 4b, no discontinuity seen to be formed in this region.

Typical interface of this weld can be seen in Fig. 5 - 4d. No cracks or voids can be seen across the interface. However, interfacial intermetallic can be formed up to 6 μm . Interfacial intermetallic this thick, as previously mentioned, is susceptible to have brittle crack across it [28], [33]. In the stir zone, in Fig. 5 - 4e it can be seen that there is mix dispersion of coarse and fine fragments of copper. The larger fragments lie in stir zone horizontally, parallel to the weld interface. This is an indication of good aluminium flow, on the contrary with the existing literature where the fragments stayed in the scribed area above the interface with no particular orientation [99], [100], [102], [104], [106], [107], [109]. These fragments, instead of blocking the flow and creating voids, they were flowed along with aluminium flow.

Typical interfacial features of weld produced with $d_{p-scriber}$ of 0.5 mm can be seen in Fig. 5 - 5a. Such $d_{p-scriber}$ means that the scriber plunged all the way into bottom of copper plate, that made the bottom surface of pin placed approximately in the Al - Cu interface. There are distinct features differences if compared with the results from previous parameter. Extensive copper flashes were formed in this weld. However, the RS copper flash that extended and slightly bent into the stir zone, unlike previous weld, as well as significantly larger fragments mixed with finer copper can be seen dispersed in stir zone. These copper fragments were positioned in the stir zone so that they resemble an onion ring configuration, on the contrary with the existing studies [99], [100], [102], [104], [106], [107], [109]. Large copper fragments above the weld interface lay vertically in stir zone, parallel with the interface. It is important to notice that no voids formed near these large copper fragments. This implies that instead of blocking the flow, the fragments flow fluidly with aluminium.

The scribed area in this weld seems narrower than the previous weld. Instead of 5 mm, the cavity of scribed area is measured at 4.2 mm. The rest of scribed area is covered by a mass of copper (area 1 in Fig. 5 - 5a). Detailed view on the mass of copper can be seen in Fig. 5 - 5b. There was aluminium trapped in this mass of copper and the length of the AS of scribed area cavity wall to the trapped aluminium closest to RS was approximately 5 mm, which is the width of scribed area. This implies that the mass of copper was folded after the occurrence of back scribing trapping some aluminium forming feature pointed by black arrow in Fig. 5 - 5b. The folding most likely happened after the pin passed the scribed area, and the copper, probably from the hook, was driven into the scribed area by the aluminium down flow just behind the pin.

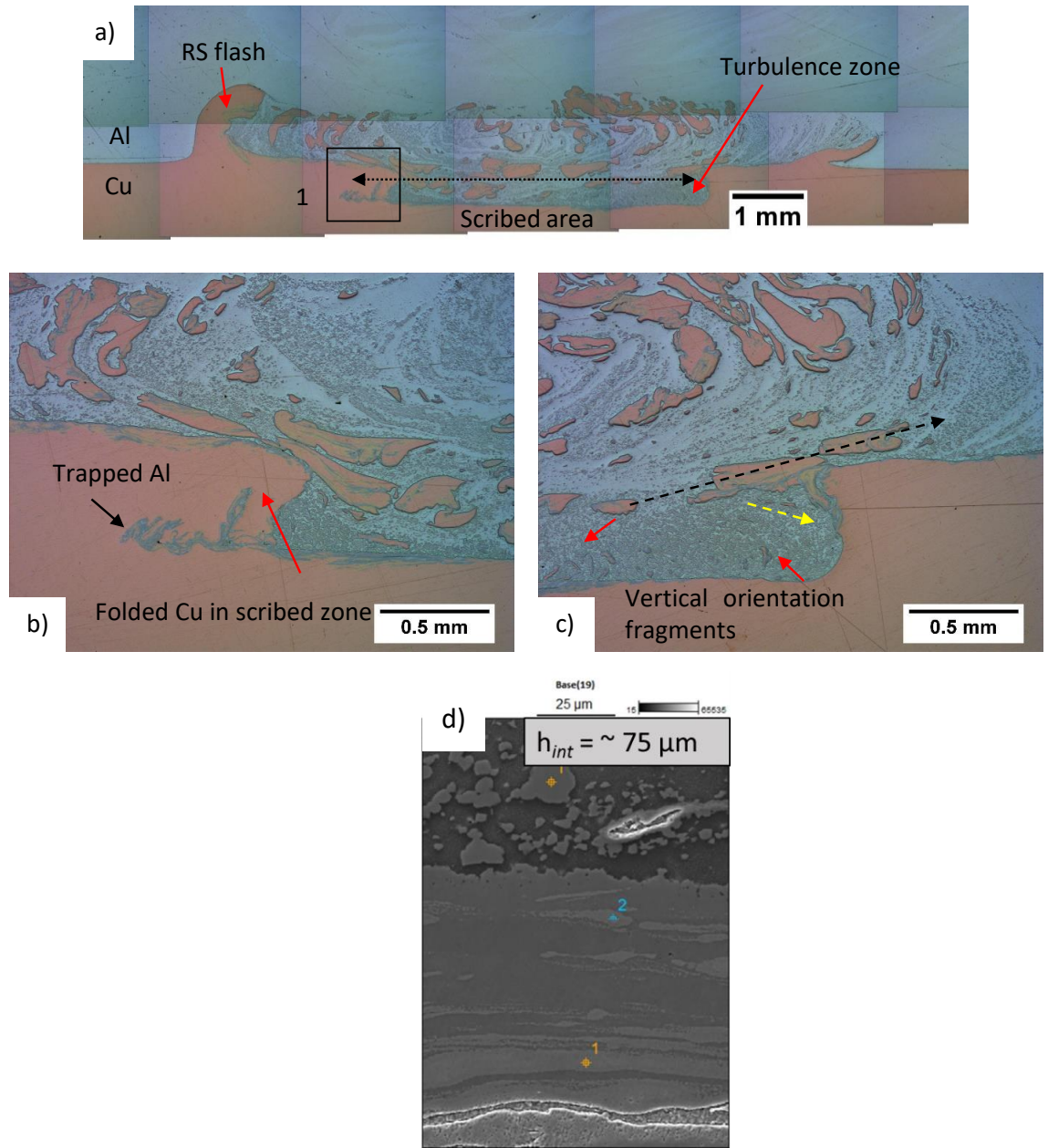


Figure 5 - 5 FSLW scribe with $\omega = 1400$ rpm, $v = 40$ mm/min and $d_{p-scriber} = 0.5$ mm
 (a) OEM image of the weld's interface; (b) Area 1 in a; (c) turbulence zone in a; (d) SEM image of mixed stir zone (MSZ) in the weld's interface.

In the scribe region in AS, specifically in the scribed cavity wall, it can be seen from Fig. 5 - 5c, the orientation of the elongated copper fragments is rather vertical, perpendicular to the weld interface. Furthermore, the fragments orientation in said area is different than the main flow, shown by the large copper fragments that flow upward out of the scribed area cavity, with the trajectory shown by the black dashed arrow. However, not all aluminium flew out of the stir zone, some went down impinging the AS cavity wall. The trajectory shown by the yellow dashed arrow is indicated by the smaller copper fragments above the yellow dashed line. This probably created turbulence in the bottom corner of the AS scribed cavity wall, indicated by the rather

vertical copper orientation, however, it is not uniform (shown in red arrows). In addition, this weld produces rather thick MSZ in the copper side near the interface, indicating that the intercalated aluminium in copper turned into intermetallic, with thickness that could reach approximately 75 μm (Fig. 5 - 5d). Intermetallic with this thickness is prone to break along the interface [28], [33].

5.2 The importance of down flow on the formation of intermetallic

To study how downward flow affects the scribed area, a weld is conducted with “faulty” threads pin (Fig. 5 - 6b) with the same parameters as weld in Fig. 5 - 5. As a comparison, normal left-hand threaded pin can be seen in Fig. 5 - 6a. The threads were deliberately made imperfect to diminish aluminium vortex down flow that supposedly functioned to drive away copper particles that was created by the scribing action. The interface of this weld can be seen in Fig. 5 - 7. Despite of difference in pin geometry, there were two features in this weld that were similar to features in weld shown in Fig. 5 - 5, which are extensive copper flash that slightly bent toward stir zone and copper mass in RS. However, in this weld, copper fragments could not escape the stir zone in scribed area. Large elongated copper fragments can be seen in Fig. 5 - 7a pointed by blue arrows that lay vertically, slightly perpendicular to the interface. There are areas that are dark in the stir zone on scribed area along with large elongated copper fragments. This dark region is most likely intermetallic formed by dense finer copper fragments that were trapped with aluminium, which then reacted, and activated by the high friction heat, converting the stir zone of scribed area into a thick region of intermetallic.

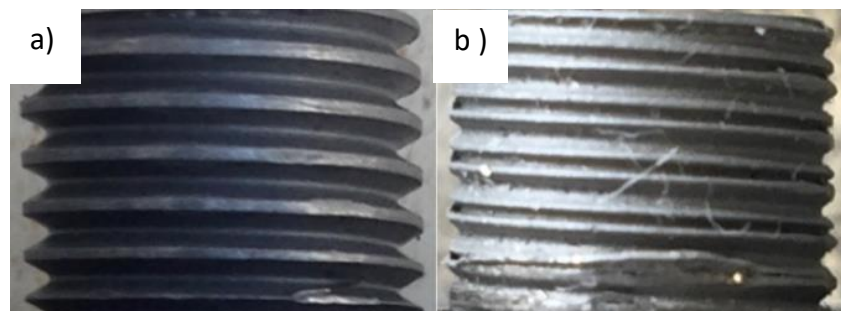


Figure 5 - 6 (a) Normal left-hand thread pin and (b) “Faulty” thread used to diminish the down flow.

This intermetallic region is 5 mm in thickness which is prone to brittle fracture [28], [32], [33]. This brittle nature of the region can be seen in cracks that are pointed by yellow arrows in Fig. 5 - 7a. The matrix region near the big cracks, red circled area in Fig. 5 - 7a, was measured at 458 HV (Fig. 5 - 7d). While the matrix of the dark area pointed by black arrow in Fig. 5 - 7a was consisted of dense grey particles, which was

identified as Al_2Cu in section 4 - 2, and also known to be prone to cracks. This area was measured at the average of 350 HV. These areas were significantly harder than the copper fragments from the same region, that was measured at 76 HV (Fig. 5 - 7c), confirming the brittle nature of the region. The cracks were formed and propagated exclusively in this brittle dark region and stopped after reaching the copper fragments, which is much softer than the surroundings matrix (Fig 5 - 7c and d).

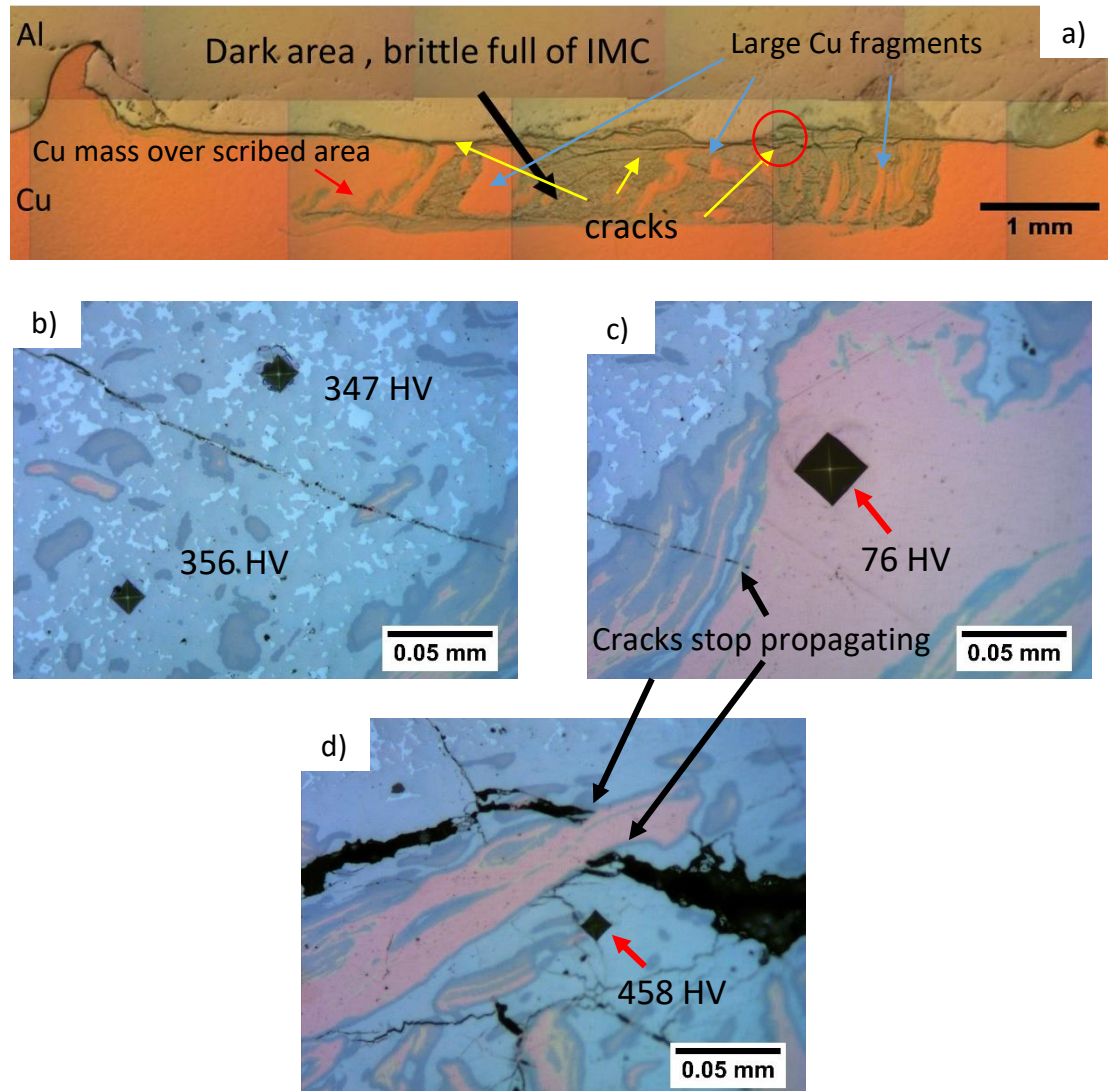


Figure 5 - 7 Weld interface using faulty thread pin (a) OEM image of the stir zone showing thick intermetallic formed by the Cu fragments and Al; (b) Hardness of matrix in intermetallic region; (c) Copper fragment hardness in intermetallic region; (d) Hardness of the region near big cracks in circled red area in a.

5.3 The effect of 2.5° tilt angle to interfacial continuity

A weld with same parameters with weld in Fig. 5 - 2 was conducted using the fourth tool, consisting of concave shoulder with left-hand threaded pin with the addition of

scriber pin. The result can be seen in Fig. 5 – 8a. Cu flash hooks in RS and AS are distinctly different in weld with 0° and 2.5° tilt. As can be seen in Fig 5 - 2, the weld that using 0° tilt, and 0.1 mm $d_{p-scriber}$ were resulting in the formation of copper flash hooks extension 0.3 mm upward from the original Al - Cu interface. However, in weld that using 2.5° tilt condition, these hooks extended only up to approximately 0.1 mm from original Al - Cu interface. Furthermore, both copper flash in RS and AS bent outward from the stir zone. There is a big chunk of copper in the left-hand side of RS copper flash, outside the stir zone. This most likely was the scribed material. But, instead of forming extensive hooks, both chunks in RS and AS were driven away from the stir zone. Above all, no extensive gap can be seen across the weld interface, on the contrary to the weld with 0° tilt.

The absence of extensive gapping interface region shows that higher downward forge force generated by the usage of tilting condition, has succeeded to further force the aluminium behind the pin to be pressed into copper surface, overcoming loss of fluidity due to the excessive distance between the scribed interface and the pin bottom surface as analysed above. Interfacial continuity can be achieved as well as interfacial intermetallic, as can be seen in Fig. 5 - 8b. However, discontinuity can also be formed in this weld. Fig. 5 - 8c shows that thickness of outer layer interfacial intermetallic, Al_2Cu , is thicker in the continuous region. However, immediately to the right, very thin-to-none layer of Al_2Cu can be seen in this region. Moreover, gap can be seen formed atop of the interface. This gap was not in the form of channel defect. There is aluminium inside the gap that was not in the same plane with the gap. This implies that, despite of the higher downward forging force induced by the tilt condition, aluminium is generally able to be forced to reach aluminium in order to scribe the copper surface, however in some area aluminium cannot reach bottom of scribed area thus forming interfacial gap. Furthermore, as the pin advanced and deposited another layer in front of the gap, the pin was not necessarily formed another gap. In addition, this gap might be initiating interfacial crack between Al_2Cu and aluminium, as pointed in Fig. 5 - 8d, indicated by the matching cracked surface.

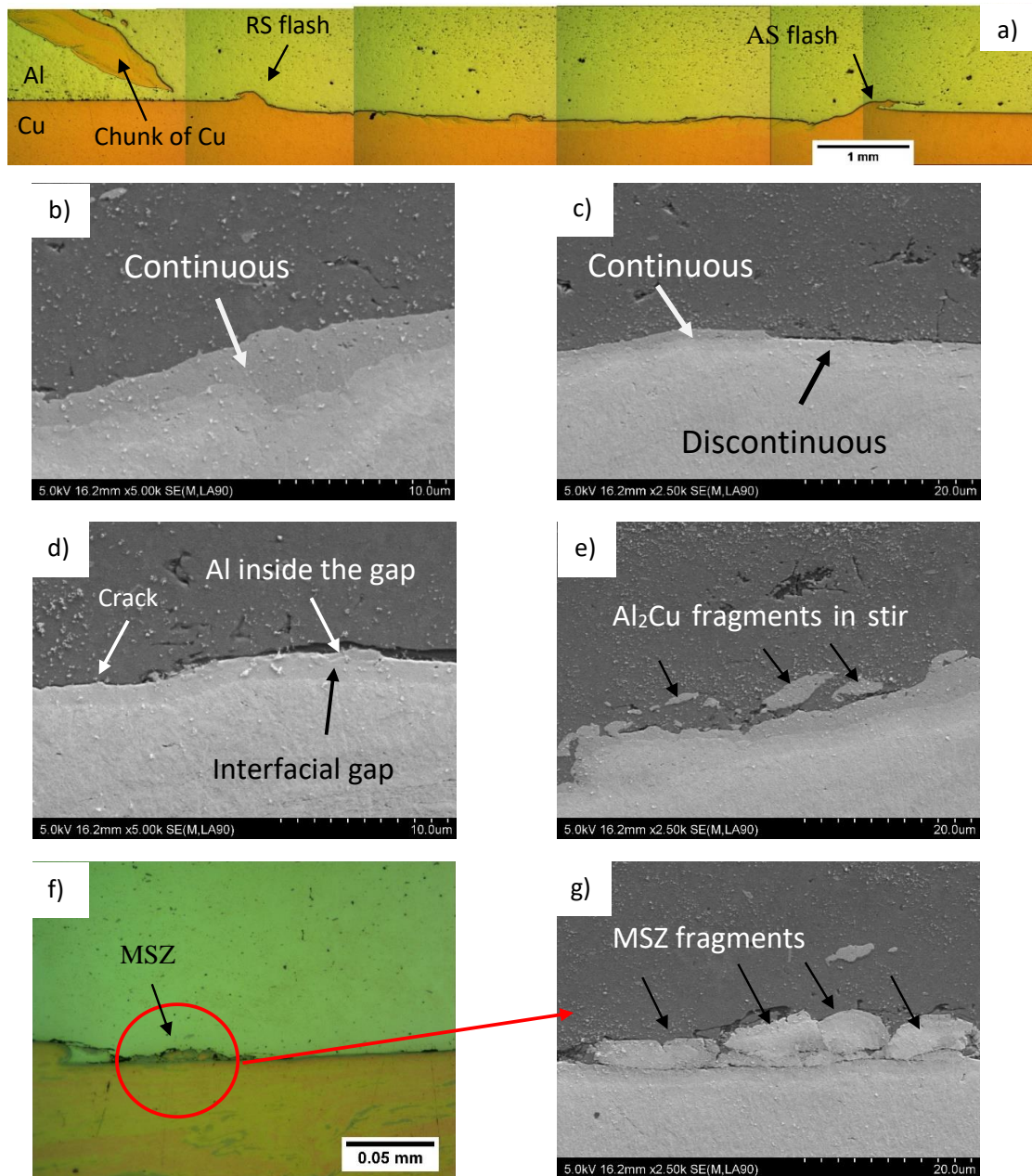


Figure 5 - 8 $\omega = 1400$ rpm, $v = 40$ mm/min, $d_{p-scriber} = 0.1$ mm, tilt angle = 2.5° (a) OM image of the interface; (b) Continuous interface of this weld; (c) Typical interface showing discontinuity formation; (d) Closer look at the gap; (e) Al₂Cu fragments in the stir zone; (f) MSZ fracturing in the interface; (g) Higher magnification of circled red area in f.

High downward forging force also contributes to the fracturing of Al₂Cu and MSZ that were probably initially formed immediately after back scribing action. The first proven by the existence of Al₂Cu fragments in aluminium above interfacial Al₂Cu layer in SEM in BE mode in Fig. 5 - 8e. Same colour gradation suggests that the fragments in aluminium with the outer layer adjacent to aluminium are in fact the same compound. In addition, in section 4 - 2, it was shown that the outer layer adjacent to aluminium is Al₂Cu. While the later was shown in Fig. 5 - 8f and g. In Fig. 5 - 8f, fracturing was not

clearly shown. However, the mixture of blue (intermetallic) and tangerine (copper) in the red-circled area and the area below it shows that area near the interface is MSZ. Further analysis of the circled area was then carried out using SEM in BE mode (Fig. 5 - 8g). It showed that the area consisted of fragments of MSZ with various sizes, suggesting MSZ fracturing occurred after backs scribing.

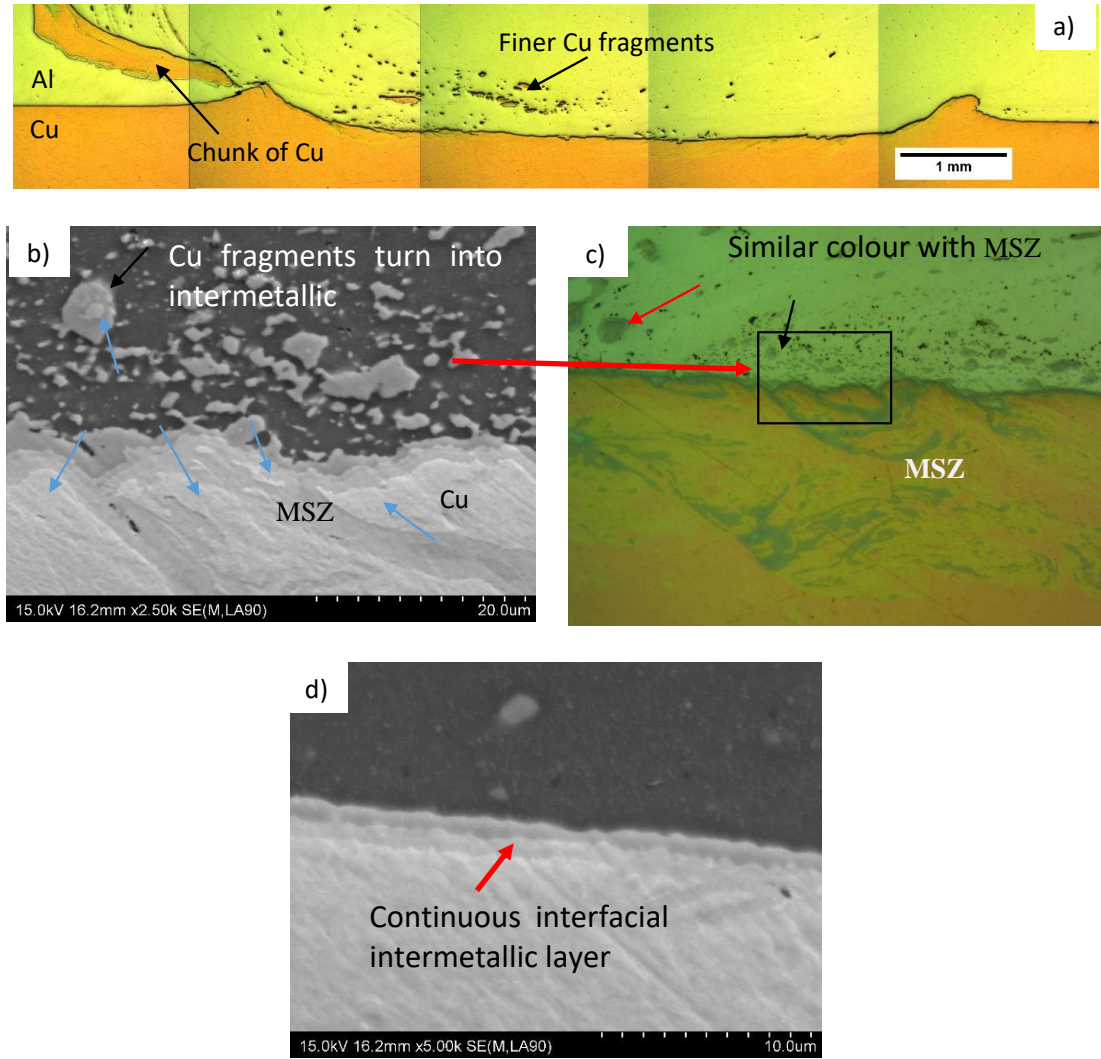


Figure 5 - 9 $\omega = 1400$ rpm, $v = 40$ mm/min, $d_{p-scriber} = 0.2$ mm, tilt angle = 2.5° (a) OM image of the interface; (b) One of typical interface above thick MSZ; (c) OM image of b; (d) Another typical interface with continuous interfacial intermetallic layer.

Further weld using deeper $d_{p-scriber}$ of 0.2 mm was then carried out. The typical interface of the weld can be seen in micrograph in Fig. 5 - 9a. Not too extensive copper flash and massive chunk of copper to the left of RS copper flash, similar to the previous weld, can also be seen formed in this weld. Except for RS, flash was not bent outward of the stir zone. The interfacial features are nowhere close to the weld with same parameters but without tilt in Fig. 5 - 4a. Finer copper fragments can be seen dispersed

in the aluminium side of the stir zone, especially in area from RS to three fourth of the interface. In this weld, continuous interface can be established. Two typical interfaces of the weld can be seen in Fig. 5 - 9b and e. Fig. 5 - 9b is one of typical interface with thick MSZ in the copper side. Light grey represents copper (pointed by blue arrow in Fig. 5 - 9b) while darker grey is Al - Cu intermetallic and the darkest grey is aluminium. The majority of the fragments dispersed in aluminium have the same colour with the intermetallic layer adjacent to aluminium (Al_2Cu). However, in some bigger fragments, judging from the colour, there are copper that exist along with Al_2Cu . Micrograph of the same interface was given in Fig. 5 - 9c for confirmation. Fragments pointed by black arrow in Fig 5 - 9b and c were compared. In SEM image, it is shown that it contained Al_2Cu and copper, while in OM image it was coloured similarly in light grey and dark grey. While in the bigger fragments (red arrow in Fig. 5 - 9c), not captured in SEM image, copper colour can be seen in the middle of the fragments with dark and light grey layer adjacent to aluminium formed in the interface, respectively. This implied that the source of the dispersed fragments in aluminium came from fractures of Al_2Cu layer and/or finer copper fragments that entirely or partially turned into Al_2Cu due to reaction with aluminium in their interface activated by the welding temperature. Another typical interface with minimal amount of MSZ can be seen in Fig. 5 - 9d. Continuous interfacial intermetallic layer, that consists of three layers were formed. With the total and Al_2Cu layer thickness are approximately 2 and 1 μm . However, thicker interfacial intermetallic layer is formed along with thicker MSZ.

5.4 Analysis on material flow in the pin bottom during FSLW

Keyholes from welding in Fig. 5 - 4a and 5 - 9a that represent FSLW with scriber pin using 0° and 2.5° tilting condition were then examined in order to understand the flow in in the vicinity of the scriber pin.

5.4.1 Flow in the bottom region in weld with 0° tilt

Keyhole from welding shown in Fig. 5 - 4a was sectioned into 4 pieces. Details about the sectioned area can be seen in section 3.7. First section that was examined was the front edge of scribing area (Fig. 5 - 10a). Original Al - Cu interface was slightly bulged, extruded by the front scribing action, when scriber pin moved from AS to RS at the front of the scribing pin. Above the bulge, there are extensive copper fragments adhere to the area that was originally occupied by the pin, extended from RS to AS and got thicker toward the middle. This fragment was separated from the interface bulge.

However, this implied that this was copper flash that pushed and extended upward, impinging the bottom pin surface and bent to the front of the scribing area as well as to the side. This was induced by $d_{p-scriber}$ and the scribing action. Judging from the copper flash features of the weld established with scriber discussed previously, the copper flash was hooking to the opposite area of stir zone or, when in process, it was forming in the front half circumference of the scribing area. This copper flash was extended to exceed the pin periphery and pushed upward by aluminium in the front of the pin due to the forward movement of the tool and immediately caught by the vortex flow in the thread pin, as can be seen in the RS in Fig. 5 - 10b. However, the flash in AS was not as extended as in RS. This might be due to lesser copper were extruded in AS. But, as the pin moved from AS to RS, the side surface of the scriber extruded more copper, and created more extended copper flash in the RS, as can clearly be seen in Fig. 5 - 11. The copper flash in the AS can be sheared into elongated fragments, driven out from the bottom of the pin, and immediately trapped by the vortex flow in the thread of the pin (Fig. 5 - 10c).

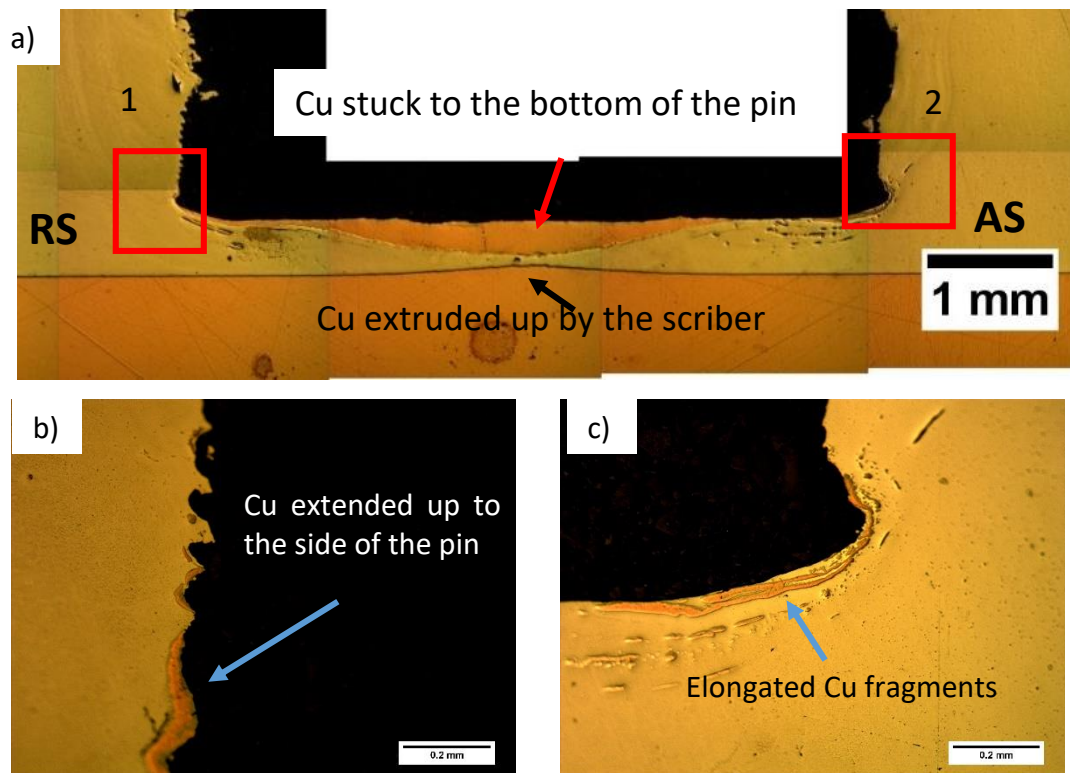


Figure 5 - 10 (a) OM image of the edge of scribed area; (b) Bottom corner of pin in RS, area 1 in a; (c) Bottom corner of pin in AS, area 2 in a.

Figure 5 - 11 is sectioned to represent the condition where the pin have passed half way through the original Al - Cu interface. The copper flash has already formed into similar form with the weld shown in Fig. 5 - 4a. The flat regions on top of the copper flash in

RS and AS pointed by blue arrows showed that during process, these two regions were directly in contact with the pin. Implying that during process, these flashes were extended upward, then impinged to the bottom of pin surface and bent, and finally pushed by the scribing action as the scriber moved from AS to RS in the front half of the scribing area. This confirms the flash hooking formation previously analysed. In the AS, there were trails of recirculation flow shown by the copper fragments just after the AS copper flash, indicating recirculation of copper fragments into the vortex flow. No aluminium extrusion got into the scribed area was perhaps because of the formation of the keyhole itself. The pin forward move was stopped, and retracted, and then its rotation was also stopped. No further extrusion of aluminium entered the scribing area.

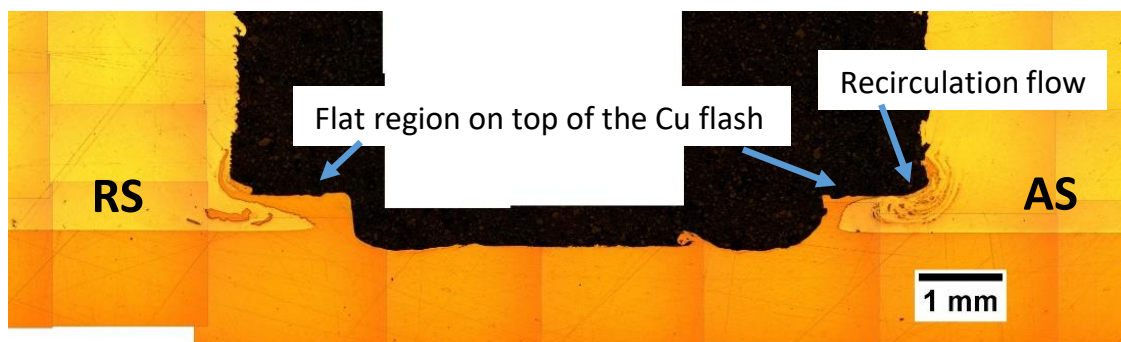


Figure 5 - 11 OM image of the middle of the keyhole.

The copper scribed is in the front half of the scribing area, either extruded out in the form of flash in the front half of circumference of the scribing area or displaced behind the scribing area as the scriber pin moved from RS to AS in the rear half of circumference of the scribing area. The mixture of large fragments of copper and aluminium in the scribed area in Fig. 5 - 12, which was taken from the rear edge of scribing area, confirmed the fragments displacement. Interface from the edge of the area behind the pin was then observed (Fig. 5 – 13). Mixture of big and finer copper can be found in the scribed area. Copper trace reveals that there were two different flows acting in the stir zone. First is flow of the pin, and second, flow in scribed area. These two flows are separated by a region of aluminium without copper fragments. The second flow can occur thanks to aluminium that went into the scribed zone from RS. The reduction in copper fragments size indicates that rigorous mixing happened in scribing area. The material from scribing area can get out of the scribing area and recirculate into the pin flow as indicated by copper fragments atop of scribed area in AS (indicated by blue arrow in Fig. 5 - 13). The flow that goes from RS, down to the bottom of the pin and rise in the AS is in accordance to Arbegast's [60], [61] finding. Voids are also formed in this area, in the vicinity of big copper fragments as well as in the RS, adjacent

to the copper flash wall inside the scribing zone. The later could be the sign that aluminium have difficulty in reaching RS copper flash wall.

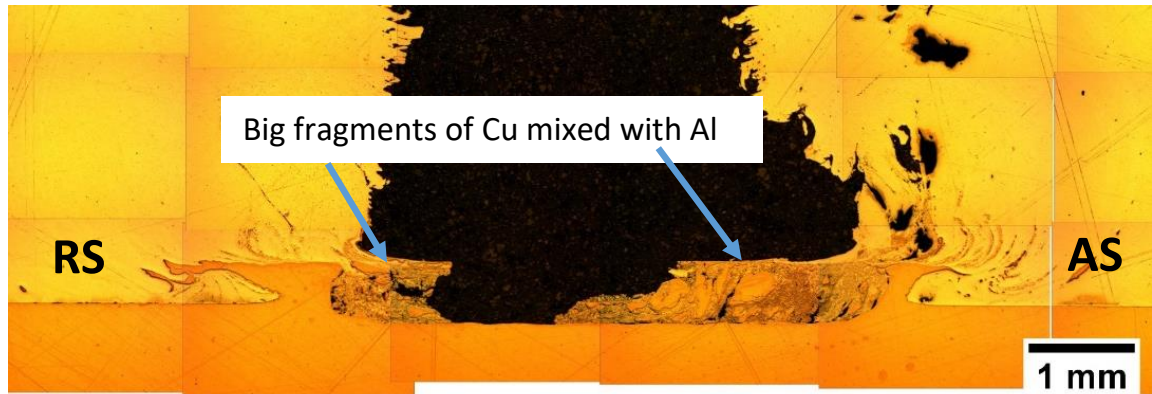


Figure 5 - 12 OM image of rear edge of the scribed area.

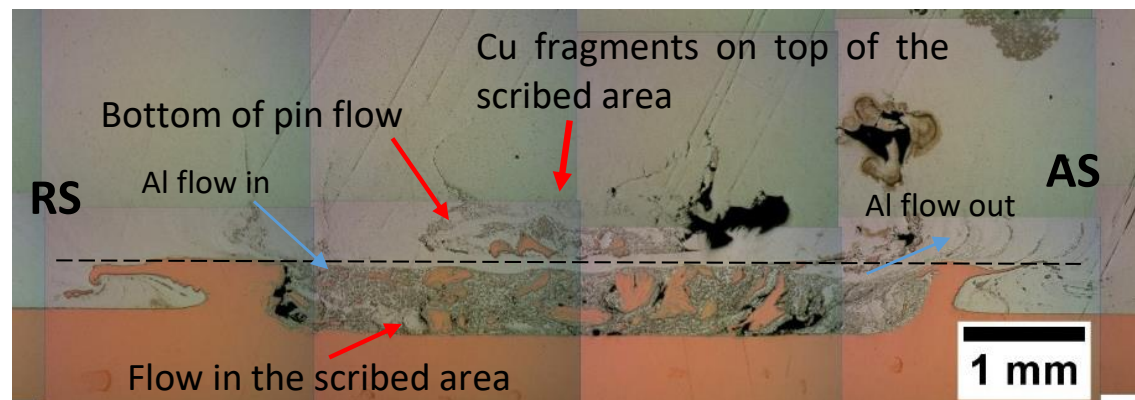


Figure 5 - 13 OM image of rear edge of the pin periphery.

To have a better understanding of the material flow, the surface from Fig. 5 - 13 was further grinded to reveal the area just outside periphery of the pin, but still inside the shoulder diameter, in order to represent the condition where the pin just left the scribed area. It was revealed that the pin flow was pushed further down to the scribed area (Fig. 5 - 14a) and further converged with the flow in scribed area (Fig. 5 - 14b) as the pin moved further away. Again, this was shown by the natural trace made by the copper fragments. Much lesser large copper fragments can be found in the scribed area. Instead, dense fine copper occupied the majority of the scribed area (Fig. 5 - 14a). However, as the pin moved further away and the pin induced flow converged with the flow in the scribed area, the dense fragments were starting to be driven away from the scribed area. This was indicated by the difference in copper fragments denseness in the scribing area shown in Fig. 5 - 14b. There was a stagnation zone, in the RS, stuck in the wall of copper flash. Higher magnification of this stagnation zone in Fig. 5 - 14c shows that it was separated with the adjacent aluminium by extensive discontinuity that started from

the top of the copper flash. It looked like the incoming aluminium could not form a joint with this stagnation zone. The fragments in stagnation zone are larger than incoming aluminium flow. The fragment's morphology, large grey fragments, in the stagnation zone indicates that this zone was not swept by aluminium flow, allowing the larger copper fragments reacted with aluminium matrix to form Al - Cu intermetallic.

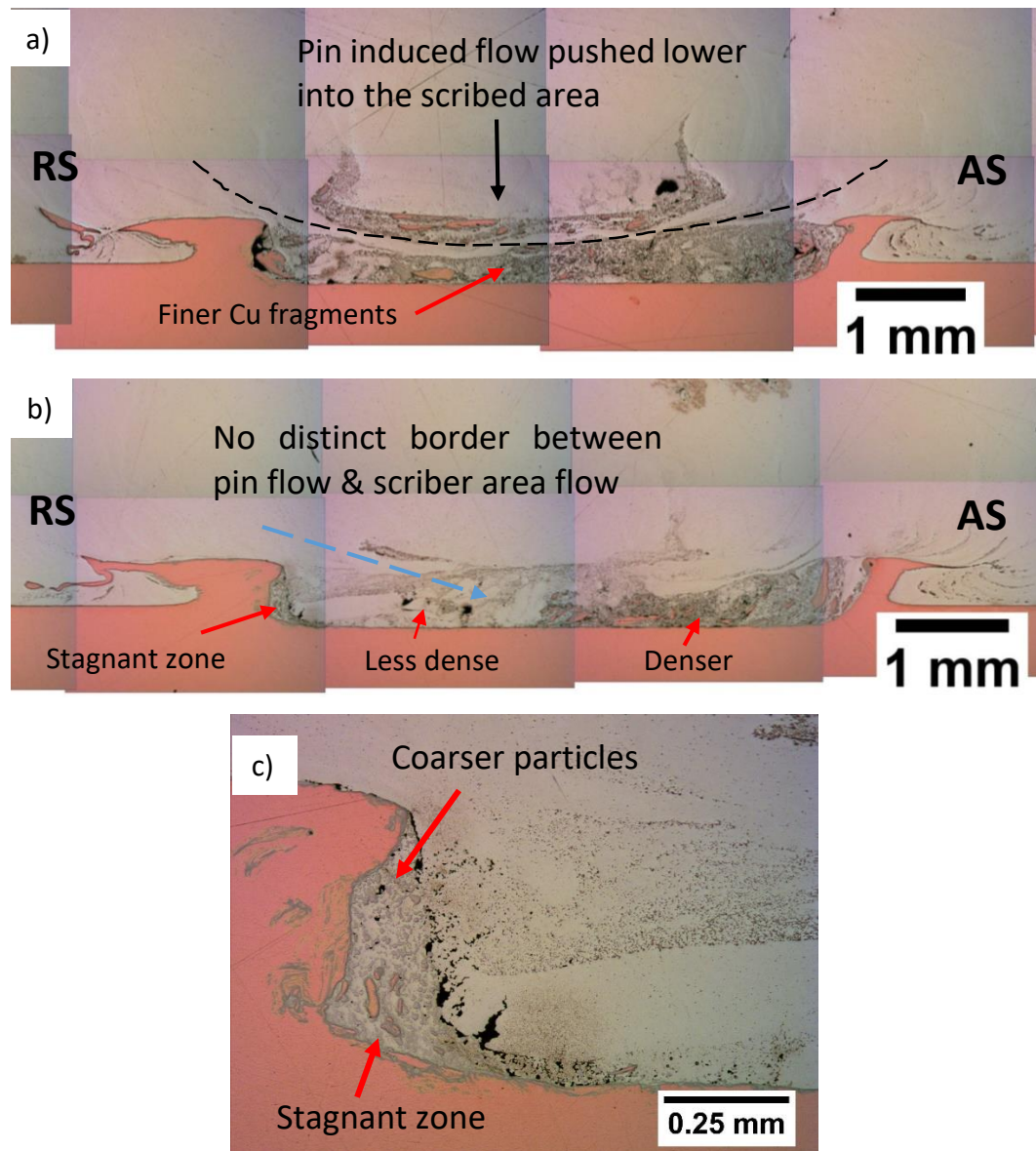


Figure 5 - 14 (a) interface of area outside the pin periphery; (b) Interface further away from a; (c) Stagnant zone from b.

5.2.2 Flow in the bottom region in weld with 2.5° tilt

To understand the material flow in FSLW with scriber pin that using 2.5° tilt condition, it is important to know the scriber positions during process. The zero-condition setting was done by pinning a piece of paper to top aluminium surface and the bottom corner of the tip of the scriber. Scriber position in zero-condition setting was the initial condition,

positioned as seen in Fig. 5 - 15a and b. The bottom corner of the scriber pin part would be the one that performs the scribing action. However, when 2.5° tilt condition was applied, as the scriber rotated with the pin, the pin penetration depth was changed, it became lesser than the initial position. Visualisation of scriber position during FSLW can be seen in Fig. 5 - 15d. As the pin rotated from initial position, behind the scribing area, to AS, flank side of the scribing area, and then to the front of scribing area, the $d_{p-scriber}$ decreased and increased again as it moved from the front, to the flank (RS) and back to the initial position. The calculation was carried by simple trigonometry with reference to the diagram in Fig. 5 - 15c with A as the tilt angle (in this case 2.5) and represented the bottom corner of scribe that performed the scribing action; B represented the bottom corner of scribe in the front (Fig. 5 - 15a) and flank side (Fig. 5 - 15b) of the scribing area; C represented the corner in front of c plane; a represented the height difference between two different scriber positions; b represented the scribed surface; and c represented the distance between two scriber bottom corners in two positions (4 and 2 mm for front and flank side position respectively).

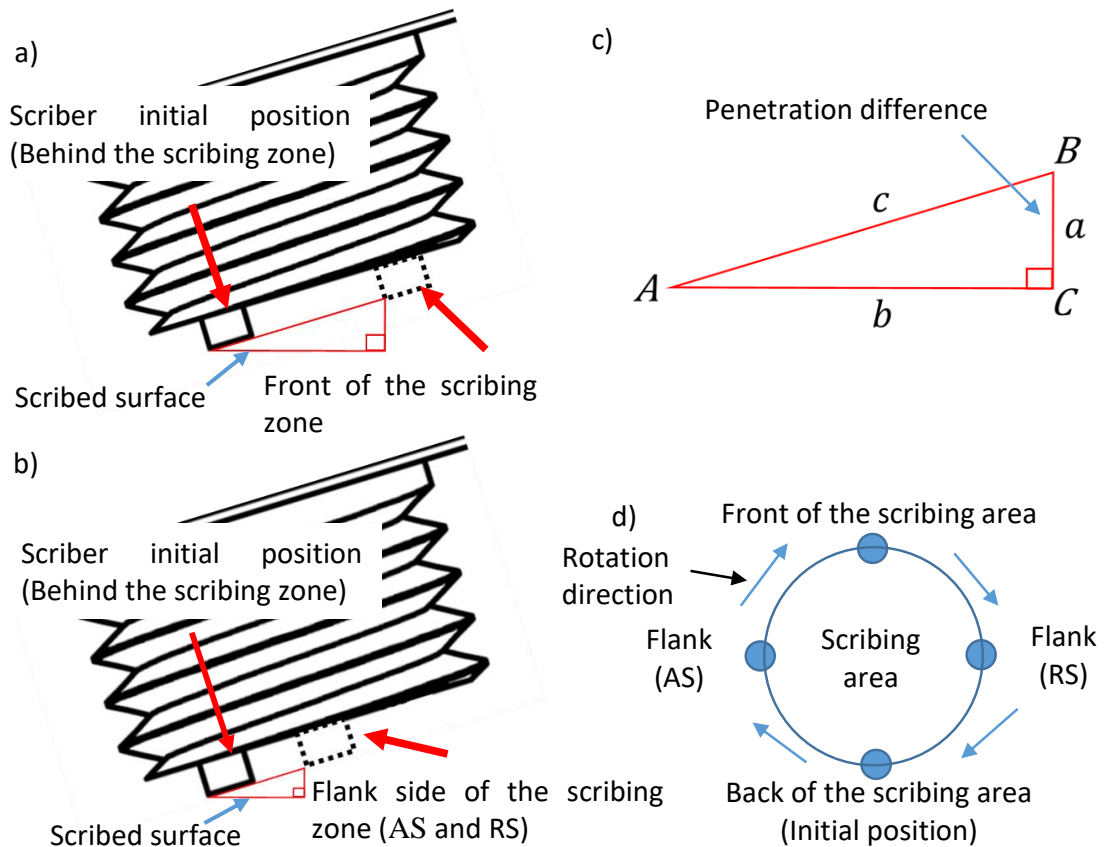


Figure 5 - 15 Scriber pin positions comparison, (a) back (initial position) and front (dashed) side; (b) back (initial position) and flank (dashed) side; (c) analysis of $d_{p-scriber}$ difference; (d) diagram of pin position.

Calculation of the penetration difference for scribe at the behind and flank side of the scribing area was conducted by using equation 18.

$$\sin A = a/c \quad \text{Eq. 18}$$

With the initial penetration being 0.1 mm and the difference between back and front scribe position being 0.17 mm, the position of scribe in the front would be 0.07 mm above the original un-scribed Al - Cu interface. While for $d_{p-scribe}$ of 0.2 mm, in front side position, the $d_{p-scribe}$ would be 0.03 mm. Calculation was made using equation 19.

$$\sin 2.5 = a/4 \quad \text{Eq.19}$$

Furthermore, the calculation for behind and flank position height difference was conducted using equation 20.

$$\sin 2.5 = a/2 \quad \text{Eq. 20}$$

This shows that in the flank sides (both AS and RS), the scribe only penetrated into the copper as far as 0.01 and 0.11 mm for $d_{p-scribe}$ of 0.1 and 0.2 mm respectively. This decrease of $d_{p-scribe}$ can clearly be seen in Fig 5 - 16a and b that sectioned from areas in the front and behind the scribing area respectively.

The absence of typical extensive copper flash hooks in AS and RS that were normally formed in FSLW with scribe in 0° tilt condition can be explained as follows. It was previously analysed that $d_{p-scribe}$ and its movement from AS to RS in the front half of the scribing area was responsible for creating the flash. In welding that using 2.5° tilt condition, with $d_{p-scribe}$ of 0.2 mm, the $d_{p-scribe}$ was reduced from 0.11 to 0.03 mm as it travelled from AS to the front of scribing area, scribing was decreasing amount of copper along the way, and increasing it again to 0.11 mm as it travelled further to RS, thus scribing increasing amount of copper. Compared to the welding using similar $d_{p-scribe}$ in 0° tilt condition, scribe penetrated constantly as it travelled from AS to RS in front half of the scribing area while picked up an increasing amount of copper. Referring to this notion, there is not enough scribed and extruded copper generated in welding using 2.5° tilt condition to even form extensive copper flash in AS and RS. Evidence of this can be seen in the image sectioned from area near the front edge of the scribing zone in Fig. 5 - 16a. In addition, the formation of massive chunk of copper in RS outside the stir zone (Fig. 5 - 9a and 5 - 10a) will most likely follow the phenomenon as follows. The copper fragments were generated when the scribe travelled from RS to AS in rear half region of the scribing area, where the scribe

penetration reached its maximum. The copper fragments generation discontinued as it reached the front of scribing area where the penetration reached its minimum. As it continued its travel and formed new fragments, the copper fragments that were formed earlier were pushed out of the scribing zone of the RS.

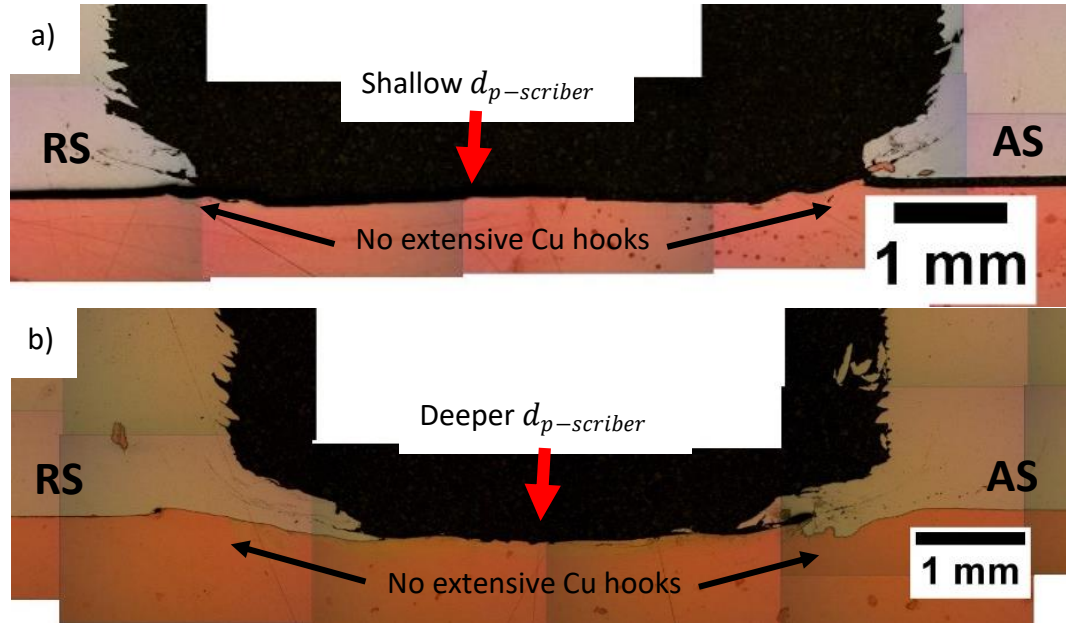


Figure 5 - 16 Keyhole analysis taken from FSLW weld with scribe using $\omega = 1400$ rpm, $v = 40$ mm/min, $d_{p-scriber} = 0.2$ mm, tilt angle = 2.5° . (a) Section taken from the region in front of the scribing area; (b) Section taken from behind of the scribing area.

5.5 Summary

It was shown that FSLW using scribe pin has succeeded to mainly overcome the narrow penetration depth occurred in welding using conventional left-hand threaded pin. Details are as follows:

1. Continuous interface can be achieved when $d_{p-scriber}$ is in a range of 0.2 - 0.5 mm, with a critical distance between bottom pin surface with the original Al - Cu interface being 0.3 mm. Lesser than that, down flow fluidity would decrease, preventing joining, for $d_{p-scriber}$ of ~ 0 , and extensive gap would form from top of the copper flash in RS to a third length of the interface in the stir zone.
2. Decreasing ω from 1400 to 710 rpm adversely affected the continuity of the weld, i.e. lack of fluidity behind the pin was forming gap in the interface
3. Downward vortex flow plays an important role. Lack of down flow was preventing scribed copper fragments to be driven out of the scribed area. The trapped copper

fragments reacted with aluminium to form a very thick region of brittle intermetallic in the scribed area, which was very susceptible to cracking.

4. Lack of fluidity can be compensated by increasing downward forging force. This can be achieved by using tilt condition. However, the critical distance between bottom of pin surface and original Al - Cu interface must be maintained to obtain discontinuity free interface.
5. Extensive hooks can be avoided because of the existence of 1.5 mm distance between scribing area and periphery of the pin that bent the extended flash copper outward of the stir zone in retreating and AS. In addition, these outward hooks were formed in half front of scribing area by scribing movement from AS to RS in the front half of the scribing area.
6. $d_{p-scribers}$ in weld using 2.5° tilt condition are different in rear, flank (RS and AS), and front side of the scribing area. In this study, zero condition was established by positioning the scriber in rear side of the scribing area, making the $d_{p-scribers}$ in flank and front side of the scribing area shallower.
7. Lesser copper scribed in the front half of the scribing area in welding using 2.5° tilt condition resulted in no extensive copper flash hooks. In addition, scribed copper fragments could easily flow out from the stir zone through the shallow RS copper flash.

Chapter 6: FSLW using pin with unthreaded portion at its bottom

This chapter attempts to validate the hypothesis made in Chapter 4 that the last thread of the pin affects the weld interface and is the main culprit of uncertainty in achieving discontinuity free interface. Validation of this hypothesis was achieved by using a pin in which the last thread at the bottom was manually filed attempting to diminish or remove the final threads influence. The influence of d_p on hook formation and interfacial continuity was explored and is presented herein. Importantly, proving the adverse effect of last thread at the bottom of the pin is conducted by studying the flow at the vicinity of the pin bottom using the keyhole method. A tensile shear test followed with fractography analysis of the pulled surface, used in validation of the weld's soundness.

6.1 Weld interface consistency and the effect of penetration (d_p) on interfacial continuity

6.1.1 Consistency of the weld

It was hypothesized in Chapter 4 that the inconsistency in forming a discontinuity free interface was the result of uneven shearing along the back of the pin caused by the last thread at the bottom of the pin. To test the hypothesis, the last thread at the bottom of the pin was manually filed as exemplified in the schematic in Fig. 3 - 15. This configuration provided constant shearing along the back of the pin, in the bottom most thread root and right after the outer periphery of the pin. It is important to note that the filed bottom region acted as the last thread root. This shearing consistency is schematically shown in Fig. 6 - 1. In the filed bottom thread, shearing height is constant as indicated by the red box in Fig. 6 - 1a. While in fully threaded pin the shearing height is affected by the position of the bottom most thread. In the configuration illustrated in Fig. 6 - 1b, the shearing height increases from retreating side (RS) to advancing side (AS), with less shearing in RS as the pin rotates and advances as indicated by the red trapezoid box.

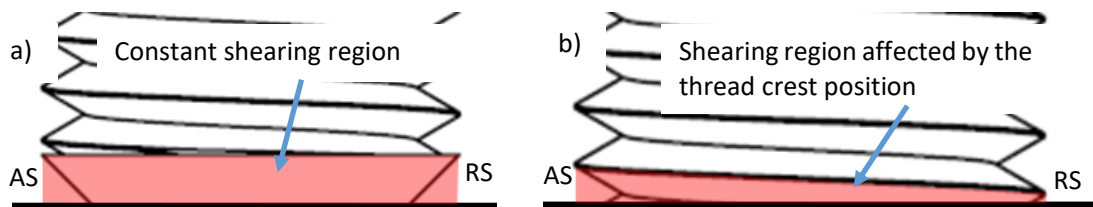


Figure 6 - 1 Back of the pin (a) filed bottom pin; (b) left hand threaded pin.

The constant shearing resulted in a uniform continuous interface throughout the weld. This is shown by interface 1 and 2 in Fig. 6 - 2a, which is taken from the same weld

produced at a $\omega = 1400$ rpm and $v = 40$ mm/min with $d_p = 0.1$ mm. The first and the second interface were taken from places near the start and end of the weld to prove the weld's continuity and is presented in Fig. 6 - 2a and 3a respectively. By using this pin, extensive copper flash was formed either in the retreating (Fig. 6 - 2a) or AS (Fig. 6 - 3a). However, unlike extensive flash in welds with the fully threaded pin, these flashes bent out of the stir zone. The majority of the interfaces in these two welds were free from discontinuities or voids. Typical interfacial features in these welds are depicted in Fig. Fig. 6 - 2. The RS to the middle of the interface was firstly characterized by a thick interfacial intermetallic layer, formed by a dense cluster of Al_2Cu particles. Above it, a cluster of lesser dense Al_2Cu particles existed, together forming a ~ 50 μm thick cluster evident in Fig. 6 - 2b and 3b.

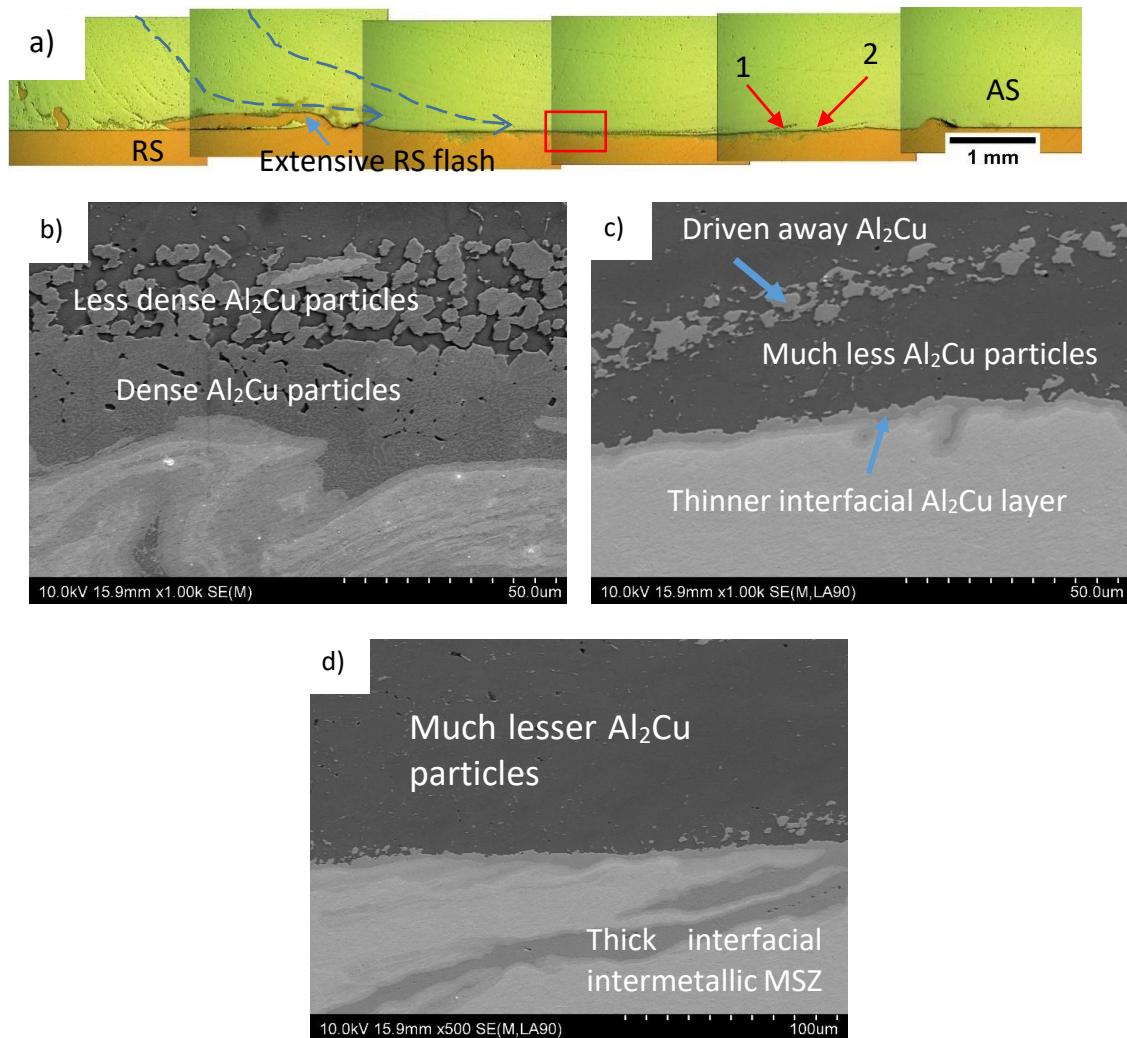


Figure 6 - 2 Interface 1 produced using parameters of $\omega = 1400$ rpm and $v = 40$ mm/min with $d_p = 0.1$ mm. (a) Interface 1 cross section; (b) SEM of typical interface from RS to mid, boxed red in a; (c) typical interface of mid to AS, marked 1 on a; (d) another typical interface of mid to AS, marked 2 on a.

In the middle to AS as seen in Fig. 6 - 2c, this cluster of Al_2Cu particles appeared to driven away from the interface. The thinner interfacial intermetallic layer in the same figure is the consequence of an absence of dense Al_2Cu clusters close to the interface. However, a thick interfacial intermetallic layer was formed in this area as seen in in interface 1 and 2 in Fig. 6 - 2d and 3c respectively. Instead of forming by a dense intermetallic particle, the intermetallic interfacial layer was formed by the dense intercalation of aluminium in copper in the mix stir zone, that was activated by the welding temperature, forming the thick intermetallic layer.

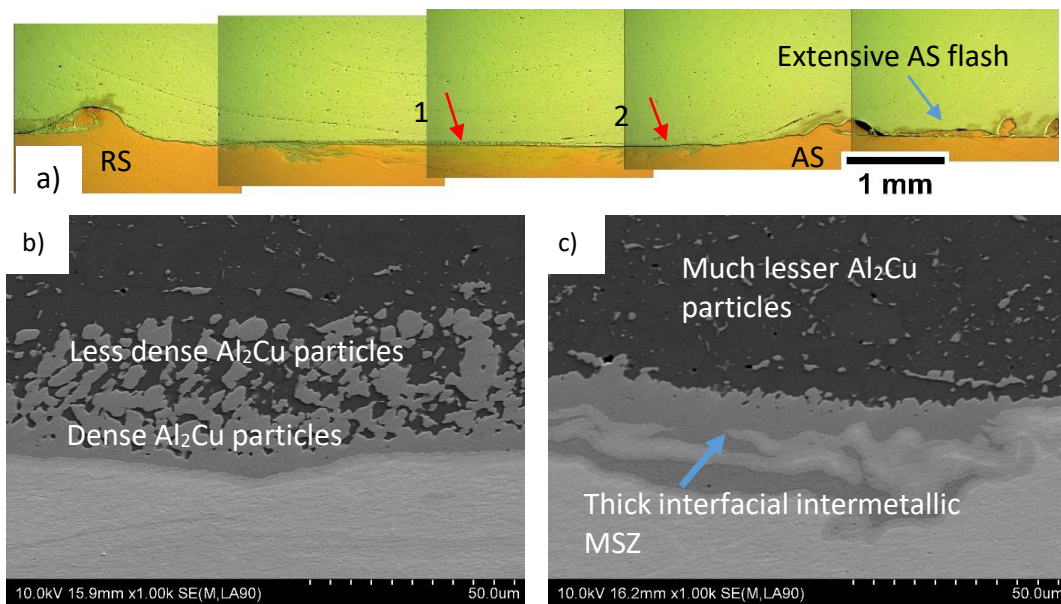


Figure 6 - 3 Interface 2 from the same weld as Fig. 6 - 2. (a) Interface 2 cross section; (b) SEM of typical interface from RS to mid, marked 1 in a; (c) SEM of typical interface from mid to AS, marked 2 in a.

6.1.2 The effect of d_p on interfacial continuity

In order to understand the influence of d_p on interfacial continuity, further welds were produced using deeper d_p 's of 0.25 (Fig. 6 - 4a) and 0.5 (Fig. 6 - 5b) mm. Copper flash in these two welds did not fold or curl back as seen in prior welds. Instead, copper flash along the RS of the weld made with d_p 's of 0.25 and 0.5 mm, extended at an angle appearing to flow in the direction of the material flow into the stir zone. As for the AS flash, welds produced with a d_p of 0.25 mm lead to flash folding all the way back to the side opposite the stir zone. Whilst, flash in welds with a d_p of 0.5 mm extended outward from the tool, likely due to the copper flash extension exceeding the height of the threadless part of the pin. Along the rear half of the pin the extended flash pushed to the side, away from the threadless pin wall, by the material coming from the top driven by the threads. However, welds made with the shallower d_p of 0.25 mm led to the

formation of less extensive copper flash, easily folding in the opposite side of the stir zone by the material flow exiting the stir zone in the AS.

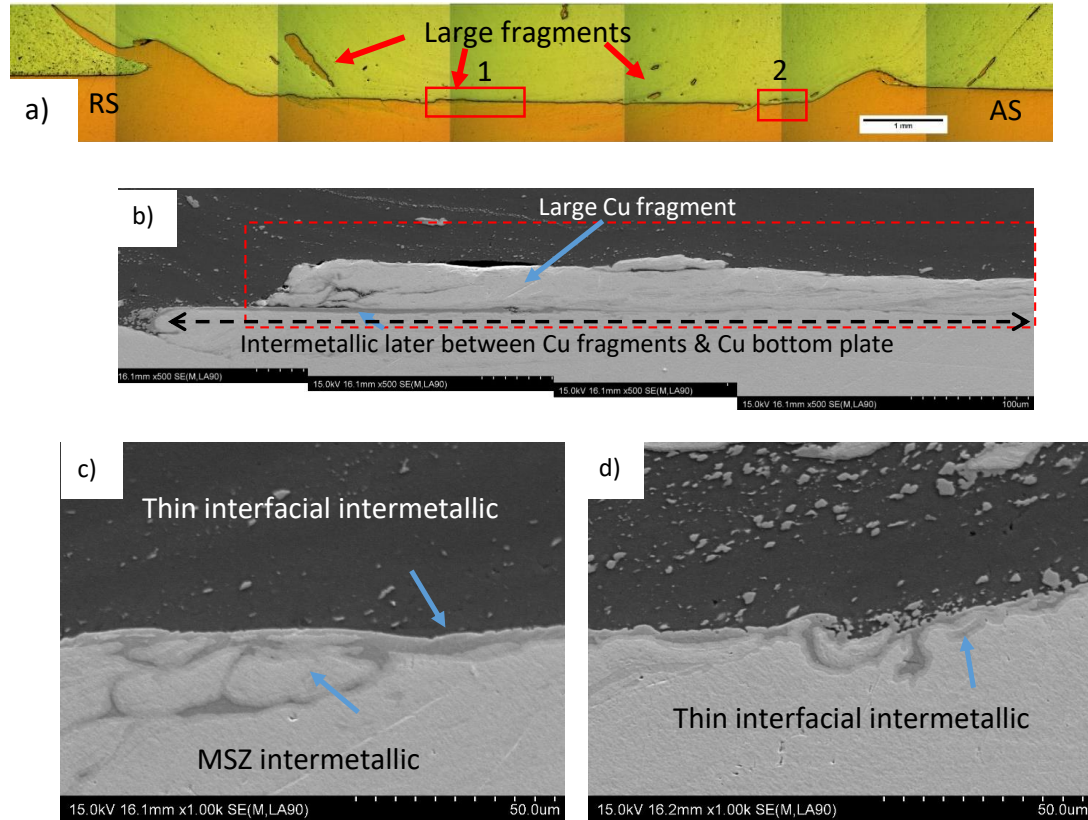


Figure 6 - 4 Weld produced with $\omega = 1400$ rpm, $v = 40$ mm/min and $d_p = 0.25$ mm (a) OM image of the interface; (b) large fragments laid on top of the interface, marked 1 in a; (c) typical interface taken from area marked 1 in a; (d) another typical interface taken from area marked 2 in a;

With respect to the interfacial intermetallic layer, owing to the absence of dense Al_2Cu particles clustering on top of the weld interface, both welds with d_p 's of 0.25 and 0.5 mm are comparably thinner to the weld produced with a d_p of 0.1 mm as seen in Fig. 6 - 4c - d and Fig. 6 - 5c and d respectively. Hence, as the d_p increases, copper fragments produced during process enlarge. These larger copper fragments in welds with d_p 's of 0.5 mm are easily spotted, due colour similarities with the copper plate, contrasted by their dispersion in the aluminium side of stir zone. While in welds with a d_p of 0.25 mm, the dispersion of the copper side of stir zone is pointed out by red arrow in Fig. 6 - 4a. The large copper fragments in the stir zone are able to flow down and deposit right on top of the interface. In the boxed area of Fig. 6 - 4b, the fragment can be seen to separate by an intermetallic layer. This intermetallic layer extended from outside the red box area to; in between the fragments (dashed black line) and copper base metal, indicating that the layer formed before the fragment deposition.

Flow in the stir zone behind the pin was visible in Fig. 6 - 2a and 3a, owing to the mixing induced marking grooves in the RS of the aluminium above the copper flash and the driven away particle cluster in the middle to the AS interface in the weld with a dp of 0.2 mm. As well as copper fragments dispersed in weld with dp of 0.5 mm seen in Fig. 6 - 5. Copper fragment orientation was seen to clearly indicate material flow in the weld produced with a dp of 0.5 mm, as depicted by the black dashed arrow in Fig. 6 - 5. Material flow was seen to enter at the stir zone from the top of RS progressing downward to the interface, about 1 mm from the edge of the weld interface in RS. Material then continued to flow horizontally for about 3 mm in the middle of the weld, finally flowing dominantly upward in middle to AS interface region out of the stir zone. The extensive copper flashes along the retreating and AS In this weld restricted flow however, copper flashes were not as extensive in welds at a dp of 0.1 mm as compared to welds with a dp of 0.5 mm. Further evident in Fig. 6 -2a is aluminium stream flow, directed down in the outside of the weld interface in addition to coming down straight to the middle of the weld interface, as indicated by the grooves.

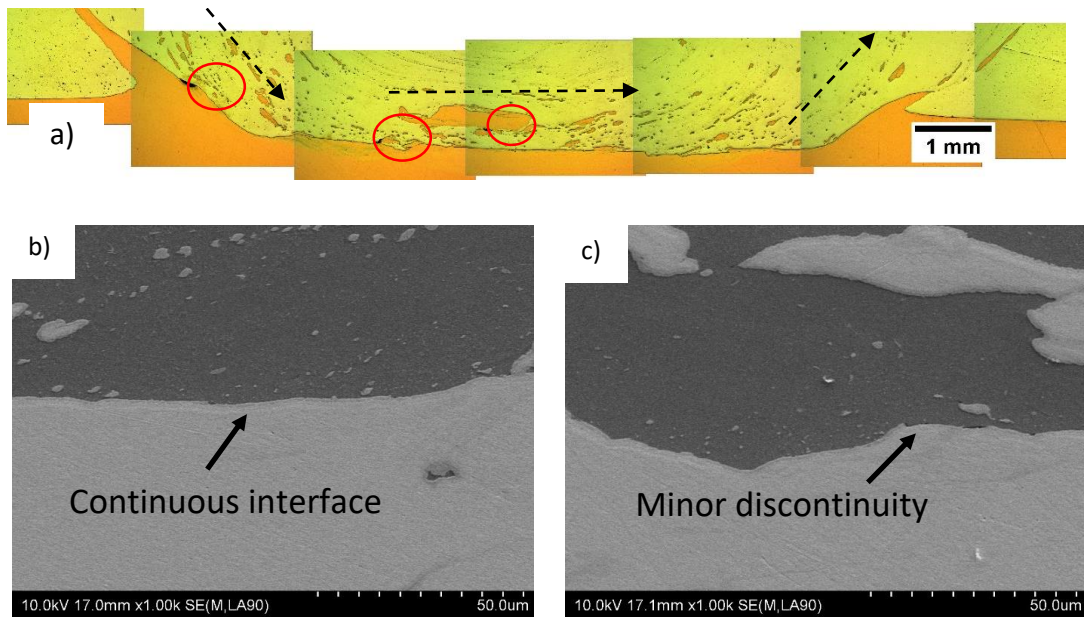


Figure 6 - 5 Weld produced with $\omega = 1400$ rpm, $v = 40$ mm/min and $dp = 0.5$ mm (a) OM image of the interface; (b) typical interface of the weld; (c) another typical interface of the weld showing minor discontinuity.

While in the weld with a dp of 0.1 mm, where the copper flash was not as extensive as that with a dp of 0.5 mm, there was aluminium stream flow that came down the outside of the weld highlighted by the dashed blue arrows in Fig. 6 - 2a. This flow was most likely responsible for the deposition of fine Al_2Cu particles just above the weld interface. A similar flow direction in the middle to AS of the weld was seen in the weld

with a d_p of 0.5 mm, as indicated by the driven away particles cluster. Comparable material flow was detailed in Arbegast's [61] study seen in Fig. 1 - 8, with material flow directed from zone II (RS) down to zone IV below the pin, rising to merge the materials in zone I (AS).

6.2 Flow analysis on the filed thread region

In order to understand the significance of omitting the last thread at the bottom of the pin with the addition of the tapering shape of the manually filed section as well as understanding of the material flow, keyhole analysis was conducted of the weld taken at a d_p of 0.1 mm. The transversal cross section taken from one fourth (Fig. 6 - 6) and three quarter (Fig. 6 - 7) of the keyhole, representing pin passing through one and three quarter of the original Al - Cu original interface were examined in this section.

A fourth of the keyhole interface can be seen in Fig. 6 - 6, showing copper flash extending extensively to about 0.7 and 1 mm in the advancing and RS respectively, despite of shallow 0.1 mm penetration. This flash pressed against the tapered threadless pin wall due to the forging action by the pin forward movement with flash curling downwards. However, whether the downward curling down action was caused by the absence of thread or the tapered shape of the bottom pin body still needs to be investigated.

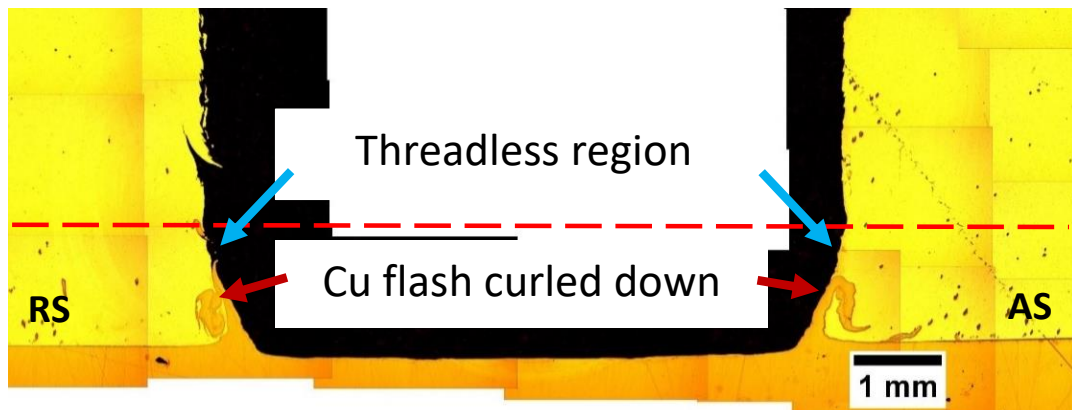


Figure 6 - 6 Transversal cross section of one fourth of the keyhole. The threadless region is ~1.4 mm in height.

After passing the front half of the keyhole, where the material flows from the retreating to the AS, the flashes curled further, pushing away from the threadless pin wall as can be seen in the three quarter of the keyhole interface in Fig. 6 - 7. The most likely cause of this phenomenon is the absence of the pin thread. For comparison, extended copper flash produced by a fully threaded pin in Fig. 4 - 15a, began bending towards the stir zone and was pulled by the vortex flow induced by the threads, particularly in the RS.

This implies that the vortex flow was either non-existent or not as intense as that produced by the fully threaded pin, and not strong enough to pull in the extended copper flash, and was dominated by downward pushing flow. However, immediately behind the threadless pin, flow behaved similar to the flow under the pin as described in the study by Arbegast [61] detailed in the previous section.

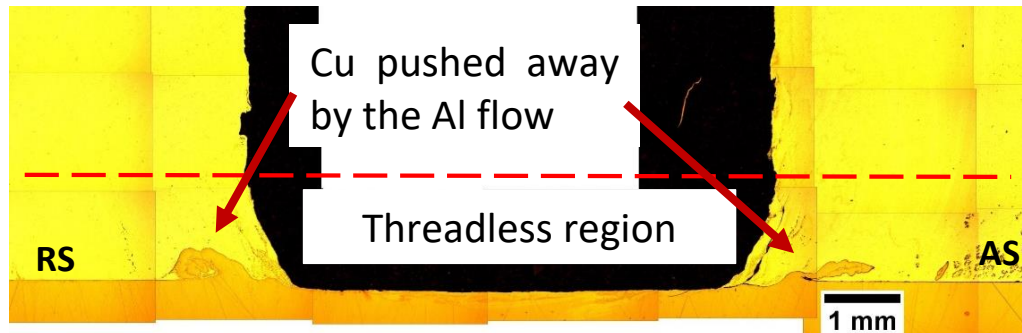


Figure 6 - 7 Transversal cross section of three fourth of the keyhole.

6.3 Mechanical properties and fracture surface analysis

Mechanical property evaluation of the welds was conducted via tensile shear tests, with fracture surfaces analysed after testing. One sample from each trial, representing welds conducted using a d_p of; 0.1, 0.2 and 0.5 mm were used, with the breaking load of these samples corresponding to; 2125, 3175 and 3400 N respectively (appendix 1 to 3). The high breaking load of the latter two samples resulted due to the anchoring action of the extensive copper flash primarily on the RS. This anchoring action also influences sample elongation as was indicated by the higher strain seen in the stress-strain curve, as can be seen in the appendix 2 and 3. The area that was plastically deformed was nearest the handle grip and the area in the vicinity of the copper flash, for welds with d_p 's of 0.2 and 0.5 mm as seen in Fig. 6 - 8b and c. While, in welds produced with a d_p of 0.1 mm, deformation only occurred nearest the handle grip due to the absence of extended copper flash (Fig. 6 - 8a). It may be noted that elongation continued after the breaking load in the stress - strain curve of the weld produced with a d_p of 0.5 mm. This is explained by further deformation of the copper flash until breakage, as the copper flash in the RS was still anchored into the aluminium after the interface was broken. Additionally, the breaking loads of 3175 and 3400N were higher than values obtained from welds with similar ω and v 's in the works of Abdollah-Zadeh et al. [69], Akbari et al.[140], and Firouzdor and Kou [93], at 1873, 3124 and 2000 N respectively.

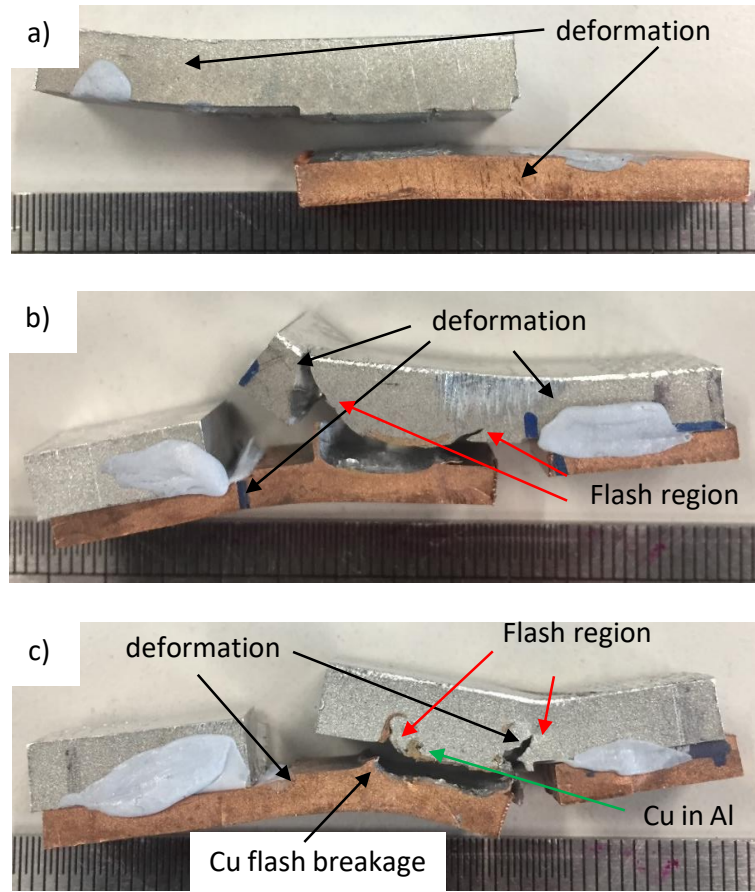


Figure 6 - 8 Fractured tensile shear sample of welds with (a) d_p of 0.1 mm; (b) d_p of 0.2 mm; (c) d_p of 0.5 mm.

In order to study the fracture mode and to assess the continuity of the welds the fracture surface was examined. Continuity of welds produced with d_p 's of 0.1 and 0.2 mm were confirmed by the fracture surface images evident in Fig. 6 - 9a and 10b respectively. The colour of the fracture surface in the copper part was similar to the aluminium fracture surface. The typical aluminium and copper weld surface at a d_p of 0.1 mm is seen in SEM imagery of Fig. 6 - 9b and c. Both surfaces exhibited a brittle fracture mode of intergranular and transgranular types, with the first dominating the fracture surface. This fracture type mixture differed to the work by Xue et al. [33], who instead of a mixed fracture mode observed clear fracture transition from intergranular to transgranular at an intermetallic thickness of $\sim 10 \mu\text{m}$. It is important to note that the interfacial intermetallic thickness for the weld with a d_p of 0.1 mm exceeded $25 \mu\text{m}$. Despite this difference in fracture mode, the protrusion shape and the cavity shape of the intergranular crack in the copper and aluminium fracture surface respectively was in an agreement with the same study [33].

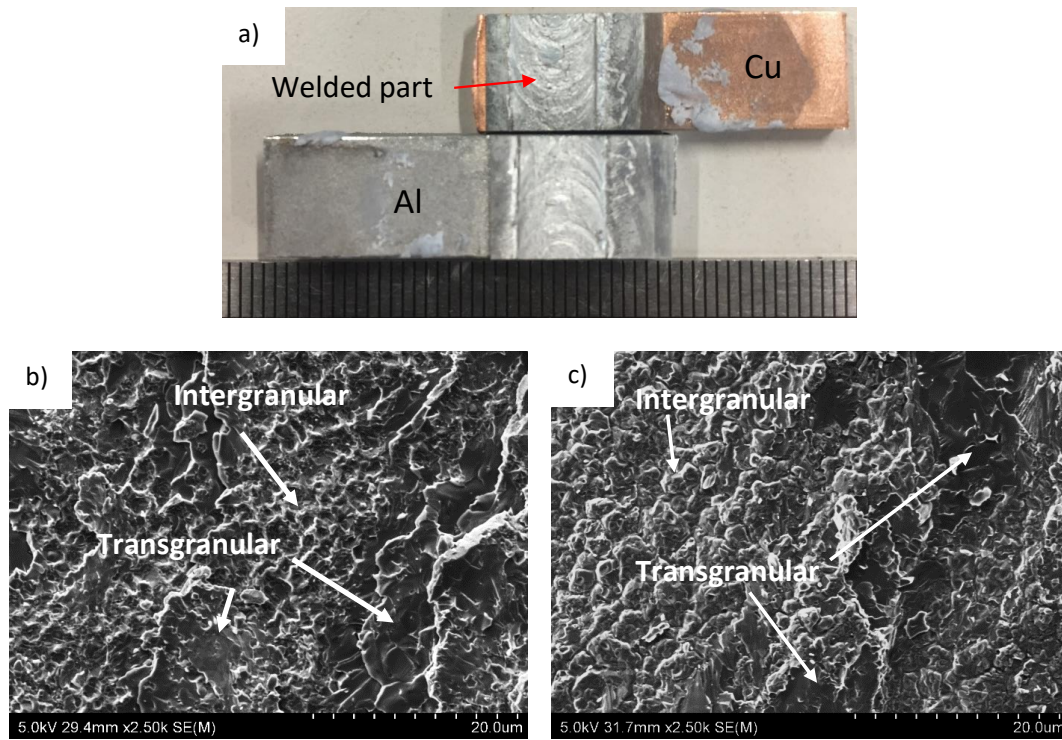


Figure 6 - 9 (a) Fracture surface of broken tensile shear test sample of weld with d_p of 0.1 mm; (b) fracture surface on the aluminium side; (c) fracture surface of copper side.

Similar to that seen above, the weld produced with a d_p of 0.2 mm has a fracture surface long the aluminium side dominated by brittle fracture of intergranular and transgranular modes as evident in Fig. 6 - 10b. Along several regions, ductile fracture features exist along with mixed brittle fracture mode as is seen by elongated dimples in Fig. 6 - 10c. EDS examination on the dimples region shows that it was composed of 99.44 at. % copper, suggesting that the fracture propagated through the mixed stir zone (MSZ), whereby the copper did not completely transform into the intermetallic. A similar mixture of fracture modes of brittle and ductile modes is evident on the copper side of the fracture surface (Fig. 6 - 10d and e). The elongated dimples together with the shear groove in Fig. 6 - 10e indicated that some of the interfacial intermetallic attached to the copper base metal was strong enough to tear the copper base metal creating the elongated dimple feature. Further, the open end of the dimple was seen to be in the opposite direction to the loading direction [141].

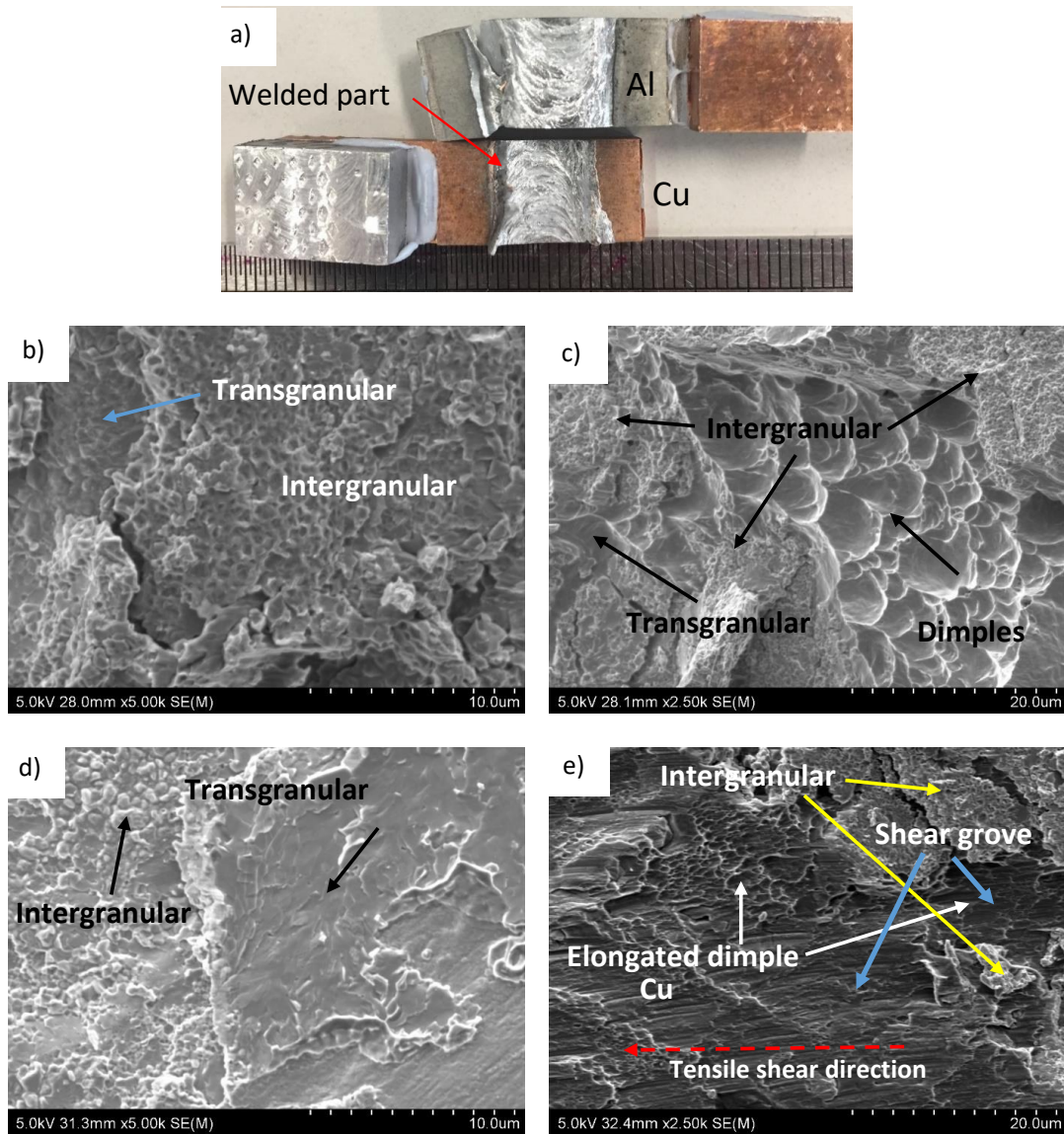


Figure 6 - 10(a) Fracture surface of broken tensile shear test sample of a weld with a d_p of 0.2 mm; (b)-(c) aluminium side fracture surface; (d)-(e) fracture surface of copper side.

Copper fragments are seen to exist in the aluminium side, and are also seen in the transversal cross section of the fractured sample in Fig. 6 - 8c. As in the copper side, in the matching side of the copper fragments seen in Fig. 6 - 11a, some areas were not covered by the intermetallic layer. The existence of copper in the matching surface implied that copper fragments might block aluminium down flow into the copper plate behind the pin, during the FSLW process. Evidence of aluminium down flow blockage by large copper fragments was presented in Section 4.1.

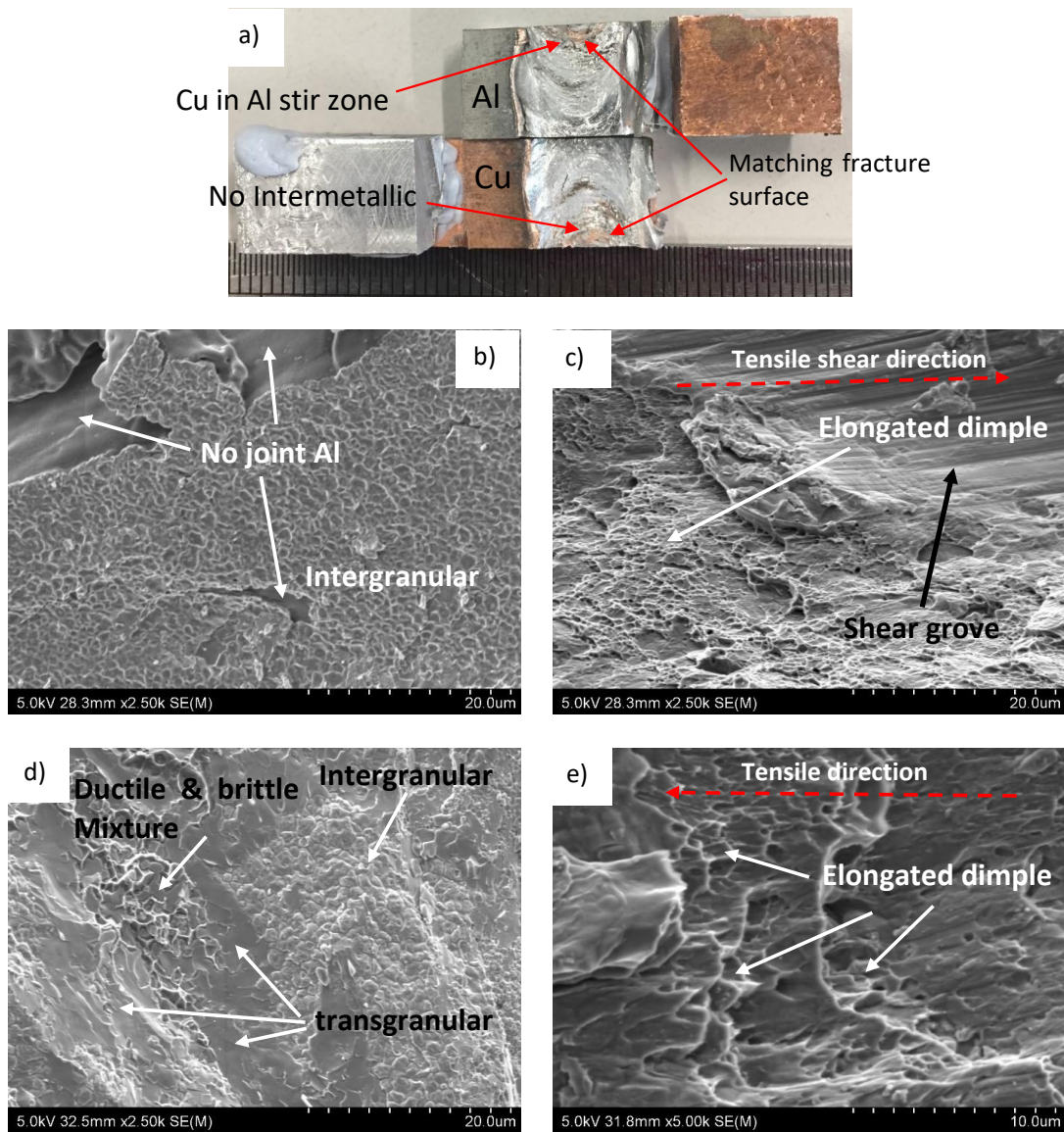


Figure 6 - 11 (a) Fracture surface of broken tensile shear test sample of a weld with a d_p of 0.5 mm; (b)-(c) aluminium side fracture surface; (d)-(e) fracture surface of copper side.

Brittle fracture is also exhibited on the aluminium side of the fracture surface in Fig. 6 - 11b, despite some areas not covered by the intermetallic. However, this uncovered aluminium is not caused by the shearing as implied by the absence of elongated dimples and shear grooves in Fig. 6 - 11b. This corresponds to the occurrence of minor discontinuities, observed in the weld's transversal cross section examination presented in Fig. 6 - 5b. Ductile fracture of aluminium caused by shearing, was apparent by the elongated dimple and shear groove in Fig. 6 - 11c. The copper side of the weld contains the usual mixture intergranular and transgranular brittle fracture modes as seen in prior fracture surfaces, and a region of ductile fracture reinforced by brittle particles broken in transgranular mode presented in Fig. 6 - 11d. This fracture mode is found to be in accordance to the work by Bisadi et al. [73], Minak et al. [142], and Yu et al. [143]. It is

hard to determine accurately the ratio of ductile and brittle fracture however, EDS examination showed that this region consisted of 57.36 and 41.64 At. % aluminium and copper respectively with spots tested seen in Fig. 6 - 12. While from the EDS result in Table 6 - 1 it can be noted that the ductile shear fracture of aluminium existed in the copper side. This supports the analysis that fracture propagated through the MSZ region.

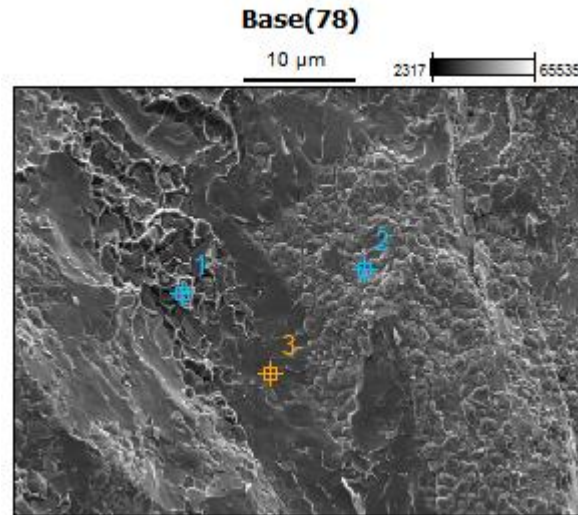


Figure 6 - 12 EDS examination spots of Fig. 6 - 11d.

Table 6 - 1 Chemical composition in atomic % of Fig 6 - 12.

<i>Atom %</i>	<i>Al</i>	<i>Cu</i>
<i>pt1</i> (ductile & brittle mix)	58.36	41.64
<i>pt2</i> (Transgranular)	38.20	61.80
<i>pt3</i> (Intergranular)	57.19	42.81

6.4 Summary

This study was conducted to prove the hypothesis drawn from Section 4.5.1, that inconsistency in achieving a continuous weld interface was the result of threads at the bottom region of the pin. Hence, this study was conducted by using a pin with its bottom most thread manually filed off, with results of as follows:

1. Constant shearing behind the pin successfully produce a continuous weld interface.
2. A continuous intermetallic layer formed across the weld interface. From the RS to the middle of the interface a thick intermetallic layer existed, mainly consisting of a MSZ and thick Al_2Cu layer, formed by a dense cluster of Al_2Cu particles. Above the dense cluster of Al_2Cu particles, a less dense cluster of the same particles was

observed, both totalling a thickness greater than 50 μm . With the cluster seen to diminish to nothing in the middle to AS region of the interface. Furthermore, there was an indication that these particles were flown away from the interface, due to the aluminium flow path, that slightly rose upward as it moved from the middle to the AS.

3. Extensive copper flash in either the retreating or AS was evident in the weld. However, flash folded in the direction opposing the stir zone.
4. Increasing d_p led to an increase of copper flash along the RS and AS. However, instead of folding completely outside, it folded to the opposite side of the stir zone at a rising angle. Furthermore, at the highest d_p of 0.5 mm, the flash restricted the flow behind the unthreaded region of the pin.
5. More copper fragments with larger sizes were observed with increasing d_p . Copper fragments were too large to form a deposition of dense Al_2Cu particles in the interface, as consistently seen in interface of the weld with a d_p of 0.1 mm.
6. A continuous intermetallic layer is produced with d_p 's up to 0.2 mm. However, the weld with a d_p of 0.5 mm resulted in minor discontinuity formation in the interface, as confirmed by fracture surface analysis of tensile shear test sample.
7. Copper fragment dispersion in stir zone of the weld made with a d_p of 0.5 mm acted as markers revealing material flow behind the unthreaded pin. Flow observed was comparable to the flow under the pin from Arbogast's [61] study.
8. Keyhole analysis revealed extensive copper flash formation, curling downward by the down flow in the unthreaded region in the front half of the pin. Further curling of the flash was evident in the back half of the pin, bending it completely towards the opposite side of the stir zone. Downward flow dominated the half back of the pin in the unthreaded area as opposed to vortex flow.
9. The tensile shear test revealed that the weld with a d_p of 0.1 mm was the weakest due to the absence of extensive copper flashes anchoring the weld together, irrespective of the continuous interfacial intermetallic layer in the weld.
10. A brittle intermetallic covered the entirety of the fracture surface of the weld with a d_p of 0.1 mm leading to intergranular fracture mode dominance with a small amount of transgranular fracture. Welds with d_p 's of 0.2 and 0.5 mm exhibited similar mixtures of brittle fracture mode and elongated ductile fracture mode. Copper's presence in the aluminium fracture side and vice versa for the same two welds, implied fracture propagation thorough a MSZ.

Chapter 7: Conclusions and future work

7.1 Conclusions

A series of experiments using various parameters such as penetration depth (d_p), tool rotation speed (ω), and pin geometry were conducted in order to produce a discontinuity-free interface of Al-to-Cu plate produced with FSLW. In addition, material flow in the pin bottom vicinity was studied by means of analysing the keyhole, as well as conducting a stop action method. Based on the findings from the previous chapters it can be concluded that:

- It is apparent that FSLW using fully threaded pin have a very narrow d_p range of 0.15 - 0.29 mm that is not convenient for manufacturing.
- FLSW performed using d_p that exceed the optimum range resulted in the formation of extensive copper flash that subsequently folded into the stir zone, pulled by the vortex flow induced by the thread. The flashes were potentially broken into elongated fragments. Together with the flashes, they blocked the aluminium downflow and subsequently forming voids in the interface vicinity.
- Despite of the known optimum d_p , however, consistently producing a continuous interface with a thin interfacial intermetallic layers between the plate was difficult. This was caused by non-uniform intermetallic shearing caused by the last thread at the bottom of the pin.
- The application of scribe extended the penetration depth, in this case scribe penetration depth ($d_{p-scribe}$) to 0.2 - 0.5 mm. Both retreating and advancing side flashes folded outside of the stir zone allowing unhampered aluminium downflow into the scribed region.
- The application of $d_{p-scribe}$ below the optimum range resulted in loss of fluidity and the formation of extensive gap that exist from the top of the flash to about a third into the middle of the weld interface. Higher downward forging force by the application of tilt angle of 2.5° can close the gap. However, for interfacial continuity, critical $d_{p-scribe}$ of 0.2 mm must be maintained.
- As the rotating scribe penetrated the copper surface, the flashes were formed extensively to reach the bottom surface of the pin. Then, they were pushed out by the movement of the scribe, arching from advancing to RS, at the front half of the pin.

- Aluminium downflow was important to drive the copper fragments, produced by the scribing action, away from the scribed area. Insufficient downflow resulted in trapped copper fragments in the scribed zone. Exposure to a high process temperature, these fragments reacted together with aluminium to transform into a region of thick and brittle intermetallic.
- Pin with manually filed bottom last thread provided a constant intermetallic shearing behind the pin. With this, consistent welds were able to be produced, validating the hypothesis drawn from the results using the left-hand threaded pin.
- Extensive copper flash formed during process was curled down instead of folded into the stir zone that indicated the absence or the diminishing of the vortex down flow which normally existed in a threaded pin.
- As the d_p increased from 0.1 to 0.5 mm, the copper flash changed from folded completely to the opposite side from the stir zone, to extended in an angle forming a sheath in the front half of the unthreaded region of the pin.
- The aluminium down flow behind the unthreaded pin was similar to flow below the pin that was shown in Arbegast's [61] work.
- In weld with d_p of 0.5 mm, aluminium downflow was restricted to flow in between the extended copper flash sheaths. Fragments of copper formed during process were becoming larger as the d_p increased. That deposited near the interface in the form of dense cluster and then formed a thick Al_2Cu interfacial intermetallic layer. Larger fragments weren't turned into intermetallic fragments; they flowed along with aluminium down flow into the stir zone.
- The extended copper flash acted as an anchor to the aluminium, strengthening the joint. Fractography analysis of the broken samples shows that, weld with d_p of 0.1 mm that have thick interfacial intermetallic layer, brittle fracture was dominating the fracture mode of the joint. While for the other two, the fracture was propagated in the mixed stir zone (MSZ).
- Composite-like structures in the stir zone formed by the reaction of copper fragments with aluminium in their surroundings. The denseness of this region is highly depended on the amount of the fragments. The supply of the copper most likely came from raised copper flash, which broken off due to vortex flow impingement and sheared from the inner wall of the flashes, during process.
- Interfacial intermetallic layer, the growth of the layer adjacent to aluminium was not fully governed by volume diffusion. It was formed by the deposition of fine

Al₂Cu and copper particles in the interface, which subsequently reacted and formed thick Al₂Cu layer with short circuit diffusion mechanism.

7.2 Future works

1. After establishing the optimum $d_{p-scriber}$, next, optimum parameters of FSLW with scriber pin, which consist of the combination of rotation speed (ω) and travel speed (v), need to be explored.
2. Various configuration of scriber such as the placement of the scriber in the pin bottom surface, the amount of scriber, and the use of curved pin bottom surface should be explored further.
3. To investigate whether the flash folding was caused by the absence of thread or the tapered shaped of the filed area, weld with tapered left-hand threaded pin needs to be conducted.
4. Further investigation into the removal of last thread at the bottom of the pin, in conjunction to the material flow, needs to be explored. A series of welding using pin where the unthreaded area is not tapered will be conducted. In addition, the effect of the length of unthreaded region along with the variations of d_p , ω , and v to find the optimum condition should be explored.

Reference

- [1] G. E. Totten and D. S. MacKenzie, *Handbook of Aluminum: Volume 2: Alloy Production and Materials Manufacturing*. New York: Marcel Dekker, 2003.
- [2] J. G. Kaufman, *Introduction to Aluminum Alloys and Tempers*. Ohio: ASM International, 2000.
- [3] J. R. Davis, "Aluminum and Aluminum Alloys," in *Alloying: Understanding the Basics*, Ohio: ASM International, 2001, p. 647.
- [4] J. R. Davis, *Alloying: Understanding the Basics*. Ohio: ASM International, 2001.
- [5] "www.makeitfrom.com." .
- [6] "http://www.aalco.co.uk/datasheets." .
- [7] J. R. Davis, *ASM Specialty Handbook: Copper and Copper Alloys*. Ohio: ASM International, 2001.
- [8] "www.totalmateria.com." .
- [9] "www.copper.org." .
- [10] M. Braunovic and N. Aleksandrov, "Intermetallic compounds at aluminum-to-copper and copper-to-tin electrical interfaces," in *Electrical Contacts - 1992 Proceedings of the Thirty-Eighth IEEE Holm Conference on Electrical Contacts*, 1992, pp. 25–34.
- [11] W. E. Veerkamp, "Copper-to-aluminum transitions in high direct-current bus systems," in *Industry Applications Society 42nd Annual Petroleum and Chemical Industry Conference*, 1995, pp. 187–195.
- [12] E. R. Waliach and G. J. Davies, "Mechanical properties of aluminium-copper solid-phase welds," *Met. Technol.*, vol. 4, no. 1, pp. 183–190, Jan. 1977.
- [13] R. W. Messler, Jr, *Joining of Advanced Materials*. Woburn, MA: butterworth-Heinemann, 1993.
- [14] R. W. Messler, Jr., *Principles of Welding: Processes, Physics, Chemistry, and Metallurgy*, 1st ed. WILEY-VCH Verlag GmbH & Co. KGaA, 2004.
- [15] S. Asai, T. Ogawa, Y. Ishizaki, T. Minemura, H. Minami, and S. Miyazaki,

- “Application of plasma MIG hybrid welding to dissimilar joints between copper and steel,” *Weld. World*, vol. 56, no. 1–2, pp. 37–42, 2012.
- [16] S. Chen, J. Huang, J. Xia, X. Zhao, and S. Lin, “Influence of processing parameters on the characteristics of stainless steel/copper laser welding,” *J. Mater. Process. Technol.*, vol. 222, pp. 43–51, 2015.
- [17] S. Chen, J. Huang, J. Xia, H. Zhang, and X. Zhao, “Microstructural characteristics of a stainless steel/copper dissimilar joint made by laser welding,” *Metall. Mater. Trans. A Phys. Metall. Mater. Sci.*, vol. 44, no. 8, pp. 3690–3696, 2013.
- [18] H. Naffakh, M. Shamanian, and F. Ashrafizadeh, “Dissimilar welding of AISI 310 austenitic stainless steel to nickel-based alloy Inconel 657,” *J. Mater. Process. Technol.*, vol. 209, no. 7, pp. 3628–3639, 2009.
- [19] R. Dehmlaei, M. Shamanian, and A. Kermanpur, “Effect of electromagnetic vibration on the unmixed zone formation in 25Cr-35Ni heat resistant steel/Alloy 800 dissimilar welds,” *Mater. Charact.*, vol. 59, no. 12, pp. 1814–1817, 2008.
- [20] M. Gao, Z. M. Wang, X. Y. Li, and X. Y. Zeng, “Laser keyhole welding of dissimilar Ti-6Al-4V titanium alloy to AZ31B magnesium alloy,” *Metall. Mater. Trans. A Phys. Metall. Mater. Sci.*, vol. 43, no. 1, pp. 163–172, 2012.
- [21] C. Tan *et al.*, “Microstructure and mechanical properties of laser welded-brazed Mg/Ti joints with AZ91 Mg based filler,” *Mater. Des.*, vol. 99, pp. 127–134, 2016.
- [22] M. Gao, Z. M. Wang, J. Yan, and X. Y. Zeng, “Dissimilar Ti/Mg alloy butt welding by fibre laser with Mg filler wire – preliminary study,” *Sci. Technol. Weld. Join.*, vol. 16, no. 6, pp. 488–496, 2011.
- [23] Y. M. Baqer, S. Ramesh, F. Yusof, and S. M. Manladan, “Challenges and advances in laser welding of dissimilar light alloys: Al/Mg, Al/Ti, and Mg/Ti alloys,” *Int. J. Adv. Manuf. Technol.*, vol. 95, no. 9–12, pp. 4353–4369, 2018.
- [24] M. Naeem, R. Jessett, and K. Withers, “Fiber laser welding of dissimilar materials,” 2012. [Online]. Available: <http://www.industrial-lasers.com/articles/2012/03/fiber-laser-welding-of-dissimilar-materials.html>.
- [25] S. J. Lee, M. Takahashi, Y. Kawahito, and S. Katayama, “Microstructural

- evolution and characteristics of weld fusion zone in high speed dissimilar welding of Ti and Al,” *Int. J. Precis. Eng. Manuf.*, vol. 16, no. 10, pp. 2121–2127, 2015.
- [26] P. Schmalen and P. Plapper, “Evaluation of laser braze-welded dissimilar Al-Cu joints,” *Phys. Procedia*, vol. 83, pp. 506–514, 2016.
 - [27] C. Otten, U. Reisgen, and M. Schmachtenberg, “Electron beam welding of aluminum to copper: mechanical properties and their relation to microstructure,” *Weld. World*, vol. 60, no. 1, pp. 21–31, 2016.
 - [28] M. Abbasi, a. Karimi Taheri, and M. T. Salehi, “Growth rate of intermetallic compounds in Al/Cu bimetal produced by cold roll welding process,” *J. Alloys Compd.*, vol. 319, no. 1–2, pp. 233–241, Apr. 2001.
 - [29] M. Braunovic and N. Aleksandrov, “Effect of electrical current on the morphology and kinetics of formation of intermetallic phases in bimetallic aluminum-copper joints,” in *Proceedings of IEEE Holm Conference on Electrical Contacts*, pp. 261–268.
 - [30] C.-Y. Chen and W.-S. Hwang, “Effect of Annealing on the Interfacial Structure of Aluminum-Copper Joints,” *Mater. Trans.*, vol. 48, no. 7, pp. 1938–1947, 2007.
 - [31] W.-B. Lee, K.-S. Bang, and S.-B. Jung, “Effects of intermetallic compound on the electrical and mechanical properties of friction welded Cu/Al bimetallic joints during annealing,” *J. Alloys Compd.*, vol. 390, no. 1–2, pp. 212–219, Mar. 2005.
 - [32] C.-Y. Chen, H.-L. Chen, and W.-S. Hwang, “Influence of Interfacial Structure Development on the Fracture Mechanism and Bond Strength of Aluminum/Copper Bimetal Plate,” *Mater. Trans.*, vol. 47, no. 4, pp. 1232–1239, 2006.
 - [33] P. Xue, B. L. Xiao, and Z. Y. Ma, “Effect of Interfacial Microstructure Evolution on Mechanical Properties and Fracture Behavior of Friction Stir-Welded Al-Cu Joints,” *Metall. Mater. Trans. A*, vol. 46, no. 7, pp. 3091–3103, Jul. 2015.
 - [34] M. Braunovic and N. Aleksandrov, “Effect of electrical current on the

morphology and kinetics of formation of intermetallic phases in bimetallic aluminum-copper joints,” in *Proceedings of IEEE Holm Conference on Electrical Contacts*, pp. 261–268.

- [35] Z. W. Chen, S. Yazdanian, and G. Littlefair, “Effects of tool positioning on joint interface microstructure and fracture strength of friction stir lap Al-to-steel welds,” *J. Mater. Sci.*, vol. 48, no. 6, pp. 2624–2634, Mar. 2013.
- [36] S. Yazdanian, “Metallurgical Studies of Friction Stir Lap Welding,” Auckland University of Technology, 2012.
- [37] Z. W. Chen and S. Yazdanian, “Microstructures in interface region and mechanical behaviours of friction stir lap Al6060 to Ti–6Al–4V welds,” *Mater. Sci. Eng. A*, vol. 634, pp. 37–45, May 2015.
- [38] R. S. Mishra and M. W. Mahoney, “Introduction,” in *Friction Stir Welding and Processing*, R. S. Mishra and M. W. Mahoney, Eds. Ohio: ASM International, 2007, p. 368.
- [39] R. S. Mishra, P. S. De, and N. Kumar, *Friction Stir Welding and Processing*. Cham: Springer International Publishing, 2014.
- [40] M. W. Mahoney, C. G. Rhodes, J. G. Flintoff, W. H. Bingel, and R. A. Spurling, “Properties of friction-stir-welded 7075 T651 aluminum,” *Metall. Mater. Trans. A*, vol. 29, no. 7, pp. 1955–1964, Jul. 1998.
- [41] W. M. Thomas, E. D. Nicholas, J. C. Needham, M. G. Murch, P. Temple-Smith, and C. J. Dawes, “Improvements relating to friction welding,” US patent no. 5 460 317; EPS 0 616 490, 1991.
- [42] W. M. Thomas, E. D. Nicholas, J. C. Needham, M. G. Murch, P. Temple-Smith, and C. J. Dawes, “Friction stir butt welding,” GB patent no. 9125978.8, 1991.
- [43] P. L. Threadgill, A. J. Leonard, H. R. Shercliff, and P. J. Withers, “Friction stir welding of aluminium alloys,” *Int. Mater. Rev.*, vol. 54, no. 2, pp. 49–93, Mar. 2009.
- [44] R. S. Mishra and Z. Y. Ma, “Friction stir welding and processing,” *Mater. Sci. Eng. R Reports*, vol. 50, no. 1–2, pp. 1–78, 2005.
- [45] N. Kumar, R. S. Mishra, and W. Yuan, *Friction Stir Welding of Dissimilar*

Alloys and Materials. Elsevier, 2015.

- [46] R. S. Mishra and M. W. Mahoney, Eds., *Friction Stir Welding and Processing*. Materials Park, OH: ASM International, 2007.
- [47] C. B. Fuller, “Friction stir tooling: tool materials and design,” in *Friction Stir Welding and Processing*, R. S. Mishra and M. W. Mahoney, Eds. Materials Park, Ohio: ASM International, 2007, pp. 7–35.
- [48] P. L. Threadgill, “No Title,” *TWI bulletin*, Mar-1997.
- [49] H. Schmidt, J. Hattel, and J. Wert, “An analytical model for the heat generation in friction stir welding,” *Model. Simul. Mater. Sci. Eng.*, vol. 12, no. 1, pp. 143–157, 2004.
- [50] J. A. Schneider, “Temperature Distribution and Resulting Metal Flow,” in *Friction Stir Welding and Processing*, R. S. Mishra and M. W. Mahoney, Eds. Ohio: ASM International, 2007, pp. 37–49.
- [51] J. A. Schneider and A. C. Nunes, “Characterization of plastic flow and resulting microtextures in a friction stir weld,” *Metall. Mater. Trans. B*, vol. 35, no. 4, pp. 777–783, Aug. 2004.
- [52] A. P. Reynolds, “Visualisation of material flow in autogenous friction stir welds,” *Sci. Technol. Weld. Join.*, vol. 5, no. 2, pp. 120–124, 2000.
- [53] H. N. B. Schmidt, T. L. Dickerson, and J. H. Hattel, “Material flow in butt friction stir welds in AA2024-T3,” *Acta Mater.*, vol. 54, no. 4, pp. 1199–1209, Feb. 2006.
- [54] T. U. Seidel and a. P. Reynolds, “Visualization of the material flow in AA2195 friction-stir welds using a marker insert technique,” *Metall. Mater. Trans. A*, vol. 32, no. November, pp. 2879–2884, 2001.
- [55] K. Colligan, “Material Flow Behavior during Friction Stir Welding of Aluminum,” *Weld. J.*, vol. 78, no. July, pp. 229–237, 1999.
- [56] A. C. Nunes and J. Schneider, “Thermo-Mechanical Processing in Friction Stir Welds,” in *Friction Stir Welding and Processing*, 2003, pp. 43–51.
- [57] M. Guerra, C. Schmidt, J. . McClure, L. . Murr, and a. . Nunes, “Flow patterns during friction stir welding,” *Mater. Charact.*, vol. 49, no. 2, pp. 95–101, Sep.

2002.

- [58] A. A. M. da Silva, E. Arruti, G. Janeiro, E. Aldanondo, P. Alvarez, and A. Echeverria, "Material flow and mechanical behaviour of dissimilar AA2024-T3 and AA7075-T6 aluminium alloys friction stir welds," *Mater. Des.*, vol. 32, no. 4, pp. 2021–2027, Apr. 2011.
- [59] Z. W. Chen, T. Pasang, and Y. Qi, "Shear flow and formation of Nugget zone during friction stir welding of aluminium alloy 5083-O," *Mater. Sci. Eng. A*, vol. 474, no. 1–2, pp. 312–316, 2008.
- [60] W. J. Arbegast, "Modeling Friction Stir Joining as a Metal Working Process," in *Hot Deformation of Aluminum Alloys III*, 2003, p. 568.
- [61] W. J. Arbegast, "A flow-partitioned deformation zone model for defect formation during friction stir welding," *Scr. Mater.*, vol. 58, no. 5, pp. 372–376, 2008.
- [62] S. Đorđević, *Electrometallurgy (In Serbian)*. Belgrade: Faculty of Technology and Metallurgy, 1972.
- [63] K. Popov, B. Grgur, and S. S. Djokić, *Fundamental Aspects of Electrometallurgy*. Boston: Kluwer Academic Publishers, 2002.
- [64] M. J. Mahon, "Dynamic Process Simulation of Zinc Electrowinning," The University Of British Columbia, 2016.
- [65] N. T. Beukes and J. Badenhorst, "Copper electrowinning: Theoretical and practical design," *J. South. African Inst. Min. Metall.*, vol. 109, no. 6, pp. 343–356, 2009.
- [66] "https://www.alibaba.com/product-detail/Durable-Aluminum-Sheet-With-Anticorrosion-Painting_60553309203.html?spm=a2700.galleryofferlist.normalList.171.143a3603r77zbc."
- [67] E. P. Wiechmann, P. Aqueveque, G. A. Vidal, and J. A. Henriquez, "Contact system design to improve energy efficiency in copper electrowinning processes," *IEEE Trans. Ind. Appl.*, vol. 49, no. 6, pp. 2461–2465, 2013.
- [68] S. Cui, Z. W. Chen, and J. D. Robson, "A model relating tool torque and its

associated power and specific energy to rotation and forward speeds during friction stir welding/processing,” *Int. J. Mach. Tools Manuf.*, vol. 50, no. 12, pp. 1023–1030, Dec. 2010.

- [69] A. Abdollah-Zadeh, T. Saeid, and B. Sazgari, “Microstructural and mechanical properties of friction stir welded aluminum/copper lap joints,” *J. Alloys Compd.*, vol. 460, no. 1–2, pp. 535–538, Jul. 2008.
- [70] A. Elrefaey, M. Takahashi, and K. Ikeuchi, “Microstructure of Aluminum/Copper Lap Joint by Friction Stir Welding and Its Performance,” *J. High Temp. Soc.*, vol. 30, no. 5, pp. 286–292, 2004.
- [71] A. Elrefaey, M. Takahashi, and K. Ikeuchi, “Preliminary Investigation of Friction Stir Welding Aluminium/Copper Lap Joints,” *Weld. World*, vol. 49, no. 3–4, pp. 93–101, Feb. 2005.
- [72] T. Saeid, a. Abdollah-zadeh, and B. Sazgari, “Weldability and mechanical properties of dissimilar aluminum–copper lap joints made by friction stir welding,” *J. Alloys Compd.*, vol. 490, no. 1–2, pp. 652–655, Feb. 2010.
- [73] H. Bisadi, A. Tavakoli, M. Tour Sangsaraki, and K. Tour Sangsaraki, “The influences of rotational and welding speeds on microstructures and mechanical properties of friction stir welded Al5083 and commercially pure copper sheets lap joints,” *Mater. Des.*, vol. 43, pp. 80–88, Jun. 2012.
- [74] X. K. Peng, R. Wuhner, G. Heness, and W. Y. Yeung, “On the interface development and fracture behaviour of roll bonded copper/aluminium metal laminates,” *J. Mater. Sci.*, vol. 34, no. 9, pp. 2029–2038, 1999.
- [75] J. Ouyang, E. Yarrapareddy, and R. Kovacevic, “Microstructural evolution in the friction stir welded 6061 aluminum alloy (T6-temper condition) to copper,” *Mater. Process. Technol.*, vol. 172, pp. 110–122, 2006.
- [76] I. Galvão, J. C. Oliveira, a Loureiro, and D. M. Rodrigues, “Formation and distribution of brittle structures in friction stir welding of aluminium and copper: influence of process parameters,” *Sci. Technol. Weld. Join.*, vol. 16, no. 8, pp. 681–689, Nov. 2011.
- [77] E. Akinlabi, A. Els-Botes, and H. Lombard, “Effect of tool displacement on defect formation in friction stir welding of aluminium and copper,” *8th Int.*

Symp. Frict. Stir Weld., pp. 18–20, 2010.

- [78] M. N. Avettand-Fenoël, R. Taillard, G. Ji, and D. Goran, “Multiscale Study of Interfacial Intermetallic Compounds in a Dissimilar Al 6082-T6/Cu Friction-Stir Weld,” *Metall. Mater. Trans. A*, vol. 43, no. 12, pp. 4655–4666, Dec. 2012.
- [79] D. M. Rodrigues, I. Galvão, D. Gesto, and D. Verdera, “Aluminum to Copper Lap Joining Using Friction Stir Welding,” in *Trends in Welding Research*, 2012, vol. 2012.
- [80] D. Parningotan, M. Tarrant, Z. W. Chen, A. Hilton, and T. Pasang, “Influence of Stir Flow on Joint Quality During Friction Stir Lap Al-to-Cu Welding,” in *Friction Stir Welding and Processing IX*, 2017, p. 360.
- [81] D. G. Andrade, I. Galvão, D. Verdera, C. Leitão, and D. M. Rodrigues, “Influence of the structure and phase composition of the bond interface on aluminium–copper lap welds strength,” *Sci. Technol. Weld. Join.*, vol. 23, no. 2, pp. 105–113, 2018.
- [82] K. P. Mehta and V. J. Badheka, “A review on dissimilar friction stir welding of copper to aluminum: Process, properties, and variants,” *Mater. Manuf. Process.*, vol. 31, no. 3, pp. 233–254, 2016.
- [83] I. Galvão, A. Loureiro, D. Verdera, D. Gesto, and D. M. Rodrigues, “Influence of Tool Offsetting on the Structure and Morphology of Dissimilar Aluminum to Copper Friction-Stir Welds,” *Metall. Mater. Trans. A*, vol. 43, no. 13, pp. 5096–5105, Aug. 2012.
- [84] S. Kahl and W. Osikowicz, “Composite Aluminum-Copper Sheet Material by Friction Stir Welding and Cold Rolling,” *J. Mater. Eng. Perform.*, vol. 22, no. August, pp. 2176–2184, Feb. 2013.
- [85] M. Sarvghad-moghaddam, R. Parvizi, A. Davoodi, M. Haddad-sabzevar, and A. Imani, “Establishing a correlation between interfacial microstructures and corrosion initiation sites in Al / Cu joints by SEM – EDS and AFM – SKPFM,” *Corros. Sci.*, vol. 79, pp. 148–158, 2014.
- [86] C. W. Tan, Z. G. Jiang, L. Q. Li, Y. B. Chen, and X. Y. Chen, “Microstructural evolution and mechanical properties of dissimilar Al–Cu joints produced by friction stir welding,” *Mater. Des.*, vol. 51, pp. 466–473, Oct. 2013.

- [87] R. Beygi, M. Kazeminezhad, a. H. Kokabi, and A. Loureiro, “Friction Stir Welding of Al-Cu Bilayer Sheet by Tapered Threaded Pin: Microstructure, Material Flow, and Fracture Behavior,” *Metall. Mater. Trans. A*, vol. 46, no. 6, pp. 2544–2553, Jun. 2015.
- [88] I. Galvão, A. Loureiro, and D. M. Rodrigues, “Critical review on friction stir welding of aluminium to copper,” *Sci. Technol. Weld. Join.*, vol. 1718, no. April, pp. 1–24, 2016.
- [89] I. Galvão, R. M. Leal, a. Loureiro, and D. M. Rodrigues, “Material flow in heterogeneous friction stir welding of aluminium and copper thin sheets,” *Sci. Technol. Weld. Join.*, vol. 15, no. 8, pp. 654–660, Nov. 2010.
- [90] H. J. Liu, J. J. Shen, L. Zhou, Y. Q. Zhao, C. Liu, and L. Y. Kuang, “Microstructural characterisation and mechanical properties of friction stir welded joints of aluminium alloy to copper,” *Sci. Technol. Weld. Join.*, vol. 16, no. 1, pp. 92–98, Jan. 2011.
- [91] M. F. X. Muthu and V. Jayabalan, “Tool travel speed effects on the microstructure of friction stir welded aluminum-copper joints,” *J. Mater. Process. Technol.*, vol. 217, pp. 105–113, 2015.
- [92] I. Galvão, D. Verdera, D. Gesto, a. Loureiro, and D. M. Rodrigues, “Influence of aluminium alloy type on dissimilar friction stir lap welding of aluminium to copper,” *J. Mater. Process. Technol.*, vol. 213, no. 11, pp. 1920–1928, Nov. 2013.
- [93] V. Firouzdor and S. Kou, “Al-to-Cu Friction Stir Lap Welding,” *Metall. Mater. Trans. A*, vol. 43, no. 1, pp. 303–315, Jul. 2011.
- [94] R. Beygi, M. Kazeminezhad, and a. H. Kokabi, “Microstructural Evolution and Fracture Behavior of Friction-Stir-Welded Al-Cu Laminated Composites,” *Metall. Mater. Trans. A*, vol. 45, no. 1, pp. 361–370, Oct. 2013.
- [95] L. Cederqvist, a P. Reynolds, and A. P. R. Cederqvist, B Y L, “Factors Affecting the Properties of Friction Stir Welded Aluminum Lap Joints,” *Weld. J.*, vol. 80, no. 12, pp. 281–287, 2001.
- [96] Z. Shen, Y. Chen, M. Haghshenas, and A. P. Gerlich, “Role of welding parameters on interfacial bonding in dissimilar steel/aluminum friction stir

- welds,” *Eng. Sci. Technol. an Int. J.*, vol. 18, no. 2, pp. 270–277, Jun. 2015.
- [97] V. Firouzdor and S. Kou, “Formation of Liquid and Intermetallics in Al-to-Mg Friction Stir Welding,” *Metall. Mater. Trans. A*, vol. 41, no. 12, pp. 3238–3251, Jul. 2010.
 - [98] M. Haghshenas, A. Abdel-Gwad, A. M. Omran, B. Gökçe, S. Sahraeinejad, and A. P. Gerlich, “Friction stir weld assisted diffusion bonding of 5754 aluminum alloy to coated high strength steels,” *Mater. Des.*, vol. 55, pp. 442–449, 2014.
 - [99] S. Jana, Y. Hovanski, G. J. Grant, and K. Mattlin, “Effect of Tool Feature on the Joint Strength of Dissimilar Friction Stir Lap Welds,” in *Friction Stir Welding and Processing VI*, Hoboken, NJ, USA: John Wiley & Sons, Inc., 2011, pp. 205–211.
 - [100] S. Jana and Y. Hovanski, “Fatigue behaviour of magnesium to steel dissimilar friction stir lap joints,” *Sci. Technol. Weld. Join.*, vol. 17, no. 2, pp. 141–145, 2012.
 - [101] Y. Hovanski, G. J. Grant, S. Jana, and K. F. Mattlin, “Friction stir welding tool and process for welding dissimilar materials,” *US Pat. US8434661 B2*, vol. 2, no. 12, 2013.
 - [102] T. Wang, H. Sidhar, R. S. Mishra, Y. Hovanski, P. Upadhyay, and B. Carlson, “Friction stir scribe welding technique for dissimilar joining of aluminium and galvanised steel,” *Sci. Technol. Weld. Join.*, vol. 1718, no. November, pp. 1–7, 2017.
 - [103] T. Curtis *et al.*, “Friction Stir Scribe Welding of Dissimilar Aluminum to Steel Lap Joints,” in *Friction Stir Welding and Processing VIII*, 2015, pp. 163–169.
 - [104] P. Upadhyay, Y. Hovanski, L. S. Fifield, and K. L. Simmons, “Friction Stir Lap Welding of Aluminum - Polymer Using Scribe Technology,” in *Friction Stir Welding and Processing VIII*, 2015, pp. 153–161.
 - [105] P. Upadhyay, Y. Hovanski, B. Carlson, E. Boettcher, R. Ruokolainen, and P. Busuttil, “Joining Dissimilar Material Using Friction Stir Scribe Technique,” in *Friction Stir Welding and Processing IX*, 2017, pp. 147–155.
 - [106] P. Upadhyay, Y. Hovanski, B. Carlson, E. Boettcher, R. Ruokolainen, and P. Busuttil, “Joining Dissimilar Material Using Friction Stir Scribe Technique,”

Miner. Met. Mater. Ser., vol. 139, no. 9783319523828, pp. 147–155, 2017.

- [107] E. I. Barker, P. Upadhyay, Y. Hovanski, and X. Sun, “Predicting Lap Shear Strength for Friction Stir Scribe Joining of Dissimilar Materials,” in *Friction Stir Welding and Processing IX*, 2017, pp. 261–267.
- [108] V. Gupta *et al.*, “Linking process and structure in the friction stir scribe joining of dissimilar materials: A computational approach with experimental support,” *J. Manuf. Process.*, vol. 32, no. February, pp. 615–624, 2018.
- [109] P. Upadhyay, Y. Hovanski, B. Carlson, E. Boettcher, R. Ruokolainen, and P. Busuttil, “Joining Dissimilar Material Using Friction Stir Scribe Technique,” in *Friction Stir Welding and Processing IX*, 2017, pp. 147–155.
- [110] V. Gupta *et al.*, “Linking process and structure in the friction stir scribe joining of dissimilar materials: A computational approach with experimental support,” *J. Manuf. Process.*, vol. 32, no. February, pp. 615–624, 2018.
- [111] H. Das, R. N. Ghosh, and T. K. Pal, “Study on the Formation and Characterization of the Intermetallics in Friction Stir Welding of Aluminum Alloy to Coated Steel Sheet Lap Joint,” *Metall. Mater. Trans. A*, vol. 45, no. 11, pp. 5098–5106, Jul. 2014.
- [112] M. Movahedi *et al.*, “Growth kinetics of Al–Fe intermetallic compounds during annealing treatment of friction stir lap welds,” *Mater. Charact.*, vol. 90, pp. 121–126, Apr. 2014.
- [113] H. Springer, a. Kostka, J. F. dos Santos, and D. Raabe, “Influence of intermetallic phases and Kirkendall-porosity on the mechanical properties of joints between steel and aluminium alloys,” *Mater. Sci. Eng. A*, vol. 528, no. 13–14, pp. 4630–4642, May 2011.
- [114] Y. Wei, J. Xiong, J. Li, F. Zhang, and S. Liang, “Microstructure and enhanced atomic diffusion of friction stir welding aluminium/steel joints,” *Mater. Sci. Technol.*, vol. 0, no. 0, pp. 1–7, 2017.
- [115] M. Movahedi, A. H. Kokabi, S. M. Seyed Reihani, W. J. Cheng, and C. J. Wang, “Effect of annealing treatment on joint strength of aluminum/steel friction stir lap weld,” *Mater. Des.*, vol. 44, pp. 487–492, 2013.
- [116] Y. H. Jin, R. G. Gan, C. F. Li, and X. J. Wang, “Growth kinetics of Al–Mg

- intermetallics during post-weld annealing treatment,” *Mater. Sci. Technol.*, vol. 32, no. 15, pp. 1632–1638, 2016.
- [117] G. Neumann and C. Tuijn, *Self-diffusion and Impurity Diffusion in Pure Metals, Volume 14*. Amsterdam: Elsevier, 2009.
- [118] E. E. Patterson, Y. Hovanski, and D. P. Field, “Microstructural Characterization of Friction Stir Welded Aluminum-Steel Joints,” *Metall. Mater. Trans. A*, vol. 47, no. 6, pp. 2815–2829, Jun. 2016.
- [119] Y. Hovanski, P. Upadhyay, S. Kleinbaum, B. Carlson, E. Boettcher, and R. Ruokolainen, “Enabling Dissimilar Material Joining Using Friction Stir Scribe Technology,” *Jom*, vol. 69, no. 6, pp. 1060–1064, 2017.
- [120] A. Simar and M.-N. Avettand-Fènoël, “State of the art about dissimilar metal friction stir welding,” *Sci. Technol. Weld. Join.*, vol. 22, no. 5, pp. 389–403, 2017.
- [121] Z. W. Chen, D. Parningotan, W. Li, and M. Tarrant, “Material flow conditions for discontinuity free friction stir lap Al-to-Cu welding,” in *11th International Symposium on Friction Stir Welding*, 2016, pp. 1–7.
- [122] “Al₂Cu (CuAl₂) Crystal Structure.” [Online]. Available: https://materials.springer.com/isp/crystallographic/docs/sd_1421272.
- [123] M. Girard, B. Huneau, C. Genevois, X. Sauvage, and G. Racineux, “Friction stir diffusion bonding of dissimilar metals,” *Sci. Technol. Weld. Join.*, vol. 15, no. 8, pp. 661–665, Nov. 2010.
- [124] J. L. Murray, “ASM Handbooks, vol.3, Alloy Phase Diagrams,” H. Okamoto, M. E. Schlesinger, and E. M. Mueller, Eds. Materials Park, OH: ASM International, 2002.
- [125] E. R. Waliach and G. J. Davies, “Mechanical properties of aluminium-copper solid- phase welds,” *Met. Technol.*, vol. 4, pp. 183–90, 1977.
- [126] D. Moreno, J. Garrett, and J. D. Embury, “A technique for rapid characterization of intermetallics and interfaces,” *Intermetallics*, vol. 7, no. 9, pp. 1001–1009, Sep. 1999.
- [127] P. Upadhyay and A. P. Reynolds, “Effects of thermal boundary conditions in

- friction stir welded AA7050-T7 sheets,” *Mater. Sci. Eng. A*, vol. 527, no. 6, pp. 1537–1543, Mar. 2010.
- [128] R. Beygi, M. Kazeminezhad, and a. H. Kokabi, “Butt joining of Al–Cu bilayer sheet through friction stir welding,” *Trans. Nonferrous Met. Soc. China*, vol. 22, no. 12, pp. 2925–2929, Dec. 2012.
 - [129] H. Liu, Y. Hu, Y. Peng, C. Dou, and Z. Wang, “The effect of interface defect on mechanical properties and its formation mechanism in friction stir lap welded joints of aluminum alloys,” *J. Mater. Process. Technol.*, vol. 238, pp. 244–254, 2016.
 - [130] I. Galvão, J. C. Oliveira, A. Loureiro, and D. M. Rodrigues, “Formation and distribution of brittle structures in friction stir welding of aluminium and copper: Influence of shoulder geometry,” *Intermetallics*, vol. 22, pp. 122–128, 2012.
 - [131] A. Fallet, G. Chichignoud, C. L. Martin, M. Suéry, and P. Jarry, “Influence of barium addition on the microstructure and the rheological behaviour of partially solidified Al-Cu alloys,” *Mater. Sci. Eng. A*, vol. 426, no. 1–2, pp. 187–193, 2006.
 - [132] D. M. Stefanescu, *Science and Engineering of Casting Solidification, Second Edition*, 2nd ed. Boston, MA: Springer US, 2009.
 - [133] M. Rappaz and J. A. Dantzig, *Solidification*, 1st ed. Lausanne, Switzerland: EPFL Press, 2009.
 - [134] Y. K. Yang, H. Dong, and S. Kou, “Liquation tendency and liquid-film formation in friction stir spot welding,” *Weld. J.*, vol. 87, no. August, pp. 202–211, 2008.
 - [135] K. V. Jata, K. K. Sankaran, and J. J. Ruschau, “Friction-Stir Welding Effects on Microstructure and Fatigue of Aluminum Alloy 7050-T7451,” vol. 31, no. September, 2000.
 - [136] Y. Li, L. . Murr, and J. . McClure, “Flow visualization and residual microstructures associated with the friction-stir welding of 2024 aluminum to 6061 aluminum,” *Mater. Sci. Eng. A*, vol. 271, no. 1–2, pp. 213–223, Nov. 1999.
 - [137] Y. S. Sato, H. Kokawa, M. Enomoto, and S. Jogan, “Microstructural Evolution of 6063 Aluminum during Friction- Stir Welding,” vol. 30, no. September, pp.

2429–2437, 1999.

- [138] Q. Zhang, W. Gong, and W. Liu, “Microstructure and mechanical properties of dissimilar Al–Cu joints by friction stir welding,” *Trans. Nonferrous Met. Soc. China*, vol. 25, no. 6, pp. 1779–1786, 2015.
- [139] A. Paul, T. Laurila, V. Vuorinen, and S. V. Divinski, “Short-Circuit Diffusion,” in *Thermodynamics, Diffusion and the Kirkendall Effect in Solids*, 2014, pp. 429–491.
- [140] M. Akbari, P. Bahemmat, M. Haghpanahi, and M.-K. Besharati Givi, “Enhancing metallurgical and mechanical properties of friction stir lap welding of Al–Cu using intermediate layer,” *Sci. Technol. Weld. Join.*, vol. 18, no. 6, pp. 518–524, Aug. 2013.
- [141] V. Kerlins, “Modes of Fracture,” in *ASM Handbook, Vol 12, Fractography*, Materials Park, OH: ASM International, 1987.
- [142] G. Minak, L. Ceschini, I. Boromei, and M. Ponte, “Fatigue properties of friction stir welded particulate reinforced aluminium matrix composites,” *Int. J. Fatigue*, vol. 32, no. 1, pp. 218–226, 2010.
- [143] L. Yu, K. Nakata, and J. Liao, “Microstructural modification and mechanical property improvement in friction stir zone of thixo-molded AE42 Mg alloy,” *J. Alloys Compd.*, vol. 480, no. 2, pp. 340–346, 2009.

Appendix

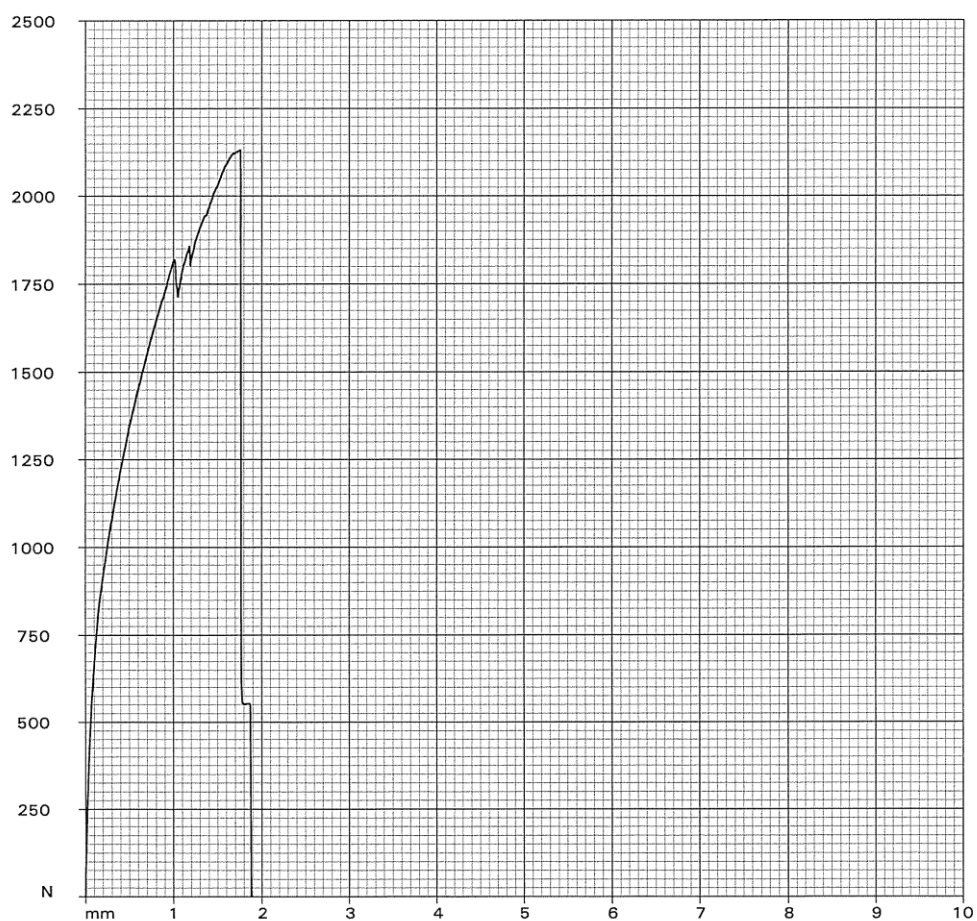
0,1

1

 Tinius Olsen
 Test Report

Product Code ...: DEST
 Date: 2018
 Batch Number ...:
 Operator:
 Test Speed.....: 3.000 {mm/min}

Max	Break	Ext @ Brk	10.000	50.000	100.000	200.000	300.000
N	N	mm	N	N	N	N	N
2133.333	-553.333	1.870	0.000	0.000	0.000	0.000	0.000



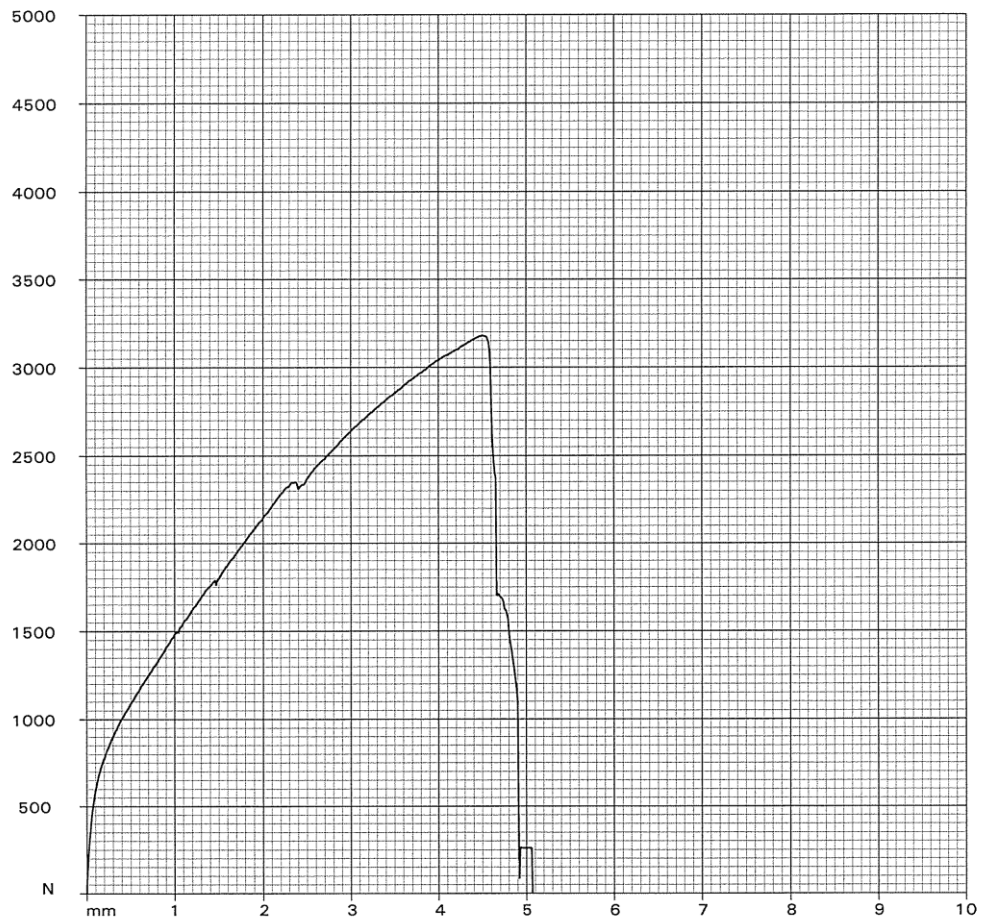
0,2

2

Tinius Olsen
Test Report

Product Code ...: DEST
Date: 2018
Batch Number ...:
Operator:
Test Speed.....: 3.000 {mm/min}

Max	Break	Ext @ Brk	10.000	50.000	100.000	200.000	300.000
N	N	mm	N	N	N	N	N
3181.667	-263.333	5.065	0.000	0.000	0.000	0.000	0.000



0,5

3

Tinius Olsen
Test Report

Product Code ...: DEST
Date: 2018
Batch Number ...:
Operator:
Test Speed.....: 3.000{mm/min}

Max	Break	Ext @ Brk	10.000	50.000	100.000	200.000	300.000
N	N	mm	N	N	N	N	N
3395.000	-23.333	7.376	0.000	0.000	0.000	0.000	0.000

